

Heat Transport Analysis of Burgers Fluid Flow Over Stretching Geometries



By

Zahoor Iqbal

Department of Mathematics

Quaid-i-Azam University

Islamabad, Pakistan

2021

Heat Transport Analysis of Burgers Fluid Flow Over Stretching Geometries



By

Zahoor Iqbal

Supervised By

Prof. Dr. Masood Khan

Department of Mathematics

Quaid-i-Azam University

Islamabad, Pakistan

2021

Heat Transport Analysis of Burgers Fluid Flow Over Stretching Geometries



By

Zahoor Iqbal

A DISSERTATION SUBMITTED IN THE PARTIAL FULFILLMENT OF THE REQUIREMENT FOR

THE DEGREE OF

DOCTOR OF PHILOSOPHY

IN

MATHEMATICS

Supervised by

Prof. Dr. Masood Khan

Department of Mathematics

Quaid-i-Azam University

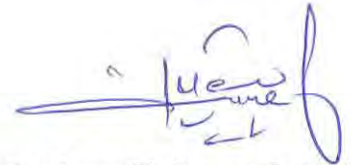
Islamabad, Pakistan

2021

Author's Declaration

I, **Zahoor Iqbal**, hereby state that my PhD thesis titled **Heat Transport Analysis of Burgers Fluid Flow Over Stretching Geometries** is my own work and has not been submitted previously by me for taking any degree from the Quaid-I-Azam University Islamabad, Pakistan or anywhere else in the country/world.

At any time if my statement is found to be incorrect even after my graduate the university has the right to withdraw my PhD degree.



Name of Student: **Zahoor Iqbal**

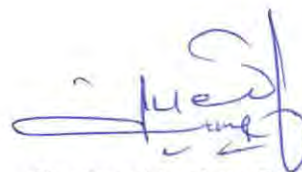
Date: **28-09-2021**

Plagiarism Undertaking

I solemnly declare that research work presented in the thesis titled "**Heat Transport Analysis of Burgers Fluid Flow Over Stretching Geometries**" is solely my research work with no significant contribution from any other person. Small contribution/help wherever taken has been duly acknowledged and that complete thesis has been written by me.

I understand the zero-tolerance policy of the HEC and **Quaid-i-Azam University** towards plagiarism. Therefore, I as an Author of the above titled thesis declare that no portion of my thesis has been plagiarized and any material used as reference is properly referred/cited.

I undertake that if I am found guilty of any formal plagiarism in the above titled thesis even afterward of PhD degree, the University reserves the rights to withdraw/revoke my PhD degree and that HEC and the University has the right to publish my name on the HEC/University Website on which names of students are placed who submitted plagiarized thesis.



Student/Author Signature

Name: **Zahoor Iqbal**

Heat Transport Analysis of Burgers Fluid Flow Over Stretching Geometries

By


Zahoor Iqbal

CERTIFICATE

A THESIS SUBMITTED IN THE PARTIAL FULFILLMENT OF THE
REQUIREMENTS FOR THE DEGREE OF THE
DOCTOR OF PHILOSOPHY IN MATHEMATICS

We accept this thesis as conforming to the required standard

1.




Prof. Dr. Sohail Nadeem
(Chairman)

2.



Prof. Dr. Masood Khan
(Supervisor)

3.



Prof. Dr. Muhammad Sajid, T.I
(External Examiner)

4.



Dr. Meraj Mustafa Hashmi
(External Examiner)

Department of Mathematics, International
Islamic University, H-10, Islamabad.

School of Natural Sciences (SNS) Sector H-
12, National University of Sciences and
Technology (NUST) Islamabad

Department of Mathematics
Quaid-I-Azam University
Islamabad, Pakistan
2021

Certificate of Approval

This is to certify that the research work presented in this thesis entitled **Heat Transport Analysis of Burgers Fluid Flow Over Stretching Geometries** was conducted by **Mr. Zahoor Iqbal** under the kind supervision of **Prof. Dr. Masood Khan**. No part of this thesis has been submitted anywhere else for any other degree. This thesis is submitted to the Department of Mathematics, Quaid-i-Azam University, Islamabad in partial fulfillment of the requirements for the degree of Doctor of Philosophy in field of Mathematics from Department of Mathematics, Quaid-i-Azam University Islamabad, Pakistan.

Student Name: **Zahoor Iqbal**

Signature: 

External committee:

a) **External Examiner 1:**

Name: **Prof. Dr. Muhammad Sajid, T.I**

Designation: Professor

Department of Mathematics, International Islamic University, H-10,
Islamabad

Signature: 

b) **External Examiner 2:**

Name: **Dr. Meraj Mustafa Hashmi**

Designation: Associate Professor

School of Natural Sciences (SNS) Sector H-12, National University of
Sciences and Technology (NUST) Islamabad

Signature: 

c) **Internal Examiner**

Name: **Prof. Dr. Masood Khan**

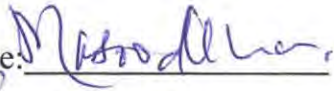
Designation: Professor

Office Address: Department of Mathematics, QAU Islamabad.

Signature: 

Supervisor Name:

Prof. Dr. Masood Khan

Signature: 

Name of Dean/ HOD

Prof. Dr. Sohail Nadeem

Signature: 

Dedicated

to

My

beloved

parents

and

wife

ACKNOWLEDGEMENT

In the name of Allah, the most Beneficent and the most Merciful Lord, the creator, and all praises for “Allah Almighty”, who has given me the chance, courage and ability to complete this thesis. I am nothing without my Allah, but I can handle everything with his blessing. Also, I cannot forget the sources of humanity, idea personality of all creation for whom Allah has created the whole universe, who is forever a torch bearer of guidance for humanity, Hazrat Muhammad (S.A.W.W).

First and foremost, I would like to express my gratitude to my worthy supervisor **Prof. Dr. Masood Khan** for his valuable suggestions and mentoring that helped me to accomplish this highly important research. His knowledge, accessibility and availability have been a critical motivational in driving this research. It would never have been possible for me to take this work to accomplish without his incredible support and encouragement. I am ever indebted and grateful to him. I would like to thank my beloved parents, dear Mrs. Amina Anwer, my sweet brothers Abdul Ghafoor, Zaheer Iqbal, Abdul Qadeer, Muhammad Kaleem and dearest sister Iqra whose love, prayers guidance are with me to follow my dream. I am very thankful to my family for their support and encouragement. I highly praise the cooperative behavior of my brothers. I have been lucky enough to have good friends in my academic and social life and cannot forget their role in my education and university life. It is a matter of great delight and pleasure for me to mention my truly wonderful friends and colleagues, **Dr. Awais Ahmed, Abdul Hafeez, Dr. Jawad Ahmed, Dr. Aamir Hamid, Dr. Lateef Ahmed, Dr. Irfan, Dr. Noor Muhammad, Dr. Mair Khan, M. Salman Khan, Dr. Nadeem Abbas, Dr. Faisal, Muhammad Yasir, Eng. Fiaz Butt and Mahnoor Sarfraz.**

Here, I would like to pay thanks to my father-in-law Eng. **Haji Anwer Malik** (Late) who was my great motivator and source of inspiration for me. I am also thankful to my mother-in-law for her prayers and support and my brother-in-law **Dr. Zia ur Rehman Malik** (Orthopaedic surgeon) for his continuously guidance and motivations. I gratefully acknowledged the Department of Mathematics,

Quaid-I-Azam University Islamabad for providing such wonderful facilities that made my work possible. At the end, I would like to thank to all my research fellows and those people who directly and indirectly helped me during my research work.

Zahoor Iqbal

Abstract

The purpose of this thesis is to expose some theoretical findings regarding non-Newtonian fluid flows. The main concern of the work presented in this thesis is to develop the mathematical model and their analytic as well as numerical solutions for the flow of non-Newtonian Burgers fluid. In addition, the heat transport in the flow of Burgers fluid is also addressed in this thesis. Consequently, the theme of thesis comprises the development of the boundary layer equations for steady two and three-dimensional flows of Burgers fluids. To provide a better understanding of pertinent physical behaviors, the development of results have been carried out for them in various circumstances. The problems encountered here contain, the forced convective heat transfer over stretching surfaces by considering different physical impacts like non-linear thermal radiation, Joule heating, uniform and non-uniform heat source/sink, magnetic field, nanofluid, Cattaneo-Christov heat and mass flux models, homogeneous heterogeneous reactions and convective thermal and solutal boundary conditions. The modelled PDEs are converted into ODEs by employing appropriate dimensionless transformations which are then tackled by employing the HAM as well as BVP midrich numerical scheme. The effects of emerging parameters on velocity, thermal and solutal profiles are plotted in the form of graphs and discussed in detail with reasonable physical arguments. Additionally, the coefficients of heat transport as well as mass transport at the surface are also computed for some dimensionless parameters and depicted in tabular form. In the limiting cases, our findings are found to be in excellent agreement with formerly published results in the literature. A noticeable finding is that the flow distribution of Burgers fluid is deteriorated for escalating magnitudes of material parameter of Burgers fluid (β_2). In addition, the thermal and concentration profiles showed rising trend for higher estimation of Burgers fluid material parameter (β_2). It is further noticed that the larger curvature parameter (α) boost up the velocity and

temperature distributions of Burgers fluid. Moreover, the higher extent of thermal relaxation time parameter (β_t) declined the temperature distribution of Burgers fluid. The results of this thesis leads to suggest a much improved understanding of the rheological characteristics of the Burgers fluid flow.

Contents

1	Research Background	5
1.1	Fundamental Laws of Continuum Mechanics	20
1.1.1	The Conservation of Mass (Continuity Equation)	21
1.1.2	The Conservation of Momentum	21
1.1.3	The Conservation of Energy	22
1.1.4	The Conservation of Concentration	23
1.1.5	The Energy Conservation for Nanofluid	24
1.1.6	The Concentration Conservation for Nanofluid	25
1.2	The Rate Type Burgers Fluid Model	25
1.3	Solution Methodologies	26
1.3.1	BVP Midrich Scheme (Midpoint Collocation Method)	26
1.3.2	Homotopy Analysis Method (HAM)	27
1.4	Contribution in Thesis	28

2 Cattaneo-Christov double diffusion theory featur-

	ing the thermal transport in the flow of Burgers	
	nanofluid due to stretching flat plate	32
2.1	Mathematical Formulation	33
2.2	Analysis of Results	38
2.3	Validation of Homotopic Solutions	42
3	Burgers nanofluid flow accelerated by bidirectional	
	stretching surface subject to Ohmic heating and	
	chemical reaction	50
3.1	Rheological Development	51
3.1.1	Flow Equations of Burgers Fluid	52
3.1.2	Energy Transport Equations	55
3.2	Physical Analysis of Results	57
3.3	Validation of Homotopic Solutions	62
4	Analysis of heat and mass transport in Burgers	
	fluid flow due to stretching cylinder	71
4.1	Mathematical Formulation	72
4.2	Validation of Homotopic Approach	76
4.3	Analysis of Results	77

5 Stagnation point flow of magnetized Burgers nanofluid

subject to thermal radiation 87

5.1 Mathematical Formulation 88
5.2 Physical Concern Parameters 91
5.3 Solution Convergence 92
5.4 Physical Analysis of Results 94

6 Burgers fluid flow in perspective of Buongiorno’s

model with improved heat and mass flux theory

over stretching cylinder 106

6.1 Mathematical Formulation 107
6.2 Validation of Optimal Homotopic Results 111
6.3 Physical Analysis of Results 112

7 Features of thermophoretic and Brownian forces

in Burgers fluid flow subject to Joule heating and

convective conditions 123

7.1 Mathematical Formulation 124
7.2 Engineering Concerned Quantities 127
7.3 Validation of Numerical Scheme 128

7.4	Discussion of Outcomes	129
8	On modified Fourier heat flux in stagnation point flow of magnetized Burgers fluid subject to homogeneous- heterogeneous reactions	140
8.1	Mathematical Formulations	141
8.1.1	Flow Profile	141
8.1.2	Thermal Features of Burgers Fluid	143
8.1.3	Relation for Chemical Species	144
8.2	Validation of Numerical Scheme	146
8.3	Discussion of Results	147
9	Conclusions and Forthcoming Work	157
9.1	Conclusions	157
9.2	Forthcoming work	159

Chapter 1

Research Background

Non-Newtonian fluids are of great importance due to their wonderful heat transform features and applications in engineering systems like, heat exchangers, solution suspensions, food processing systems, biochemical progressing and geophysical developments. There are different non-Newtonian fluid models which exhibit the behavior of diverse non-Newtonian fluids. Because of their different characteristics several kinds of non-Newtonian models have been established. These materials are being classified as differential, integral and rate type materials. Rate type models include, for instance, Maxwell, Oldroyd-B and Burgers fluids. Burgers model is considered as the comprehensive viscoelastic rate type fluid model which is broadly developed and delineates the complete features of several non-Newtonian fluids. Burgers fluid model explains the relaxation and retardation times properties of fluid. Burgers fluid model has tendency to explain the viscous and elastic responses of fluid and to setup the stress relaxation of several polymeric liquids. Initially, Maxwell introduced the viscoelastic fluid model for explaining the behavior of fluids like air, in place of polymeric liquids. Additionally, at this time Maxwell did not understand in sense of mechanical point of view of adopting spring and dashpot in his

demonstration of the model, but he worked in a direction of method for storage of energy and its dissipation. In contrast of this, Burgers investigated the model in mechanical perspective and familiarized spring and dashpot as sources of mechanism for energy storage and its dissipation. Burgers [1] presented a one-dimensional rate type fluid model that contains one dimensional Maxwell model [2] as a special case to explain the viscoelastic behavior of fluid materials. This model also includes the Oldroyd-B fluid model presented in the memorial paper of Oldroyd [3]. In this paper, Oldroyd presented a precise method to interact with three dimensional rate-type fluid models which are appropriately invariant of frame. Due to this model, Burgers has been used to explain a diversity of non-Newtonian materials which provided a debate about the use of Burgers fluid model to describe the characteristics of viscoelastic type fluids. Regardless of its diverse applications, Burgers fluid model has not gained considerable consideration in the past. But, some works on Burgers fluid model have done in past which we mention here like, Ravindran *et al.* [4] investigated the flow of Burgers fluid between two parallel surfaces which are rotating along non-coincident axes. Hayat *et al.* [5] examined the simple flow of a Burgers fluid. Additionally, Hayat [6] inspected the rotational Burgers fluid flow due to a flat surface. He found that the velocity of fluid initially grows up and then depreciates afterwards. Khan *et al.* [7] examined the flow of Burgers fluid in a pipe by considering the effects of Hall current. They disclosed that the flow curves of Burgers magnetic fluid build up for higher scales of Hall parameter. Hayat *et al.* [8] presented a mathematical model to study the flow of Burgers fluid due to a stretching sheet. Further, Hayat *et al.* [9] explored the flow of magneto Burgers fluid in view of heat source. They observed that the flow distribution of nanofluid escalates due to growing magnitude of retardation time parameter. Khan *et al.* [10] analyzed the boundary layer flow of Burgers nanofluid with the effects of nonlinear radiation. They reported that the

thermal distribution of nanofluid rises for improving scales of radiation constant. Recently, Waqas *et al.* [11] employed the non-Fourier's and Fick's laws to study the heat transform features in flow of Burgers fluid due to stretching surface. Khan *et al.* [12] examined the flow of Burgers fluid near a stagnation point by incorporating the effects of thermal radiation. They exposed that the fluid velocity builds up by intensifying the scales of velocity ratio parameter. Iqbal *et al.* [13] investigated the magneto Burgers nanofluid by employing modified heat and mass fluxes over a stretchable sheet. They noted that the thermal energy flow deteriorates for higher scales of thermal relaxation parameter.

Heat transfer mechanism of fluid flow due to unidirectional stretching and bidirectional stretching sheets is a topic of great interest since last few decades. Heat transfer due to stretching surfaces has significant applications in thermal advancement of devices, extrusion process and in polymer industry. Wang [14] was the first who studied a 3D flow due to bidirectional stretching surface. This idea of Wang is utilized by several researchers and analysts to examine the 3D flow of different types of fluids. Like, Ariel [15] presented a numerical simulation to a 3D flow of fluid caused by bidirectional stretching sheet. He obtained the perturbation solution of the flow problem. Liu and Andersson [16] analyzed the thermal transport in the flow of viscous fluid caused by bidirectional stretching geometry. They noticed that the larger sheet temperature corresponds to thinner thermal boundary layer thickness. Thermal properties of three-dimensional Jeffrey fluid are investigated by Hayat *et al.* [17] under the influence of heat source sink. They noticed that the thermal distribution of Jeffrey fluid significantly enhances due to developing magnitude of heat source. Mahanthesh *et al.* [18] numerical explored the thermal and momentum transport in the flow of nanofluid caused by bidirectional stretching surface by considering the effects of Lorentz forces. Momentum transport is declined for higher

strength of Lorentz force in their investigation. Khan and Khan [19] explored the momentum and thermal transport in the flow of Burgers fluid due to bidirectional stretching of surface by employing the non-Fourier heat flux theory. Moreover, Khan *et al.* [20,21] investigated the thermal transport in flow of Burgers fluid by employing the impact of chemical reaction and non-Fourier heat law for bidirectional stretching case. Hina *et al.* [22] employed the bidirectional stretching of surface to scrutinize the thermal behavior of Oldroyd-B nanofluid flow. Diminution in thermal penetration depth is perceived by them for growing values of thermal relaxation time constraint. Khan *et al.* [23] studied the heat transfer characteristics in the steady flow of Sisko fluid caused by bidirectional stretching of the surface. They manifested that the increasing strength of thermal relaxation time constraint leads to depreciate the thermal transport in the flow. Gupta and Gupta [24] developed a model to study the momentum transport in the viscoelastic Oldroyd-B nanofluid flow accelerated by bidirectional stretching plate. They employed DTM-Pade technique to solve the developed model of flow. Thermal features in the flow of Carreau nanofluid by employing thermal conductivity are investigated by Lu *et al.* [25]. They noticed that the thermal conductivity constraint helps to accelerate the heat transport in the fluid flow. Alsabery *et al.* [26] concentrated to explore the heat transfer properties in the free and forced convection flow of fluid inside the cavity by utilizing entropy generation. They employed FEM numerical technique to analyze the flow and thermal properties for various involved parameters. Iqbal *et al.* [27] employed improved heat flux theory to examine the heat transfer rate in the Burgers fluid flow driven by a stretching surface. Khan *et al.* [28] proposed a heat transport model for the flow of Burgers fluid caused by stretching surface by considering hat rise/fall effects. They informed the higher thermal transport for improving scales of heat rise parameter. Recently, Upreti *et al.* [29] implemented a Joule heating effects to study the

thermal energy transport in the Darcy flow of viscous nanofluid consists of CNTs. They found that the thermal profile becomes stronger for higher extent of Eckert number. Furthermore, Iqbal *et al.* [30] investigated the momentum and thermal transport in the Burgers fluid flow caused by stretching surface. Javed *et al.* [31] numerically explored the flow of Eyring-Powell nanofluid influenced by bidirectional stretching surface. They employed numerical technique to explore the effects of physical constraints occurring in the momentum and energy equations and exposed that the growing strength of thermophoretic force constraint serve to reduce the rate of solutal transport in the flow.

The thermal transport and flow induced by stretching cylinder has propitious applications in industrial manufacturing and engineering advances. The flow of fluid induced by a stretching cylinder was primarily investigated by Crane [32]. The motion of time independent viscous fluid at rest outside the hollow stretching cylinder was studied by Wang [33]. The slip flow due to stretched cylinder was examined by Wang *et al.* [34]. They investigated that the slip strictly diminishes the velocity profile and shear stress measures. The characteristics of MHD nanofluid induced by a stretching cylinder were assessed by Ashorynejad *et al.* [35]. Moreover, Sheikholeslami *et al.* [36] analyzed heat and mass transfer characteristics on permeable stretching cylinder by considering the effects of nanoparticles and thermal radiation. They found that concentration of nanoparticles and solutal thickness of boundary layer boosted by increasing values of curvature parameter. The magneto Casson fluid flow by a stretching cylinder was inspected by Tamoor *et al.* [37]. Hashim *et al.* [38] investigated the heat and mass transfer mechanism of Williamson fluid induced by a stretching cylinder incorporated with thermal conductivity effects. Khan *et al.* [12] conducted the heat transport analysis in the flow of viscoelastic Burgers fluid generated by stretching cylinder by incorporating the impact of thermal

radiation. They found that the temperature curves significantly rise by intensifying the scale of radiation parameter. Moreover Iqbal *et al.* [39] deliberated an analysis on thermal energy transport in the flow of rate type fluid caused by stretching surface. A diminution in thermal curves is being detected in this study by escalating the extent of Prandtl number. A complete analysis on transfer of heat due to stretching cylinder in the flow of Maxwell fluid is carried out by Khan *et al.* [40].

Thermal analysis by the addition of heat rise/fall and Joule heating effects in the moving fluids is of great significance and has many physical applications in industries and engineering like, it takes place during chemical reaction and the situations regarding dissociating of fluids. The thermal distribution of the fluid may be changed due to the occurrence of heat rise or fall phenomenon in the system which results in the deposition of particle rate in procedure like, semiconductor wafers, nuclear reactors as well as in electronic chips. Many researchers utilized this effect on different types of fluid flows to investigate the thermal features of the flow and some of them are discussed here. Pal and Mondal [41] investigated the hydromagnetic boundary layer flow by considering the combined effects of variable viscosity and the non-uniform heat source sink. They found that the flow distribution of fluid depressed for larger magnitude of magnetic number. Sivaraaj and Kumar [42] employed the non-uniform heat source/sink effects to study the reactive non-Newtonian Walter-B fluid flow past a moving cone and a flat porous surface. They reported an elevation in the thermal curves of the viscoelastic fluid for intensifying ranges of heat source parameter. Mythili and Sivaraaj [43] utilized the non-uniform heat rise/fall effects to examine the thermal transport in the flow of Casson fluid past a cone. Crank-Nicolson type finite element numerical scheme is being adopted by them to tackle the governing equations of the problem. Durairaj *et al.* [44] inspected the non-Darcy flow of Casson fluid by employing the

effect of heat generation/absorption. They concluded that the heat is elevated in the system by higher effects of heat rise parameter. Hayat *et al.* [45] incorporated the non-uniform heat generation/absorption effects in the mixed convective flow of viscoelastic fluid due to stretching cylinder. They detected that the higher thermal Biot number promotes the heat transfer rate. Hayat *et al.* [46] considered the effects of Joule heating and non-uniform heat source sink to examine the thermal characteristics in the flow of magnetized non-Newtonian fluid caused by slandering geometry. Irfan *et al.* [47] analysed the Oldroyd-B nanofluid flow caused by stretching cylinder by enforcing the effect of non-uniform heat source sink. Additionally, Ijaz *et al.* [48] employed Joule heating effect to study the Casson nanofluid by using improved heat and mass fluxes theory. They employed shooting numerical technique to deal the nonlinear models. Ghadikolaie *et al.* [49] explored the effect of Joule heating in radiative flow of magneto Eyring-Powell fluid. They found that the temperature curves of nanofluid elevate by an increment in the Eckert number magnitude. Recently, Khashi'e *et al.* [50] explored the thermal features in the flow of hybrid nanofluid by considering the impact of Joule heating.

The mechanism of the transfer of heat is an amazing process which occurs in the universe. This process occurs due to difference of temperature in two surfaces of the body. Which means that the thermal state of two surfaces or objects is not same. This is important to note that, this process stops when both the surfaces adopt the equilibrium in temperature. To understand this mechanism first of all, Fourier [51] done a great job and he established a basic law of heat conduction. Many studies have been performed based on Fourier's law of thermal conduction since past few decades. The mathematical form of Fourier's law confesses the parabolic type differential equation which reveals that the entire system is instantaneously affected due to initially disturbance in the system. With the passage of time, Cattaneo [52]

came to know that the entire system requires time to change its thermal state after producing an initially disturbance in temperature of the system. Hence, he introduced the thermal relaxation time to amend the Fourier's law. The thermal relaxation time is the time which a body requires to transform the heat from one surface to another. The Cattaneo's expression was regardless of material invariant model and depicts the hyperbolic partial differential equation. Later on, to overcome this issue Christov [53] done a great job and improved the Cattaneo's expression by introducing the Oldroyd upper-convected derivative. Hence, a modified theory named as Cattaneo-Christov theory matured in 2009 which was utilized by several scientists and researchers to perform their analysis. At first, Cattaneo-Christov heat flux model was employed by Straughan [54] to investigate the characteristics of temperature in the flow of an incompressible fluid. Additionally, the uniqueness and stability of Cattaneo-Christov heat flux model was obtained by Ciarletta and Straughan [55]. Haddad [56] examined the thermal instability in porous media by utilizing Cattaneo-Christov heat flux model. The uniqueness of this model was further studied by Tribullo and Zampoli [57]. Moreover, the features of temperature distribution in combination with Cattaneo-Christov heat flux model were examined by Han *et al.* [58]. The thermal aspects of an incompressible fluid were studied by Hayat *et al.* [59] by incorporating Cattaneo-Christov heat flux model. They exposed that the temperature profile of Jeffrey liquid depreciates for varying magnitude of thermal relaxation time. The phenomenon of heat transport was further inspected by Waqas *et al.* [60] by using Cattaneo-Christov heat flux model in the flow of generalized Burgers liquid. They also scrutinized that the temperature of Burgers liquid diminishes for greater values of thermal relaxation time parameter. Furthermore, the numerical investigation of Sisko fluid flow was carried out by Malik *et al.* [61] by employing the Cattaneo-Christov heat flux model. Khan *et al.* [62] employed the

Cattaneo-Christov heat flux model to examine the flow features of Sisko fluid. In near past, the mechanism of heat transfer in differential type flow of fluids by utilizing modified Fourier's law is numerically studied by Irfan *et al.* [63]. Recently, Alamri *et al.* [64] employed Cattaneo-Christov heat flux model to examine the solutal transport in the flow of magnetized second grade fluid. They explored that the thermal profile of magnetized liquid becomes thinner for varying effects of Prandtl number. Additionally, Iqbal *et al.* [65] utilized the Cattaneo-Christov heat and mass flux theory to investigate the flow of magnetized Burgers nanofluid caused due to a stretching surface near a stagnation point. They perceived that the flow distribution diminishes for greater magnetic force parameter. Shafiq *et al.* [66] examined the micropolar flow of nanofluid by employing Cattaneo-Christov heat flux model and considering slip effects. They reported that the entropy generation profile falls off for varying magnitude of Bejan number.

Magnetohydrodynamic (MHD) is a topic of great interest in which we deal fluids conduction with the effects of magnetic field. There are several practical applications of MHD flows in physics, medical field, industries and in engineering. Attention in this field has been initiated since 1918, when first time an electromagnetic pump was designed by a scientist named Hartmann. After that, many researchers extended their investigations on MHD flows. Initially, Rossow [67] examined the magnetized fluid flow on a flat surface. Andersson [68] presented the exact solutions of viscoelastic fluid incorporating with magnetic field properties. Bhargava *et al.* [69] presented the numerical solutions of magnetized micropolar fluid flow between two parallel surfaces. They concluded that the flow profile for Hartmann number is the decreasing function. Hence, flow profile diminishes for higher Hartmann number. Datti *et al.* [70] investigated the features of viscoelastic type fluid flow over stretching surfaces by considering

the effects of magnetic fields. They presented numerical and analytical solutions and made a comparison between them. They also found that the thermal profile of the fluid deteriorates for higher Prandtl number. Hayat *et al.* [71] investigated the viscoelastic fluid by imposing the magnetic field in normal direction of the flow. They employed the fractional calculus method to solve the governing equations and found that the temperature profile of generalized Burgers fluid boosts up by increasing the magnetic parameter. Sajid and Hayat [72] presented the analytic solutions of magnetized viscous fluid flow by shrinking surface by incorporating the effects of suction. They reported that the velocity of the fluid enhances by increasing the suction parameter. Nadeem and Akram [73] studied the magnetized flow of hyperbolic tangent fluid in a channel. Munawar *et al.* [74] examined the heat transport in the oscillatory flow of magnetized viscous fluid. They employed finite difference methodology to tackle the governing partial differential equations. Mukhopadhyay [75] investigated the slip flow of magnetized viscous fluid induced due to stretching cylinder. He determined that the flow velocity of fluid diminishes for larger rate of velocity slip parameter. Afterwards, Rajesh *et al.* [76] explored the effects of viscous dissipation in the flow of magnetized nanofluid induced due to a suddenly moving porous plate. They employed “Tiwari-Das model” to study the features of nanofluid. Moreover, they deployed Galerkin finite element scheme to explore the effects of pertinent physical parameters. Akbar *et al.* [77] investigated the thermal transport phenomenon in flow of nanofluid due to an elastic surface. They performed numerical integration to solve the governing model. Moreover, Shukla *et al.* [78] utilized entropy generation to investigate the thermal features of magnetized nanofluid flow caused by stretching cylinder. Elevation in the thermal curves of nanofluid is being detected by them for escalating scales of magnetic constraint. Suleman *et al.* [79] developed the model to study the energy transfer in the flow of viscous nanofluid

influenced by nonlinear stretching surface and considered the magnetic field effects. Khan *et al.* [80] explored the magnetized convective flow of nanofluid in a rotating surface by considering entropy generation. They concluded that the escalating effects of magnetic field lead to ascend the entropy generation. Vo *et al.* [81] implemented the MHD effects to analyze the thermal energy conversion within the porous cavity. Nguyen *et al.* [82] studied the entropy generation solidification by implementing the magnetic effects on it. They reported that the solidification expedites for larger effects of Hartmann number. Recently, Nadeem *et al.* [83] explored the magnetic field effects on the stagnation point oscillatory flow of nanofluid caused due to stretching/shrinking surface. Recently Khan *et al.* [84] explored the magneto Burgers nanofluid flow over a stretching cylinder by considering the effects of stagnation point and thermal radiations. They concluded that the Burgers fluid flow profile diminishes by increasing the magnetic field magnitude. Moreover, Awais *et al.* [85] investigated the magnetized Maxwell nanofluid flow over a disk by incorporating the impacts of Joule heating and they reported that the thermal profile of nanofluid builds up by intensifying the impacts of Eckert number. Nanofluids are also of great importance in since a decade. Many researchers explored the nanofluid properties in their studies.

The combination of very small sized particles with base fluid form new class of fluids termed as nanofluid. Usually nanoparticles are composed by oxides, carbides, carbon nanotubes and metals. The thermophysical features of nanofluid are slightly distinct than their respective base fluids. Nanofluids have several domestic and industrial utilizations like heating of solar water, cooling of engines, electronics cooling, cooling of transformer oil, cooling of refrigerators and freezers etc. Due to such applications, different researchers paid their attention towards this field and explored the characteristics of nanofluids. Initially, Choi [86, 87] explored the thermo-

physical features of nanofluids experimentally. Actually, he included nano sized components in base fluid to examine the characteristics of nanofluids. He exposed that the nanofluids are much efficient as compared to base fluids. He also reported that particularly the thermal conductivity of nanofluid is much better than the base fluid. Subsequently, many researchers have made their contributions in this field after this fruitful experiment. Kang *et al.* [88] and Yoo *et al.* [89] studied the thermal conductivity of nanofluid experimentally. They considered base fluids (glycol, water etc.) incorporated with nanoparticles (copper, iron etc.) in their investigations. They determined that the nanofluids have much higher thermal conductivity than their relative base fluids. Analysis of squeezing flow of nanofluid between two parallel surfaces was done by Ganji *et al.* [90]. Investigation of natural convection of different non-Newtonian nanofluid flow along two vertical plates was done by Hatami and Ganji [91]. Malik *et al.* [92] scrutinized the flow of magneto Eyring-Powell nanofluid over a stretching cylinder. Seiyed *et al.* [93] analyzed nanoparticles effect on peristaltic fluid flow in systems of drug delivery. Additionally, Ellahi *et al.* [94] discussed the mixed convection flow of nanofluids on a wedge incorporated with entropy generation. They disclosed that the flow distribution of the nanofluid deteriorates for larger values of particle concentration. Akbar *et al.* [95] explored the magnetic effects in peristalsis motion of nanofluid. Irfan *et al.* [96] inspected the flow of 3D Carreau nanofluid incorporated with the influences of thermal conductivity over a stretched surface. They informed that the thermal and solutal profiles of the Carreau nanofluid boost up by increasing thermophoresis parameter. Characteristics of Lorentz forces on flow of nanofluid generated by movable parallel plates are examined by Hosseinzadeh *et al.* [97]. They adopted CM and FEM to investigate the flow phenomenon of nanofluid. Moreover, theoretical investigation of thermal boundary layer flow of nanofluid over a porous cylinder was done by Nourazar *et al.* [98]. They utilized

(OCM) and numerical method to examine the flow characteristics. Hsiao [99, 100] investigated the flows of micropolar and Carreau nanofluids over different geometries. A numerical analysis on natural convection heat transfer of Fe_3O_4 -water nanofluid in a half-annulus cavity by considering the variable magnetic field effect have been carried out by Hatami *et al.* [101]. Hashim *et al.* [102] investigated the impacts of Williamson nanofluid flow on a wedge geometry with convective boundary conditions. They reported that the heat transfer rate is boosted up by intensifying the Brownian motion and thermophoresis effects. Nasir *et al.* [103] discussed the flow of carbon nanotubes on a stretching surface by considering the effect of non linear radiation. Aamir *et al.* [104] exposed the impacts of non-linear radiation against Williamson nanofluid flow generated by a moving wedge. Their finding reveals that the intensifying effects of temperature ratio parameter boosts up the thermal profile and the associated boundary layer thickness. Recently, Ahmad *et al.* [105] scrutinized the flow of nanofluid incorporated with the impacts of Cattaneo-Christov double diffusion theory on a stretching surface. They reported that the augmentation in thermophoresis parameter and Brownian motion constraint corresponds to rise in temperature distribution of the nano liquid. They also explored that the solutal profile of nano fluid boosts up by rising thermophoresis parameter. Moreover, Ellahi *et al.* [106] investigated the two phase nanofluid flow of hybrid fluid by considering the slip effects. They explored that the higher slip parameter corresponds to diminishes the flow profile of nanofluid. Some other studies on nanofluids can be found in *Refs.* [107 – 109].

In the era of fluid mechanics, the investigation of the stagnation-point flow has great importance and real-world applications in industry like flows detected over the tip of jets and submarines and the spinning and blowing of fiber glass etc. Due to such practical applications researchers gained much attention in stagnation point flows and investigated such types

of flows theoretically. Initially, 2D stagnation point flow and its exact solutions were studied by Hiemenz [110]. Later on, Homann [111] introduced axisymmetric stagnation-point flow while non axisymmetric stagnation point flow was investigated by Howarth [112]. Subsequently numerous researchers made their contributions in investigation of flows concerning stagnation point phenomenon, like Chiam [113], Mahapatra and Gupta [114, 115], Nazar *et al.* [116], Reza and Gupta [117], Lok *et al.* [118, 119], etc. Problems of boundary layer flows past a stretching sheet are encountered in these studies. In 1994, Chiam revealed that flow profile closer to stretching surface and far away to the surface show similar behavior while Mahapatra and Gupta reported in contrast to this. Additionally, Farooq *et al.* [120] studied the stagnation point flow of viscoelastic fluid incorporated with radiation effects over a stretching surface. They assessed that the velocity and the amount of heat transport of the viscoelastic nano liquid enhance for increasing values of velocity ratio parameter. Hsiao [121] examined the free and forced convective stagnation point flow of nanofluid over a stretching surface with slip conditions. He reported that the temperature profile of nanofluid enhances for escalating values of stagnation parameter. After that Ghadikolaei *et al.* [122] discussed the flow near a stagnation point of hybrid nanofluid over a stretching surface. They reported that the thermal profile of hybrid nanofluid diminishes for improving values of velocity ratio parameter. Additionally, Hsiao [123] examined the flow of Maxwell fluid near a stagnation point by incorporating radiation effects. He informed that the transfer of heat increases for larger values of Prandtl number. Likewise, Abbas *et al.* [124] explored the micropolar fluid flow near a stagnation point past a circular cylinder. They came to know that maximum amount of heat transfer and the shear stresses at the wall are also maximum for copper–water nanofluid related to the alumina–water and titania–water nanofluids. Recently, Khan *et al.* [125] addressed the stagnation point flow of

bioconvection nanoliquid with quartic chemical reaction towards a nonlinear stretching surface. They noted that flow velocity increases by rising velocity ratio parameter while thermal profile shows opposite trend.

Recently, scientists and engineers are concerned to encounter the problems regarding flows of fluids incorporated with chemical reactions. Chemical reactions could be homogeneous or heterogeneous. If a reaction arises within the entire domain that reaction termed as homogeneous reaction while, the reaction which reacts inside of some specific region or within the boundary of the region that could be heterogeneous reaction. Homogeneous heterogeneous reactions are also taking part in different chemically reactive systems. Here it is important to note that, some reactions grow on very low speed and some of them does not progress at all, without the existence of a catalyst. A variety of chemical reactions exists, most of them have significant uses in industries and in chemical engineering systems. Particularly, chemical reactions have substantial effects in production of polymers, food dispensation, ceramics manufacturing, hydrometallurgical industry, chemically equipment designs and crops damage through freezing and groves of different trees. Many investigators utilized homogeneous heterogeneous reactions in their studies to investigate different type of flow phenomena. Initially, Chaudhary and Markin [126] presented a simple model by employing homogeneous heterogeneous reactions in flow of a viscous fluid near a stagnation point. Additionally, Markin [127] numerically explored the boundary layer flow by utilizing homogeneous heterogeneous reactions. Hayat *et al.* [128] employed homogeneous heterogeneous reactions along with Cattaneo-Christov heat flux model on flow of Maxwell fluid to examine the thermal features of the viscoelastic fluid. They scrutinized that the thermal profile of non-Newtonian fluid deteriorates for larger thermal relaxation time parameter. Later on, Xu [129] presented a model to examine the thermal aspects of fluid

flow near a stagnation point by incorporating the effects of homogeneous heterogeneous reactions. Hayat *et al.* [130] incorporated homogeneous heterogeneous reactions and demonstrated a model to study the convective heat transport in the flow of nanofluid due to rotating 3D surface. They indicated that the rate of heat transport at the boundary improved by intensifying the effects of nano particles volume fraction. Hayat *et al.* [131] established a three-dimensional flow model of nanofluid by utilizing the impacts of homogeneous heterogeneous reactions. They reported that the solutal rate rises for growing values of Schmidt number. Numerical simulation of Maxwell fluid flow due to spiraling surface is recently carried out by Ahmed *et al.* [132]. They analyzed that the concentration rate diminishes for larger homogeneous heterogenous reactions parameter. Khan *et al.* [133] presented a modified thermal conduction model by employing homogeneous heterogenous reactions in swirling flow of Maxwell fluid. They also discussed that the nano particles volume fraction distribution weakens for homogeneous heterogenous reactions parameter.

1.1 Fundamental Laws of Continuum Mechanics

The conservation laws of classical mechanics provide base to the fluid dynamics. The basic conservation laws comprise mass conservation law, momentum conservation law and energy conservation law. They are specified by employing Reynolds transport theorem. It is worth mentioning that the conservation laws are applicable to a specific region of the flow and this region is particularly termed as control volume (CV). The integral or differential forms of conservation laws are stated below.

1.1.1 The Conservation of Mass (Continuity Equation)

According to this law, mass in the control volume (CV) remains conserved for the fluids with constant density. It means that, the entire mass which enters the CV must be equivalent to the entire mass which leaves the CV and the mass accumulating in the CV. Mathematically, the conservation of any thing is generally expressed by the equation given below

$$\frac{\partial \Psi}{\partial t} + \nabla \cdot (F + \Psi \mathbf{V}) - R_1 = 0. \quad (1.1)$$

In continuum mechanics, all the physical conservation laws are represented by this equation. In case, $F = 0$, $\Psi = \rho_f$ and with no source/sink i.e. $R_1 = 0$. The above equation (1.1) admits the subsequent form represents the equation of continuity which demarcates the conservation of mass, mathematically as:

$$\frac{\partial \rho_f}{\partial t} + \nabla \cdot (\rho_f \mathbf{V}) = 0, \quad (1.2)$$

where ρ_f is the fluid density, \mathbf{V} the liquid velocity and t the time.

The steady and incompressible flow version admits the following form

$$\nabla \cdot \mathbf{V} = 0. \quad (1.3)$$

1.1.2 The Conservation of Momentum

Newton's second law demarcates the conservation of momentum which narrates that in a control volume the time rate of change of momentum is equal to the resultant of the external forces acting on volume. According to Newton's second law, which narrates that time rate of increase

of momentum of a control volume equals the resultant force acting on it. It can be expressed in mathematical form as

$$\int_{\zeta(t)} \left[\frac{\partial(\rho \mathbf{V}_\alpha)}{\partial t} + (\rho \mathbf{V}_\alpha \mathbf{V}_\beta)_{,\beta} \right] d\zeta = \int_{\zeta(t)} [\rho \mathbf{B} + \boldsymbol{\tau}_{\alpha\beta,\beta}] d\zeta. \quad (1.4)$$

On simplification, we get

$$\frac{\partial(\rho \mathbf{V}_\alpha)}{\partial t} + (\rho \mathbf{V}_\alpha \mathbf{V}_\beta)_{,\beta} = \rho \mathbf{B} + \boldsymbol{\tau}_{\alpha\beta,\beta}. \quad (1.5)$$

where \mathbf{B} is the body forces per unit volume and $\boldsymbol{\tau}_{\alpha\beta}$ the stress tensor.

In a more appropriate form the conservation of momentum admits the following form

$$\rho \left[\frac{\partial \mathbf{V}}{\partial t} + (\mathbf{V} \cdot \boldsymbol{\nabla}) \mathbf{V} \right] = \text{div } \boldsymbol{\tau} + \rho \mathbf{B}. \quad (1.6)$$

1.1.3 The Conservation of Energy

The first law of thermodynamics demarcates the conservation of energy which mathematically states that

$$\rho c_p \frac{dT}{dt} = \boldsymbol{\tau} \cdot \mathbf{L} - \text{div } \mathbf{q}, \quad (1.7)$$

where c_p represents the specific heat of the liquid, T the liquid temperature and \mathbf{L} be the velocity gradient. Moreover, in Eq. (1.7), $\boldsymbol{\tau} \cdot \mathbf{L}$ is the viscous dissipation term, $(\text{div } \mathbf{q}$ and $\text{div } \mathbf{q}_r)$ signifies the thermal and radiative fluxes, respectively, while the term on the left hand side of Eq. (1.7) represents the internal energy.

The thermal flux \mathbf{q} is given by the relation

$$\mathbf{q} = -k\nabla T, \quad (1.8)$$

with k denotes the thermal conductivity of the liquid.

By making use of Eq. (1.8) in Eq. (1.7) and in the absence of viscous dissipation we obtain the energy equation as:

$$\rho c_p \frac{dT}{dt} = k\nabla^2 T. \quad (1.9)$$

1.1.4 The Conservation of Concentration

This law narrates that, in a control volume (CV) the growth in the total mass of species must be remains balanced to the total amount of mass flow in CV plus the rate of increase of species in CV. In other words, it means that the net concentration of the system under perception must be constant. By employing Fick's second law in the presence of chemical reaction, it takes the form as

$$\frac{\partial \phi}{\partial t} + \mathbf{V} \cdot \nabla \phi = -\nabla \cdot \mathbf{j} + R_1, \quad (1.10)$$

where ϕ represents the fluid concentration, \mathbf{j} the normal mass flux and R_1 source/sink for ϕ .

The normal mass flux is given by Fick's first law as

$$\mathbf{j} = -D\nabla \phi, \quad (1.11)$$

where D is the mass diffusivity.

By utilizing Eq. (1.11) in Eq. (1.10) and by substituting $R_1 = 0$ we arrived at

$$\frac{\partial \phi}{\partial t} + \mathbf{V} \cdot \nabla \phi = D \nabla^2 \phi. \quad (1.12)$$

1.1.5 The Energy Conservation for Nanofluid

The energy conservation law in view of an incompressible nanofluid is stated as

$$\rho c_p \frac{dT}{dt} = -h_p \nabla \cdot \mathbf{j}_p - \text{div } \mathbf{q}_p, \quad (1.13)$$

where \mathbf{q}_p , \mathbf{j}_p and h_p symbolize the nanofluid thermal flux, nanofluid mass flux and specific enthalpy of nanofluids, respectively.

Also, \mathbf{q}_p and \mathbf{j}_p admit the following relations, respectively.

$$\mathbf{q}_p = -k \nabla T + h_p \mathbf{j}_p, \quad (1.14)$$

$$\mathbf{j}_p = -\rho_p D_B \nabla \phi - \rho_p D_T \frac{\nabla T}{T_\infty}. \quad (1.15)$$

Here, ρ_p signifies the nanofluid density, D_B the Brownian motion and D_T the thermophoresis diffusion coefficients.

In view of Eqs. (1.14) and (1.15), Eq. (1.13) yields the subsequent form

$$\rho c_p \frac{dT}{dt} = k \nabla^2 T + \rho_p c_p D_B \left[D_T \frac{\nabla T \cdot \nabla T}{D_B T_\infty} + \nabla \phi \cdot \nabla T \right]. \quad (1.16)$$

1.1.6 The Concentration Conservation for Nanofluid

The concentration conservation law for nanofluid admits the following form

$$\frac{\partial \phi}{\partial t} + \mathbf{V} \cdot \nabla \phi = -\frac{1}{\rho_p} \nabla \cdot \mathbf{j}_p. \quad (1.17)$$

By substituting Eq. (1.15) into Eq. (1.17) yields the subsequent form

$$\frac{\partial \phi}{\partial t} + \mathbf{V} \cdot \nabla \phi = D_B \nabla^2 \phi + D_T \frac{\nabla^2 T}{T_\infty}. \quad (1.18)$$

1.2 The Rate Type Burgers Fluid Model

Because of the diverse characteristics several kinds of non-Newtonian models have been established. Amongst all, the rate type models gained special consideration. Specially, Burgers fluid model is considered as the comprehensive viscoelastic rate type fluid model which is broadly developed and delineates the complete features of several non-Newtonian fluids. Burgers fluid model explains the relaxation and retardation times properties of fluid. Burgers fluid model has tendency to explain the viscous and elastic responses of fluid and to setup the stress relaxation of several polymeric liquids. Other rate type models such as, Maxwell fluid model and Oldroyd-B fluid model are the sub classes of Burgers fluid model. The constitutive equation for rate type models is given in the following relation

$$\boldsymbol{\tau} + p\mathbf{I} - \mathbf{S} = 0, \quad (1.19)$$

where $\boldsymbol{\tau}$ elucidates the Cauchy stress tensor, p the fluid pressure, \mathbf{I} the identity tensor and

\mathbf{S} the Burgers fluid extra stress tensor defined by

$$\left(1 + \lambda_1 \frac{D}{Dt} + \lambda_2 \frac{D^2}{Dt^2}\right) \mathbf{S} = \mu \left(1 + \lambda_3 \frac{D}{Dt}\right) \mathbf{A}_1, \quad (1.20)$$

where λ_1 is the fluid relaxation time, λ_2 the material parameter of Burgers fluid, μ the dynamic viscosity, λ_3 the fluid retardation time, $\mathbf{A}_1 = \nabla \mathbf{V} + (\nabla \mathbf{V})^t$ is the Rivlin-Ericksen tensor and $\frac{D}{Dt}$ the upper convected derivative defined as follows

$$\frac{D\mathbf{S}}{Dt} = \frac{\partial \mathbf{S}}{\partial t} + (\mathbf{V} \cdot \nabla) \mathbf{S} - (\nabla \mathbf{V})^t \cdot \mathbf{S} - \mathbf{S} \cdot (\nabla \mathbf{V}). \quad (1.21)$$

1.3 Solution Methodologies

1.3.1 BVP Midrich Scheme (Midpoint Collocation Method)

In order to find the numerical solution of two-point boundary value problem the efficient numerical techniques like midrich, middefer, traprich and trapdefer can be employed by utilizing Maple software. The midrich and middefer techniques are based on midpoint collocation method while the trapdefer and traprich techniques are depends upon on trapzoid methods in which the Richardson extrapolation or deferred correction enhancement is utilized. We utilized the Maple software for the numerical simulation of the boundary value problems. The complete solution methodology of Midrich technique base on modified Euler method or explicit midpoint method is described by the following general algorithm

$$Z^{*'}(t^*) = F(t^*, Z^*(t^*)), \quad Z^*(t_0^*) = Z_0^*, \quad (1.22)$$

The modified Euler's method relation is given by

$$Z_{n+1}^* = Z_n^* + h^* F \left(t_n^* + \frac{h^*}{2}, Z_n^* + \frac{h^*}{2} F(t_n^*, Z_n^*) \right), \quad (1.23)$$

where h^* is considered as the step size and $t_n^* = t_0^* + nh^*$. The implicit strategy of the mid-point method is stated as

$$Z_{n+1}^* = Z_n^* + h^* F \left(t_n^* + \frac{h^*}{2}, Z_n^* + \frac{1}{2}(Z_n^*, Z_{n+1}^*) \right), \quad n = 0, 1, 2, 3... \quad (1.24)$$

Here it is worth mentioning that the order of the local error of mid-point method is $O(h^3)$ while, that of global error is $O(h^2)$. Also, it is important to note that, the reduction of the error in mid-point formula implies the more stable solution. Moreover, the reduction in the step size ($h^* \rightarrow 0$) leads to rapid decay in the error of mid-point formula.

1.3.2 Homotopy Analysis Method (HAM)

Here we are presenting the solution methodology of HAM to gain the analytic series solution of our problem. We need linear operators and initial guesses to start the process. so that we choose $(\mathcal{L}_f, \mathcal{L}_\theta, \mathcal{L}_\phi)$ as linear operators and (f_0, θ_0, ϕ_0) as the initial guesses which are defined as follows

$$f_0(\eta) = 1 - e^{-\eta}, \quad \theta_0(\eta) = e^{-\eta}, \quad \phi_0(\eta) = e^{-\eta}, \quad (1.25)$$

$$\mathcal{L}_f[f(\eta)] = f''' - f', \quad \mathcal{L}_\theta[\theta(\eta)] = \theta'' - \theta, \quad \mathcal{L}_\phi[\phi(\eta)] = \phi'' - \phi, \quad (1.26)$$

with the properties mentioned below

$$\mathcal{L}_f[D_1^* + D_2^*e^\eta + D_3^*e^{-\eta}] = 0, \quad \mathcal{L}_\theta[D_4^*e^\eta + D_5^*e^{-\eta}] = 0, \quad \mathcal{L}_\phi[D_6^*e^\eta + D_7^*e^{-\eta}] = 0, \quad (1.27)$$

where D_i^* ($i = 1 - 7$) represent constants.

The zeroth order deformation problem is defined below

$$(1 - c) \mathcal{L}_f[\tilde{f}(\eta; c) - f_0(\eta)] = c\hbar_f \dot{N}_f[\tilde{f}(\eta; c)], \quad (1.28)$$

$$(1 - c) \mathcal{L}_\theta[\tilde{\theta}(\eta; c) - \theta_0(\eta)] = c\hbar_\theta \dot{N}_\theta[\tilde{f}(\eta; c), \tilde{\theta}(\eta; c), \tilde{\phi}(\eta; c)], \quad (1.29)$$

$$(1 - c) \mathcal{L}_\phi[\tilde{\phi}(\eta; c) - \phi_0(\eta)] = c\hbar_\phi \dot{N}_\phi[\tilde{f}(\eta; c), \tilde{\theta}(\eta; c), \tilde{\phi}(\eta; c)]. \quad (1.30)$$

1.4 Contribution in Thesis

This thesis is designed to explore the heat transfer properties in the flow of Burgers fluid generated by different stretching surfaces. The mathematical models are developed for the flow of Burgers fluid caused by unidirectional stretching sheet, bidirectional stretching sheet and stretching cylinder. Moreover, the improved $2D$ and $3D$ models of heat transport in nanofluids are also formulated by employing the modified Fourier's heat flux and certain other physical effects. The analytical as well as numerical solutions of the flow and energy transport equations are established. The work done in this thesis is published in reputed international journals which is clearly mentioned in this section. The contribution made in each chapter is mentioned below as:

Chapter 1: This chapter contains the literature survey related to contents of present work.

The physical importance of the different flows of non-Newtonian fluids, heat transfer and other physical effects are also depicted in this chapter. The solution methodologies we utilized in this thesis are deliberated.

Chapter 2: This chapter is devoted to investigate the thermal transform features in the stagnation point flow of magnetized Burgers nanofluid accelerated by stretching sheet. Moreover, uniform heat source/sink and Cattaneo-Christov double diffusion theory are employed to examine the thermal energy transport. The transport of solutal energy is also examined under the influence of chemical reaction and solutal relaxation time effects. The impacts of physical parameters arising in flow and energy transport equations are explored by adopting the homotopy analysis method. The contents of this chapter have been published in "**Appl. Nanosci.**, **10 (2020) 5331-5342**".

Chapter 3: In this chapter, the Burgers nanofluid flow due to bidirectional stretching surface is addressed. Mathematical modelling for the phenomenon of heat, mass and fluid flow is formulated in view of bidirectional stretching inspired by the combined effects of thermal and solutal relaxation time, chemical reaction and heat rise/fall. The governing equations are analytically examined by employing the homotopy analysis method. The results of this chapter are published in "**J. Proc. Mech. Eng., Part E, (2021), doi: 10.1177/0954408921999613**".

Chapter 4: This chapter focuses on the mathematical modelling of the magnetized Burgers fluid flow accelerated by stretching cylinder. Moreover, the heat and mass transport features in the flow due to stretching cylinder are also addressed under the influence of magnetic field and heat generation/absorption effect. The dimensionless similarity transformations are incorporated to transmute the partial differential equations into ordinary differential equations. Homotopy analysis method (HAM) is being considered for the solution of governing

ordinary differential equations. The impacts of physical parameters on flow and energy transport distributions are drafted in the form of graphs and discussed by reasonable arguments. The effort made in this chapter is published in "**J. Therm. Anal. Calorim., (2020), <https://doi.org/10.1007/s10973-020-10224-w>**".

Chapter 5: This chapter is the extension of the work made in chapter 4. In this chapter, the flow of Burgers nanofluid is discussed near a stagnation point. The Buorgiano's model is utilized for the study of Brownian motion and thermophoresis diffusion of nanoparticles. Furthermore, the non-linear thermal radiation in the form of Rosseland approximation is employed to investigate the behavior of thermal distribution of the Burgers nanofluid. The mass transport in the flow is also examined by utilizing chemical reaction effects. The solution methodology of homotopy analysis is employed for the scrutiny of physical parameters effects on flow and energy transport distributions. The contents of this chapter are published in "**Appl. Nanosci., 10 (2020) 5233-5246**".

Chapter 6: Here, an improved thermal conduction model is presented for stretching cylinder case to study the heat transport in Burgers nanofluid flow by employing modified Fourier's heat flux in accordance with Bourgiano's model for nanofluid. Moreover, the impacts of Joule heating and heat source/sink are also incorporated in thermal conduction model to investigate the heat transform features in the flow. The optimal homotopy analysis method (OHAM) is employed to investigate the behavior of flow and thermal distributions for several physical parameters. The impacts of different parameters are depicted through graphs and discussed physically. The contents of this chapter are published in "**Eur. Phys. J. Appl. Phys., 92 (2020) 31101**".

Chapter 7: The main concern of this chapter is to present the numerical solutions of the

flow and energy transport equations. We analyzed the convective heat and mass transport at the surface of the cylinder by utilizing Joule heating and non-uniform heat source sink effects with convective boundary conditions. Furthermore, the prescribed surface temperature (PST) is also considered rather than constant wall temperature (CWT) in this chapter. The BVP midrich numerical technique in Maple software is being utilized to numerically investigate the contained parameters effects on flow, thermal and solutal distributions. The work furnished in this chapter is published in "**Phys. Scr., 96 (2021) 015211**".

Chapter 8: This chapter numerically explores the thermal energy transport in the flow of magnetized Burgers fluid caused by stretching cylinder under the influence of thermal relaxation time and heat generation/absorption. The cardinal concern of this chapter is to explore the solutal energy transport by employing the effects of homogeneous-heterogeneous reactions. BVP midrich numerical scheme based on mid point collocation method in Maple is adopted to explore the outcomes of physical parameters. The results are depicted in graphical form and discussed with physical explanations. The contents of this chapter are published in **J. Therm. Analy. Calorim., (2020), doi.org/10.1007/s10973-020-10308**"

Chapter 9: Finally the conclusions of this work are presented in this chapter and some extensions of this work are also mentioned as future work.

Chapter 2

Cattaneo-Christov double diffusion theory featuring the thermal transport in the flow of Burgers nanofluid due to stretching flat plate

In this chapter, the heat transport mechanism in the Burgers nanofluid flow above stretchable sheet is investigated under the influence of uniform transverse magnetic field. For the analysis of thermal and solutal energy distributions, we have employed the Cattaneo-Christov double diffusion theory instead of Classical Fourier's and Fick's laws. The Buongiorno model for movement of nanoparticles in Burgers liquid is first time utilized in the perspective of Cattaneo-Christov model. Suitable similarity transformations are employed to transform the governing partial differential equations into ordinary differential equations. Homotopic approach is being utilized to expose the effects of different physical parameters on the flow of Burgers nanofluid. The results pertained by homotopic analysis method are depicted in the form of graphs and discussed with reasonable judgments. The validity of the homotopic approach is shown by depicting comparison tables. Furthermore, it is analyzed that the thermal and solutal distributions of Burgers nanofluid are diminished by escalating the magnitude of thermal relaxation time

and solutal relaxation time parameters, respectively. Additionally, the enhancing trend of thermal and solutal distributions is being perceived for higher strength of thermophoretic force.

2.1 Mathematical Formulation

In this section a mathematical model is developed for a $2D$ stagnation point flow of Burgers nanofluid induced by stretching sheet. The flow phenomenon is modelled by imposing a uniform magnetic field of strength $B = [0, B_0, 0]$ in the direction normal to the flow (see Fig. 2.1). Moreover, the mechanisms of heat and mass transport in the flow are also modelled by employing modified heat and mass fluxes in combination with the Buongiorno model for the nanoparticles. Additionally, the effects of uniform heat source/sink and chemical reaction are also incorporated in the modelling of heat and mass transport respectively. The velocity components in x and y directions are taken as u and v respectively. Also it is assumed that the sheet is stretched along x -direction with velocity $u = \frac{U_0 x}{l}$, where l is the specific length and U_0 the reference velocity.

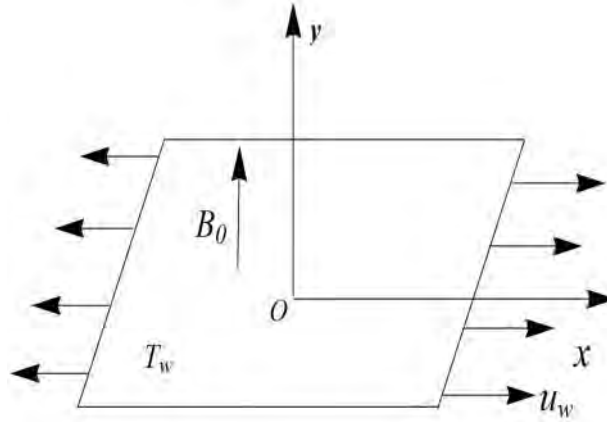


Fig. 2.1: Flow configuration and coordinates system.

The rheology of viscoelastic rate type fluid described by the Burgers model is given by following expression

$$\left(1 + \lambda_1 \frac{D}{Dt} + \lambda_2 \frac{D^2}{Dt^2}\right) \mathbf{S} = \mu \left(1 + \lambda_3 \frac{D}{Dt}\right) \mathbf{A}_1. \quad (2.1)$$

In the above mentioned equations, \mathbf{S} is the extra stress tensor, $\mathbf{A}_1 = (\nabla \mathbf{V}) + (\nabla \mathbf{V})^t$ the first Rivlin-Ericksen tensor, μ the dynamic viscosity of fluid and $\frac{D}{Dt}$ represents the upper convective derivative.

The basic continuity and momentum equations for flow analysis are as follows

$$\nabla \cdot \mathbf{V} = 0, \quad (2.2)$$

$$\rho_f \frac{d\mathbf{V}}{dt} = -\nabla p + \text{div } \mathbf{S} + \mathbf{J}_1 \times \mathbf{B}. \quad (2.3)$$

The conservation of energy law for current problem is

$$(\rho c_p) \frac{dT}{dt} - (\rho c_p) \left[D_B \nabla C \cdot \nabla T + \frac{D_T}{D_\infty} (\nabla T)^2 \right] = -\nabla \cdot \mathbf{q} + Q_0(T - T_\infty), \quad (2.4)$$

where \mathbf{q} is the heat flux satisfying the relation

$$\mathbf{q} + \lambda_t \left[\frac{\partial \mathbf{q}}{\partial t} + \mathbf{V} \cdot \nabla \mathbf{q} - \mathbf{q} \cdot \nabla \mathbf{V} + (\nabla \cdot \mathbf{V}) \mathbf{q} \right] = -k \nabla T. \quad (2.5)$$

The concentration equation for current situation is

$$\frac{dC}{dt} - \frac{D_T}{D_\infty} \nabla^2 T = -\nabla \cdot \mathbf{J} - k_c(C - C_\infty), \quad (2.6)$$

where \mathbf{J} is the mass flux satisfying the relation

$$\mathbf{J} + \lambda_c \left[\frac{\partial \mathbf{J}}{\partial t} + \mathbf{V} \cdot \nabla \mathbf{J} - \mathbf{J} \cdot \nabla \mathbf{V} + (\nabla \cdot \mathbf{V}) \mathbf{J} \right] = -D_B \nabla C. \quad (2.7)$$

Here λ_1 is the fluid relaxation time, λ_2 the material parameter of Burgers fluid, λ_3 ($\leq \lambda_1$) the fluid retardation time, λ_t the thermal relaxation time, λ_c the mass relaxation time, ν the kinematics viscosity, (T, C) the liquid temperature and concentration respectively, (T_∞, C_∞) the ambient temperature and concentration respectively, D_B the diffusion coefficient, \mathbf{J}_1 the current density, \mathbf{q} and \mathbf{J} are the heat and mass fluxes which are defined from Fourier's and Fick's laws, respectively.

By eliminating \mathbf{S} between Eqs. (2.1) and (2.3), \mathbf{q} between Eqs. (2.4) and (2.5) and \mathbf{J} between Eqs. (2.6) and (2.7) we obtained the following PDEs governing the flow

$$\frac{\partial u}{\partial x} + \frac{\partial v}{\partial y} = 0, \quad (2.8)$$

$$\begin{aligned} & u \frac{\partial u}{\partial x} + v \frac{\partial u}{\partial y} + \lambda_1 \left[u^2 \frac{\partial^2 u}{\partial x^2} + v^2 \frac{\partial^2 u}{\partial y^2} + 2uv \frac{\partial^2 u}{\partial x \partial y} \right] \\ & + \lambda_2 \left[\begin{aligned} & u^3 \frac{\partial^3 u}{\partial x^3} + v^3 \frac{\partial^3 u}{\partial y^3} + u^2 \left(\frac{\partial v}{\partial x} \frac{\partial^2 u}{\partial x \partial y} - \frac{\partial u}{\partial y} \frac{\partial^2 v}{\partial x^2} + \frac{\partial u}{\partial x} \frac{\partial^2 u}{\partial x^2} \right) \\ & + 3v^2 \left(\frac{\partial v}{\partial y} \frac{\partial^2 u}{\partial y^2} + \frac{\partial u}{\partial y} \frac{\partial^2 u}{\partial x \partial y} \right) + 3uv \left(u \frac{\partial^3 u}{\partial x^2 \partial y} + v \frac{\partial^3 u}{\partial x \partial y^2} \right) \\ & + 2uv \left(\frac{\partial v}{\partial y} \frac{\partial^2 u}{\partial x \partial y} + \frac{\partial v}{\partial x} \frac{\partial^2 u}{\partial y^2} + \frac{\partial u}{\partial y} \frac{\partial^2 u}{\partial x^2} - \frac{\partial u}{\partial y} \frac{\partial^2 v}{\partial x \partial y} \right) \end{aligned} \right] \\ & = \nu \lambda_3 \left[v \frac{\partial^3 u}{\partial y^3} + u \frac{\partial^3 u}{\partial x \partial y^2} - \frac{\partial u}{\partial x} \frac{\partial^2 u}{\partial y^2} - \frac{\partial u}{\partial y} \frac{\partial^2 v}{\partial y^2} \right] + \nu \left[\frac{\partial^2 u}{\partial y^2} \right] \\ & + \frac{dU_e}{dx} - \frac{\sigma B_0^2}{\rho} \left[\begin{aligned} & u - U_e + \lambda_1 v \frac{\partial u}{\partial y} + \\ & \lambda_2 \left(u \frac{\partial v}{\partial x} \frac{\partial u}{\partial y} - v \frac{\partial u}{\partial x} \frac{\partial u}{\partial y} + uv \frac{\partial^2 u}{\partial x \partial y} + u^2 \frac{\partial^2 u}{\partial y^2} \right) \end{aligned} \right], \quad (2.9) \end{aligned}$$

$$\begin{aligned}
\left(u \frac{\partial T}{\partial x} + v \frac{\partial T}{\partial y}\right) &= \alpha_1 \left(\frac{\partial^2 T}{\partial y^2}\right) + \frac{Q_0}{\rho c_p} (T - T_\infty) + \lambda_t \frac{Q_0}{\rho c_p} \left(v \frac{\partial T}{\partial y} + u \frac{\partial T}{\partial x}\right) \\
-\lambda_t \left[u^2 \frac{\partial^2 T}{\partial x^2} + v^2 \frac{\partial^2 T}{\partial y^2} + 2uv \frac{\partial^2 T}{\partial x \partial y} + \frac{\partial T}{\partial x} \left(u \frac{\partial u}{\partial x} + v \frac{\partial u}{\partial y}\right) + \frac{\partial T}{\partial y} \left(u \frac{\partial v}{\partial x} + v \frac{\partial v}{\partial y}\right) \right] \\
&+ \lambda_t \tau D_B \left[u \frac{\partial^2 C}{\partial x \partial y} \frac{\partial T}{\partial y} + u \frac{\partial C}{\partial y} \frac{\partial^2 T}{\partial x \partial y} + v \frac{\partial^2 C}{\partial y^2} \frac{\partial T}{\partial y} + v \frac{\partial C}{\partial y} \frac{\partial^2 T}{\partial y^2} \right] \\
&+ 2\lambda_t \tau \frac{D_T}{D_\infty} \left[u \frac{\partial T}{\partial y} \frac{\partial^2 T}{\partial x \partial y} + v \frac{\partial^2 T}{\partial y^2} \frac{\partial T}{\partial y} \right], \tag{2.10}
\end{aligned}$$

$$\begin{aligned}
u \frac{\partial C}{\partial x} + v \frac{\partial C}{\partial y} &= D_B \left(\frac{\partial^2 C}{\partial y^2}\right) - \frac{D_T}{T_\infty} \left[u \frac{\partial^3 T}{\partial x \partial y^2} + v \frac{\partial^3 T}{\partial y^3} + \frac{\partial^2 T}{\partial y^2} \right] \\
-\lambda_c \left[u^2 \frac{\partial^2 C}{\partial x^2} + v^2 \frac{\partial^2 C}{\partial y^2} + 2uv \frac{\partial^2 C}{\partial x \partial y} + \frac{\partial C}{\partial x} \left(u \frac{\partial u}{\partial x} + v \frac{\partial u}{\partial y}\right) + \frac{\partial C}{\partial y} \left(u \frac{\partial v}{\partial x} + v \frac{\partial v}{\partial y}\right) \right] \\
&- k_c (C - C_\infty) - \lambda_c k_c \left(v \frac{\partial C}{\partial y} + u \frac{\partial C}{\partial x}\right). \tag{2.11}
\end{aligned}$$

with boundary conditions

$$u = \frac{U_0 x}{l}, \quad v = 0, \quad T = T_w, \quad C = C_w \quad \text{at } y = 0, \tag{2.12}$$

$$v \rightarrow 0, \quad \frac{\partial v}{\partial y} \rightarrow 0, \quad T \rightarrow T_\infty, \quad C \rightarrow C_\infty \quad \text{as } y \rightarrow \infty. \tag{2.13}$$

Here $\alpha_1 = \left(\frac{k}{\rho c_p}\right)$ is the thermal diffusivity, in which ρ is the density and p the pressure of liquid, c_p the specific heat capacity at constant pressure, k the thermal conductivity of the liquid and (T_w, C_w) are the temperature and concentration at the surface of the sheet, respectively.

Presenting the following conversions

$$\begin{aligned}
u &= cx f'(\eta), \quad v = -\sqrt{c\nu} f(\eta), \quad \theta(\eta) = \frac{T - T_\infty}{T_w - T_\infty}, \\
\phi(\eta) &= \frac{C - C_\infty}{C_w - C_\infty}, \quad \eta = y \sqrt{\frac{c}{\nu}}. \tag{2.14}
\end{aligned}$$

By making use of the above mentioned conversions, Eq. (2.8) is satisfied automatically and Eqs. (2.9) – (2.11) yield

$$\begin{aligned}
& f''' + ff'' - (f')^2 + \beta_1 [2ff'f'' - f^2f'''] - \beta_2 [3f^2(f'')^2 + 2f(f')^2f'' - f^3f^{iv}] \\
& + \beta_3 [(f'')^2 - ff^{iv}] - M^2 [\beta_2ff''' - \beta_1ff'' + f'] + A^2 + M^2A = 0, \quad (2.15)
\end{aligned}$$

$$\begin{aligned}
& \theta'' + \text{Pr}(f\theta' + N_b\theta'\phi' + N_t(\theta')^2) + \delta\theta + \delta\beta_t f\theta' \\
& + \text{Pr}\beta_t[-ff'\theta' - f^2\theta'' - 2N_t f\theta'\theta'' - N_b f\theta'\phi'' - N_b f\theta''\phi'] = 0, \quad (2.16)
\end{aligned}$$

$$\begin{aligned}
& \phi'' + Le\text{Pr}f\phi' - k_1\phi - k_1\beta_c f\phi' \\
& + Le\text{Pr}\beta_c[-ff'\phi' - f^2\phi'' - \frac{N_t}{N_b}\theta'''f + \frac{N_t}{N_b}\theta''] = 0, \quad (2.17)
\end{aligned}$$

and transformed boundary conditions are follows

$$f = 0, f' = 1, \theta = 1, \phi = 1 \text{ at } \eta = 0, \quad (2.18)$$

$$f' \rightarrow A, f'' \rightarrow 0, \theta \rightarrow 0, \phi \rightarrow 0 \text{ as } \eta \rightarrow \infty, \quad (2.19)$$

where the Deborah numbers (β_1, β_3) Burgers fluid parameter (β_2) , Prandtl number (Pr) , Lewis number (Le) , magnetic parameter (M) , thermal relaxation parameter (β_t) , the mass relaxation parameter (β_c) , thermophoresis parameter (N_t) and Brownian motion parameter

(N_b) are defined as follows:

$$\begin{aligned}
\beta_1 &= \lambda_1 \frac{U_0}{l}, \quad \beta_2 = \lambda_2 \left(\frac{U_0}{l}\right)^2, \quad \beta_3 = \lambda_3 \frac{U_0}{l}, \quad \beta_t = \lambda_t \frac{U_0}{l}, \\
\beta_c &= \lambda_c \frac{U_0}{l}, \quad k_1 = \frac{k_c l}{U_0}, \quad \delta = \frac{l Q_0}{U_0 (\rho c)_f}, \quad \text{Pr} = \frac{\nu}{\alpha_1}, \quad Le = \frac{\alpha_1}{D_B}, \\
M &= \left(\frac{\sigma B_0^2}{\rho_f U_0}\right)^{1/2}, \quad N_t = \frac{\tau D_T (T_w - T_\infty)}{\nu T_\infty}, \quad N_b = \frac{\tau D_B (C_w - C_\infty)}{\nu}.
\end{aligned} \tag{2.20}$$

2.2 Analysis of Results

This segment of research is devoted to expose the noticeable features of several physical parameters. To disclose the characteristics of essential parameters, homotopy analysis method (HAM) is taken into account. Numerical solution of non linear ordinary differential equations (2.15 – 2.17) are developed by imposing boundary conditions written in Eqs. (2.18) and (2.19). We explored the features of all involved parameters, for instance, Burgers fluid parameter (β_2), retardation time parameter (β_3), magnetic parameter (M) on velocity $f'(\eta)$, thermal $\theta(\eta)$ and solutal $\phi(\eta)$ profiles. Moreover the characteristics of Brownian motion parameter (N_b), thermophoresis parameter (N_t), Prandtl number (Pr), and thermal relaxation parameter (β_t) on thermal distribution while the impacts of thermophoresis parameter (N_t), Brownian motion parameter (N_b), Lewis number (Le), chemical reaction parameter (k_1) and mass relaxation parameter (β_c) on solutal distribution are also exposed and depicted through *Figs. 2.2 – 2.10*. We have assigned fixed values for leading parameters such as $\alpha = 0.2$, $A = 0.5$, $\beta_1 = 0.7$, $\beta_2 = 0.25$, $\beta_3 = 0.5$, $M = 0.7$, $Pr = 5.0$, $\beta_t = 0.2$, $\beta_c = 0.15$, $Le = 4.0$, $N_b = 0.4$, $N_t = 0.6$ and $k_1 = 0.6$ during the entire computations except they are mentioned.

We discuss the impact of each parameter with complete logic as follows. To express the influence of Burgers fluid parameter (β_2) on flow, thermal and solutal distributions *Figs. 2.2(a–c)*

are portrayed. From these Figs., it is clear that the flow profile of Burgers liquid deteriorates while the thermal and solutal profiles enhance for higher magnitude of β_2 . Moreover, Figs. 2.3(a – c) are drafted to explore the impact of retardation time parameter (β_3) on velocity, thermal and concentration distributions. It is examined that the flow distribution and momentum boundary layer thickness of the Burgers liquid boost up for higher values of β_3 whereas, the thermal and concentration distributions depict converse trend to that of flow distribution. This behavior is according to the physical judgment. As β_3 is directly proportional to the retardation time (λ_3). Since retardation time increases by increasing β_3 . As it is physically examined that the retardation time is a specific time which is required to create the shear stress in the liquid. Hence, obviously higher retardation time corresponds to create more shear stress in the liquid and more shear stress in liquid boosts up the flow velocity. Additionally, it is also physically examined that when retardation time increases the fluid become more thinner due to which the resistance in the fluid decreases and consequently the temperature of the fluid declines in the system. Figs. 2.4(a, b) disclose the impacts of velocity ratio parameter (A) and magnetic force parameter (M) on flow profile of Burgers nanofluid. It is assessed that the velocity of the fluid diminishes for escalating values of M while it increases for varying values of A in both the cases ($A > 1$ and $A < 1$). The case ($A > 1$) corresponds to the situation when velocity of free stream is higher than the stretching velocity of the cylinder while the case ($A < 1$) is the situation when free stream velocity is inferior to the stretching velocity of the cylinder. Furthermore, the case ($A = 1$) is the case when both the velocities are equal in magnitude. Physically the results exposed in Fig. 2.4(a) are according to the reality as physically A is directly proportional to the free stream velocity and when we increase the values of A then free stream velocity enhances and consequently the flow velocity and momentum

boundary layer thickness of nano Burgers fluid boosts up. While, it is noted that boundary layer is not achieved at $A = 0$ because in this situation velocity of the fluid and the stretching velocity of the cylinder are equal. The results depicted in Fig. 2.4(b) reveal that fluid velocity deteriorates for intensifying magnetic force, it is due to the fact that intensification in magnetic field produces more drag force in fluid motion due to which the motion of the fluid slow down and consequently the velocity profile and velocity boundary layer thickness decay within the region of convergence. Figs. 2.5(a,b) are drafted to envision the features of Brownian motion parameter (N_b) on thermal and solutal distributions of nano Burgers fluid. It is clear from these graphs that temperature is an increasing while concentration is decreasing function of N_b . Physically, the mechanism behind this is that the kinetic energy of the fluid particles rises due to increase in the magnitude of Brownian motion constraint (N_b). Ultimately, the temperature of the fluid enhances due to increase in kinetic energy of the fluid molecules. Furthermore, diffusion of nanofluid particles is controlled by the Brownian motion. Hence, intensifying magnitude of Brownian motion constraint leads to decline the solutal profile of Burgers nanofluid. To enlighten the influence of thermophoresis parameter (N_t) on thermal and solutal profile of Burgers liquid Figs. 2.6(a,b) are portrayed. It is observed that the thermal and solutal profiles of Burgers liquid show enhancing trend for improving numbers of thermophoresis constraint. Also the thermal and solutal boundary conditions satisfied asymptotically within the region of convergence. Thermal and solutal boundary layer thickness of Burgers liquid improve for higher values of N_t . Actually, in process of thermophoresis the molecules from hotter region move towards colder region and this mechanism leads to increase the temperature of the system. Figs. 2.7(a,b) are inserted to disclose the impact of Prandtl number (Pr) and Lewis number (Le) on temperature and concentration distributions of nanofluid. From these graphs it is examined

that the thermal and solutal distributions decline for larger values of Pr and Le respectively. In fact, Prandtl number is inversely proportional to the thermal diffusivity of liquid which declines with an intensification in the values of Prandtl number. Finally, the decreasing thermal diffusivity of the liquid results in reduction of temperature profile of the nanofluid. Furthermore, Lewis number is inversely proportional to mass diffusivity and stronger Lewis number corresponds to weaker mass diffusivity which results in reduction of concentration distribution of Burgers nanofluid. To enlighten the influence of thermal relaxation time parameter (β_t) and concentration relaxation parameter (β_c) on temperature and solutal profiles Figs. 2.8(*a, b*) are inserted. It is assessed that both the thermal and solutal distributions of nanofluid diminish for augmented values of β_t and β_c respectively. Actually, the reason is that the heat conduction requires additional time by increasing the values of thermal relaxation time parameter and consequently the temperature of the fluid decreases. Similarly, further time is required to transfer the mass in fluid by increasing the magnitude of solutal relaxation time parameter. Hence, the concentration of Burgers nanofluid is decreasing function of the solutal relaxation time parameter. Figs. 2.9(*a, b*) are sketched to examine the features to the thermal distribution of Burgers nanofluid by employing the effect of heat generation/absorption. It is observed that the stimulus of temperature profile is enhanced for intensified magnitude of heat generation constraint ($\delta > 0$) while at the other hand it is diminished by increasing the heat absorption parameter ($\delta < 0$). It is obvious that because the source of heat adds more heat in the system and consequently temperature distribution enhances. In a similar manner, when heat is absorbed from the system then temperature of the fluid falloff. At the end of the analysis, the impact of chemical reaction parameter (k_1) at solutal distribution of the nano Burgers fluid is observed and variations are depicted in Figs. 2.10(*a, b*). It is analyzed that for positively in-

creasing values of chemical reaction parameter ($k_1 > 0$) the solutal profile of Burgers nanofluid shows decreasing trend while for negatively increasing values of chemical reaction parameter ($k_1 < 0$) the solutal distribution of nanofluid enhances. Physically, it is analyzed that when we increase the reaction rate in the liquid then more amount of mass utilizes in occurrence of chemical reaction and hence the solutal distribution of nanofluid diminishes. In a similar manner, when we decrease the chemical reaction rate in a fluid then we get extra amount of mass in the system and consequently the concentration distribution of the system enhances.

2.3 Validation of Homotopic Solutions

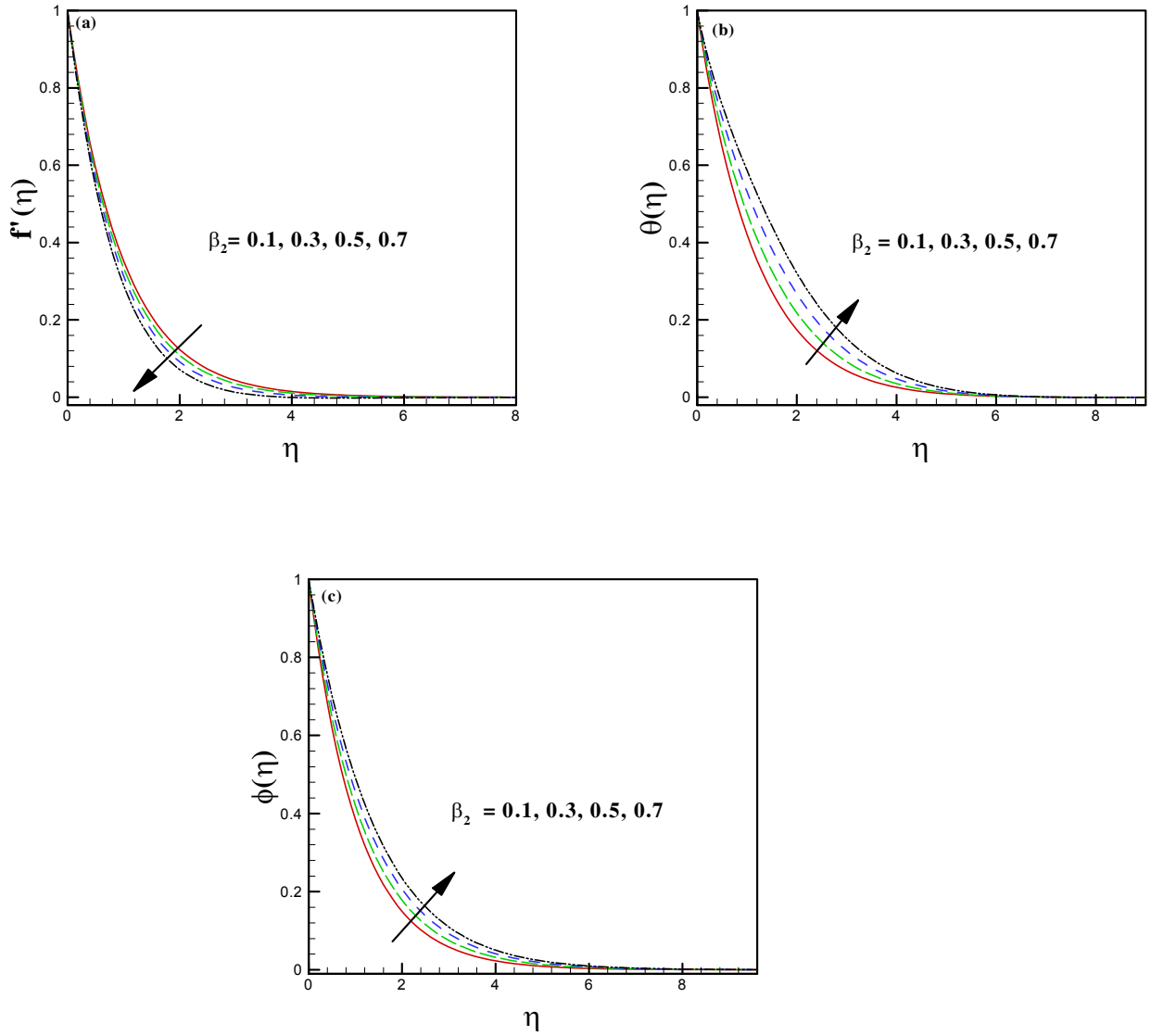
In this segment of the research the adopted homotopic approach is proved valid by computing the values of $-f''(0)$ and $-\theta'(0)$ for different values of β_1 and Pr respectively by fixing all other constraints. The obtained iterations are depicted in the form of table (2.1) and table (2.2). It is analyzed that the adopted approach is valid as the obtained values are found identical when compared with some previously investigated studies.

Table 2.1: A comparison table for $-f''(0)$ against different values of β_1 in limiting case when $\alpha = A = \beta_2 = \beta_3 = M = 0$.

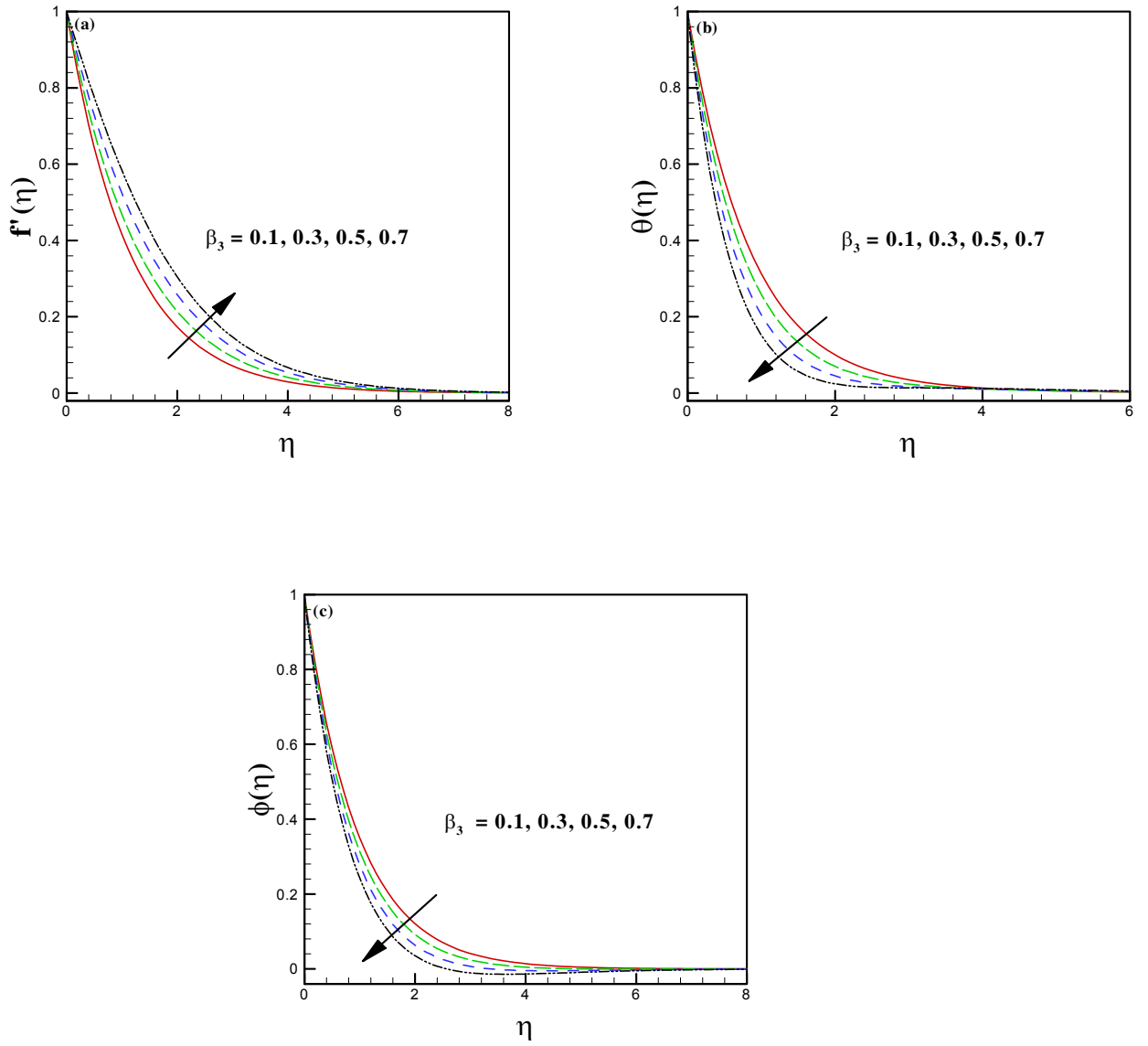
β_1	Mukhopadhyay <i>et al.</i> [134]	Hayat <i>et al.</i> [135]	Present study
0.0	0.9999963	1.000000	1.0000011
0.2	1.051949	1.051995	1.0519889
0.4	1.101851	1.10193	1.1019299
0.6	1.150162	1.150175	1.1501711
0.8	1.196693	1.197689	1.1966712

Table 2.2: A comparison table for $-\theta'(0)$ against different values of Pr in limiting case when $\alpha = A = \beta_1 = \beta_2 = \beta_3 = M = \beta_t = \beta_b = N_t = N_b = \delta = Le = k_1 = 0$.

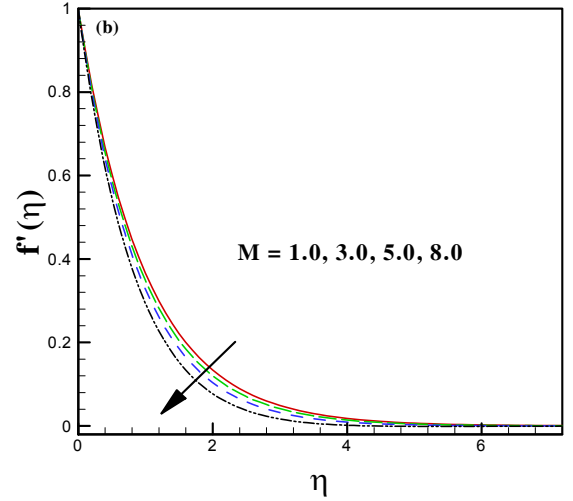
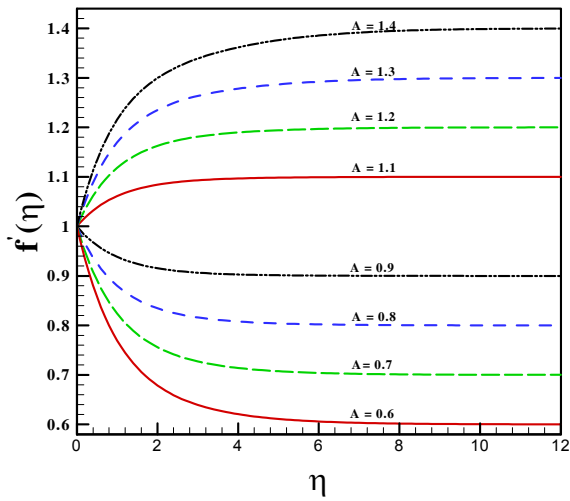
Pr	Wang [136]	Gorla and sidwai [137]	Present study
0.7	0.4539	0.4539	0.45312
2.0	0.9114	0.9114	0.90894
7.0	1.8954	1.8954	1.88986



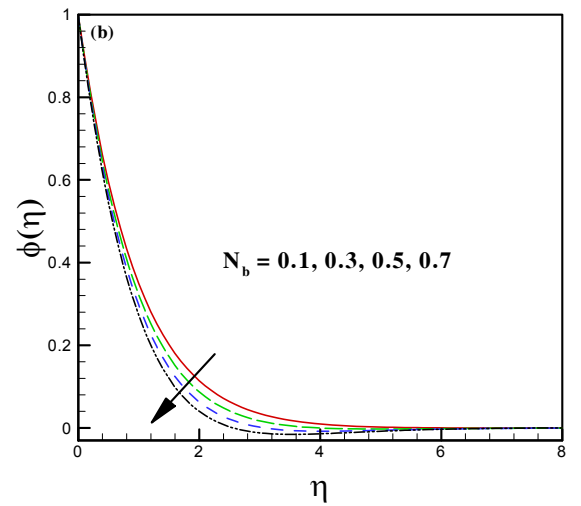
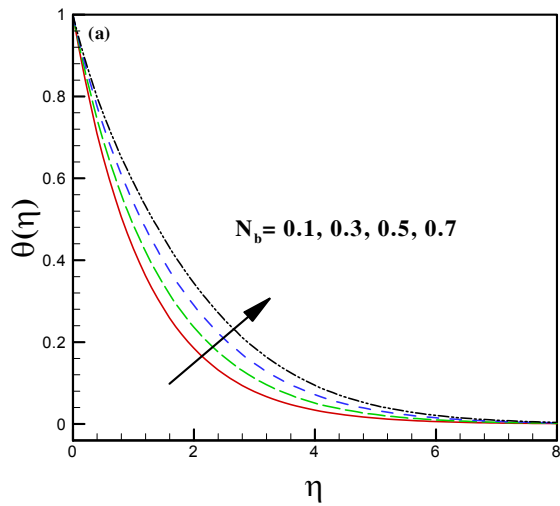
Figs. 2.2(a – c): Impact of β_2 on f' , θ and ϕ .



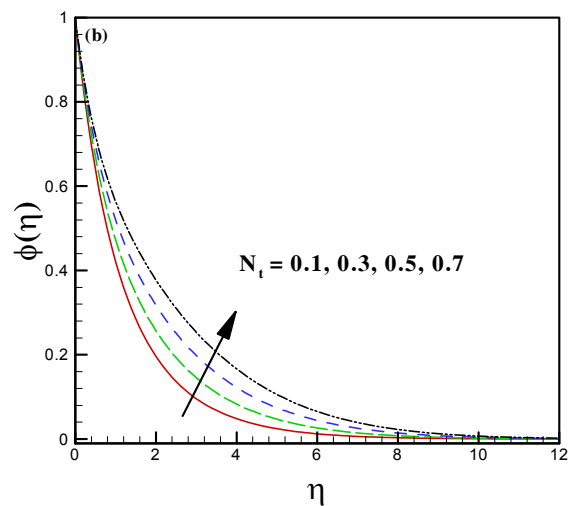
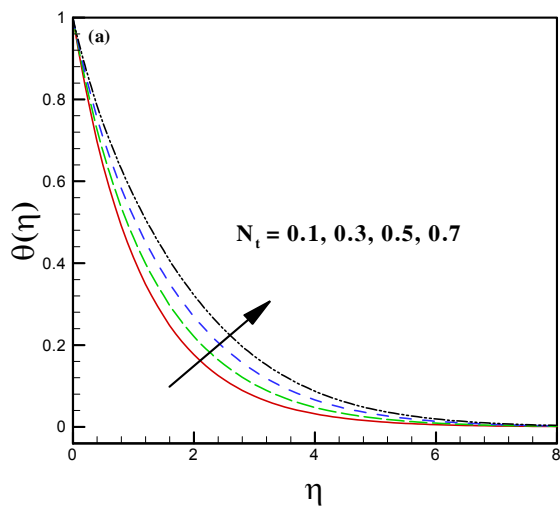
Figs. 2.3(a – c): Impact of β_3 on f' , θ and ϕ .



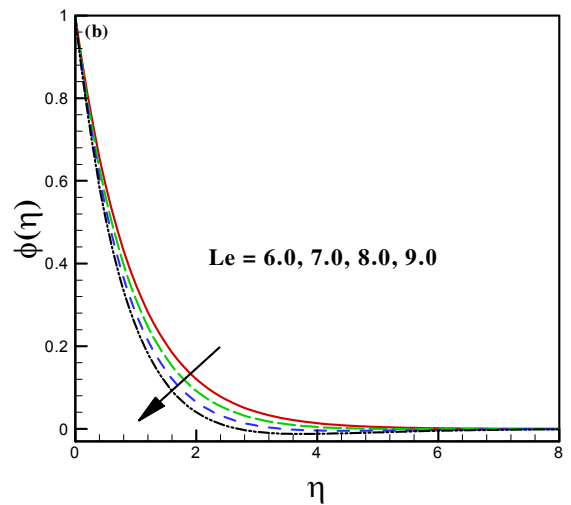
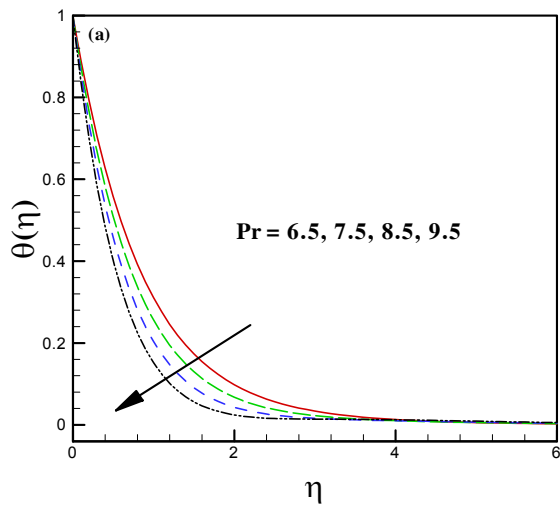
Figs. 2.4(a, b): Effect of A and M on f' .



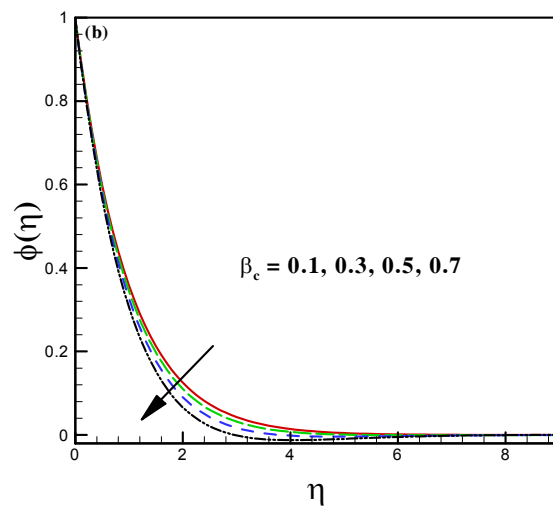
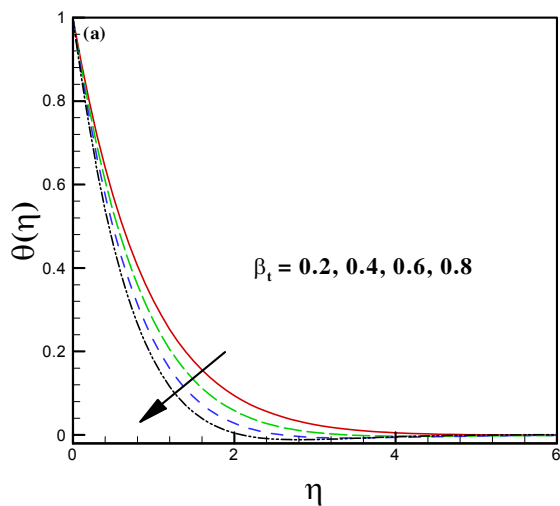
Figs. 2.5(a, b): Effect of N_b on θ and ϕ .



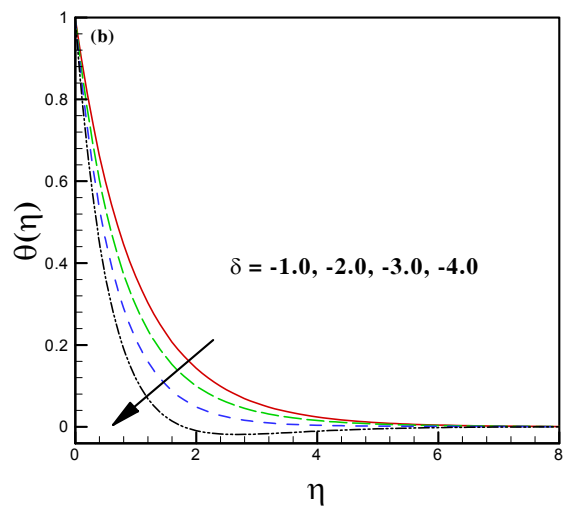
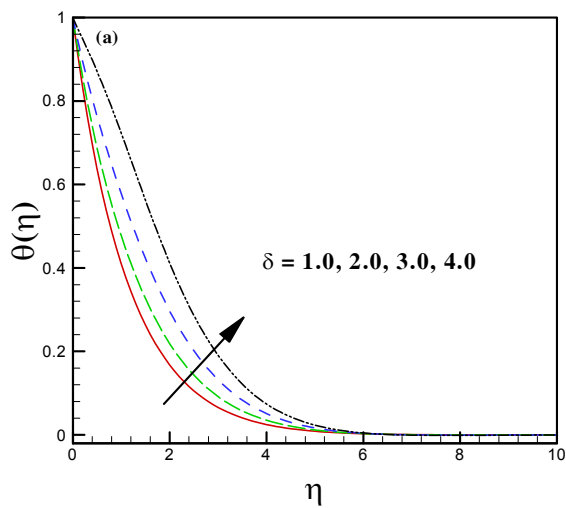
Figs. 2.6(a, b): Effect of N_t on θ and ϕ .



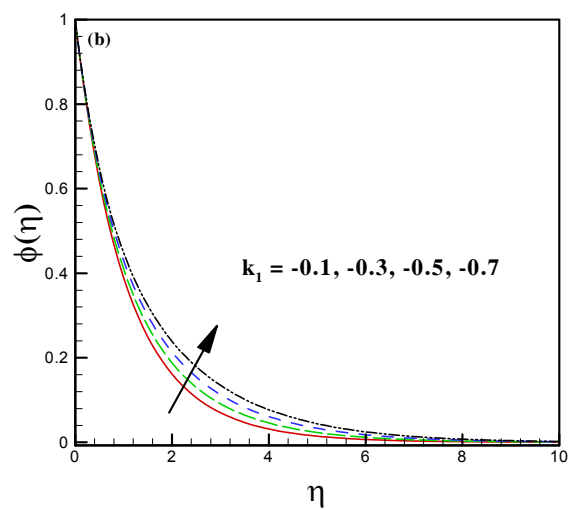
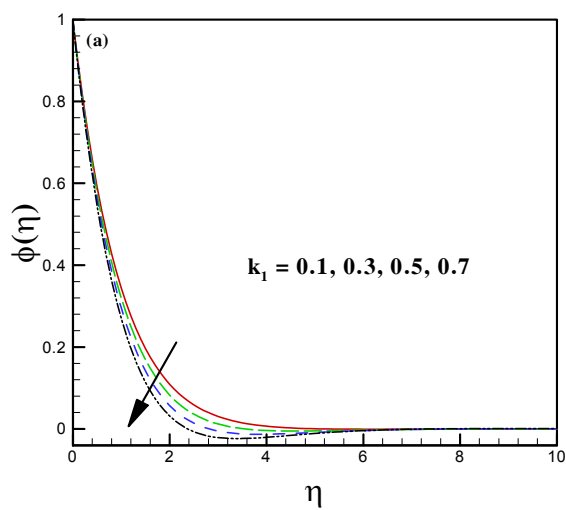
Figs. 2.7(a, b): Impact of Pr on θ and Le on ϕ .



Figs. 2.8(a, b): Impact of β_t on θ and β_c on ϕ .



Figs. 2.9(a, b): Impact of $\delta > 0$ and $\delta < 0$ on θ .



Figs. 2.10(a, b): Impact of $k_1 > 0$ and $k_1 < 0$ on ϕ .

Chapter 3

Burgers nanofluid flow accelerated by bidirectional stretching surface subject to Ohmic heating and chemical reaction

Thermal transport in a 3D flow of Burgers nanofluid due to bidirectional stretching is an interesting topic with large number of applications. Motivated by this fact, in this chapter, we formulated the mathematical modelling for 3D flow of viscoelastic Burgers nanofluid accelerated by bidirectional stretching surface. We studied the fluid relaxation and retardation times effects on the momentum and thermal transport of Burgers fluid. Moreover, we considered the effects of heat rise/fall and Ohmic heating to analyze the heat transport features in the flow of viscoelastic nanofluid. A momentous feature of this study is to incorporate the thermal relaxation time phenomenon to observe the properties of heat flow in nanofluid. Additionally, the mass transport phenomenon is explored by employing modified mass flux model and chemical reaction effects. Results are attained by employing the homotopy analysis method (HAM) and illustrated through graphical representation. The main finding of the study exposes that the thermal transport in the flow is accelerated due to building strength of Eckert number. Moreover,

the depreciating trend of concentration profile is being detected for building strength of constructive chemical reaction parameter. Also, it is seen that the escalating magnitude of thermal relaxation time parameter serves to decline the heat flow rate.

3.1 Rheological Development

In this section, 3D incompressible and unsteady flow of Burgers nanofluid accelerated by bidirectional stretching sheet is modelled. Additionally, the thermal transport in the flow is also studied in view of non-Fourier heat flux model by employing the effects of Ohmic heating and heat rise/fall. The mass transfer phenomenon is inspected under the influence of chemical reaction by employing modified mass flux theory. Flow is considered along x – axis as well as along y – axis with linear velocities $u = ax$ and $v = by$, respectively, where a and b are taken as constants. The region of fluid flow is considered as $z > 0$. The pattern of the flow is displayed in Fig. 3.1.

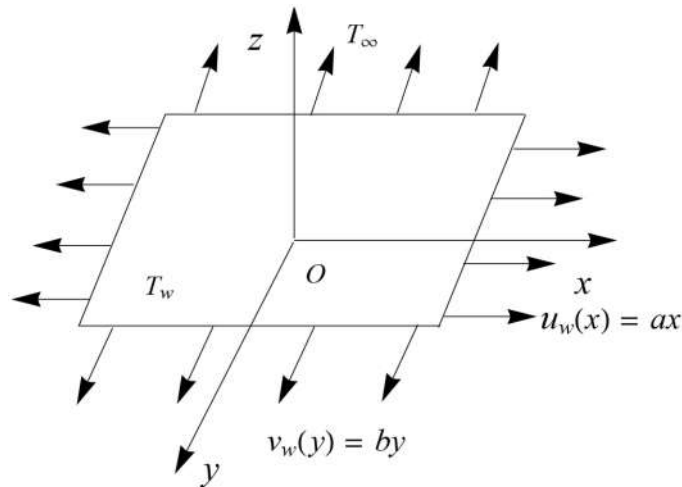


Fig. 3.1: The configuration of the flow.

3.1.1 Flow Equations of Burgers Fluid

The basic continuity and momentum equations (2.2) and (2.3) (cf. Chapter 2) for current flow analysis are as follows

$$\frac{\partial u}{\partial x} + \frac{\partial v}{\partial y} + \frac{\partial w}{\partial z} = 0, \quad (3.1)$$

$$\begin{aligned}
& u \frac{\partial u}{\partial x} + v \frac{\partial u}{\partial y} + w \frac{\partial u}{\partial z} + \lambda_1 \left[u^2 \frac{\partial^2 u}{\partial x^2} + v^2 \frac{\partial^2 u}{\partial y^2} + w^2 \frac{\partial^2 u}{\partial z^2} + 2uv \frac{\partial^2 u}{\partial x \partial y} + 2wv \frac{\partial^2 u}{\partial y \partial z} + 2wu \frac{\partial^2 u}{\partial x \partial z} \right] \\
& + \lambda_2 \left(\begin{aligned}
& u^2 \frac{\partial u}{\partial x} \frac{\partial^2 u}{\partial x^2} + 2u^2 \frac{\partial v}{\partial x} \frac{\partial^2 u}{\partial x \partial y} - u^2 \frac{\partial u}{\partial y} \frac{\partial^2 v}{\partial x^2} + 3u^2 v \frac{\partial^3 u}{\partial x^2 \partial y} + 2uv \frac{\partial u}{\partial y} \frac{\partial^2 u}{\partial x^2} + 3wv^2 \frac{\partial^3 u}{\partial x \partial y^2} - v^2 \frac{\partial u}{\partial x} \frac{\partial^2 u}{\partial y^2} \\
& + u^3 \frac{\partial^3 u}{\partial x^3} + v^3 \frac{\partial^3 u}{\partial y^3} + 2uv \frac{\partial v}{\partial x} \frac{\partial^2 u}{\partial y^2} - 2uv \frac{\partial u}{\partial y} \frac{\partial^2 v}{\partial x \partial y} + 2uv \frac{\partial v}{\partial y} \frac{\partial^2 u}{\partial x \partial y} + 2v^2 \frac{\partial u}{\partial y} \frac{\partial^2 u}{\partial x \partial y} \\
& + 2v^2 \frac{\partial v}{\partial y} \frac{\partial^2 u}{\partial y^2} - 2vw \frac{\partial u}{\partial x} \frac{\partial^2 u}{\partial y \partial z} + 3u^2 w \frac{\partial^3 u}{\partial x^2 \partial z} + 2uw \frac{\partial u}{\partial z} \frac{\partial^2 u}{\partial x^2} + 6uvw \frac{\partial^3 u}{\partial x \partial y \partial z} + 2vw \frac{\partial u}{\partial y} \frac{\partial^2 u}{\partial x \partial z} \\
& - v^2 \frac{\partial u}{\partial y} \frac{\partial^2 v}{\partial y^2} + 2vw \frac{\partial u}{\partial z} \frac{\partial^2 u}{\partial x \partial y} + 3v^2 w \frac{\partial^3 u}{\partial y^2 \partial z} + 2uw \frac{\partial v}{\partial x} \frac{\partial^2 u}{\partial y \partial z} - 2uw \frac{\partial u}{\partial y} \frac{\partial^2 v}{\partial x \partial z}
\end{aligned} \right) \\
& + \lambda_2 \left(\begin{aligned}
& 2vw \frac{\partial v}{\partial y} \frac{\partial^2 u}{\partial y \partial z} - 2vw \frac{\partial u}{\partial y} \frac{\partial^2 v}{\partial y \partial z} + 2uw \frac{\partial v}{\partial z} \frac{\partial^2 u}{\partial x \partial y} + 2vw \frac{\partial v}{\partial z} \frac{\partial^2 u}{\partial y \partial y} + 3uw^2 \frac{\partial^3 u}{\partial x \partial z \partial z} + 2w^2 \frac{\partial u}{\partial z} \frac{\partial^2 u}{\partial x \partial y^2} \\
& + 3uw^2 \frac{\partial^3 u}{\partial x \partial y \partial z} + 2w^2 \frac{\partial u}{\partial z} \frac{\partial^2 u}{\partial x \partial z} - w^2 \frac{\partial u}{\partial x} \frac{\partial^2 u}{\partial z^2} + 3vw^2 \frac{\partial^3 u}{\partial y \partial z^2} + 2w^2 \frac{\partial v}{\partial z} \frac{\partial^2 u}{\partial y \partial z} - w^2 \frac{\partial u}{\partial y} \frac{\partial^2 v}{\partial z^2} \\
& + w^3 \frac{\partial^3 u}{\partial z^3} + 2uw \frac{\partial w}{\partial x} \frac{\partial^2 u}{\partial y \partial z} + 2uw \frac{\partial w}{\partial x} \frac{\partial^2 u}{\partial z \partial z} - u^2 \frac{\partial u}{\partial z} \frac{\partial^2 w}{\partial x^2} - 2uv \frac{\partial u}{\partial z} \frac{\partial^2 w}{\partial x \partial y} \\
& - 2uw \frac{\partial u}{\partial z} \frac{\partial^2 w}{\partial x \partial z} + 2uv \frac{\partial w}{\partial y} \frac{\partial^2 u}{\partial x \partial z} + 2v^2 \frac{\partial w}{\partial y} \frac{\partial^2 u}{\partial y \partial z} + 2vw \frac{\partial w}{\partial y} \frac{\partial^2 u}{\partial z \partial z} \\
& - v^2 \frac{\partial u}{\partial z} \frac{\partial^2 w}{\partial y^2} - 2vw \frac{\partial u}{\partial z} \frac{\partial^2 w}{\partial y \partial z} + 2uw \frac{\partial w}{\partial z} \frac{\partial^2 u}{\partial x \partial z} + 2vw \frac{\partial w}{\partial z} \frac{\partial^2 u}{\partial y \partial z} + 2w^2 \frac{\partial w}{\partial z} \frac{\partial^2 u}{\partial z^2} - w^2 \frac{\partial u}{\partial z} \frac{\partial^2 w}{\partial z \partial z}
\end{aligned} \right) \\
& = \nu \lambda_3 \left[u \frac{\partial^3 u}{\partial x \partial z^2} + v \frac{\partial^3 u}{\partial y \partial z^2} + w \frac{\partial^3 u}{\partial z^3} - \frac{\partial u}{\partial x} \frac{\partial^2 u}{\partial z^2} - \frac{\partial u}{\partial z} \frac{\partial^2 w}{\partial z^2} - \frac{\partial u}{\partial y} \frac{\partial^2 v}{\partial z^2} \right] + \nu \left[\frac{\partial^2 u}{\partial z^2} \right] \quad (3.2)
\end{aligned}$$

$$\begin{aligned}
& u \frac{\partial v}{\partial x} + v \frac{\partial v}{\partial y} + w \frac{\partial v}{\partial z} + \lambda_1 \left[u^2 \frac{\partial^2 v}{\partial x^2} + v^2 \frac{\partial^2 v}{\partial y^2} + w^2 \frac{\partial^2 v}{\partial z^2} + 2uv \frac{\partial^2 v}{\partial x \partial y} + 2wv \frac{\partial^2 v}{\partial y \partial z} + 2wu \frac{\partial^2 v}{\partial x \partial z} \right] \\
& + \lambda_2 \left(\begin{aligned}
& u^3 \frac{\partial^3 v}{\partial x^3} + 2u^2 \frac{\partial u}{\partial x} \frac{\partial^2 v}{\partial x^2} + 2uv \frac{\partial u}{\partial y} \frac{\partial^2 v}{\partial x^2} + uv^2 \frac{\partial^3 u}{\partial x^2 \partial y} + 2uvw \frac{\partial u}{\partial z} \frac{\partial^2 v}{\partial x^2} + u^2 w \frac{\partial^3 v}{\partial x^2 \partial z} - u^2 \frac{\partial v}{\partial y} \frac{\partial^2 u}{\partial x^2} \\
& - u^2 \frac{\partial v}{\partial y} \frac{\partial^2 u}{\partial x^2} - u^2 \frac{\partial v}{\partial z} \frac{\partial^2 w}{\partial x^2} + 2uv \frac{\partial v}{\partial x} \frac{\partial^2 v}{\partial y^2} + uv^2 \frac{\partial^3 v}{\partial x \partial y^2} + 2v^2 \frac{\partial v}{\partial y} \frac{\partial^2 v}{\partial y^2} + v^3 \frac{\partial^3 v}{\partial y^3} + 2vw \frac{\partial v}{\partial z} \frac{\partial^2 v}{\partial y^2} \\
& + v^2 w \frac{\partial^3 v}{\partial z \partial y^2} - v^2 \frac{\partial v}{\partial y} \frac{\partial^2 u}{\partial y^2} - v^2 \frac{\partial v}{\partial y} \frac{\partial^2 v}{\partial y^2} - v^2 \frac{\partial v}{\partial z} \frac{\partial^2 w}{\partial y^2} + 2uvw \frac{\partial w}{\partial x} \frac{\partial^2 v}{\partial z^2} + vw^2 \frac{\partial^3 v}{\partial x \partial z^2} \\
& 2vw \frac{\partial w}{\partial y} \frac{\partial^2 v}{\partial z^2} + vw^2 \frac{\partial^3 v}{\partial y \partial z^2} + 2w^2 \frac{\partial w}{\partial z} \frac{\partial^2 v}{\partial z^2} + w^3 \frac{\partial^3 v}{\partial z^3} - w^2 \frac{\partial v}{\partial x} \frac{\partial^2 v}{\partial z^2} \\
& - w^2 \frac{\partial v}{\partial y} \frac{\partial^2 v}{\partial z^2} - w^2 \frac{\partial v}{\partial z} \frac{\partial^2 w}{\partial z^2} + 2uv \frac{\partial u}{\partial x} \frac{\partial^2 v}{\partial x \partial y} + 2u^2 \frac{\partial v}{\partial x} \frac{\partial^2 v}{\partial x \partial y} \\
& 2u^2 v \frac{\partial^3 v}{\partial x^2 \partial y} + 2v^2 \frac{\partial u}{\partial y} \frac{\partial^2 v}{\partial x \partial y} + 2uv \frac{\partial v}{\partial y} \frac{\partial^2 v}{\partial x \partial y} + 2uv^2 \frac{\partial^3 v}{\partial x \partial y^2}
\end{aligned} \right) \\
& + \lambda_2 \left(\begin{aligned}
& + 2uvw \frac{\partial v}{\partial z} \frac{\partial^2 u}{\partial x \partial y} + 2uvw \frac{\partial^3 u}{\partial x \partial y \partial z} - 2uv \frac{\partial v}{\partial x} \frac{\partial^2 u}{\partial x \partial y} - 2vu \frac{\partial v}{\partial y} \frac{\partial^2 v}{\partial x \partial y} - 2uw \frac{\partial v}{\partial z} \frac{\partial^2 w}{\partial x \partial y} + 2uw \frac{\partial v}{\partial x} \frac{\partial^2 v}{\partial z \partial y} \\
& + 2uv \frac{\partial w}{\partial x} \frac{\partial^2 v}{\partial z \partial y} + 2uvw \frac{\partial^3 v}{\partial x \partial y \partial z} + vw \frac{\partial v}{\partial y} \frac{\partial^2 v}{\partial y \partial z} + 2v^2 \frac{\partial w}{\partial y} \frac{\partial^2 v}{\partial y \partial z} - 2vwv \frac{\partial v}{\partial y} \frac{\partial^2 v}{\partial y \partial z} + 2v^2 w \frac{\partial^3 v}{\partial z \partial y^2} \\
& + 2w^2 \frac{\partial v}{\partial z} \frac{\partial^2 v}{\partial y \partial z} + 2vw \frac{\partial w}{\partial z} \frac{\partial^2 v}{\partial y \partial z} + 2vw^2 \frac{\partial^3 v}{\partial z^2 \partial y} - 2vw \frac{\partial u}{\partial x} \frac{\partial^2 w}{\partial z \partial y} + 2uw \frac{\partial u}{\partial x} \frac{\partial^2 v}{\partial x \partial z} \\
& + 2u^2 \frac{\partial w}{\partial x} \frac{\partial^2 v}{\partial x \partial z} + 2u^2 w \frac{\partial^3 u}{\partial x^2 \partial z} + 2vw \frac{\partial u}{\partial y} \frac{\partial^2 v}{\partial x \partial z} + 2uv \frac{\partial w}{\partial y} \frac{\partial^2 v}{\partial x \partial z} + 2uvw \frac{\partial^3 v}{\partial x \partial y \partial z} \\
& + 2w^2 \frac{\partial u}{\partial z} \frac{\partial^2 v}{\partial x \partial z} + 2uw \frac{\partial w}{\partial z} \frac{\partial^2 v}{\partial x \partial z} + 2uw^2 \frac{\partial^2 v}{\partial x \partial z} - 2uw \frac{\partial v}{\partial x} \frac{\partial^2 u}{\partial x \partial z} - 2uw \frac{\partial v}{\partial y} \frac{\partial^2 v}{\partial x \partial z} - uw \frac{\partial w}{\partial z} \frac{\partial^2 w}{\partial x \partial z}
\end{aligned} \right) \\
& = \nu \lambda_3 \left[u \frac{\partial^3 v}{\partial x \partial z^2} + v \frac{\partial^3 v}{\partial y \partial z^2} + w \frac{\partial^3 v}{\partial z^3} - \frac{\partial v}{\partial y} \frac{\partial^2 v}{\partial z^2} - \frac{\partial v}{\partial z} \frac{\partial^2 w}{\partial z^2} - \frac{\partial v}{\partial x} \frac{\partial^2 u}{\partial z^2} \right] + \nu \left[\frac{\partial^2 v}{\partial z^2} \right], \quad (3.3)
\end{aligned}$$

with boundary conditions

$$u = u_w = ax, \quad v = v_w = by, \quad w = 0 \text{ at } z = 0, \quad (3.4)$$

$$u \rightarrow 0, \quad v \rightarrow 0 \text{ as } z \rightarrow \infty, \quad (3.5)$$

where λ_1 is the fluid relaxation time, λ_2 the Burgers fluid parameter, λ_3 ($\leq \lambda_1$) the fluid retardation time and ν the kinematic viscosity of the fluid.

Presenting the following similarity transformations

$$\begin{aligned}
u &= axf'(\eta), \quad v = ayf'(\eta), \quad w = -\sqrt{av}(f + g), \quad \eta = z\sqrt{\frac{a}{v}}. \\
\theta(\eta) &= \frac{T-T_\infty}{T_w-T_\infty}, \quad \phi(\eta) = \frac{C-C_\infty}{C_w-C_\infty}.
\end{aligned} \tag{3.6}$$

By employing the above conversions, equation (3.1) satisfied automatically and equations (3.2) and (3.3) yield

$$\begin{aligned}
&f''' + (f + g)f'' - (f')^2 + \beta_1 [2(f + g)f'f'' - (f + g)^2f'''] \\
&- \beta_2 \left[\begin{aligned} &2(f + g)^2(f'')^2 + 2(f + g)(f' + g')f'f'' - (f + g)^3f^{iv} \\ &+ (f + g)^2f''(f'' + g'') + 2g'(f + g)^3f''' \end{aligned} \right] \\
&+ \beta_3 [(f'' + g'')f'' - (f + g)f^{iv}] = 0,
\end{aligned} \tag{3.7}$$

$$\begin{aligned}
&g''' + (f + g)g'' - (g')^2 + \beta_1 [2(f + g)g'g'' - (f + g)^2g'''] \\
&- \beta_2 \left[\begin{aligned} &2(f + g)^2(g'')^2 + 2(f + g)(f' + g')g'g'' - (f + g)^3g^{iv} \\ &+ (f + g)^2g''(f'' + g'') + 2f'(f + g)^3g''' \end{aligned} \right] \\
&+ \beta_3 [(f'' + g'')g'' - (f + g)g^{iv}] = 0,
\end{aligned} \tag{3.8}$$

with transformed boundary conditions

$$f(0) = 0, \quad g(0) = 0, \quad f'(0) = 1, \quad g'(0) = R, \tag{3.9}$$

$$f'(\infty) = 0, \quad g'(\infty) = 0. \tag{3.10}$$

In the above equations, the Deborah number $\beta_1 = \lambda_1 a$ is the fluid relaxation time parameter, $\beta_2 = \lambda_2 a^2$ the Burgers fluid parameter and the Deborah number $\beta_3 = \lambda_3 a$ the fluid retardation time parameter and R the stretching strength parameter.

3.1.2 Energy Transport Equations

The conservation laws of heat and mass transport (2.4) and (2.6) (cf. Chapter 2) in view of modified heat and mass fluxes (2.5) and (2.7) (cf. Chapter 2), respectively, under above assumptions take the following forms

$$\begin{aligned}
& u \frac{\partial T}{\partial x} + v \frac{\partial T}{\partial y} + w \frac{\partial T}{\partial z} - \tau \left[D_B \left(\frac{\partial C}{\partial z} \frac{\partial T}{\partial z} \right) + \frac{D_T}{T_\infty} \left(\frac{\partial T}{\partial z} \right)^2 \right] \\
& + \lambda_t \left[u^2 \frac{\partial^2 T}{\partial x^2} + v^2 \frac{\partial^2 T}{\partial y^2} + w^2 \frac{\partial^2 T}{\partial z^2} + 2uv \frac{\partial^2 T}{\partial x \partial y} + 2vw \frac{\partial^2 T}{\partial y \partial z} + 2uw \frac{\partial^2 T}{\partial x \partial z} + u \frac{\partial u}{\partial x} \frac{\partial T}{\partial x} + u \frac{\partial v}{\partial x} \frac{\partial T}{\partial y} \right. \\
& \quad \left. + u \frac{\partial w}{\partial x} \frac{\partial T}{\partial z} + v \frac{\partial u}{\partial y} \frac{\partial T}{\partial x} + v \frac{\partial v}{\partial y} \frac{\partial T}{\partial y} + u \frac{\partial w}{\partial x} \frac{\partial T}{\partial z} + w \frac{\partial u}{\partial z} \frac{\partial T}{\partial x} + w \frac{\partial v}{\partial z} \frac{\partial T}{\partial y} + w \frac{\partial w}{\partial z} \frac{\partial T}{\partial z} \right] \\
& - \lambda_t \tau D_B \left[u \frac{\partial^2 C}{\partial x \partial z} \frac{\partial T}{\partial z} + u \frac{\partial C}{\partial z} \frac{\partial^2 T}{\partial x \partial z} + v \frac{\partial^2 C}{\partial y \partial z} \frac{\partial T}{\partial z} + v \frac{\partial C}{\partial z} \frac{\partial^2 T}{\partial y \partial z} + w \frac{\partial^2 C}{\partial z^2} \frac{\partial T}{\partial z} + w \frac{\partial C}{\partial z} \frac{\partial^2 T}{\partial z^2} \right] \\
& - 2\lambda_t \tau \frac{D_T}{T_\infty} \left[u \frac{\partial T}{\partial z} \frac{\partial^2 T}{\partial x \partial z} + v \frac{\partial T}{\partial z} \frac{\partial^2 T}{\partial y \partial z} + w \frac{\partial T}{\partial z} \frac{\partial^2 T}{\partial z^2} \right] = \alpha_1 \left[\frac{\partial^2 T}{\partial z^2} \right] \\
& + \frac{\sigma B_0^2}{\rho c_p} \left[u^2 + v^2 + 2\lambda_t \left(u^2 \frac{\partial u}{\partial x} + v^2 \frac{\partial v}{\partial x} + uv \frac{\partial v}{\partial x} + uv \frac{\partial u}{\partial y} + uw \frac{\partial u}{\partial z} + vw \frac{\partial v}{\partial z} \right) \right] \\
& + \lambda_t \frac{Q_0}{\rho c_p} \left(u \frac{\partial T}{\partial x} + v \frac{\partial T}{\partial y} + w \frac{\partial T}{\partial z} \right) + Q_0 (T - T_w), \tag{3.11}
\end{aligned}$$

$$\begin{aligned}
& u \frac{\partial C}{\partial x} + v \frac{\partial C}{\partial y} + w \frac{\partial C}{\partial z} + \lambda_c \left[u^2 \frac{\partial^2 C}{\partial x^2} + v^2 \frac{\partial^2 C}{\partial y^2} + w^2 \frac{\partial^2 C}{\partial z^2} + 2uv \frac{\partial^2 C}{\partial x \partial y} + 2vw \frac{\partial^2 C}{\partial y \partial z} + 2uw \frac{\partial^2 C}{\partial x \partial z} \right. \\
& \quad \left. + u \frac{\partial u}{\partial x} \frac{\partial C}{\partial x} + u \frac{\partial v}{\partial x} \frac{\partial C}{\partial y} + u \frac{\partial w}{\partial x} \frac{\partial C}{\partial z} + v \frac{\partial u}{\partial y} \frac{\partial C}{\partial x} + v \frac{\partial v}{\partial y} \frac{\partial C}{\partial y} \right. \\
& \quad \left. + v \frac{\partial w}{\partial y} \frac{\partial C}{\partial z} + w \frac{\partial u}{\partial z} \frac{\partial C}{\partial x} + w \frac{\partial v}{\partial z} \frac{\partial C}{\partial y} + w \frac{\partial w}{\partial z} \frac{\partial C}{\partial z} \right] \\
& - \lambda_c \frac{D_T}{T_\infty} \left[u \frac{\partial^3 T}{\partial x \partial z^2} + v \frac{\partial^3 T}{\partial y \partial z^2} + w \frac{\partial^3 T}{\partial z^3} \right] = D_B \left[\frac{\partial^2 C}{\partial z^2} \right] + \frac{D_T}{T_\infty} \left(\frac{\partial^2 T}{\partial z^2} \right), \\
& -k^* (C - C_\infty) - \lambda_c k^* \left(u \frac{\partial C}{\partial x} + v \frac{\partial C}{\partial y} + w \frac{\partial C}{\partial z} \right), \tag{3.12}
\end{aligned}$$

with boundary conditions

$$T = T_w, C = C_w \text{ at } z = 0, \quad (3.13)$$

$$T \rightarrow T_\infty, C \rightarrow C_\infty \text{ as } z \rightarrow \infty. \quad (3.14)$$

Here $\alpha_1 = \left(\frac{k}{\rho c_p}\right)$ is the thermal diffusivity, in which ρ is the density of the liquid, c_p the specific heat capacity at constant pressure and k the thermal conductivity of the liquid and (T_∞, C_∞) the ambient temperature and concentration respectively.

By utilizing the transformation in equation (3.6) into equations (3.11) and (3.12) we get the following equations

$$\begin{aligned} & \theta'' + \text{Pr} (f + g) \theta' + \text{Pr}(N_b \theta' \phi' + N_t \theta'^2) - \text{Pr} \beta_t \left[(f + g) (f' + g') \theta' + (f + g)^2 \theta'' \right] \\ & - \text{Pr} \beta_t N_b \left[(f + g) \theta'' \phi' + (f + g) \theta' \phi'' \right] - 2 \text{Pr} \beta_t N_t (f + g) \theta' \theta'' \\ & + 2 \text{Pr} M \beta_t \left[E c_1 f'^3 + E c_2 g'^3 - E c_1 f' f'' (f + g) - E c_2 g' g'' (f + g) \right] \\ & + \text{Pr} \delta \left[\theta + \beta_t (f + g) \theta' \right] + \text{Pr} M (E c_1 f'^2 + E c_2 g'^2) = 0, \end{aligned} \quad (3.15)$$

$$\begin{aligned} & \phi'' + Le \text{Pr} (f + g) \phi' + \frac{N_t}{N_b} Le \text{Pr} \theta'' - Le \text{Pr} \beta_c \left[(f + g) (f' + g') \phi' + (f + g)^2 \phi'' \right] \\ & - Le \text{Pr} \frac{N_t}{N_b} (f + g) \theta''' - Le \text{Pr} \left[K \phi + \beta_c k_1 (f + g) \phi' \right] = 0, \end{aligned} \quad (3.16)$$

with transformed boundary conditions

$$\theta(0) = 1, \quad \phi(0) = 1, \quad (3.17)$$

$$\theta(\infty) = 0, \quad \phi(\infty) = 0. \quad (3.18)$$

In the above equations, Prandtl number is defined as $Pr = \frac{\nu}{\alpha_1}$, thermal relaxation time parameter $\beta_t = \lambda_t a$, Lewis number $Le = \frac{\alpha_1}{D_B}$, the mass relaxation time parameter $\beta_c = \lambda_c a$, the stretching strength parameter $R = \frac{b}{a}$, thermophoretic force parameter $N_t = \frac{\tau D_T \Delta T}{\nu T_\infty}$, Brownian motion force parameter $N_b = \frac{\tau D_B \Delta C}{\nu}$, Eckert numbers due to stretching along x and y directions, respectively, are $Ec_1 = \frac{u_w^2}{c_p \Delta T}$ and $Ec_2 = \frac{v_w^2}{c_p \Delta T}$, heat rise/fall parameter $\delta = \frac{Q_0}{\rho c_p a}$ and the chemical reaction parameter $k_1 = \frac{k^*}{a}$.

3.2 Physical Analysis of Results

This section of the chapter is proposed to analyze the effects of different physical parameters on momentum and energy transport profiles of Burgers nanofluid. In this study, we investigated the 3D flow of Burgers nanofluid accelerated due to bidirectional stretching sheet. The thermal transport in the flow is analyzed by utilizing non-Fourier heat flux in addition with the impact of heat rise/fall and Joule heating. The mass diffusion phenomenon is explored under the influence of chemical reaction and modified mass flux theory. Governing equations of flow and energy transport are mentioned in equations (3.7, 3.8) and (3.15, 3.16) with associated boundary conditions (3.9, 3.10) and (3.17, 3.18) are solved by employing the HAM. The properties of momentum transport along x and y directions $f'(\eta)$, $g'(\eta)$, heat transport $\theta(\eta)$ and mass transport $\phi(\eta)$ are scrutinized for different involved physical constraints like, relaxation time

parameter (β_1), Burgers fluid parameter (β_2), retardation time parameter (β_3), Eckert number (Ec), thermal relaxation time parameter (β_t), thermophoresis parameter (N_t), heat source/sink parameter (δ), Brownian motion parameter (N_b), mass relaxation time parameter (β_c) and chemical reaction parameter (k_1) represented through *Figs. 3.3 – 3.9*. Fixed magnitude is accorded for leading parameters such as $\beta_1 = 0.75$, $R = 0.3$, $\beta_2 = 0.18$, $\beta_3 = 0.45$, $Pr = 7.0$, $Ec = 0.9$, $\beta_t = 0.8$, $\delta = 1.0$, $\beta_c = 0.7$, $Le = 6.0$, $K = 0.6$, $N_b = 0.3$ and $N_t = 0.4$ during the entire computations except they are mentioned.

We are going to present the physical judgment of the parameters involved in this study. Here, it is necessary to mention that the flow is generated due to bidirectional stretching along x and y directions of the surface while, $f'(\eta)$ and $g'(\eta)$ respectively are corresponding velocity components. Furthermore, the thermal and solutal transport in the flow is represented by $\theta(\eta)$ and $\phi(\eta)$, respectively. The stimulus of stretching strength parameter (R) over flow profiles $f'(\eta)$, $g'(\eta)$, thermal transport profile $\theta(\eta)$ and mass transport profile $\phi(\eta)$ is demonstrated through *Figs. 3.3(a – d)*. These figures illustrate that the curves representing $f'(\eta)$ depict the reducing trend while the curves of $g'(\eta)$ grow up for larger scales of R . Additionally, it is observed that the higher extent of R does not promote the rate of heat transfer $\theta(\eta)$ and mass transfer $\phi(\eta)$ in the flow of nanofluid. Mathematically, R is defined as the ratio of stretching rates “ b ” and “ a ” in y and x directions, respectively. In which, b is directly proportional and a is inversely proportional to R . It clearly refers that the larger extent of R corresponds to increase the stretching rate along y direction and reduce along x direction of the surface. Hence, the fluid motion along y –direction becomes quicker and along x direction it becomes slower. Additionally, the reduction in the thermal transport is due to the entrainment of chiller fluid from the ambient. It is of worth mentioning that the case $R = 0$ corresponds to $2D$ flow

while, the case $R = 1$ corresponds to axisymmetric flow. The velocity profiles $f'(\eta)$, $g'(\eta)$, temperature profiles $\theta(\eta)$ and solutal profiles $\phi(\eta)$ for various magnitudes of fluid relaxation time parameter (β_1) are delineated in Figs. 3.4(a–d). It is anticipated that the incrementing values of β_1 reduce the flow velocity of nanofluid along both x and y directions. Moreover, it is observed that both $\theta(\eta)$ and $\phi(\eta)$ improved for incremented β_1 . The thermal and solutal curves adhere to the surface when β_1 magnifies representing that the thermal boundary layer is the increasing function of β_1 . Basically, growing strength of β_1 serves to stimulate the resistance between fluid elements which causes reduced flow velocity along x and y directions. The rising trend of thermal transport is also the consequence of this resistance in the motion. As resistance generates more heat in the system which obviously accelerates the thermal transport in the flow. The behavior of material parameter of Burgers fluid (β_2) on $f'(\eta)$, $g'(\eta)$, $\theta(\eta)$ and $\phi(\eta)$ is demonstrated in Figs. 3.5(a–d). It is perceived that enlargement in the magnitude of β_2 implies that the flow is retarded along x and y directions. Additionally, the rate of heat conduction $\theta(\eta)$ and the rate of mass transfer $\phi(\eta)$ is seems to be accelerated for incrementing values of β_2 . Figs. 3.6(a–d) are interleaved to highlight the response of fluid retardation time parameter (β_3) over flow distributions $f'(\eta)$, $g'(\eta)$ and energy transport profiles $\theta(\eta)$, $\phi(\eta)$ of Burgers nanofluid. Figs. 3.6(a, b) reveal that the flow velocities along x and y directions $f'(\eta)$, $g'(\eta)$ respectively, are accelerated by enlarging the magnitude of β_3 . It depicts that the momentum transport is boosted by the developing strength of β_3 . Additionally, it is confirmed that augmented β_3 de-escalates the thermal and solutal transport curves of Burgers fluid. Actually, the developing strength of β_3 builds up the shear stress in the fluid which serves to accelerate the flow velocity of nanofluid. Additionally, larger β_3 corresponds to lower creep phenomenon of the Burgers fluid. Some energy is required to lower down the creep phenomenon of the fluid hence, this loss of

energy refers to decline the thermal as well as the solutal transport in the fluid. Figs. 3.7(a–d) elucidate the thermophoretic force (N_t) and Brownian motion force (N_b) response on thermal and nanoparticles volume fraction profile of nanofluid. In Figs. 3.7(a, b) it is investigated that the incremented N_t serves to accelerate the thermal transport $\theta(\eta)$ and solutal transport $\phi(\eta)$. These results are according to our expectations because during the process of thermophoresis particles move from hotter to chiller regions and this movement of fluid particles generate friction which drives up the thermal transport $\theta(\eta)$ and solutal transport $\phi(\eta)$ in the flow. The response of Brownian motion force parameter (N_b) over $\theta(\eta)$ and $\phi(\eta)$ is manifested in Figs. 3.7(c, d). A clear magnification is detected in the thermal curves of nanofluid for growing strength of N_b . Additionally, it is assessed that the curves indicating the solutal transport are depicting the diminishing trend for incrementing values of N_b . Basically, enhanced kinetic energy of the system due to random movement of molecules in Brownian motion phenomenon refers to accelerate the heat flow rate in the flow which intensifies the thermal distribution. Infact, incremented N_b implies lower mass diffusivity because building strength of N_b resists the mass diffusion which deteriorate the solutal curves of fluid. Figs. 3.8(a–d) are drafted to visualize the response of thermal relaxation time parameter (β_t), Eckert numbers Ec_1 and Ec_2 due to stretching along x and y directions, respectively, on thermal transport profile and mass transfer relaxation time parameter (β_c) on solutal transport profiles. The plots in Figs. 3.8(a, b) infer that the thermal transport de-accelerates for incremented β_t and solutal transport also declines for augmented β_c . Physically, accretion in β_t implies that more time is utilized for convection of heat in the material. Hence, an intensification in the β_t refers to decline the thermal transport curves of fluid. Same reason is in the case of diminution of solutal profile for incremented β_c , i.e, larger time is needed for mass transfer. Figs. 3.8(c, d) are depicted to

disclose the thermal transport characteristics of Burgers nanofluid influenced by Eckert numbers (Ec_1) and (Ec_2) in x and y directions, respectively. These Figs. demonstrate that the higher extent of both Ec_1 and Ec_2 promote the transport of thermal energy in the flow of nanofluid. As Ec_1 is the Eckert number produced due to stretching along x -axis while, Ec_2 is the Eckert number appears due to stretching of the surface along y direction. It is worth mentioning that due to accumulation in the magnitude of Ec_1 and Ec_2 implies that the stretching rate in x and y directions respectively, increases which is responsible for the enhancement of kinetic energy of the fluid particles and consequently the thermal profiles of nanofluid build up. Figs. 3.9(a – d) elucidate the nature of thermal curves for influence of heat source/sink constraint (δ) and the nature of solutal curves for the influence of chemical reaction constraint (k_1). Clearly, an improvement in the thermal enhancement is detected from Figs. 3.9(a, b) for magnifying scales of heat source parameter ($\delta > 0$) while, it is assessed that the higher values of heat sink constraint ($\delta < 0$) de-escalates the thermal contours in the flow. Obviously, intensifying effects of heat source parameter correspond to sum up more heat in the system due to which heat transport boosts up and the larger heat sink parameter indicates that the more amount of heat absorbs from the system which surely refers to reduce the heat flow in the fluid. Moreover, to detect the impact of chemical reaction constraint (k_1) on solutal distribution of nanofluid Figs. 3.9(c, d) are portrayed. From these plots, it is exposed that the for larger extent of constructive chemical reaction parameter ($k_1 > 0$) the solutal distribution of Burgers fluid become weaker while, it strengthens for developing destructive chemical reaction parameter ($k_1 < 0$). Actually, some amount of energy consumes in construction of chemical reaction which refers that the rate of mass transfer declines in the flow whereas, the energy adds back in the system when destruction in rate of chemical reaction is started which in result promotes the mass transfer

rate in the flow.

3.3 Validation of Homotopic Solutions

In this section we computed the values of $-f''(0)$, $-g''(0)$ and $-\theta'(0)$ for some values of stretching strength parameter R in reduced case and depicted in tables 3.1(a) and 3.1(b) and compared these values with already published studies. We found that our computed values are accurate when compared to previously published studies, which proves that our adopted homotopic approach is a valid technique. Also the \hbar curve is depicted in Fig. 3.2 for 15th order of approximation, which illustrates the acceptable values of \hbar are lie in the interval $-1.3 \leq \hbar \leq -0.8$.

Table 3.1(a): A comparison table for $-f''(0)$ and $-g''(0)$ for several magnitudes of stretching strength parameter (R) in reduced case when $\beta_1 = \beta_2 = \beta_3 = 0$.

R	Khan <i>et al.</i> [21]		Present study	
	$-f''(0)$	$-g''(0)$	$-f''(0)$	$-g''(0)$
0.0	1.0	0.0	1.0	0.0
0.2	1.03949	0.14874	1.03937	0.14863
0.4	1.07578	0.34921	1.07567	0.34901
0.6	1.10994	0.59053	1.10913	0.59048
0.8	1.14249	0.86668	1.14229	0.86654
1.0	1.17372	1.17372	1.17121	1.17361

Table 3.1(b): An assessment table for $-\theta'(0)$ for pertinent ranges of R in reducing case when $\beta_1 = \beta_2 = \beta_3 = \beta_t = N_t = Ec = \delta = N_b = 0$ and $Pr = 1$.

R	[16]	[138]	Present study
0.25	-0.665933	-0.66593	-0.665929
0.50	-0.735334	-0.73533	-0.735326
0.75	-0.796472	-0.79472	-0.796469

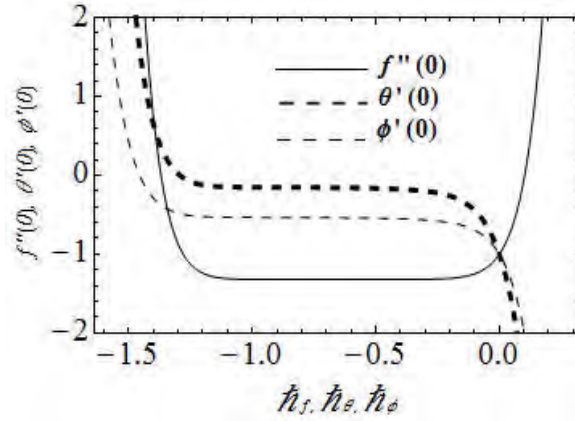
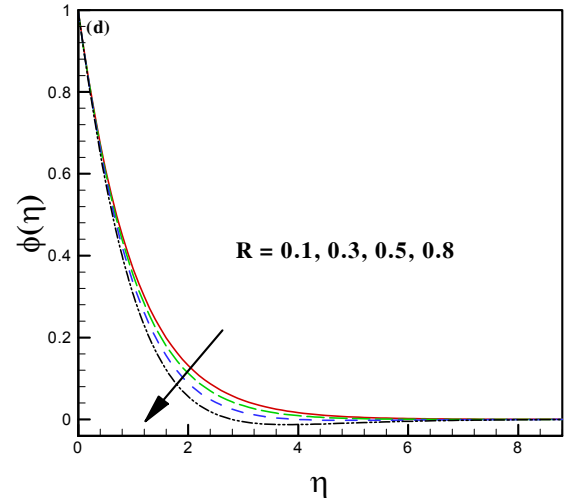
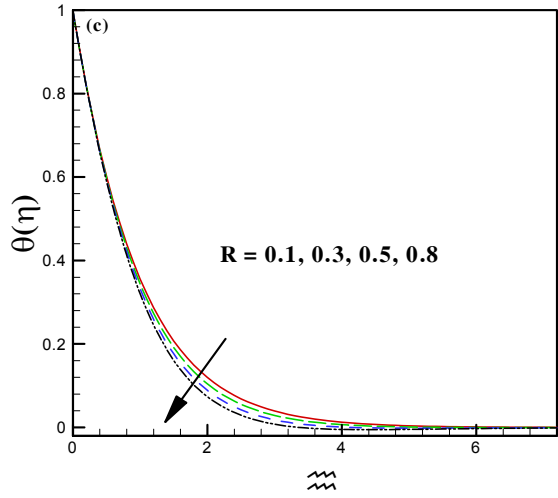
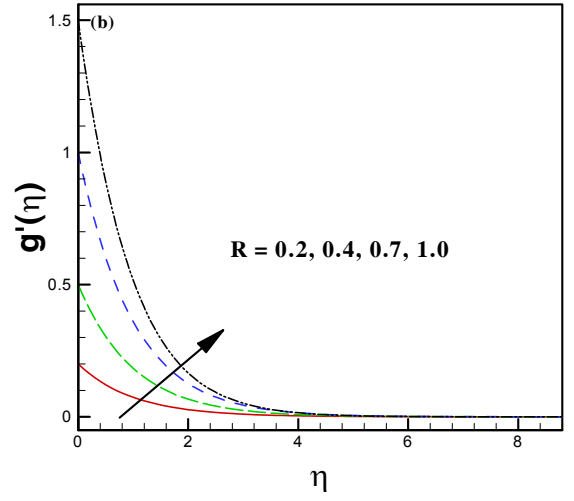
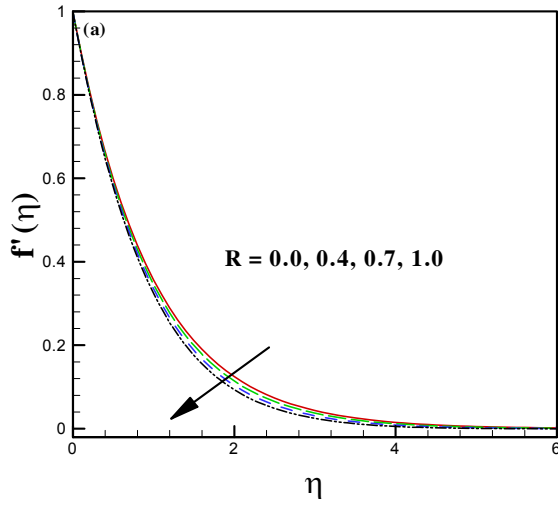
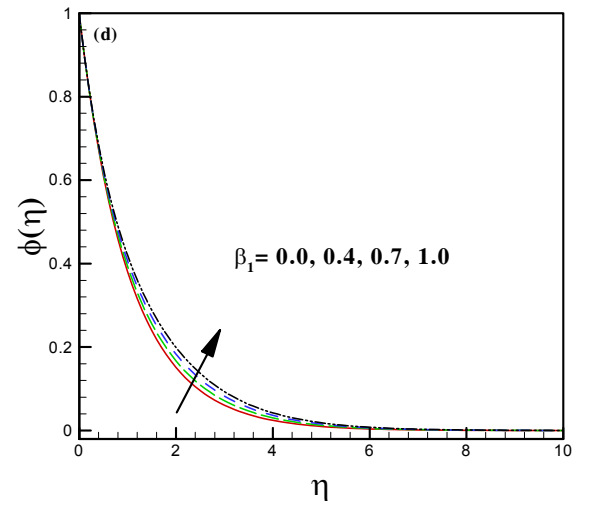
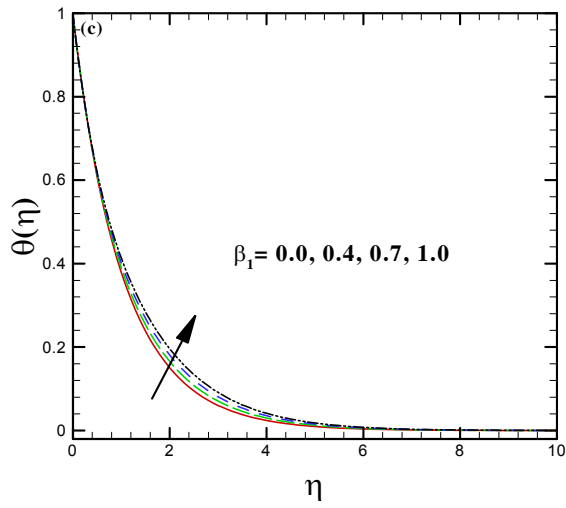
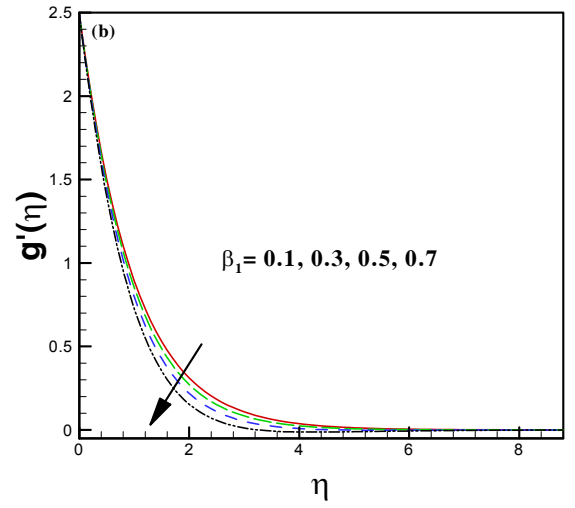
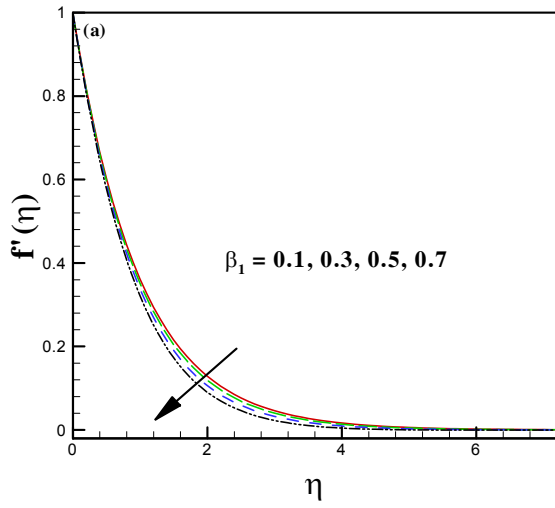


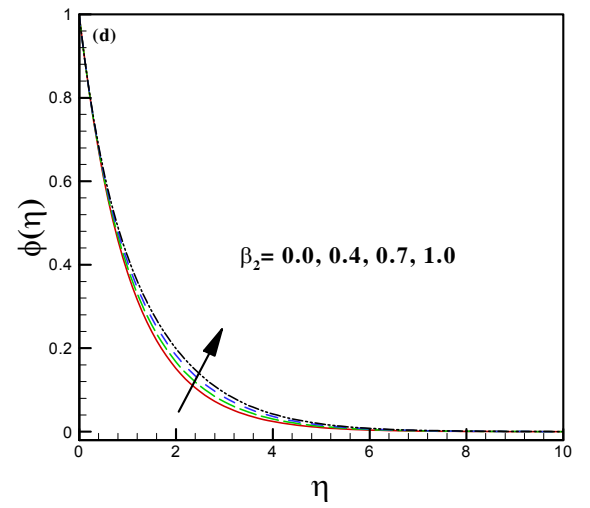
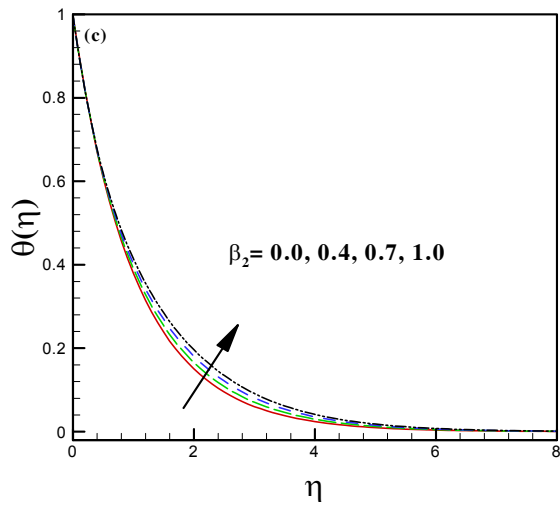
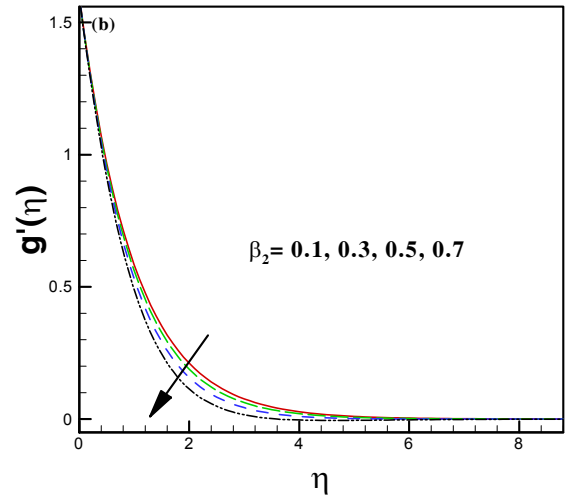
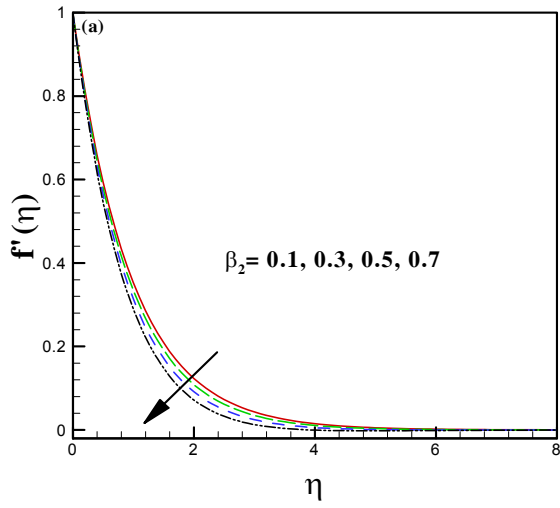
Fig. 3.2: The \hbar curves for 15th order of approximation.



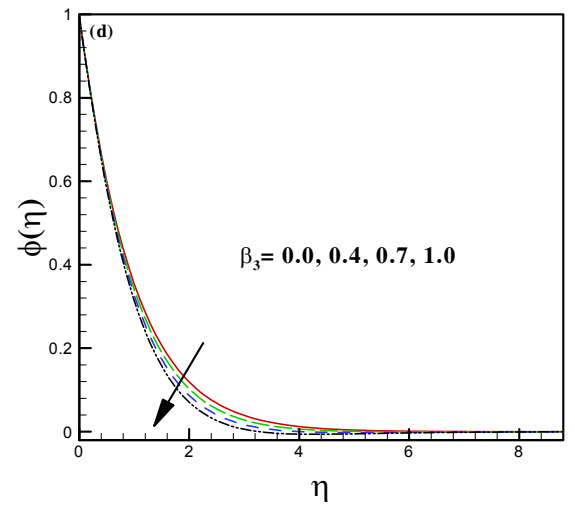
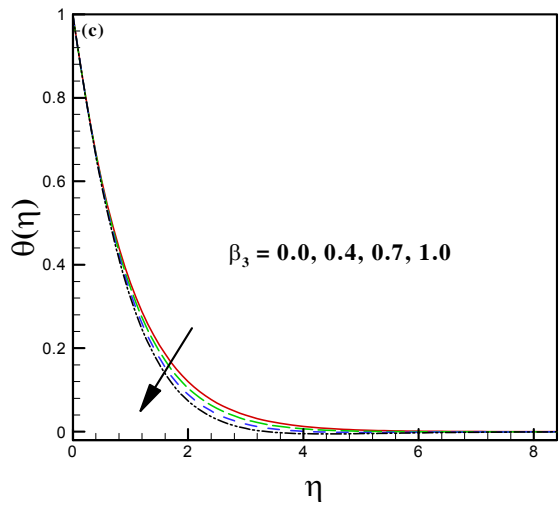
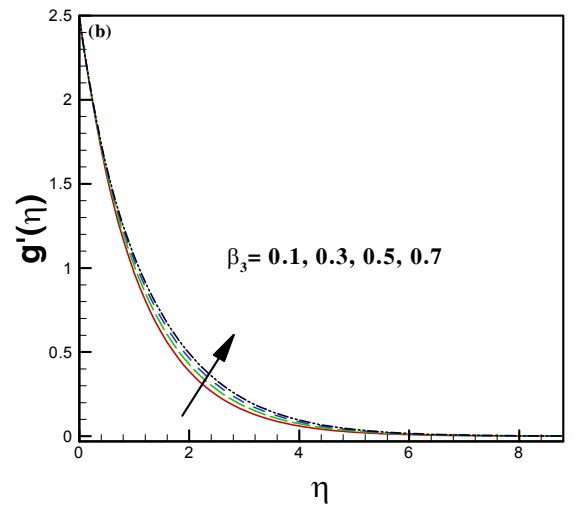
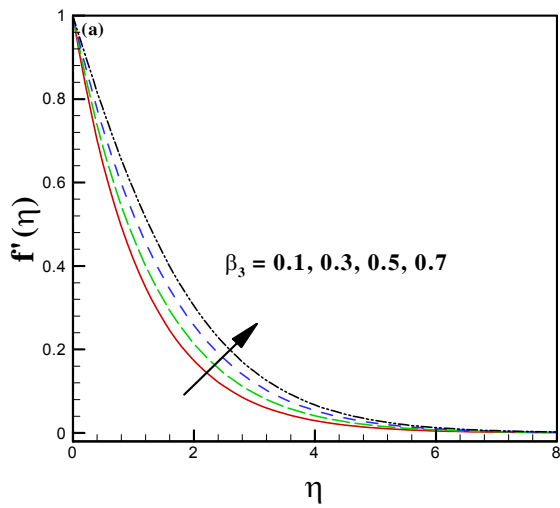
Figs. 3.3(a – d): Impact of R on f' , g' , θ and ϕ .



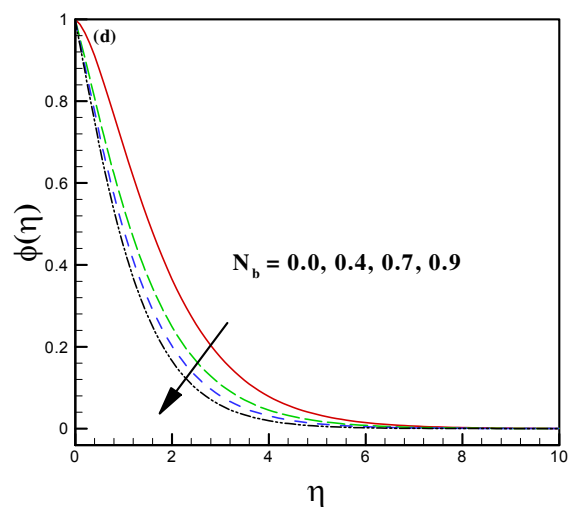
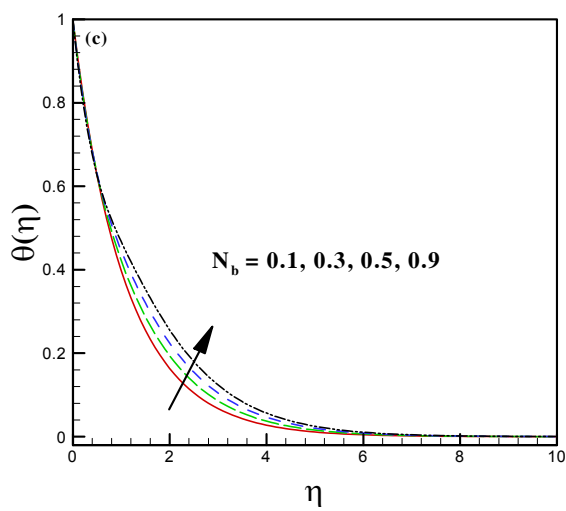
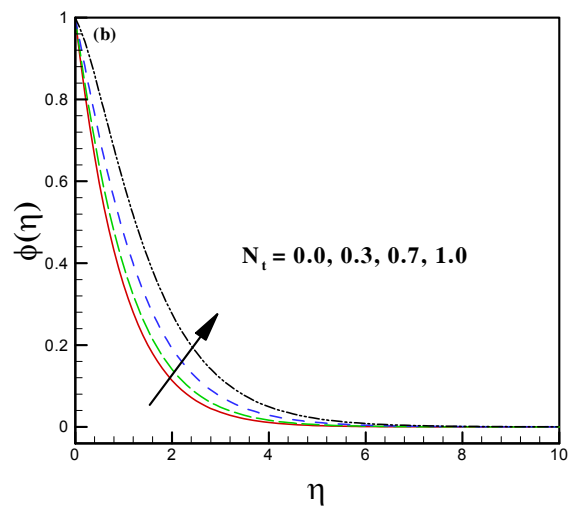
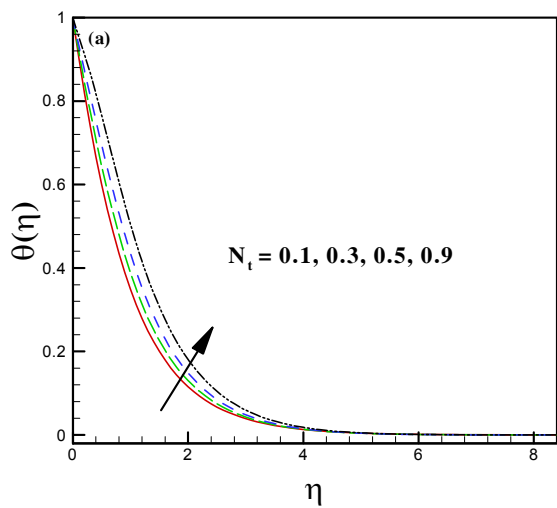
Figs. 3.4(a – d): Impact of β_1 on f' , g' , θ and ϕ .



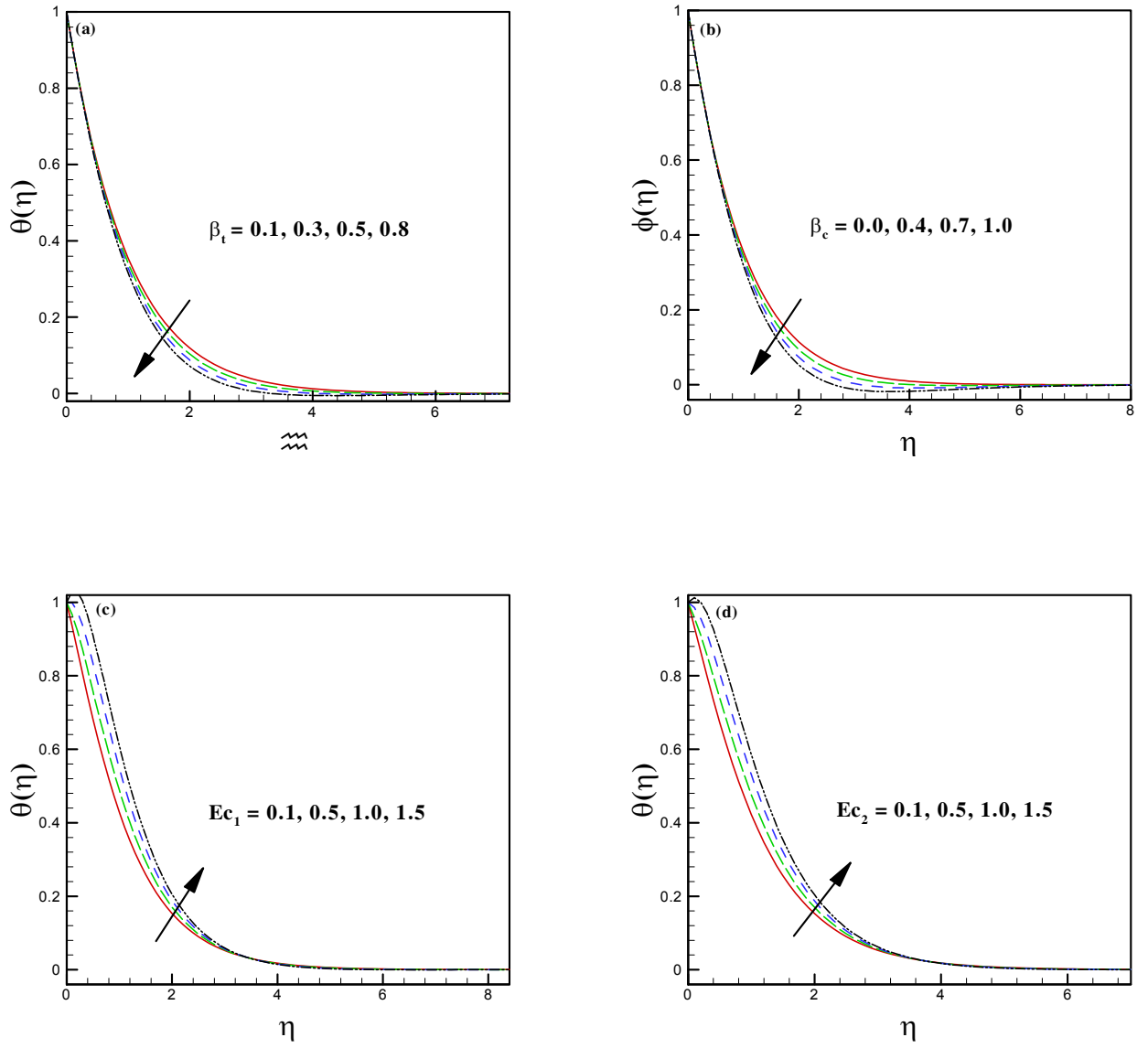
Figs. 3.5(a – d): Impact of β_2 on f' , g' , θ and ϕ .



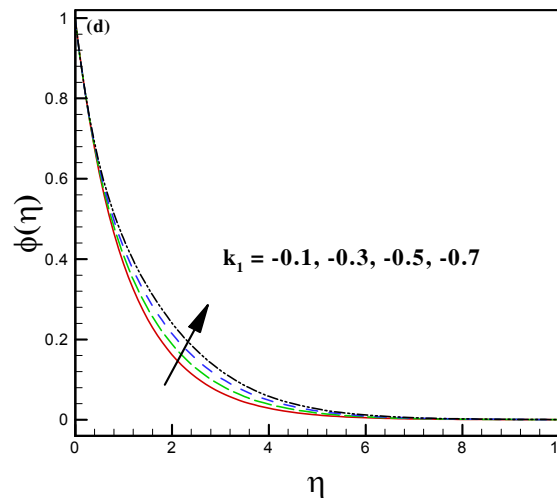
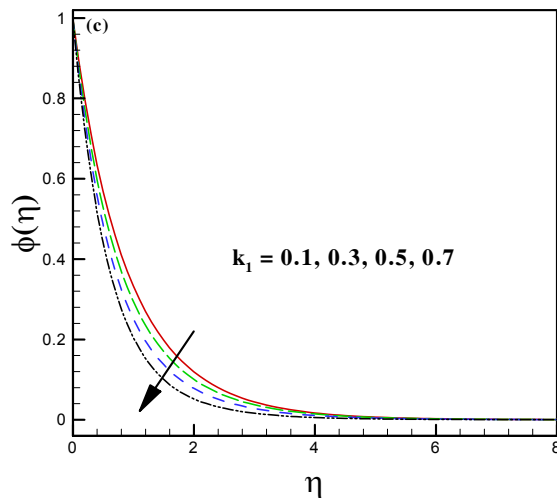
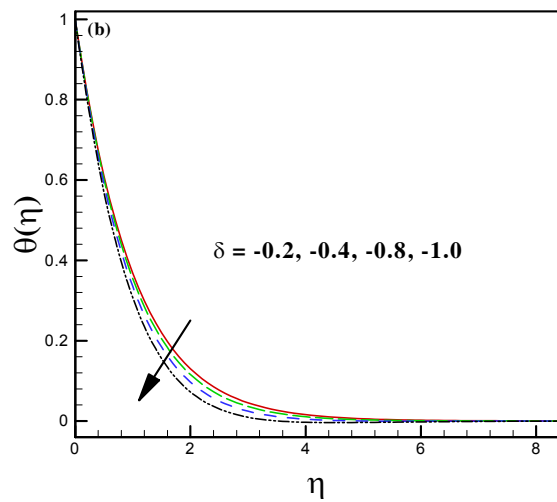
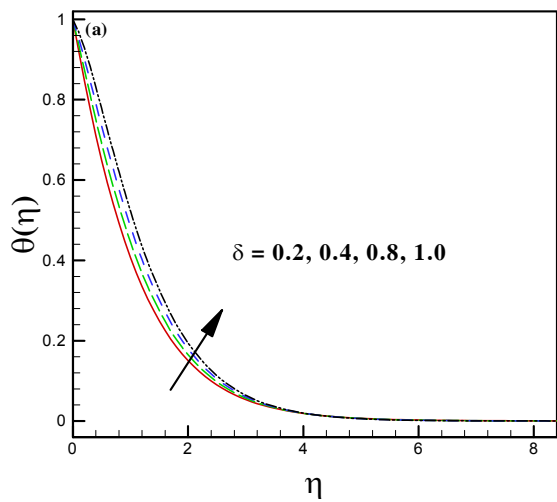
Figs. 3.6(a – d): Impact of β_3 on f' , g' , θ and ϕ .



Figs. 3.7(a – d): Effect of N_t and N_b on θ and ϕ .



Figs. 3.8(a – d): Impact of β_t , E_{c1} and E_{c2} on θ and β_c and on ϕ .



Figs. 3.9(a – d): Impact of δ on θ and k_1 on ϕ .

Chapter 4

Analysis of heat and mass transport in Burgers fluid flow due to stretching cylinder

In this chapter, a new mathematical modelling is presented for the flow of Burgers fluid induced by a stretching cylinder in the presence of magnetic field. Moreover, the mechanisms of heat and mass transport are also examined by using the laws of conservation of energy with Fourier's and Fick's laws for thermal and solutal energy, respectively. The ordinary differential equations (ODEs) are attained from partial differential equations (PDEs) by making the use of dimensionless similarity transformations. The homotopic approach is being adopted to solve the developed ODEs. The influences of different physical parameters on velocity, thermal and concentration profiles are pondered through graphs and physical behaviors of these parameters are enlightened with the realistic verdicts. The basic physical intimation of pertained results is that the temperature and solutal curves of Burgers liquid show the enhancing trend for larger scales of relaxation time parameter and for material parameter of Burgers fluid while, opposing behavior is being observed for retardation time parameter. Moreover, it is assessed that the concentration rate and solutal boundary layer thickness decline with an intensification in Lewis number. Further, it is noted that the temperature distribution enhances/declines with higher values of

heat source/sink parameter, respectively.

4.1 Mathematical Formulation

We are considering the steady $2D$ incompressible flow of Burgers fluid induced by a stretched cylinder of radius R . Let cylindrical polar coordinates (r, θ, z) are taken to be in such a way that z - axis is settled along the axis of the cylinder while, r - axis is considered along the radial direction as illustrated in Fig. 4.1. The velocity field for present flow is considered as $\mathbf{V} = [u, 0, w]$. Here u and w are taken as the velocity components along r and z axes, respectively with a uniform magnetic field $B = [B_0, 0, 0]$ applied normal to the flow direction. Moreover, $w_s = \frac{U_0 z}{l}$ is taken as the stretching velocity of the cylinder in z -direction, where U_0 is the reference velocity and l the specific length.

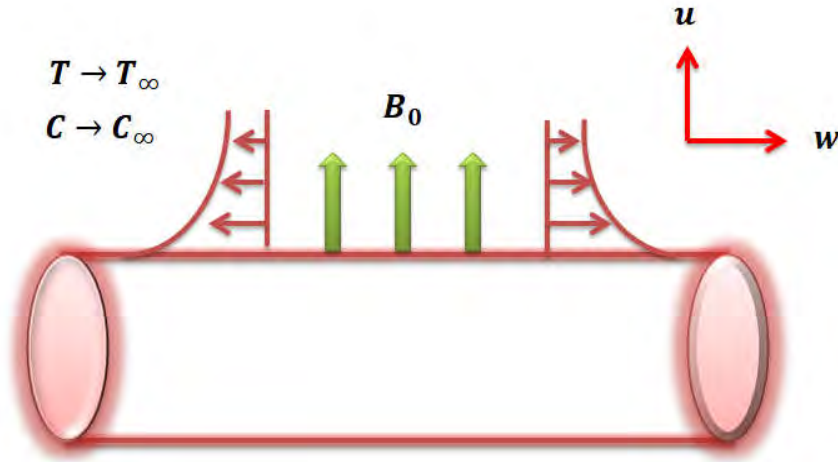


Fig. 4.1: Flow configuration and coordinates system.

In view of above assumptions, the continuity equation (2.2) (cf. Chapter 2) and the momentum equation by the elimination of \mathbf{S} from equations (2.1) and (2.3) (cf. Chapter 2) take

the subsequent forms for current flow analysis

$$\frac{\partial u}{\partial r} + \frac{u}{r} + \frac{\partial w}{\partial z} = 0, \quad (4.1)$$

$$\begin{aligned} & u \frac{\partial w}{\partial r} + w \frac{\partial w}{\partial z} + \lambda_1 \left[u^2 \frac{\partial^2 w}{\partial r^2} + w^2 \frac{\partial^2 w}{\partial z^2} + 2uw \frac{\partial^2 w}{\partial z \partial r} \right] \\ + \lambda_2 & \left[u^3 \frac{\partial^3 w}{\partial r^3} + w^3 \frac{\partial^3 w}{\partial z^3} + 2u^2 \left(\frac{\partial u}{\partial r} \frac{\partial^2 w}{\partial r^2} + \frac{\partial w}{\partial r} \frac{\partial^2 w}{\partial r \partial z} \right) - u^2 \left(\frac{\partial w}{\partial r} \frac{\partial^2 u}{\partial r^2} + \frac{\partial w}{\partial z} \frac{\partial^2 w}{\partial r^2} \right) \right. \\ & \left. + 2w^2 \frac{\partial u}{\partial z} \frac{\partial^2 w}{\partial r \partial z} + w^2 \left(\frac{\partial w}{\partial z} \frac{\partial^2 w}{\partial z^2} - \frac{\partial w}{\partial r} \frac{\partial^2 u}{\partial z^2} \right) + 3uw \left(u \frac{\partial^3 w}{\partial r^2 \partial z} + w \frac{\partial^3 w}{\partial z^2 \partial r} \right) \right. \\ & \left. + 2uw \left(\frac{\partial u}{\partial r} \frac{\partial^2 w}{\partial z \partial r} + \frac{\partial u}{\partial z} \frac{\partial^2 w}{\partial r^2} + \frac{\partial w}{\partial r} \frac{\partial^2 w}{\partial z^2} - \frac{\partial w}{\partial r} \frac{\partial^2 u}{\partial r \partial z} \right) \right] \\ = \nu \lambda_3 & \left[u \frac{\partial^3 w}{\partial r^3} + w \frac{\partial^3 w}{\partial r^2 \partial z} + \frac{u}{r} \frac{\partial^2 w}{\partial r^2} - \frac{\partial w}{\partial r} \frac{\partial^2 u}{\partial r^2} + \frac{w}{r} \frac{\partial^2 w}{\partial r \partial z} - \right. \\ & \left. \frac{1}{r} \frac{\partial u}{\partial r} \frac{\partial w}{\partial r} - \frac{1}{r} \frac{\partial w}{\partial r} \frac{\partial w}{\partial z} - \frac{\partial w}{\partial z} \frac{\partial^2 w}{\partial r^2} \right] \\ + \nu & \left[\frac{\partial^2 w}{\partial r^2} + \frac{1}{r} \frac{\partial w}{\partial r} \right] - \frac{\sigma B_0^2}{\rho} \left[\begin{array}{c} w + \lambda_1 u \frac{\partial w}{\partial r} + \\ \lambda_2 \left(w \frac{\partial u}{\partial z} \frac{\partial w}{\partial r} - u \frac{\partial w}{\partial z} \frac{\partial w}{\partial r} + uw \frac{\partial^2 w}{\partial r \partial z} + w^2 \frac{\partial^2 w}{\partial r^2} \right) \end{array} \right]. \quad (4.2) \end{aligned}$$

By adopting current assumptions, the heat transport and mass transport equations (1.7) and (1.10) (cf. Chapter 1) in view of Fourier's and Fick's heat and mass fluxes given in equations (1.8) and (1.11) (cf. Chapter 1) we arrived at the following PDEs

$$u \frac{\partial T}{\partial r} + w \frac{\partial T}{\partial z} = \alpha_1 \frac{1}{r} \left[\frac{\partial}{\partial r} \left(r \frac{\partial T}{\partial r} \right) \right] + \frac{Q_0(T - T_\infty)}{\rho c_p}, \quad (4.3)$$

$$u \frac{\partial C}{\partial r} + w \frac{\partial C}{\partial z} = \frac{D_B}{r} \frac{\partial}{\partial r} \left(r \frac{\partial C}{\partial r} \right), \quad (4.4)$$

with boundary conditions

$$w = w_s = \frac{U_0 z}{l}, \quad u = 0, \quad T = T_w, \quad C = C_w \quad \text{at } r = R, \quad (4.5)$$

$$w \rightarrow 0, \quad \frac{\partial w}{\partial r} \rightarrow 0, \quad T \rightarrow T_\infty, \quad C \rightarrow C_\infty \quad \text{as } r \rightarrow \infty. \quad (4.6)$$

Here λ_1 is the relaxation time, λ_2 the material parameter of Burgers fluid, λ_3 ($\leq \lambda_1$) the retardation time, ν the kinematics viscosity, Q_0 the heat generation /absorption coefficient, (T, C) the liquid temperature and concentration respectively, (T_∞, C_∞) the ambient temperature and concentration respectively, D_B the diffusion coefficient and $\alpha_1 = \left(\frac{k}{(\rho c)_f}\right)$ the thermal diffusivity, in which ρ_f is the density of liquid, c_f the specific heat and k the thermal conductivity of the liquid.

Introducing the following conversions

$$u = -\frac{R}{r} \sqrt{\frac{U_0 \nu}{l}} f(\eta), \quad w = \frac{U_0 z}{l} f'(\eta), \quad \theta(\eta) = \frac{T - T_\infty}{T_w - T_\infty},$$

$$\phi(\eta) = \frac{C - C_\infty}{C_w - C_\infty}, \quad \eta = \sqrt{\frac{U_0}{\nu l}} \left(\frac{r^2 - R^2}{2R} \right). \quad (4.7)$$

By utilizing the overhead transformations equation (4.1) is explicitly satisfied while equations (4.2) – (4.6) yield

$$\begin{aligned} & (1 + 2\alpha\eta)^3 f''' + (1 + 2\alpha\eta)^2 \left[f f'' - (f')^2 \right] + (1 + 2\alpha\eta)^2 \beta_1 \left[2f f' f'' - f^2 f''' \right] \\ & - (1 + 2\alpha\eta)^2 \beta_2 \left[3f^2 (f'')^2 + 2f (f')^2 f'' - f^3 f^{iv} \right] + (1 + 2\alpha\eta)^3 \beta_3 \left[(f'')^2 - f f^{iv} \right] \\ & + (1 + 2\alpha\eta) \alpha \beta_2 \left[3f^2 f' f'' + f^3 f''' \right] + 2\alpha (1 + 2\alpha\eta)^2 f'' + 4\alpha \beta_3 (1 + 2\alpha\eta)^2 f f''' \\ & - (1 + 2\alpha\eta) \alpha \beta_1 f^2 f'' - 4\alpha^2 \beta_2 f''' f'' - (1 + 2\alpha\eta)^2 M^2 \left[\beta_2 f f''' - \beta_1 f f'' + f' \right] = 0, \quad (4.8) \end{aligned}$$

$$(1 + 2\alpha\eta)\theta'' + 2\alpha\theta' + \text{Pr} f\theta' + \text{Pr} \delta\theta = 0, \quad (4.9)$$

$$(1 + 2\alpha\eta)\phi'' + 2\alpha\phi' + Le \text{Pr} f\phi' = 0, \quad (4.10)$$

$$f = 0, f' = 1, \theta = 1, \phi = 1 \text{ at } \eta = 0, \quad (4.11)$$

$$f' \rightarrow 0, f'' \rightarrow 0, \theta \rightarrow 0, \phi \rightarrow 0 \text{ as } \eta \rightarrow \infty, \quad (4.12)$$

where the curvature parameter (α), Deborah numbers (β_1 and β_3), Burgers fluid parameter (β_2), heat source ($\delta > 0$) and sink ($\delta < 0$) parameter, magnetic parameter (M), Prandtl number (Pr), and Lewis number (Le) are defined as follows:

$$\begin{aligned} \alpha &= \frac{1}{R} \sqrt{\frac{\nu l}{U_0}}, \quad \beta_1 = \lambda_1 \frac{U_0}{l}, \quad \beta_3 = \lambda_3 \frac{U_0}{l}, \quad \delta = \frac{lQ_0}{U_0(\rho c)_f}, \\ \beta_2 &= \lambda_2 \left(\frac{U_0}{l}\right)^2, \quad M = \left(\frac{\sigma l B_0^2}{\rho_f U_0}\right)^{1/2}, \quad \text{Pr} = \frac{\nu}{\alpha_1}, \quad Le = \frac{\alpha_1}{D_B}. \end{aligned} \quad (4.13)$$

4.2 Validation of Homotopic Approach

We have depicted table 4.1 which is a comparison table of $-f''(0)$ for pertinent magnitudes of β_1 with some formerly published studies. Therefore, we can say that our work is valid as it is identical with formerly published results.

Table 4.1: A comparison table for $-f''(0)$ against different values of β_1 when $\alpha = \beta_2 = \beta_3 = M = 0$.

β_1	Abel <i>et al.</i> [139]	Waqas <i>et al.</i> [140]	Irfan <i>et al.</i> [141]	Present study
0.0	1.000000	1.000000	1.0000000	1.0000000
0.2	1.051948	1.051889	1.0518890	1.0518891
0.4	1.101850	1.101903	1.1019035	1.1019036
0.6	1.150163	1.150137	1.1501374	1.1501375
0.8	1.196692	1.196711	1.1967114	1.1967015
1.0	–	–	1.2417477	1.2417699
1.2	1.285257	1.285363	1.2853630	1.2853701
1.4	–	–	1.3276675	1.3276669
1.6	10368641	1.368758	1.3687582	1.3687579
1.8	–	–	1.4087264	1.4087310
2.0	1.447617	1.447651	1.4476526	1.4476519

4.3 Analysis of Results

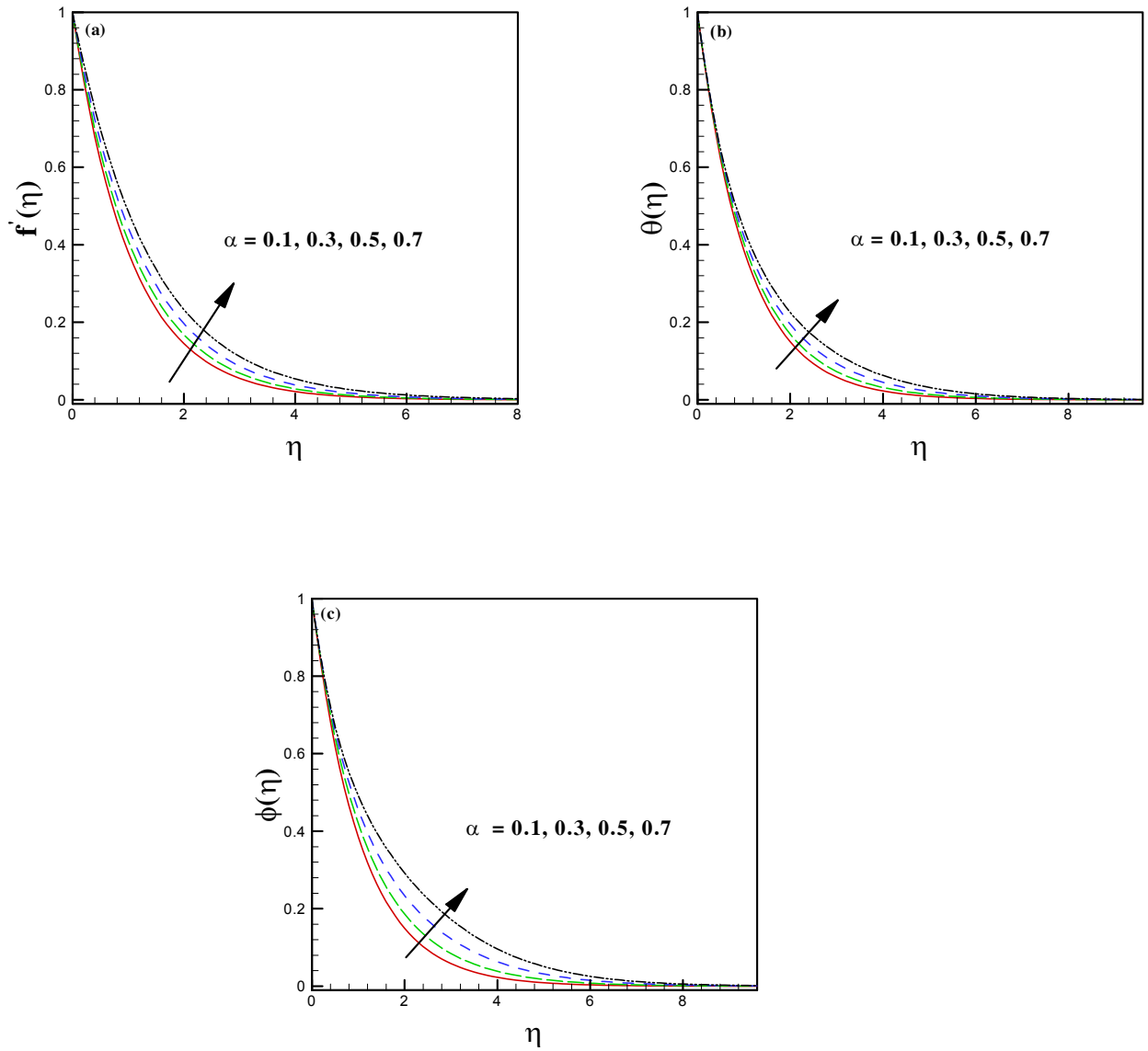
In this section of the chapter we are discussing the physical interpretation of various parameters which are involved in our non linear differential equations (4.8 – 4.10) along with associated boundary conditions mentioned in Eqs. (4.11) and (4.12). We have employed the homotopy analysis method (HAM) to explore the impact of physical parameters on flow, thermal and concentration distributions of Burgers fluid. The impact of all essential physical parameters is explored and discussed with complete physical understandings and the pertained outcomes are depicted in Figs. 4.2 – 4.9. We examined the effects for the constraints of curvature (α), fluid relaxation time (β_1), material parameter of Burgers fluid (β_2), fluid retardation time (β_3) and magnetic force (M) on flow $f'(\eta)$, thermal $\theta(\eta)$ and concentration $\phi(\eta)$ distributions of Burgers fluid while, the impact of Prandtl number (Pr) and heat source/sink (δ) are seen on thermal curves and impact of Lewis number (Le) is noted on solutal curves of the Burgers magneto fluid. Scales of involved parameters are fixed to find the convergence of the solutions i.e., $\alpha = 0.7$, $\beta_1 = 0.65$, $\beta_2 = 0.25$, $\beta_3 = 0.41$, $M = 0.5$, $Pr = 4.0$, $\delta = 2.0$, $Le = 2.0$ during the overall simulations and some are mentioned in Figs. (4.2 – 4.9).

We deliberate the complete physical interpretation to behaviors of involved parameters. Firstly, we have depicted Figs. 4.2(a – c) to observe the impact of curvature parameter (α) against flow, temperature and solutal distributions of Burgers fluid. Through these Figs., it is assessed that the flow curves of the fluid become higher for larger curvature parameter. The reason is that the radius of the cylinder shrinks by enhancing the curvature and as a result interaction region of fluid with the geometry also become limited. Hence, diminution is produced in the resistance due to exterior and ultimately the fluid velocity and the associated thickness

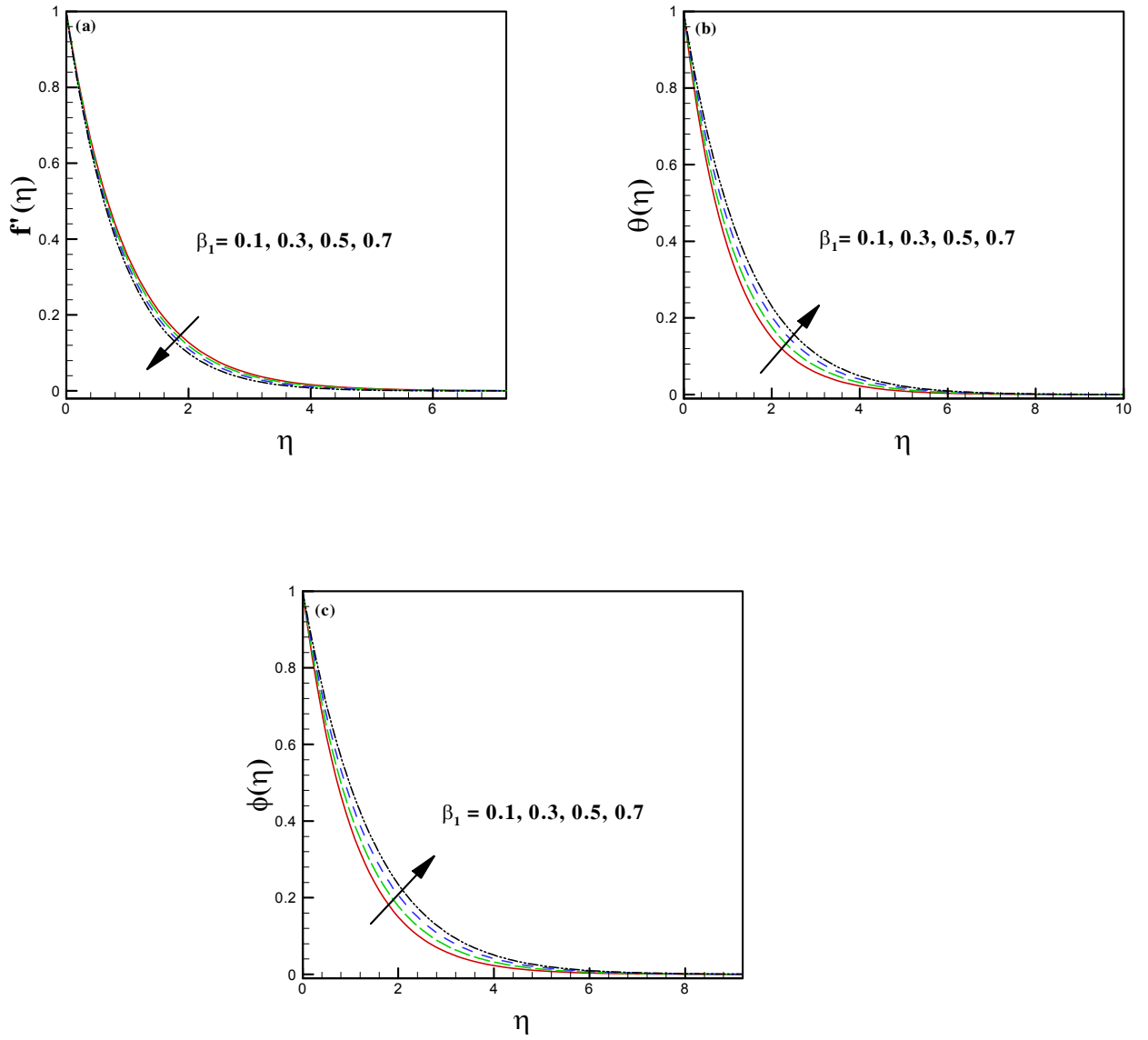
of boundary layer build up. Also, an upsurge is noted in thermal and solutal curves of Burgers fluid due to intensifying the values of curvature parameter. The impact of fluid relaxation time (β_1) against flow, temperature and concentration curves is depicted through Figs. 4.3(a – c). We scrutinized that the larger values of β_1 leads to diminish the flow profile as well as the thickness of the momentum boundary layer of Burgers fluid. Whereas, at the other hand, thermal and solutal curves of Burgers fluid build up for escalating magnitude of fluid relaxation time parameter. Physically, β_1 is dependent upon the relaxation time (λ_1) and an escalation in the Deborah number (β_1) corresponds to augmentation in the fluid relaxation time which means that fluid motion opposes with greater effects and consequently, the flow curves of the Burgers liquid become the victim of diminution in their strength. Furthermore, due to intensification in Deborah number (β_1) an escalation in fluid relaxation time is produced which leads to increase the interface among fluid elements and finally, the thermal as well as solutal energy transport rises in the flow of Burgers fluid. We analyzed that the range of values for β_1 can be selected between 0.1 to 0.7. Figs. 4.4(a – c) disclose the influence of material parameter of Burgers fluid (β_2) against flow, thermal and concentration distributions of Burgers fluid. Attenuation in the flow curves and velocity boundary layer thickness is perceived by enlarging the magnitude of β_2 however, an augmentation is noted in the variation of thermal and concentration profile of Burgers liquid for varying scales of Burgers fluid parameter. To highlight the influence of fluid retardation time parameter β_3 on flow, temperature and solutal profiles of Burgers fluid we have inserted Figs. 4.5(a – c). Increasing trend (contrary to β_1) of the flow distribution is assessed for varying scales of fluid retardation time constraint (β_3) while, diminution in the thermal and solutal transport of energy is detected for higher magnitude of β_3 . We know that β_3 is dependent to retardation time (λ_3). So that λ_3 also rises due to rise in β_3 and

consequently, the burgers fluid flow is accelerated, and fluid velocity enhances. Additionally, augmentation in Deborah number β_3 is accountable for diminishing behavior of temperature curves and thermal boundary layer thickness. Furthermore, practically it is detected that our non-Newtonian viscoelastic fluid model reduced in viscous fluid model in two situations. i.e, (i) $\lambda_1 = \lambda_2 = \lambda_3$ (ii) $\lambda_2 = 0$ and $\lambda_1 = \lambda_3$. That means that in first situation the fluid relaxation time, Burgers fluid parameter and fluid retardation time all become equal and in second case it elaborates that Burgers fluid parameter vanishes and relaxation time become equal to retardation time then in these two cases current model will reduce into Newtonian fluid model and the case that $\lambda_2 = 0$ corresponds that Burgers model will reduce into Oldroyd-B fluid model and the situation that $\lambda_2 = \lambda_3 = 0$ describes that Burgers fluid model will be reduced into Maxwell viscoelastic fluid model. Additionally, we came to know that the flow distribution has completely converse influences for relaxation time β_1 when compared by fluid retardation time β_3 . To enlighten the stimulus of magnetic force parameter (M) on velocity, thermal and concentration contours we have portrayed Figs. 4.6(a – c). It is analyzed from these graphs that thermal boundary conditions are asymptotically satisfied and flow pattern of the Burgers fluid is significantly affected and depicts the reducing behavior by escalating the extent of magnetic force parameter (M). Actually, when we intensify the effect of magnetic force parameter then a drag force is generated in larger extent which oppose the flow motion of the liquid and hence the velocity of the liquid deteriorates. Additionally, it is perceived that the thermal and solutal energy transport in the flow of Burgers fluid is decline for higher extent of magnetic parameter. Basically, larger magnetic parameter is responsible for the stronger Lorentz force and this force ultimately leads to develop the thermal as well as the solutal profile of the Burgers liquid. Note that, here $M \neq 0$ is corresponds to hydromagnetic flow situation

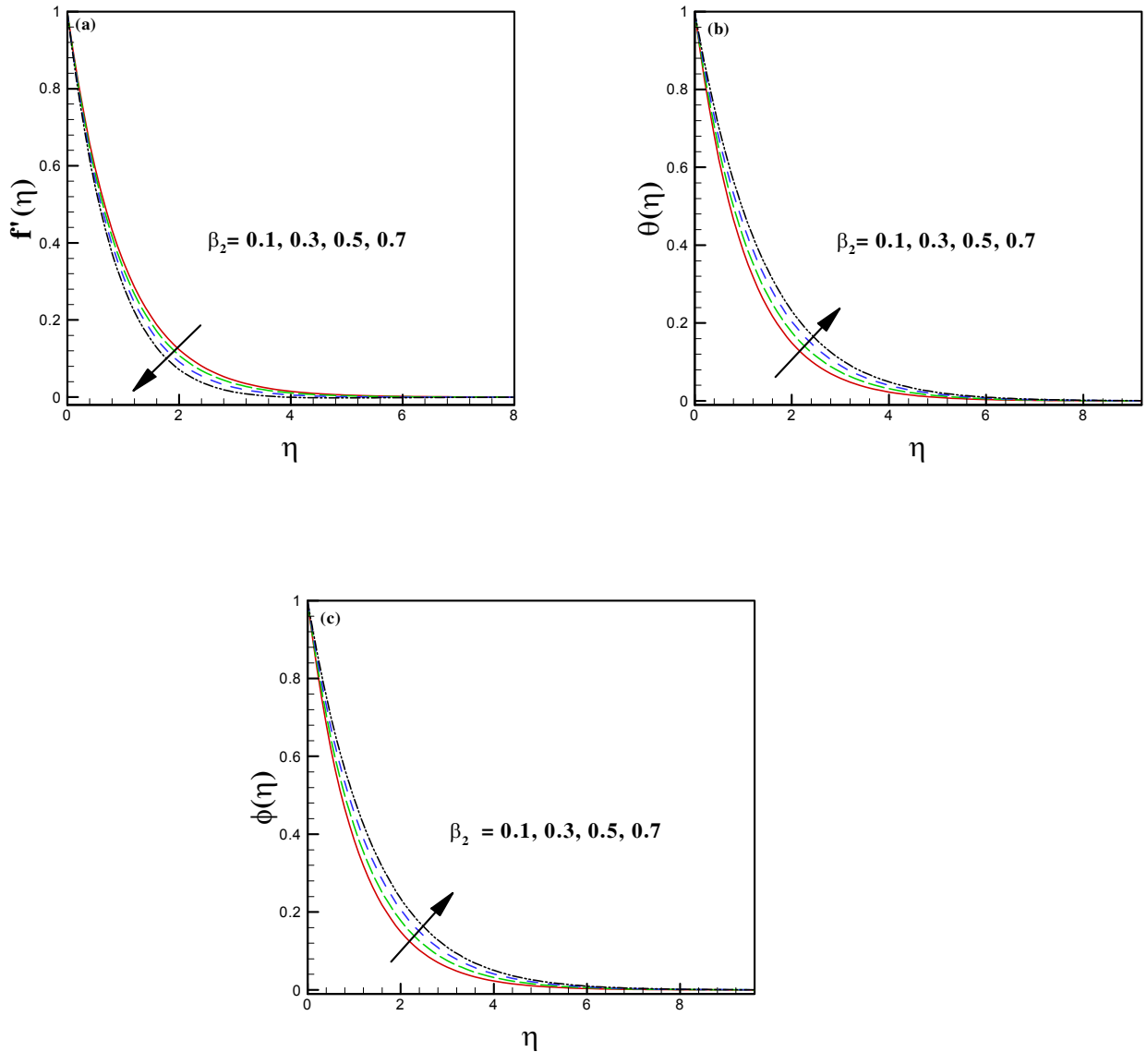
and $M = 0$ classifies as the hydrodynamic flow pattern. We analyzed that the range of M can be taken in between 1.0 to 10.0. To disclose the temperature features of Burgers fluid against the Prandtl number (Pr) we have drafted Fig. 4.7(a). Through this Fig., it is inspected that the thermal contours of the magneto Burgers liquid descend for varying extent of Prandtl number. Physically, Prandtl number is the function of thermal diffusivity and is inversely proportional to the Pr . So that we can easily assess that higher extent of Prandtl number leads to diminish the temperature diffusion coefficient and due to this reason thermal profile of Burgers liquid deteriorates and temperature thickness of the boundary layer also declines. It is realized that the range of Prandtl number can be chosen between 1.0 to 12.0. The stimulus of Lewis number (Le) against solutal curves of Burgers liquid is delineated in Fig. 4.7(b). It is inferred that the concentration rate and solutal boundary layer thickness lessen for enlarged scales of Lewis number (Le). As Lewis number is the fraction of mass and momentum diffusion coefficients and has inverse relation to the mass diffusivity. Thus, an intensification in Lewis number corresponds to a decrease in diffusion which ultimately leads to diminish the concentration rate and the solutal thickness of the boundary layer of the Burgers fluid. Figs. 4.8(a, b) disclose the temperature characteristics for the effects of heat source/sink constraint. It is investigated that the thermal curves of Burgers liquid depict ascending trend for heat source parameter ($\delta > 0$) while depict descending behavior for heat sink constraint ($\delta < 0$). Its reason is simple, i.e, when effect of any source of heat is augmented in the system the surely more quantity of heat sums up in the system due to which thermal distribution of the fluid ascends and in contrast to this when we escalate the values of heat sink constraint then more amount of heat waves leave the system then obviously temperature of the system depreciates. We observed that the range of heat source can be taken between 1.0 to 8.0 for the present investigation.



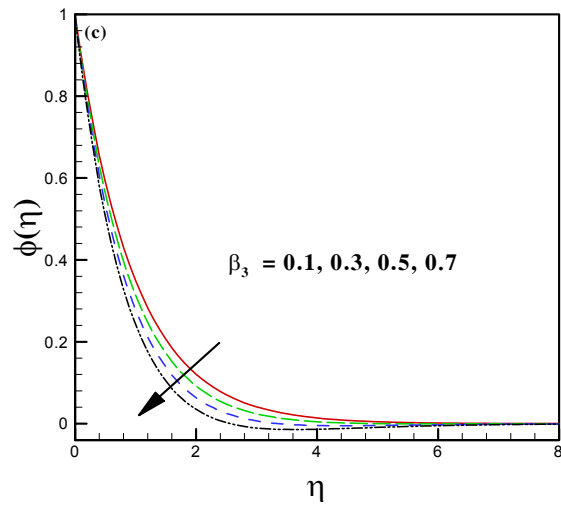
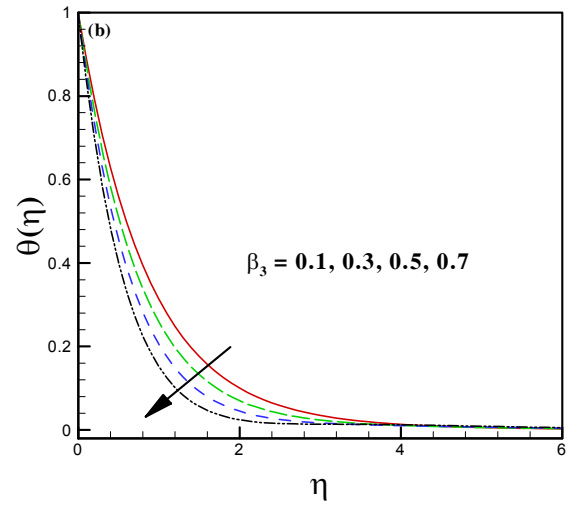
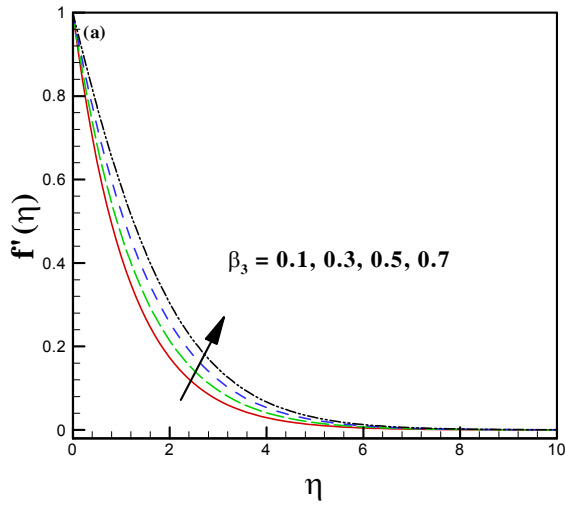
Figs. 4.2(a – c): Impact of α on f', θ and ϕ .



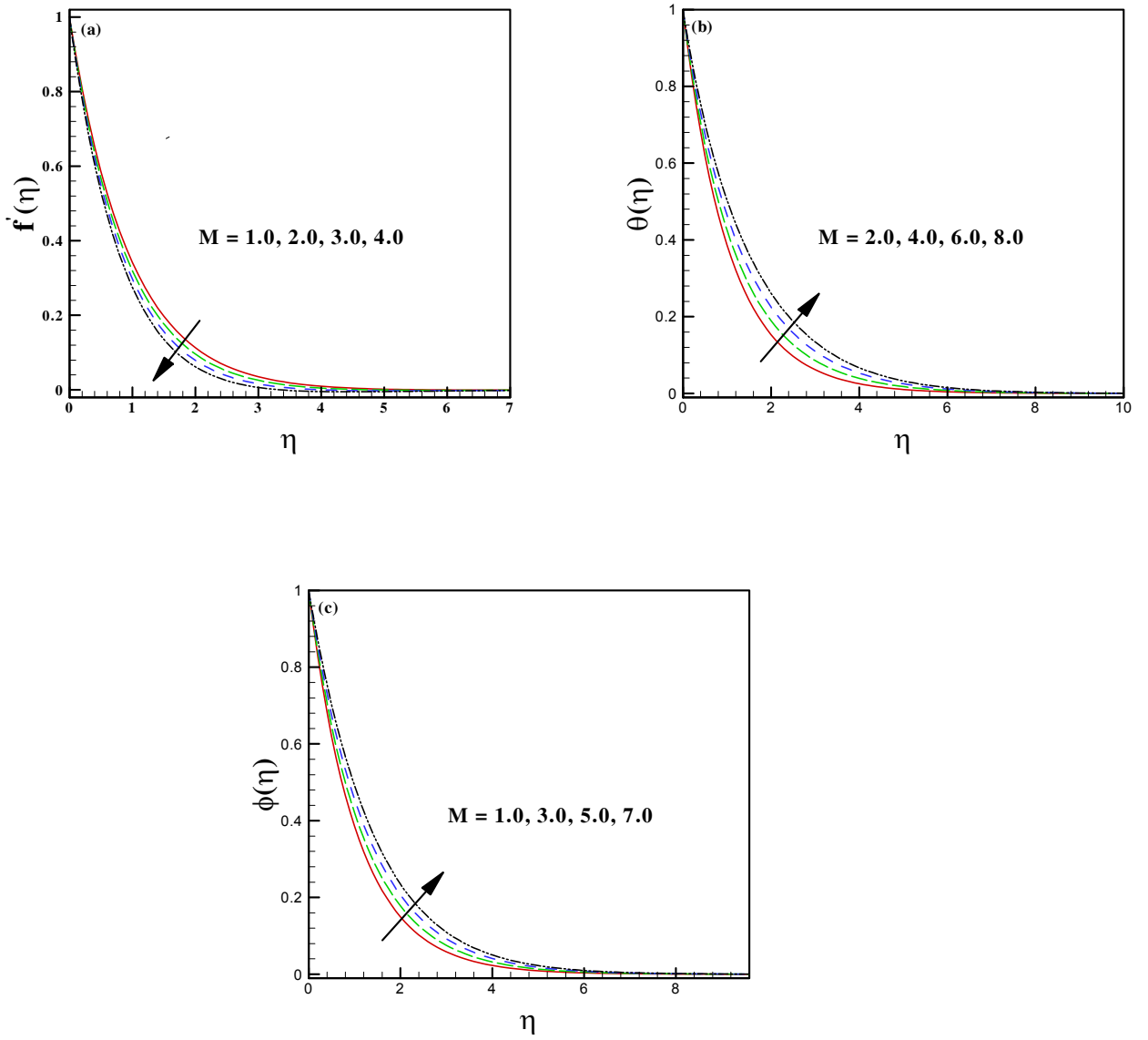
Figs. 4.3(a – c): Effect of β_1 on f' , θ and ϕ .



Figs. 4.4(a – c): Effect of β_2 on f' , θ and ϕ .



Figs. 4.5(a – c): Effect of β_3 on f' , θ and ϕ .



Figs. 4.6(a – c): Impact of M on f' , θ and ϕ .

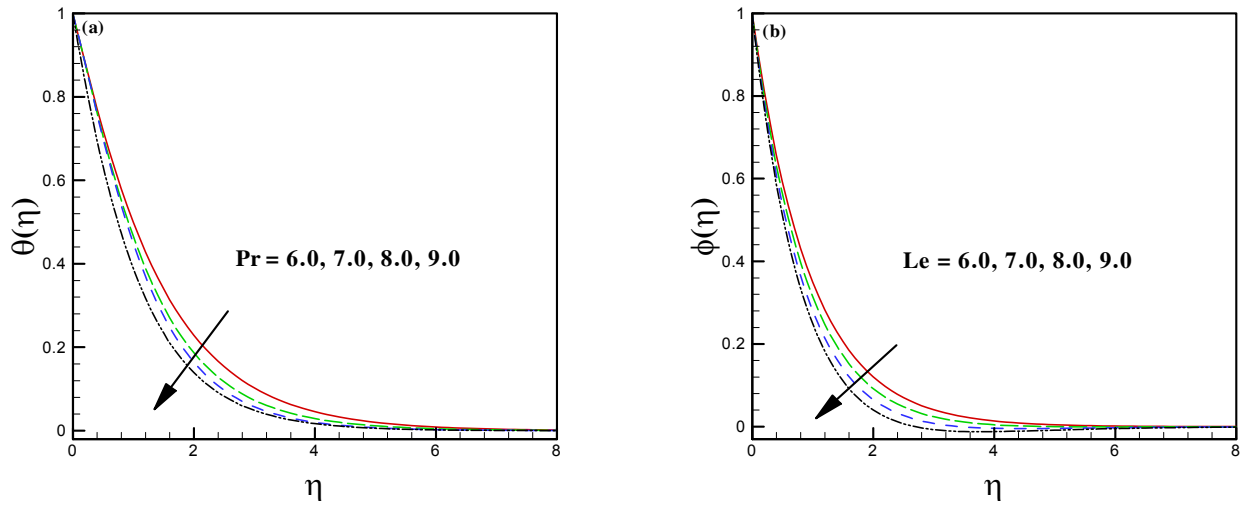
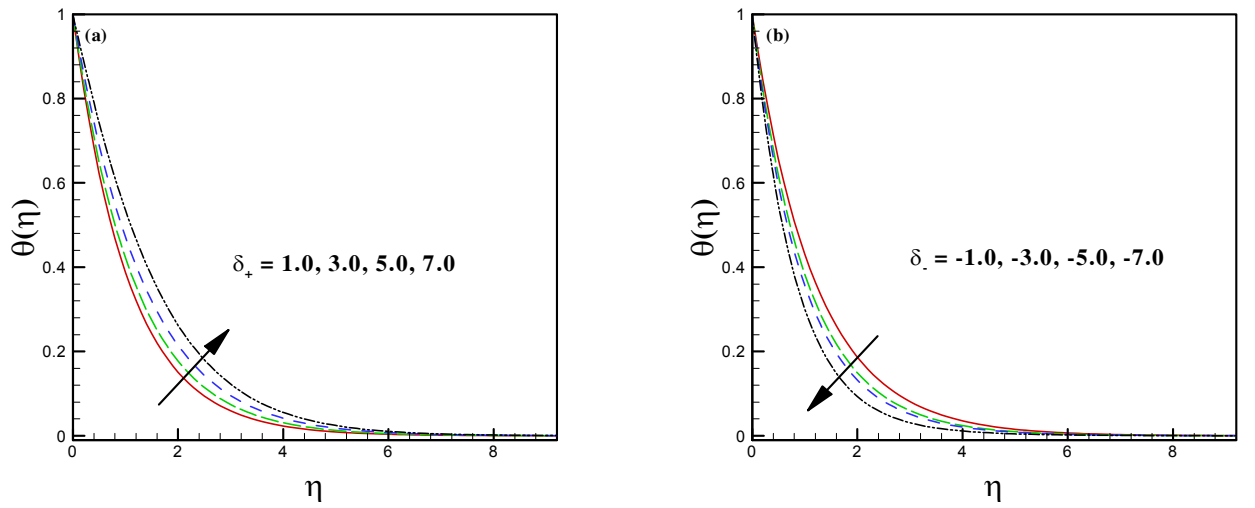


Fig. 4.7(a, b): Influence of Pr and Le on thermal and solutal profile.



Figs. 4.8(a, b): Influence of heat rise ($\delta > 0$) and heat sink ($\delta < 0$) against thermal profiles.

Chapter 5

Stagnation point flow of magnetized Burgers nanofluid subject to thermal radiation

This chapter explores the impact of non linear thermal radiation on magnetohydrodynamics MHD flow of Burgers nanofluid induced by stretching cylinder. The effects of thermal radiation and chemical reaction are also taken into account to investigate the heat and mass transportation in flow of Burgers fluid. Mathematical formulation is obtained by utilizing boundary layer theory and then similarity transformations are introduced to alter the governing partial differential equations into set of ordinary differential equations. The solutions of velocity, thermal and solutal equations are attained by adopting homotopy analysis method (HAM). Thermophysical properties of numerous physical parameters on flow, thermal and solutal profiles are depicted in graphs and outcomes are explained with realistic judgements. The essential physical declaration of obtained outcomes explore that the flow profile of Burgers nanofluid boosts up for growing values of velocity ratio parameter. Additionally, it is noticed that the thermal and solutal boundary layers of magneto Burgers nanofluid become more thicker for augmented values of Burgers material parameter while contrasting behavior is observed for retardation time parameter. Moreover, it is assessed that thermal profile and thermal thickness of boundary layer of nanofluid

enhance for growing values of temperature ratio parameter and radiation parameter. Also, it is explored that the solutal thickness of Burgers fluid weakens for positively increasing values of chemical reaction parameter.

5.1 Mathematical Formulation

In present problem we are dealing with steady 2D incompressible flow of magneto Burgers nanofluid. Moreover, we consider that the flow is induced by a stretching cylinder having radius R near a stagnation point. Let cylindrical polar coordinates (r, z) are taken to be in such an approach that z – axis taken along the axis of the cylinder and r – axis is taken along the radial direction as demonstrated through Fig. 4.1 (cf. Chapter 4). The velocity field for present flow is considered as $\mathbf{V} = [u, 0, w]$. Here u and w are taken as the velocity components along r and z axis respectively. Flow equation of Burgers nano liquid over a stretching cylinder is modelled incorporated with uniform magnetic field $B = [B_0, 0, 0,]$ applied perpendicular to the flow direction. Additionally, the energy equation is modelled incorporating with the characteristics of non linear thermal radiation. While nano particles and chemical reactions are also considered to model the concentration equation. Furthermore, it is presumed that the cylinder is stretched along z –direction with velocity $w = \frac{U_0 z}{l}$, here U_0 is considered as reference velocity and l the specific length. Moreover, it is presumed that the temperature and concentration at the wall of the cylinder is (T_w, C_w) respectively.

By adopting above assumptions in equations (2.1 – 2.3) (cf. Chapter 2), the continuity equation and momentum equation, respectively, for the current flow analysis are given by

$$\frac{\partial u}{\partial r} + \frac{u}{r} + \frac{\partial w}{\partial z} = 0, \quad (5.1)$$

$$\begin{aligned}
& u \frac{\partial w}{\partial r} + w \frac{\partial w}{\partial z} + \lambda_1 \left[u^2 \frac{\partial^2 w}{\partial r^2} + w^2 \frac{\partial^2 w}{\partial z^2} + 2uw \frac{\partial^2 w}{\partial z \partial r} \right] \\
& + \lambda_2 \left[\begin{aligned}
& u^3 \frac{\partial^3 w}{\partial r^3} + w^3 \frac{\partial^3 w}{\partial z^3} + 2u^2 \left(\frac{\partial u}{\partial r} \frac{\partial^2 w}{\partial r^2} + \frac{\partial w}{\partial r} \frac{\partial^2 w}{\partial r \partial z} \right) - u^2 \left(\frac{\partial w}{\partial r} \frac{\partial^2 u}{\partial r^2} + \frac{\partial w}{\partial z} \frac{\partial^2 w}{\partial r^2} \right) \\
& + 2w^2 \frac{\partial u}{\partial z} \frac{\partial^2 w}{\partial r \partial z} + w^2 \left(\frac{\partial w}{\partial z} \frac{\partial^2 w}{\partial z^2} - \frac{\partial w}{\partial r} \frac{\partial^2 u}{\partial z^2} \right) + 3uw \left(u \frac{\partial^3 w}{\partial r^2 \partial z} + w \frac{\partial^3 w}{\partial z^2 \partial r} \right) \\
& + 2uw \left(\frac{\partial u}{\partial r} \frac{\partial^2 w}{\partial z \partial r} + \frac{\partial u}{\partial z} \frac{\partial^2 w}{\partial r^2} + \frac{\partial w}{\partial r} \frac{\partial^2 w}{\partial z^2} - \frac{\partial w}{\partial r} \frac{\partial^2 u}{\partial r \partial z} \right)
\end{aligned} \right] \\
& = w_e \frac{\partial w_e}{\partial r} + \nu \lambda_3 \left[\begin{aligned}
& u \frac{\partial^3 w}{\partial r^3} + w \frac{\partial^3 w}{\partial r^2 \partial z} + \frac{u}{r} \frac{\partial^2 w}{\partial r^2} - \frac{\partial w}{\partial r} \frac{\partial^2 u}{\partial r^2} + \frac{w}{r} \frac{\partial^2 w}{\partial r \partial z} \\
& - \frac{1}{r} \frac{\partial u}{\partial r} \frac{\partial w}{\partial r} - \frac{1}{r} \frac{\partial w}{\partial r} \frac{\partial w}{\partial z} - \frac{\partial w}{\partial z} \frac{\partial^2 u}{\partial r^2}
\end{aligned} \right] \\
& + \nu \left[\frac{\partial^2 w}{\partial r^2} + \frac{1}{r} \frac{\partial w}{\partial r} \right] - \frac{\sigma B_0^2}{\rho} \left[\begin{aligned}
& (w - w_e) + \lambda_1 u \frac{\partial w}{\partial r} + \\
& \lambda_2 \left(w \frac{\partial u}{\partial z} \frac{\partial w}{\partial r} - u \frac{\partial w}{\partial z} \frac{\partial w}{\partial r} + uw \frac{\partial^2 w}{\partial r \partial z} + w^2 \frac{\partial^2 w}{\partial r^2} \right)
\end{aligned} \right]. \quad (5.2)
\end{aligned}$$

By adopting current assumptions, the heat transport and mass transport equations for nanofluids (1.7) and (1.10) (cf. Chapter 1), we arrived at the following PDEs

$$u \frac{\partial T}{\partial r} + w \frac{\partial T}{\partial z} = \alpha_1 \frac{1}{r} \left[\frac{\partial}{\partial r} \left(r \frac{\partial T}{\partial r} \right) \right] - \frac{1}{(\rho c)_f} \frac{\partial q_r}{\partial r} + \tau \left[D_B \frac{\partial C}{\partial r} \frac{\partial T}{\partial r} + \frac{D_T}{T_\infty} \left(\frac{\partial T}{\partial r} \right)^2 \right], \quad (5.3)$$

$$u \frac{\partial C}{\partial r} + w \frac{\partial C}{\partial z} = \frac{D_B}{r} \frac{\partial}{\partial r} \left(r \frac{\partial C}{\partial r} \right) + \frac{D_T}{T_\infty} \frac{1}{r} \frac{\partial}{\partial r} \left(r \frac{\partial T}{\partial r} \right) - k_1 (C - C_\infty), \quad (5.4)$$

with boundary conditions

$$w = w_s = \frac{U_0 z}{l}, \quad u = 0, \quad T = T_w, \quad C = C_w \quad \text{at } r = R, \quad (5.5)$$

$$w \rightarrow w_e = \frac{U_\infty z}{l}, \quad \frac{\partial w}{\partial r} \rightarrow 0, \quad T \rightarrow T_\infty, \quad C \rightarrow C_\infty \quad \text{as } r \rightarrow \infty. \quad (5.6)$$

Here (u, w) are the components of velocity in r and z directions, respectively, ν the kinematics viscosity, λ_1 the relaxation time, λ_2 the material parameter of Burgers fluid, $\lambda_3 (\leq \lambda_1)$ the retardation time, (T, C) the liquid temperature and concentration respectively, (T_∞, C_∞)

the ambient temperature and the ambient concentration, D_B the diffusion coefficient, w_s the stretching velocity, w_e the free stream velocity, and $\alpha_1 = \left(\frac{k}{(\rho c)_f}\right)$ the thermal diffusivity, in which (ρ_f, c_f) is the density of liquid and specific heat respectively, and k the thermal conductivity of the liquid.

By utilizing the transformations mentioned in equation (4.7) (cf. Chapter 4), equation (5.1) satisfied automatically and equations (5.2) – (5.5) yield

$$\begin{aligned}
& (1 + 2\alpha\eta)^3 f''' + (1 + 2\alpha\eta)^2 [ff'' - (f')^2] + (1 + 2\alpha\eta)^2 \beta_1 [2ff'f'' - f^2f'''] - 4\alpha^2\beta_2 f''' f'' \\
& - (1 + 2\alpha\eta)^2 \beta_2 [3f^2(f'')^2 + 2f(f')^2 f'' - f^3 f^{iv}] + 4\alpha\beta_3 (1 + 2\alpha\eta)^2 ff''' - (1 + 2\alpha\eta) \alpha\beta_1 f^2 f'' \\
& + (1 + 2\alpha\eta) \alpha\beta_2 [3f^2 f' f'' + f^3 f'''] + 2\alpha (1 + 2\alpha\eta)^2 f'' + (1 + 2\alpha\eta)^3 \beta_3 [(f'')^2 - ff^{iv}] \\
& + (1 + 2\alpha\eta)^2 A^2 - (1 + 2\alpha\eta)^2 M^2 [-A + \beta_2 ff''' - \beta_1 ff'' + f'] = 0, \tag{5.7}
\end{aligned}$$

$$\begin{aligned}
& [\{R_d(1 + \theta(\theta_w - 1))^3\}\theta' (1 + 2\alpha\eta)]' + \text{Pr} \theta' f + \text{Pr} N_b \phi' \theta' (1 + 2\alpha\eta) + \text{Pr} N_t \theta'^2 (1 + 2\alpha\eta) = 0, \\
& \tag{5.8}
\end{aligned}$$

$$(1 + 2\alpha\eta) \phi'' + 2\alpha\phi' + Le \text{Pr} f \phi' + (1 + 2\alpha\eta) \left(\frac{N_t}{N_b}\right) \theta'' + 2\alpha \left(\frac{N_t}{N_b}\right) \theta' - Le \text{Pr} k_1 \phi = 0. \tag{5.9}$$

The transformed boundary conditions are as follows

$$f = 0, f' = 1, \theta = 1, \phi = 1 \text{ at } \eta = 0, \tag{5.10}$$

$$f' \rightarrow A, f'' \rightarrow 0, \theta \rightarrow 0, \phi \rightarrow 0 \text{ as } \eta \rightarrow \infty, \tag{5.11}$$

where $A = \frac{U_\infty}{U_0}$ is the velocity ratio parameter, U_∞ the velocity of free stream, U_0 the stretching velocity of the cylinder. Moreover, the curvature parameter α , Deborah numbers β_1 and β_3 , Burgers fluid parameter β_2 , magnetic parameter M , Prandtl number Pr , Lewis number Le ,

Chemical reaction parameter k_1 , Radiation parameter R_d , Temperature ratio parameter θ_w , Thermophoresis parameter N_t and Brownian motion parameter N_b are defined as follows:

$$\begin{aligned}\alpha &= \frac{1}{R} \sqrt{\frac{\nu l}{U_0}}, \quad \beta_1 = \lambda_1 \frac{U_0}{l}, \quad \beta_3 = \lambda_3 \frac{U_0}{l}, \quad \beta_2 = \lambda_2 \left(\frac{U_0}{l}\right)^2, \\ M &= \left(\frac{\sigma l B_0^2}{\rho_f U_0}\right)^{1/2}, \quad Le = \frac{\alpha_1}{D_B}, \quad Pr = \frac{\nu}{\alpha_1}, \quad k_1 = \frac{k_c l}{U_0}, \quad \theta_w = \left(\frac{T_w}{T_\infty}\right), \\ R_d &= \frac{16\sigma T_\infty^3}{3kk^*}, \quad N_t = \frac{\tau D_T (T_w - T_\infty)}{\nu T_\infty}, \quad N_b = \frac{\tau D_B (C_w - C_\infty)}{\nu}.\end{aligned}\tag{5.12}$$

5.2 Physical Concern Parameters

Relations for the rate of heat transfer (Nu_z) and rate of mass transport (Sh_z) are

$$Nu_z = \frac{z q_s}{k(T_w - T_\infty)}, \quad Sh_z = \frac{z j_s}{D_B(C_w - C_\infty)},\tag{5.13}$$

where q_s and j_s are the heat and mass flux respectively

$$q_s = -k \left(\frac{\partial T}{\partial r}\right)_{r=R} - \frac{16\sigma T^3}{3k^*} \left(\frac{\partial T}{\partial r}\right)_{r=R}, \quad j_s = -D_B \left(\frac{\partial C}{\partial r}\right)_{r=R}.\tag{5.14}$$

The dimensionless form of Eq. (5.13) is given by

$$Nu_z Re^{-\frac{1}{2}} = -\left(1 + \frac{4}{3} (R_d(1 + (\theta_w - 1)\theta(0)))^3 \theta'(0)\right), \quad Sh_z Re^{-\frac{1}{2}} = -\phi'(0).\tag{5.15}$$

where $Re_z = \frac{w_s z}{\nu}$ is the local Reynolds number.

5.3 Solution Convergence

We used homotopy analysis method written in section (1.3.2) (cf. Chapter 1) which always gives convergent solutions. This segment is proposed to discuss the convergence of such analytical solutions which contain auxiliary parameters (\hbar_f, \hbar_θ and \hbar_ϕ). It is compulsory to mention that convergence of the homotopic results can be adjusted by these influential parameters (\hbar_f, \hbar_θ and \hbar_ϕ). The accompanying value of these assisting parameters is assessed by employing least square error which is given by

$$F_{f,m} = \frac{1}{N+1} \sum_{j=0}^N \left[N_f \sum_{i=0}^m F_j(i\Delta\eta) \right]^2. \quad (5.16)$$

To verify authentication of the convergence of these analytic results, Table 5.1 is inserted. From which it is clear that convergence of velocity accomplished at 20th order of approximation, whereas convergence for thermal and solutal profiles attained at 22nd order of approximations. Also we have plotted the \hbar curves in Fig. 5.2 upto 14th order of approximation for the present investigation. It can be seen from Fig. 5.2 that the acceptable interval for \hbar is $-1.2 \leq \hbar \leq -0.7$.

Table 5.1: Convergence of homotopic results for $\alpha = 0.2$, $\beta_1 = 0.65$, $\beta_2 = 0.25$, $\beta_3 = 0.45$, $N_t = 0.5$, $N_b = 0.6$, $R_d = 0.5$, $\theta_w = 0.4$, $A = 0.5$, $M = 0.5$, $\text{Pr} = 5.0$, $k_1 = 0.7$, $Le = 0.5$.

No of approximations	$-f''(0)$	$-\theta'(0)$	$-\phi'(0)$
1	-0.5000708	-0.9621234	-0.9976667
5	-0.4999938	-0.8492961	-1.007009
10	-0.4990878	-0.7652028	-1.037145
12	-0.4984736	-0.7424222	-1.049929
15	-0.4972827	-0.7159114	-1.067577
19	-0.4963091	-0.7087028	-1.072900
20	-0.4963091	-0.7021749	-1.077916
22	-0.4963091	-0.7021749	-1.077916

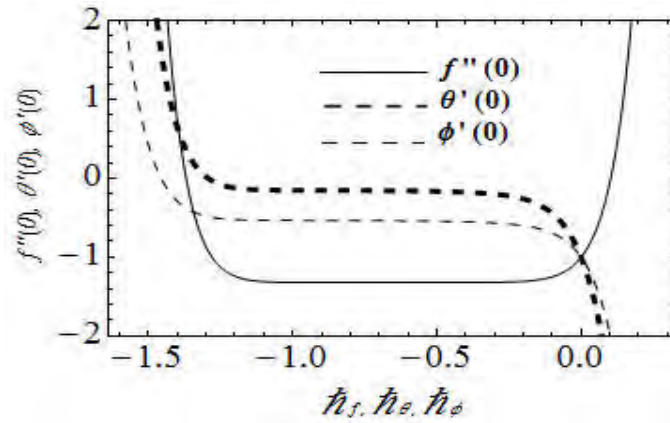


Fig. 5.1: The \hbar curves for 14th order of approximation.

5.4 Physical Analysis of Results

The analytical solutions of coupled non linear ordinary differential equations (5.7 – 5.9) with boundary conditions given in Eqs. (5.10) and (5.11) have been obtained by homotopy analysis method (HAM). In order to analyze the effects of varying values of pertinent physical parameters on velocity, thermal and solutal profiles this section is proposed. We investigated the physical behavior of all involved dimensionless parameters, for instance, relaxation time parameter β_1 , Burgers fluid parameter β_2 , retardation time parameter β_3 , magnetic parameter M , velocity ratio parameter A , curvature parameter α , radiation parameter R_d , temperature ratio parameter θ_w , Brownian motion parameter N_b , thermophoresis parameter N_t , Prandtl number Pr , Lewis number Le and chemical reaction parameter k_1 on velocity $f'(\eta)$, thermal $\theta(\eta)$ and solutal $\phi(\eta)$ profiles, which are depicted through Figs. (5.2 – 5.12). We have put the following fixed values for leading parameters such as $\alpha = 0.2$, $\beta_1 = 0.65$, $\beta_2 = 0.25$, $\beta_3 = 0.45$, $N_t = 0.5$, $N_b = 0.6$, $R_d = 0.5$, $\theta_w = 0.4$, $A = 0.5$, $M = 0.5$, $Pr = 5.0$, $k_1 = 0.7$, $Le = 0.5$, during the entire computations.

We discuss the impact of each parameter with complete logic as follows. Initially, Figs. 5.2(a – b) are drafted to envision the stimulus of velocity ratio parameter (A) towards velocity and thermal profiles of Burgers fluid. Fig. 5.2(a) interprets the increasing trend of velocity distribution for both cases $A > 1$ and $A < 1$ while the momentum boundary layer thickness shows reverse trend for $A > 1$ (when the free stream velocity is larger than the stretching velocity of the cylinder) as compared with $A < 1$ (when the free stream velocity is lower than the the stretching velocity of the cylinder). From this Fig., it is also exposed that boundary layer is not achieved for $A = 1$ because the fluid particles and boundary of the cylinder moves with

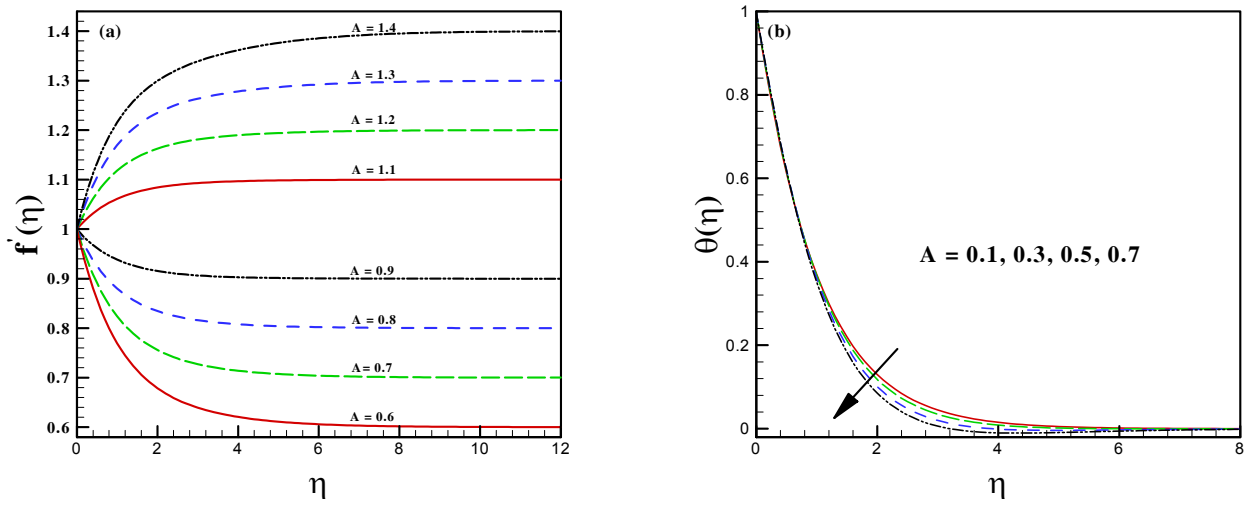
same velocity. Physically, augmentation in A corresponds to the higher free stream velocity which is responsible for an intensification in the velocity of fluid. Fig. 5.2(b) shows that temperature profile of Burgers liquid diminishes for $A < 1$. The characteristics of temperature ratio parameter against thermal profile of nano Burgers liquid are delineated in Fig. 5.3. This Fig. demonstrates that the temperature profile and associated thickness of the boundary layer of Burgers liquid boosts for intensifying values of temperature ratio parameter (θ_w). Actually, it is due to the fact that an increase in θ_w enhances the thermal state of the fluid consequently the temperature of the fluid increases. To visualize the effects of thermophoresis parameter (N_t) against thermal and solutal distributions of nano Burgers fluid Figs. 5.4(a, b) are drafted. It is scrutinized that temperature and nano particles volume fraction of Burgers liquid enhance due to growth in N_t . Additionally, it is seen that momentum and solutal boundary layers become more thicker for increasing values of N_t . These findings relate with physical phenomenon of thermophoresis, i.e, the particles which are heated moves from hotter regions towards colder regions and consequently the fluid temperature grows up. Figs. 5.5(a, b) disclose the characteristics of Brownian motion parameter (N_b) against temperature and solutal profiles. It is seen that thermal profile and thickness of thermal boundary layer enhances by increasing values of N_b . At the other hand, solutal profile and solutal boundary layer thickness of nano Burgers liquid diminish by enhancing N_b . Physically, intensification in N_b corresponds to enhance the kinetic energy of nanoparticles within the liquid which lead to rise the rate of heat transfer and boundary layer thickness and consequently temperature field of Burgers liquid increases. Moreover, Brownian motion controls the diffusion of the nanoparticles in the regime away from the boundary. Hence enlargement of Brownian motion parameter results in decrease of nano particles volume fraction profile. Figs. 5.6(a – c) demonstrate the stimulus of curvature

parameter (α) against flow, thermal and concentration profiles. It is exposed that the flow velocity as well as nano particles volume fraction profiles of Burgers nano liquid enhances for progressive values of α . Also it is noted that momentum, thermal and solutal thicknesses of boundary layer improve with augmented values of α . The reason behind this is the radius of curvature deteriorates due to which the interaction space of the cylinder with the fluid declines. As a result, resistance occurred by the exterior decreases, hence the flow profile and momentum boundary layer thickness of Burgers fluid enhance. Moreover, it is analyzed that the higher values of α boost both the thermal profile and associated thickness of boundary layer. It is due to the reason that amount of heat transport rises which result in rise of thermal and nano particles volume fraction profiles of Burgers nano fluid. Figs. 5.7(*a-c*) are drafted to enlighten the effects of β_2 (Burgers fluid parameter) against velocity, thermal and nano particles volume fraction distributions. It is explored that the velocity and associated boundary layer thickness of Burgers nano fluid reduce with intensification in β_1 whereas reverse trend is being noticed for thermal and solutal profiles. Actually, relaxation time enhances with an intensification in Deborah number, as a result resistance in fluid motion rises which causes to diminish the velocity profile. Moreover, when β_2 enhances the relaxation time also enhances due to which collision between fluid elements increases consequently thermal and concentration distributions of the nano liquid boost. Furthermore, it is observed that if $\lambda_1 = \lambda_2 = \lambda_3$ or $\lambda_2 = 0$ and $\lambda_1 = \lambda_3$ in both cases our work reduce to Newtonian fluid model and when $\lambda_2 = 0$ our model reduces to Oldroyd B fluid model and when $\lambda_2 = \lambda_3 = 0$ our model reduces to Maxwell fluid model. Further, it is noticed that due to presence of relaxation and retardation times we examined that velocity has totally reverse effects for β_1 and β_2 as compared with β_3 . Figs. 5.8(*a, b*) demonstrate the influences of chemical reaction parameters (k_1) against concentration

distribution of Burgers nano liquid for both positive and negative values. From these graphs it is inferred that nano particles volume fraction decreases and associated boundary layer becomes more thinner for increasing values of $k_1 > 0$. In contrast of this, it is observed that solutal profile of Burgers nano liquid builds up and thickness of boundary layer improves with intensification in values of $k_1 < 0$. It is because of the reason that strong chemical reaction parameter ($k_1 > 0$) corresponds to decline the mass transfer and enhances for higher values of $k_1 < 0$. Figs. 5.9(a, b) are depicted to envision the characteristics of Prandtl number (Pr) and Lewis number (Le) towards temperature and solutal profiles respectively. Diminution in thermal distribution of nano Burgers liquid is presumed for increasing values of Prandtl number. At the other hand the thermal boundary layer thickness also becomes thinner for higher Pr . It is due to the fact that Pr depends upon thermal diffusivity which becomes weaker for higher Prandtl number. Obviously, weaker thermal diffusivity results in falloff of the temperature profile and also the thermal boundary layer thickness reduces. Additionally, as Lewis number is the ratio of mass diffusivity and momentum diffusivity and is inversely proportional to the mass diffusion coefficient. Thus an intensification in Lewis number leads to decrease the diffusion which results in a decline of mass of nano particles volume fraction and solutal boundary layer thickness. To highlight the effects of radiation parameter (R_d) against temperature distribution of Burgers nanofluid, Fig. 5.10 is inserted. It is scrutinized that the thermal profile of nano liquid builds up and thermal thickness of boundary layer improves for larger number of R_d . It is because of the reason that more heat is generated within the liquid due to increase in R_d which corresponds to boosts up the temperature profile of nanoliquid.

The variation in dimensionless Nusselt number $Re^{\frac{-1}{2}} Nu$ against distinct values of Brownian motion parameter (N_b) and thermophoresis parameter (N_t) is plotted in Fig. 5.11(a). It is

seen that magnitude of heat transport rate is boosts up with rise in N_b and in N_t . It means that the rate of heat transfer at that boundary enhances for augmenting values of N_b and N_t . Additionally, Fig. 5.11(b) is inserted to envision the impacts of Brownian motion parameter (N_b) and Prandtl number (Pr) against the rate of heat transport at the boundary. It is noticed that the amount of heat transfer at the surface rises for higher values of Pr and N_b . Fig. 5.12 is portrayed to highlight the variations of N_b and Le for dimensionless sherwood number. It is found that rate of mass transport decreases for varying effects of N_b and Le . Table 5.2 is an assessment table of $-f''(0)$ for distinct values of M with some studies. As a consequence, from this table, we are guaranteed that the recent outcomes are very accurate.



Figs. 5.2(a, b): Impact of velocity ratio parameter (A) on velocity and temperature fields.

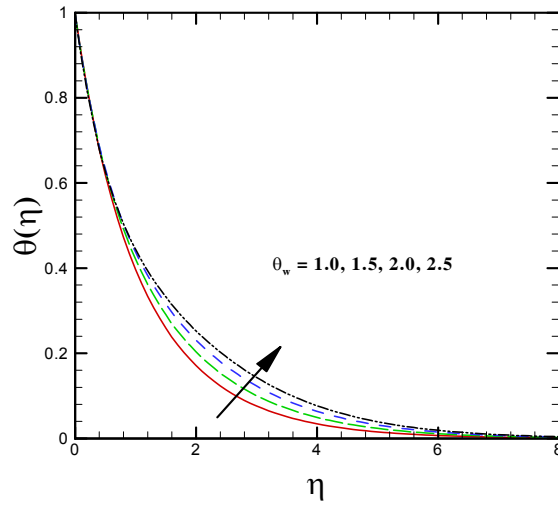
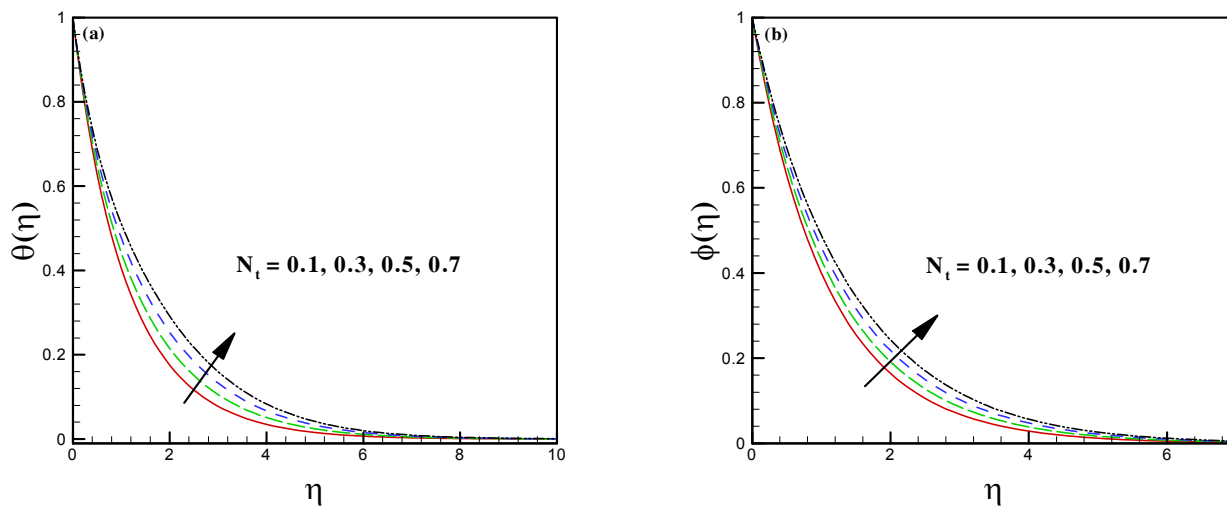
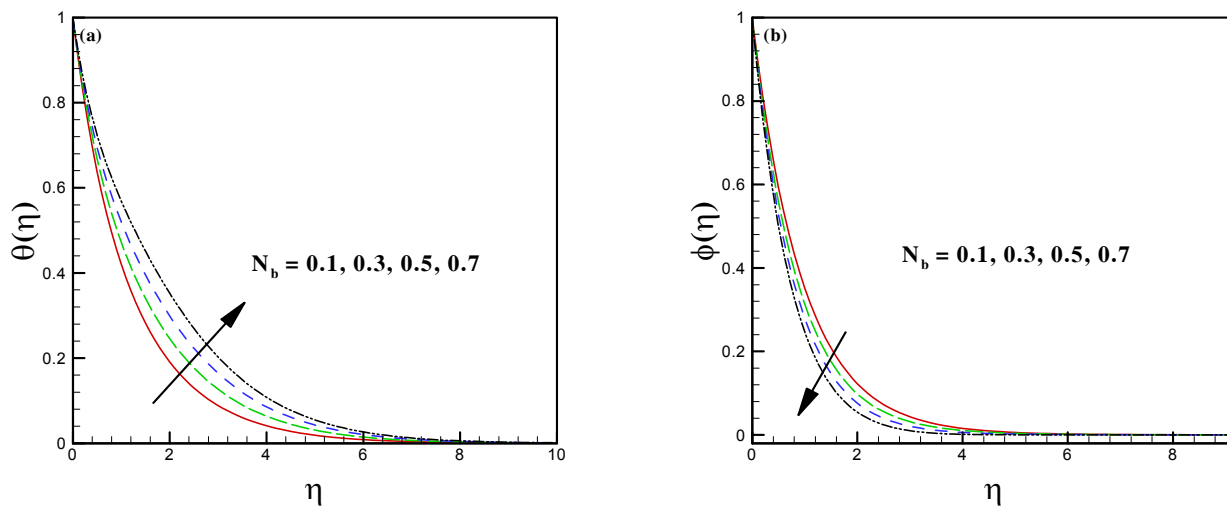


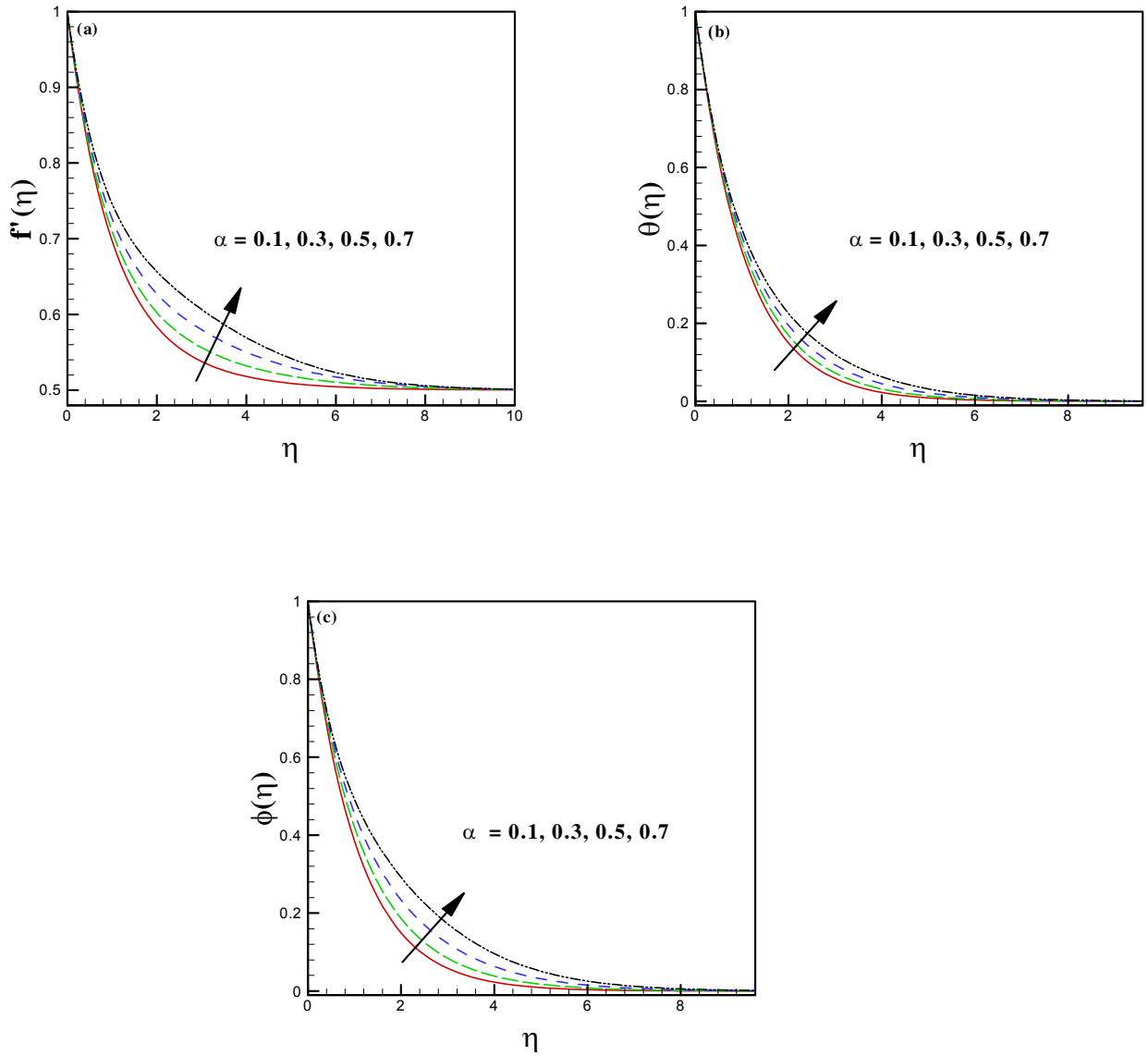
Fig. 5.3: Impact of temperature ratio parameter (θ_w) on temperature field.



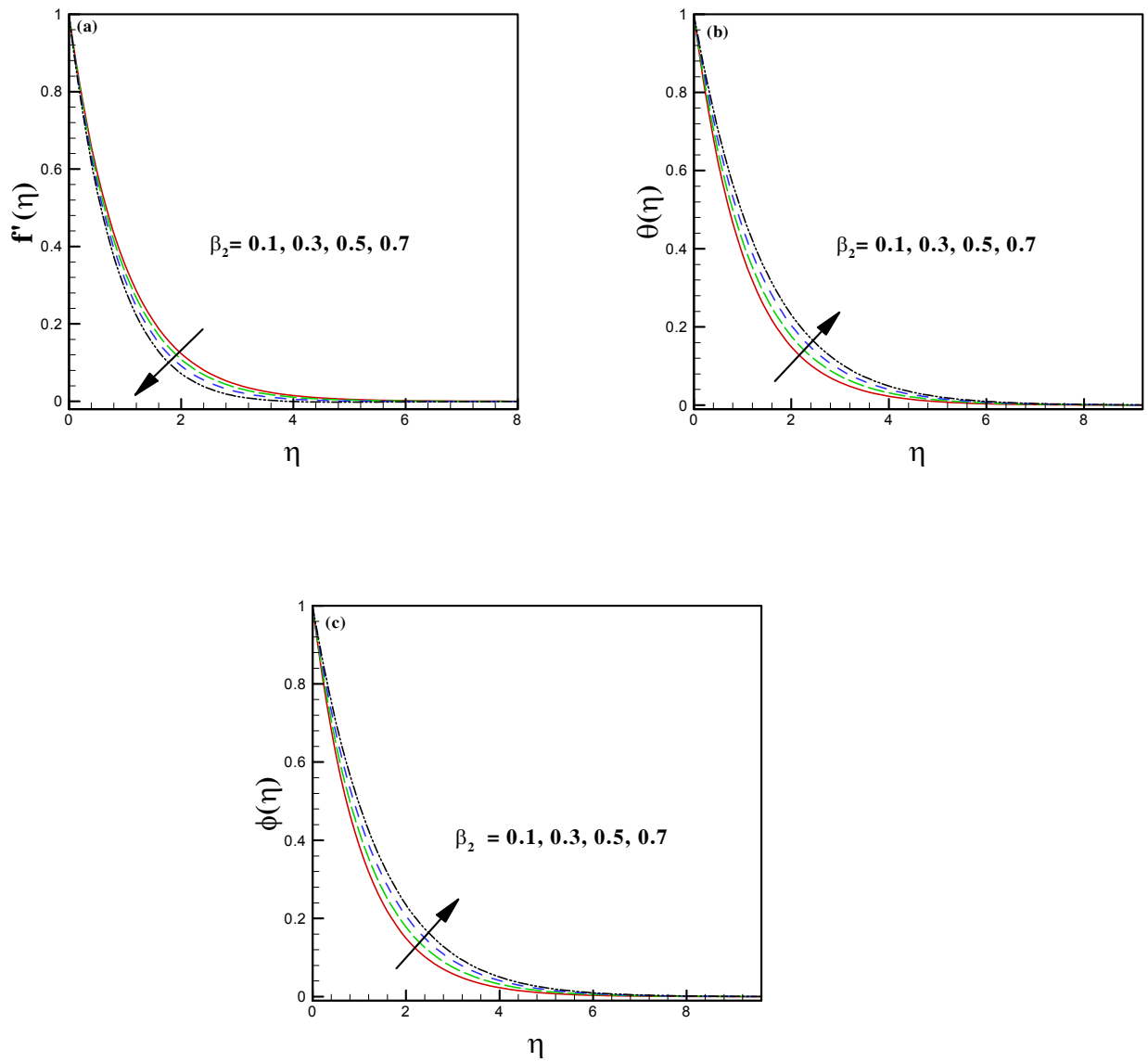
Figs. 5.4(a, b): Variation of N_t on thermal and solutal profiles.



Figs. 5.5(a, b): Impact of N_b on thermal and solutal profiles.



Figs. 5.6(a – c): Impact of α on flow, thermal and solutal profiles.



Figs. 5.7(a – c): Impact of β_2 on flow, thermal and solutal profiles.

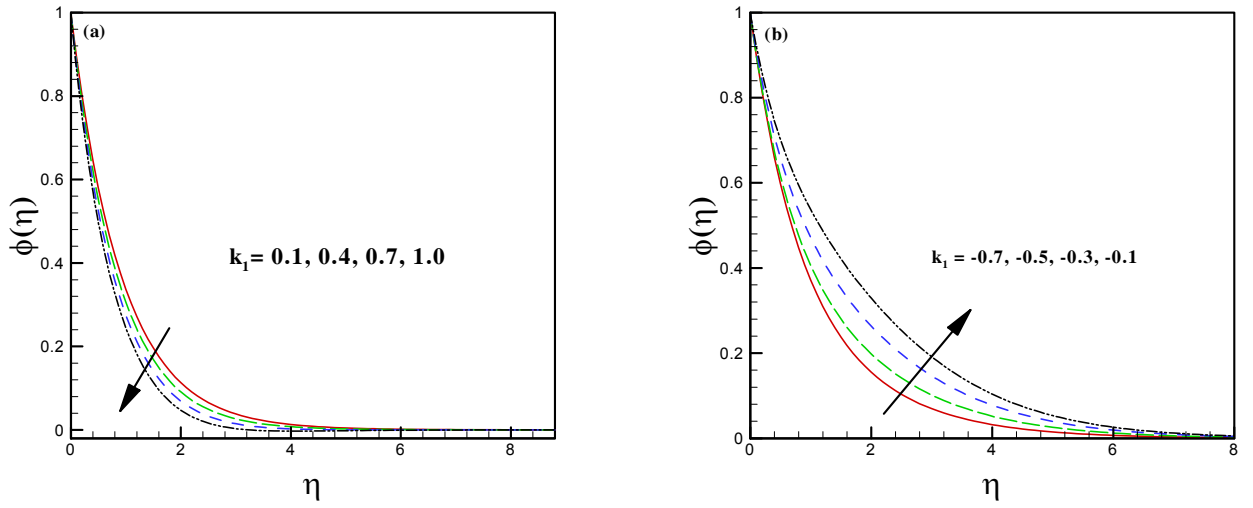
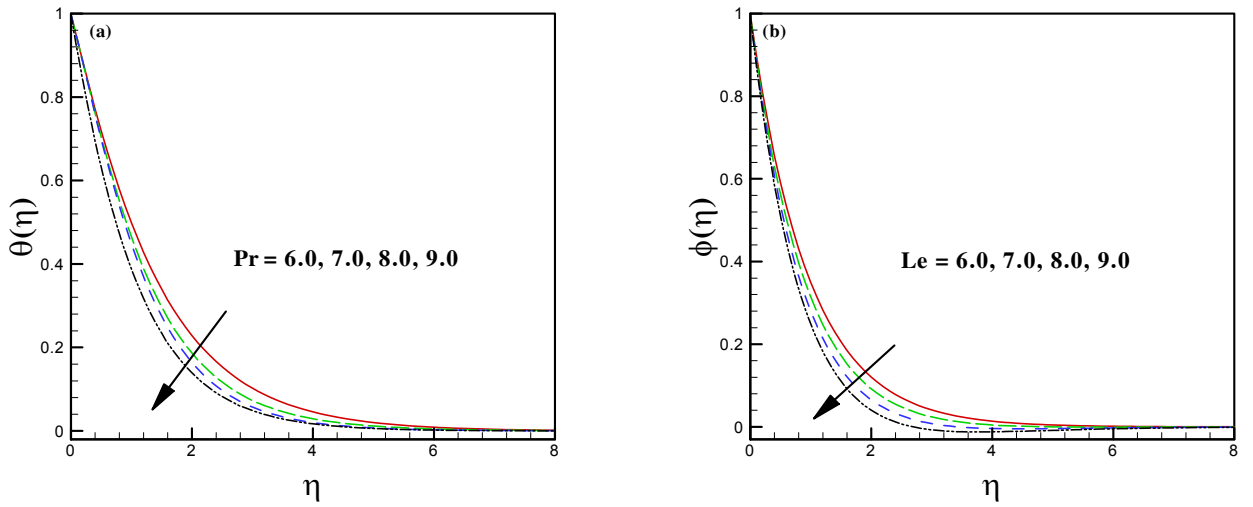


Fig. 5.8(a, b): Impact of k_1 on concentration profile.



Figs. 5.9(a, b): Impact of Pr on thermal profile and Le on concentration profile.

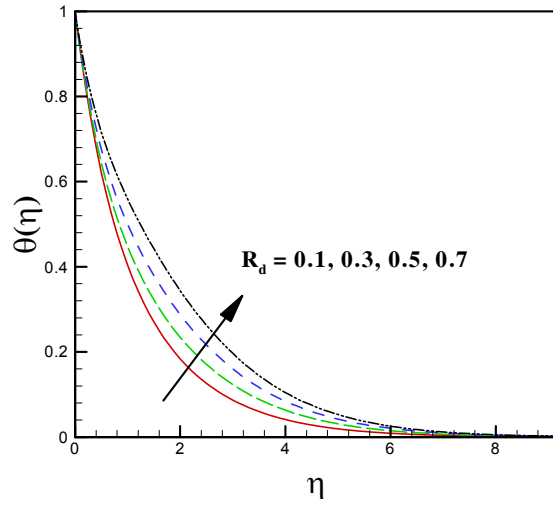


Fig. 5.10: Impact of R_d on thermal profile.

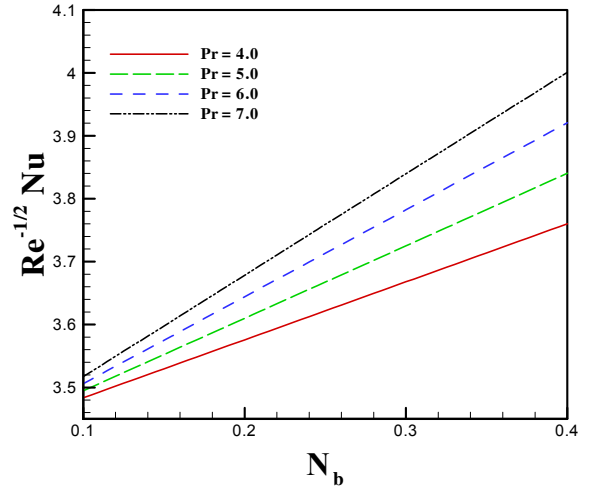
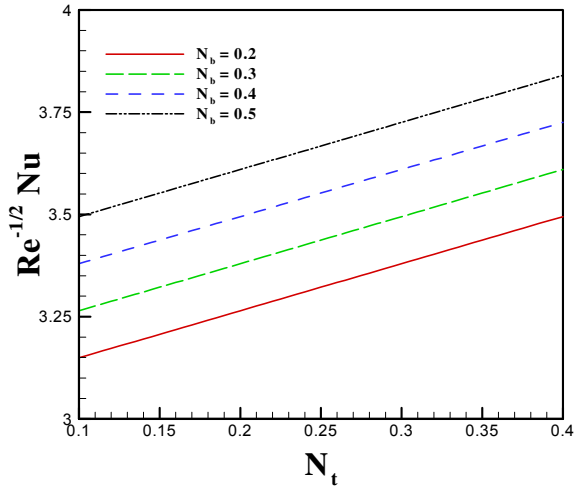


Fig. 5.11(a, b): (a) Impact of N_t and N_b on Nusselt number (b) Impact of N_b and Pr on Nusselt number.

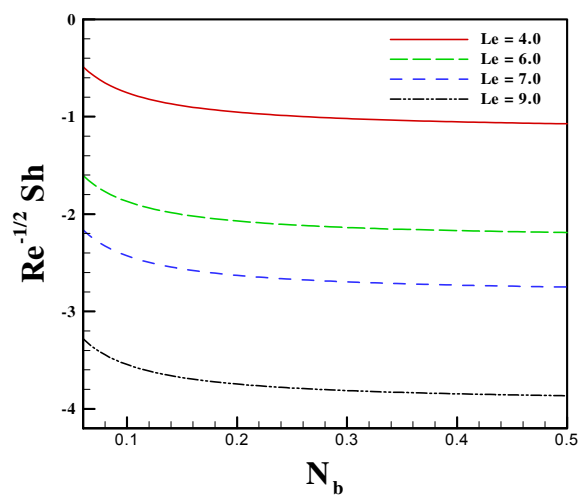


Fig. 5.12: Impact of N_b and L_e on Sherwood number.

Table 5.2: A comparison table for values of $-f''(0)$ for different values of M when $\alpha = \beta_2 = \beta_3 = \beta_1 = A = 0$.

M	Shehzad <i>et al.</i> [142]	Hayat <i>et al.</i> [143]	Present study
0.0	1.00000	1.00000	1.000000
0.2	1.01980	1.01980	1.019801
0.5	1.11803	1.11803	1.118029
0.8	1.28063	1.28063	1.280633
1.0	1.41421	1.41421	1.414221
1.2	1.56205	1.56205	1.562048
1.5	1.80303	1.80303	1.803044

Chapter 6

Burgers fluid flow in perspective of Buongiorno's model with improved heat and mass flux theory over stretching cylinder

In this chapter, an effort is made to model the thermal conduction and mass diffusion phenomena in perspective of Buongiorno's model and Cattaneo-Christov theory for 2D flow of magnetized Burgers nanofluid due to stretching cylinder. Moreover, the impacts of Joule heating and heat source are also included to investigate the heat flow mechanism. Additionally, mass diffusion process in flow of nanofluid is examined by employing the influence of chemical reaction. Mathematical modelling of momentum, heat and mass diffusion equations is carried out in mathematical formulation section of the manuscript. Optimal homotopy analysis method (OHAM) in Wolfram Mathematica is utilized to analyze the effects of physical dimensionless constants on flow, temperature and solutal distributions of Burgers nanofluid. Graphical results are depicted and physically justified in results and discussion section. At the end of the manuscript the section of closing remarks is also included to highlight the main findings of this study. It is revealed that an escalation in thermal relaxation time constant leads to ascend the temperature

curves of nanofluid. Additionally, depreciation is assessed in mass diffusion process due to escalating amount of thermophoretic force constant.

6.1 Mathematical Formulation

We are considering a $2D$ axisymmetric flow of Burgers nanofluid with the effect of uniform magnetic field which is applied in direction normal to the flow. The flow under discussion is further considered as steady and incompressible. Moreover, it is assumed that the flow is conducted by stretching the boundary of the cylinder along z – *axis* with stretching velocity $w = \frac{U_0 z}{l}$. Here U_0 represents the reference velocity and l denotes the specific length. We are considering cylindrical polar coordinates (r, θ, z) to model the flow, temperature and concentration equations. Here, z – *axis* is taken along the axis of the cylinder while r – *axis* is considered along the normal to the flow direction, i.e, radial direction as depicted in Fig. 4.1 (cf. Chapter 4). Here, $\mathbf{V} = [u, 0, w]$ is taken as the velocity field for the flow where, u and w are represent the velocities along r and z directions, respectively, respectively. Furthermore, the flow of Burgers nanofluid is modelled in terms of uniform magnetic field of strength $\mathbf{B} = [B_0, 0, 0,]$. Additionally, the equation representing the heat transport in the flow of nanofluid is modelled by employing the Cattaneo-Christov heat flux in addition with the effects of Joule heating and heat source/sink. The concentration of nanoparticles is modelled by utilizing modified mass flux and the effect of chemical reaction. Furthermore, (T_w, C_w) are considered as the temperature and concentration at the wall of the cylinder respectively.

By utilizing above assumptions in equations (2.1 – 2.7) (cf. Chapter 2), the equation of continuity, flow, temperature and concentration equations for the present problem take the

subsequent forms

$$\frac{\partial u}{\partial r} + \frac{u}{r} + \frac{\partial w}{\partial z} = 0, \quad (6.1)$$

$$\begin{aligned} & u \frac{\partial w}{\partial r} + w \frac{\partial w}{\partial z} + \lambda_1 \left[u^2 \frac{\partial^2 w}{\partial r^2} + w^2 \frac{\partial^2 w}{\partial z^2} + 2uw \frac{\partial^2 w}{\partial z \partial r} \right] \\ + \lambda_2 & \left[u^3 \frac{\partial^3 w}{\partial r^3} + w^3 \frac{\partial^3 w}{\partial z^3} + 2u^2 \left(\frac{\partial u}{\partial r} \frac{\partial^2 w}{\partial r^2} + \frac{\partial w}{\partial r} \frac{\partial^2 w}{\partial r \partial z} \right) - u^2 \left(\frac{\partial w}{\partial r} \frac{\partial^2 u}{\partial r^2} + \frac{\partial w}{\partial z} \frac{\partial^2 w}{\partial r^2} \right) \right. \\ & \left. + 2w^2 \frac{\partial u}{\partial z} \frac{\partial^2 w}{\partial r \partial z} + w^2 \left(\frac{\partial w}{\partial z} \frac{\partial^2 w}{\partial z^2} - \frac{\partial w}{\partial r} \frac{\partial^2 u}{\partial z^2} \right) + 3uw \left(u \frac{\partial^3 w}{\partial r^2 \partial z} + w \frac{\partial^3 w}{\partial z^2 \partial r} \right) \right. \\ & \left. + 2uw \left(\frac{\partial u}{\partial r} \frac{\partial^2 w}{\partial z \partial r} + \frac{\partial u}{\partial z} \frac{\partial^2 w}{\partial r^2} + \frac{\partial w}{\partial r} \frac{\partial^2 w}{\partial z^2} - \frac{\partial w}{\partial r} \frac{\partial^2 u}{\partial r \partial z} \right) \right] \\ = \nu & \left[\frac{\partial^2 w}{\partial r^2} + \frac{1}{r} \frac{\partial w}{\partial r} \right] - \frac{\sigma B_0^2}{\rho} \left[\begin{array}{c} w + \lambda_1 u \frac{\partial w}{\partial r} + \\ \lambda_2 \left(w \frac{\partial u}{\partial z} \frac{\partial w}{\partial r} - u \frac{\partial w}{\partial z} \frac{\partial w}{\partial r} + uw \frac{\partial^2 w}{\partial r \partial z} + w^2 \frac{\partial^2 w}{\partial r^2} \right) \end{array} \right] \\ + \nu \lambda_3 & \left[\begin{array}{c} u \frac{\partial^3 w}{\partial r^3} + w \frac{\partial^3 w}{\partial r^2 \partial z} + \frac{u}{r} \frac{\partial^2 w}{\partial r^2} - \frac{\partial w}{\partial r} \frac{\partial^2 u}{\partial r^2} + \frac{w}{r} \frac{\partial^2 w}{\partial r \partial z} \\ - \frac{1}{r} \frac{\partial u}{\partial r} \frac{\partial w}{\partial r} - \frac{1}{r} \frac{\partial w}{\partial r} \frac{\partial w}{\partial z} - \frac{\partial w}{\partial z} \frac{\partial^2 u}{\partial r^2} \end{array} \right], \quad (6.2) \end{aligned}$$

$$\begin{aligned} & u \frac{\partial T}{\partial r} + w \frac{\partial T}{\partial z} - \tau \frac{D_t}{T_\infty} \left[\left(\frac{\partial T}{\partial r} \right)^2 + 2\lambda_t \left(u \frac{\partial T}{\partial r} \frac{\partial^2 T}{\partial r^2} + w \frac{\partial T}{\partial z} \frac{\partial^2 T}{\partial z^2} \right) \right] \\ - \tau D_b & \left[\frac{\partial C}{\partial r} \frac{\partial T}{\partial r} - \lambda_t \left(u \frac{\partial^2 T}{\partial r^2} \frac{\partial C}{\partial z} + u \frac{\partial^2 C}{\partial r^2} \frac{\partial T}{\partial r} + w \frac{\partial^2 T}{\partial r \partial z} \frac{\partial C}{\partial r} + w \frac{\partial^2 C}{\partial r \partial z} \frac{\partial T}{\partial r} \right) \right] \\ + \lambda_t & \left[u^2 \frac{\partial^2 T}{\partial r^2} + w^2 \frac{\partial^2 T}{\partial z^2} + 2uw \frac{\partial^2 T}{\partial r \partial z} + u \frac{\partial u}{\partial r} \frac{\partial T}{\partial r} + u \frac{\partial w}{\partial r} \frac{\partial T}{\partial z} + w \frac{\partial u}{\partial z} \frac{\partial T}{\partial r} + w \frac{\partial w}{\partial z} \frac{\partial T}{\partial z} \right] \\ = \alpha_1 & \left[\frac{1}{r} \frac{\partial}{\partial r} \left(\frac{\partial T}{\partial r} \right) \right] + \frac{Q_0}{\rho c_p} \left[(T - T_\infty) + \lambda_t \left(u \frac{\partial T}{\partial r} + w \frac{\partial T}{\partial z} \right) \right] \\ & + \frac{\sigma B_0^2}{\rho c_p} \left[w^2 + \lambda_t \left(2w^2 \frac{\partial w}{\partial z} + 2uw \frac{\partial u}{\partial r} \right) \right], \quad (6.3) \end{aligned}$$

$$\begin{aligned}
& u \frac{\partial C}{\partial r} + w \frac{\partial C}{\partial z} - \frac{D_t}{T_\infty} \left(\frac{\partial^2 T}{\partial r^2} + \frac{1}{r} \frac{\partial T}{\partial r} \right) + \lambda_c \left[\begin{aligned} & u^2 \frac{\partial^2 C}{\partial r^2} + w^2 \frac{\partial^2 C}{\partial z^2} + 2uw \frac{\partial^2 C}{\partial r \partial z} + u \frac{\partial u}{\partial r} \frac{\partial C}{\partial r} \\ & + u \frac{\partial w}{\partial r} \frac{\partial C}{\partial z} + w \frac{\partial u}{\partial z} \frac{\partial C}{\partial r} + w \frac{\partial w}{\partial z} \frac{\partial C}{\partial z} \end{aligned} \right] \\
& = D_b \left[\frac{\partial^2 C}{\partial r^2} + \frac{1}{r} \frac{\partial C}{\partial r} \right] + \lambda_c \frac{D_t}{T_\infty} \left(u \frac{\partial^3 T}{\partial r^3} + \frac{u}{r^2} \frac{\partial T}{\partial r} + \frac{u}{r} \frac{\partial^2 T}{\partial r^2} + w \frac{\partial^3 T}{\partial r^2 \partial z} + \frac{w}{r^2} \frac{\partial^2 T}{\partial r \partial z} \right) \\
& \quad - k_c \left[(C - C_\infty) + \lambda_c \left(u \frac{\partial C}{\partial r} + w \frac{\partial C}{\partial z} \right) \right], \tag{6.4}
\end{aligned}$$

with boundary conditions

$$w = w_s = \frac{U_0 z}{l}, \quad u = 0, \quad T = T_w, \quad C = C_w \quad \text{at } r = R, \tag{6.5}$$

$$w \rightarrow 0, \quad \frac{\partial w}{\partial r} \rightarrow 0, \quad T \rightarrow T_\infty, \quad C \rightarrow C_\infty \quad \text{as } r \rightarrow \infty. \tag{6.6}$$

Here ν is the kinematics viscosity, λ_1 the relaxation time, λ_2 the material parameter of Burgers fluid, λ_3 ($\leq \lambda_1$) the retardation time, (T, C) the liquid temperature and concentration respectively, (T_∞, C_∞) the ambient temperature and the ambient concentration, D_B the diffusion coefficient and $\alpha_1 = \left(\frac{k}{(\rho c)_f} \right)$ the thermal diffusivity, in which (ρ_f, c_f) are the density of liquid and specific heat respectively, and k the thermal conductivity of the liquid.

By adopting the dimensionless transformations depicted in Eq. (4.7) (cf. Chapter 4), Eq. (6.1) satisfied automatically and equations (6.2) – (6.4) yield

$$\begin{aligned}
& (1 + 2\alpha\eta)^2 \beta_1 \left[2ff'f'' - f^2f''' \right] - (1 + 2\alpha\eta) \alpha\beta_1 f^2 f'' + (1 + 2\alpha\eta)^3 f''' \\
& + (1 + 2\alpha\eta) \alpha\beta_2 \left[3f^2 f' f'' + f^3 f''' \right] + (1 + 2\alpha\eta)^2 \left[2\alpha f'' + f f'' - (f')^2 \right] \\
& - (1 + 2\alpha\eta)^2 \beta_2 \left[3f^2 (f'')^2 + 2f (f')^2 f'' - f^3 f^{iv} \right] - 4\alpha^2 \beta_2 f''' f'' \\
& + (1 + 2\alpha\eta)^3 \beta_3 \left[(f'')^2 - f f^{iv} \right] - 4\alpha\beta_3 (1 + 2\alpha\eta)^2 f f''' \\
& - (1 + 2\alpha\eta)^2 M^2 \left[\beta_2 f f''' - \beta_1 f f'' + f' \right] = 0, \tag{6.7}
\end{aligned}$$

$$\begin{aligned}
& (1 + 2\alpha\eta)\theta'' + 2\alpha\theta' + \Pr [\theta'f - \beta_t(f'f\theta' + f^2\theta'')] + \Pr \delta [\theta + \beta_t(f\theta')] \\
& + \Pr N_b \left[\phi' \theta' (1 + 2\alpha\eta) - \beta_t \{ 2\alpha f \theta' \phi' + (1 + 2\alpha\eta) (f\theta'' \phi' + f\theta' \phi'') \} \right] \\
& \Pr N_t \left[\theta'^2 (1 + 2\alpha\eta) - 2\beta_t \{ (1 + 2\alpha\eta) f\theta' \theta'' + \alpha f \theta'^2 \} \right] \\
& + 2\Pr MEc \left[f'^2 + \beta_1 (f'^3 - f f' f'') \right] = 0, \tag{6.8}
\end{aligned}$$

$$\begin{aligned}
& (1 + 2\alpha\eta)\phi'' + 2\alpha\phi' + Sc[f\phi' - \beta_c(f'f\phi' + f^2\phi'')] - Sck_1 [\phi + \beta_c(f\phi')] \\
& + \left(\frac{N_t}{N_b} \right) \left[(1 + 2\alpha\eta)\theta'' - \beta_c(f\theta''' - 4\alpha f\theta'') \right] = 0, \tag{6.9}
\end{aligned}$$

and transformed boundary conditions are as follows

$$f = 0, f' = 1, \theta = 1, \phi = 1 \text{ at } \eta = 0, \tag{6.10}$$

$$f' \rightarrow 0, f'' \rightarrow 0, \theta \rightarrow 0, \phi \rightarrow 0 \text{ as } \eta \rightarrow \infty. \tag{6.11}$$

Here, $M = \left(\frac{\sigma l B_0^2}{\rho_f U_0} \right)^{1/2}$ is the magnetic parameter, $\alpha \left(= \frac{1}{R} \sqrt{\frac{\nu l}{U_0}} \right)$ the curvature parameter, $\beta_1 \left(= \lambda_1 \frac{U_0}{l} \right)$ the fluid relaxation time constant, $\beta_3 \left(= \lambda_3 \frac{U_0}{l} \right)$ the fluid retardation time constant, $\beta_2 \left(= \lambda_2 \left(\frac{U_0}{l} \right)^2 \right)$ the Burgers fluid parameter, $\Pr \left(= \frac{\nu}{\alpha_1} \right)$ the Prandtl number, $Ec \left(= \frac{w^2}{c_p(T_w - T_\infty)} \right)$ the Eckert number, $\delta \left(= \frac{lQ_0}{U_0(\rho c_p)} \right)$ the heat source/sink parameter, $Sc \left(= \frac{\nu}{D_B} \right)$ the Schmidt number, $k_1 \left(= \frac{k_c l}{U_0} \right)$ the chemical reaction parameter, $N_t \left(= \frac{\tau D_T (T_w - T_\infty)}{\nu T_\infty} \right)$ the thermophoresis parameter and $N_b \left(= \frac{\tau D_B (C_w - C_\infty)}{\nu} \right)$ the Brownian motion parameter.

6.2 Validation of Optimal Homotopic Results

We computed several values of $-f''(0)$ for different magnitudes of β_1 and M in tables 6.1 and 6.2 respectively. These values are compared with already published studies and we find that our values are in good agreement with these studies which clarify that the used optimal homotopic approach is valid. The optimal convergence control parameters are chosen as $\hbar_f = -0.601$, $\hbar_\theta = -1.132$ and $\hbar_\phi = -0.901$.

Table 6.1: A comparison table for $-f''(0)$ for distinct scales of β_1 when $\alpha = \beta_2 = \beta_3 = M = 0$.

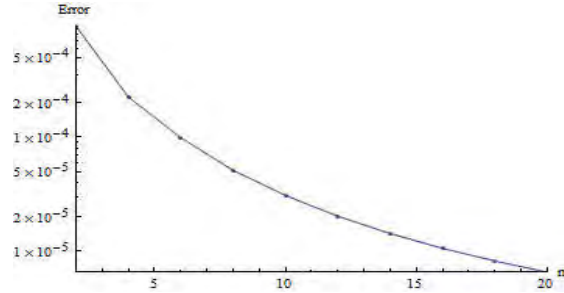
β_1	Abel <i>et al.</i> [139]	Irfan <i>et al.</i> [141]	Present study
0.0	1.00000	1.0000000	1.0000000
0.2	1.051948	1.0518890	1.0518799
0.4	1.101850	1.1019035	1.1019100
0.6	1.150163	1.1501374	1.1501368
0.8	1.196692	1.1967114	1.1967121
1.2	1.285257	1.2853630	1.2853578

Table 6.2: A comparison table for $-f''(0)$ for distinct scales of M when $\alpha = \beta_1 = \beta_2 =$

$\beta_3 = 0$.

M	Fathizadeh <i>et al.</i> [144]	Ahmed <i>et al.</i> [145]	Present study
0.5		1.224745	1.224739
1.0	1.41421	1.414213	1.414211
1.5			1.581028
2.0			1.731939
5.0	2.44948	2.449474	2.449396

The total residual error is (TRE) depicted in the following plot.



6.3 Physical Analysis of Results

We employed optimal homotopy analysis method (OHAM) to investigate the behaviors of physical parameters occur in ODEs (6.7 – 6.9) with associated boundary conditions (6.10) and (6.11).

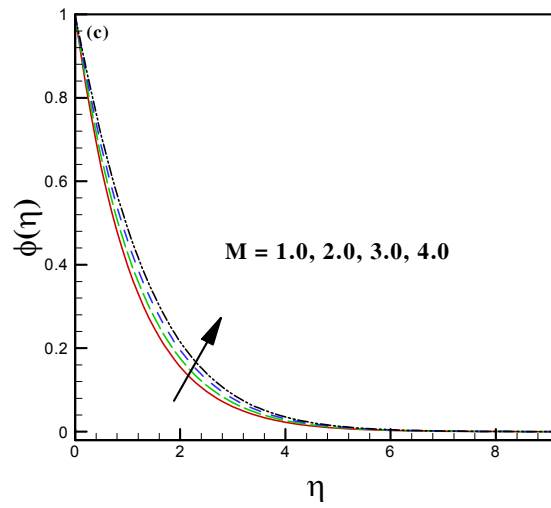
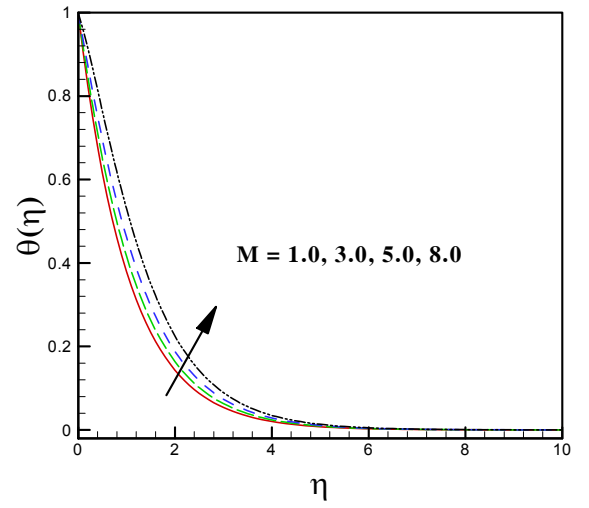
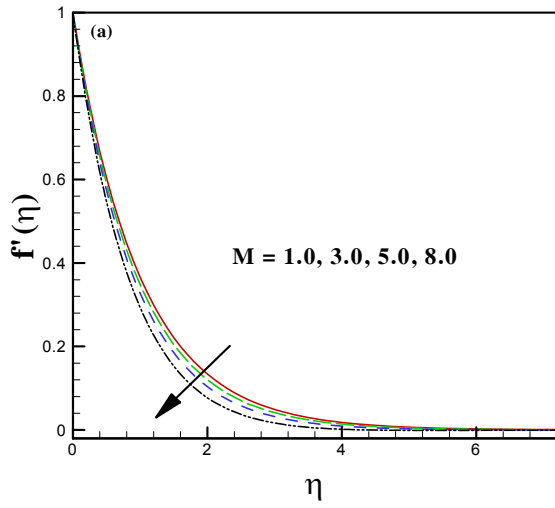
We checked the impact of involved parameters on velocity $f'(\eta)$, thermal $\theta(\eta)$ and solutal $\phi(\eta)$ distributions of Burgers nanofluid. The impact of physical parameters is depicted in the form of graphs and discussed with suitable arguments. Moreover fixed values are assigned to leading dimensionless parameters such as $\alpha = 0.25$, $\beta_1 = 0.75$, $\beta_2 = 0.3$, $\beta_3 = 0.5$, $N_t = 0.6$, $N_b = 0.4$, $\beta_t = 0.5$, $\beta_c = 0.4$, $Ec = 1.5$, $M = 2.0$, $\delta = 1.5$, $Pr = 5.0$, $k_1 = 0.7$, $Sc = 4.0$, during the entire

computations.

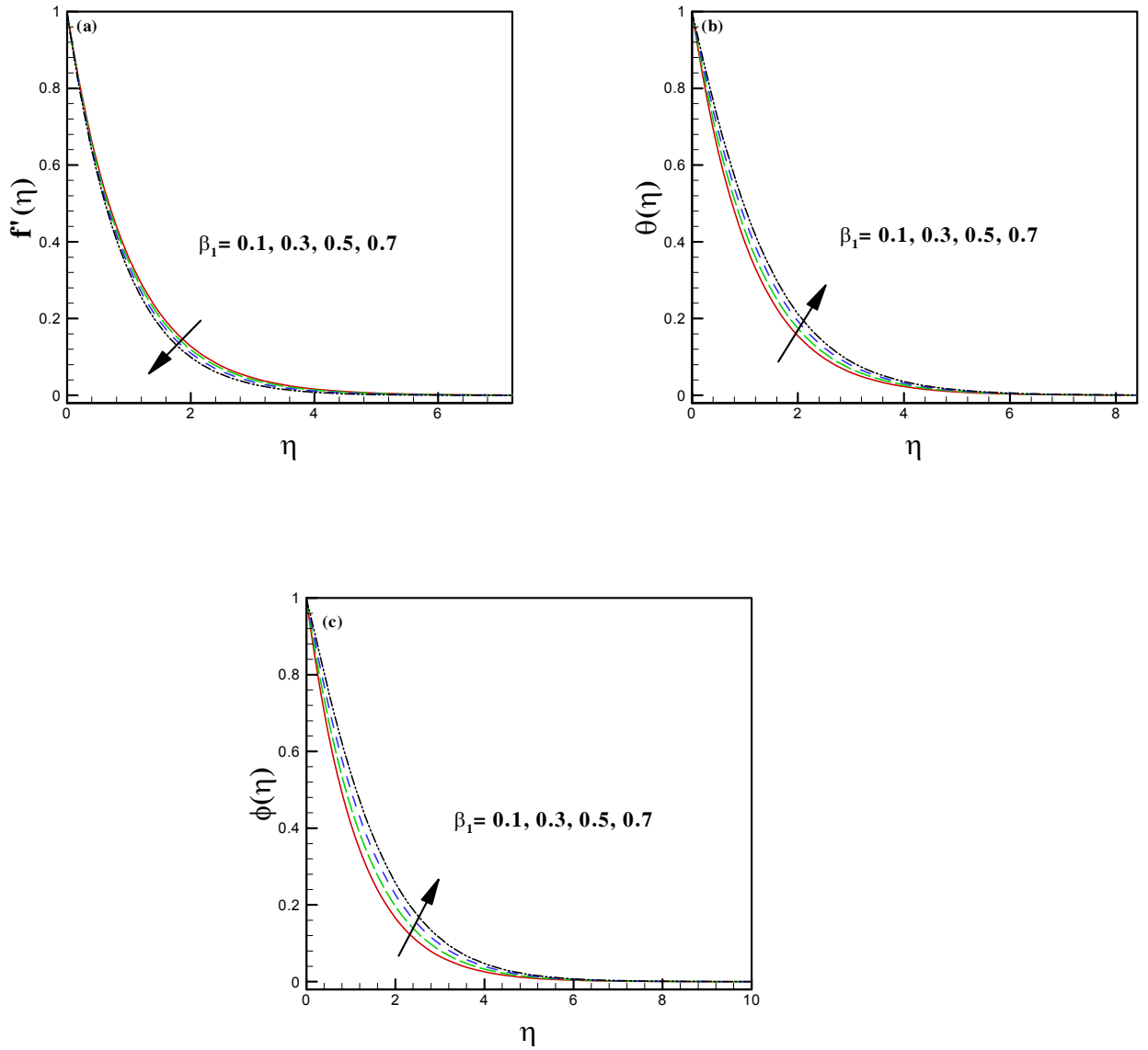
Figs. 6.1(a – c) expose the features of thermal curves for distinct scales of magnetic parameter. It is analyzed that the flow curves of Burgers nano liquid decline for higher intensity of magnetic force constant while in contrast of this the thermal and solutal curves of nanofluid depict mounting trend for intensifying magnitude of magnetic force variable. These behaviors are as expected because, larger scales of magnetic force constant lead to produce the escalating amount of Lorentz force which opposes the fluid motion and enhance the temperature and solutal distributions of fluid. Growing amount of Lorentz force generates friction due to which it happens. The influence of relaxation time constant (β_1) towards flow, thermal and solutal distributions is illustrated through Figs. 6.2(a – c). It is depicted that the motion of the fluid retards while heat transport and mass diffusion augments for higher values of β_1 . Physical justification of these behaviors is that, the larger relaxation time corresponds to rise the resistance between fluid particles and therefore flow profile of fluid depreciates while thermal and solutal energy transport enhance. The importance of Burgers fluid parameter (β_2) for motion, temperature and concentration distributions of Burgers fluid is represented in Figs. 6.3(a – c). These Figs. indicate that the motion of the nanofluid depreciates while the thermal and solutal energy transport curves show ascending trend for higher amount of (β_2). The role of thermal and solutal relaxation time constants (β_t, β_c) on temperature and concentration distributions, respectively, is demonstrated through Figs. 6.4(a, b). It is observed that both the thermal and concentration curves of Burgers nanofluid deteriorate for magnifying effects of thermal and solutal relaxation time constants. These results are according to reality that, further time requires for transportation of heat waves to nearby particles of liquid when thermal relaxation time rises therefore the temperature curves of nanofluid weaken. Moreover, mass diffusion needs addi-

tional time by intensifying the values of solutal relaxation time constant and consequently, the diminution in the nano particles volume fraction profile is assured. Fig. 6.5 irradiates the impact of Eckert number (Ec) on thermal distribution of reactive Burgers nanofluid. It is analysed that due to accretion in the Eckert number the magnitude of kinetic energy magnifies throughout in the system and this situation leads to improve the transport of temperature in the flow and hence thermal curves of Burgers fluid seem to be strengthen in the graph. Furthermore, Figs. 6.6(*a, b*) are depicted to highlight the significance of thermophoretic force constant (N_t) on temperature and solutal distribution of nanofluid. These plots demonstrate that the thermal as well as nano particles concentration distributions of nanofluid both build up for amplifying magnitudes of thermophoresis constant. The values taken for N_t are mentioned in graphs. In thermophoresis process, because of change in temperature the fluid particles start moving from warmer to chiller zone and hence the thermal energy and concentration of the system boost up as represented in plots. Moreover, the effect of Brownian motion constant (N_b) on thermal and concentration profiles of Burgers fluid is illustrated through Figs. 6.7(*a, b*). It is evident from these Figs. that transport of thermal energy in the flow shows the boosting trend while the nanoparticles concentration depreciates for amplifying values of (N_b). Due to Brownian motion, particles go under rapid motion due to which kinetic energy of the particles enhance which lead to magnify the thermal distribution of magnetized nanofluid. Since, the diffusion of nano-species is controlled by the Brownian motion hence, escalating amount of Brownian motion constraint depreciate the diffusion rate of nano particles and therefore the solutal curves of nanofluid diminish. Fig. 6.8(*a*) exposes the consequence of Prandtl number (Pr) on transport of heat while, Fig. 6.8(*b*) illustrates the stimulus of Schmidt number (Sc) for diffusion of mass in the system. The decay in the heat transfer rate is envisioned for magnifying values of Pr

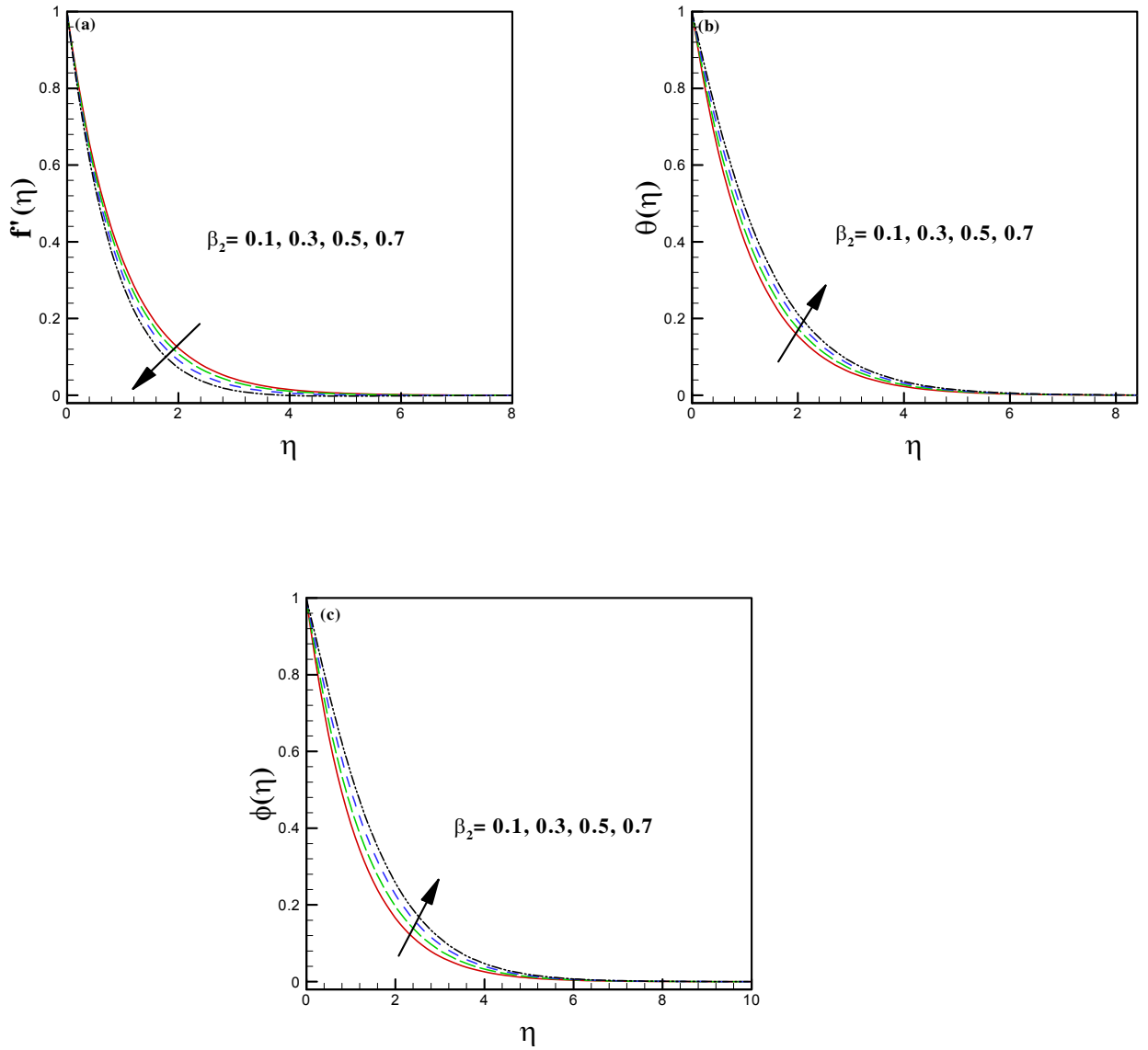
and the same trend is being detected for escalating amount of Sc on solutal energy transport curves. As, intensification in the strength of Pr enlarges the viscosity as well as the specific heat while the thermal conductivity of the liquid deteriorates in this regard as it can be observe from the relation, i.e, $Pr = \frac{\nu}{\alpha_1}$. Where, α_1 is the thermal conduction while, ν represents the momentum diffusivity. Also, note that here the heat transfers due to convection. Moreover, a magnification in the intensity of Sc corresponds to decline the mass diffusion coefficient that's why nanoparticles concentration depreciates. We depicted Figs. 6.9(*a, b*) to ensure the effect of hat source/sink variable for thermal curves of nanofluid. From these plots, it is clear that the thermal energy transport builds up in the flow for magnifying values of heat source constant ($\delta > 0$). On the other hand, it is seen that the thermal curves of nanofluid weakens for escalating amount of heat sink parameter ($\delta < 0$). Obviously, due to existence of heat source in the system the radiations produce extra amount of heat which magnify the temperature distribution and when heat sinks then temperature falls from the system. Hence, our theoretical outcomes are according to expectations. The influences of constructive and destructive chemical reaction parameters on solutal energy transport curves of nanofluid are demonstrated through Figs. 6.10(*a, b*). Depreciating trend of the mass diffusion curves is noticed for amplifying scales of constructive chemical reaction constant ($k_1 > 0$) while diminishing trend is achieved for larger amount of destructive chemical reaction parameter ($k_1 < 0$). Energy absorbs to some extent for execution of chemical reaction which leads to decline the solutal contours. Moreover, when the reaction rate deteriorates, the less magnitude of energy employs and system gain more energy to transfer therefore, transfer of solutal energy curves build up for larger values of destructive reaction parameter.



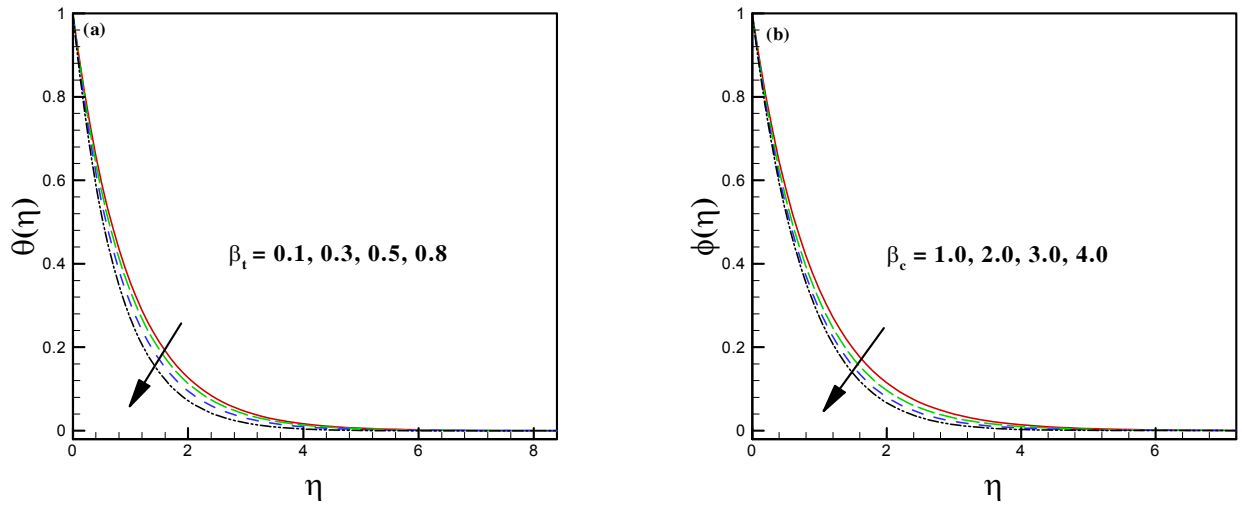
Figs. 6.1(a – c): Impact of M on flow, temperature and concentration fields.



Figs. 6.2(a – c): Impact of β_1 on flow, temperature and concentration fields.



Figs. 6.3(a – c): Impact of β_2 on flow, thermal and solutal profiles.



Figs. 6.4(a, b): Impact of β_t and β_c on thermal and solutal profiles.

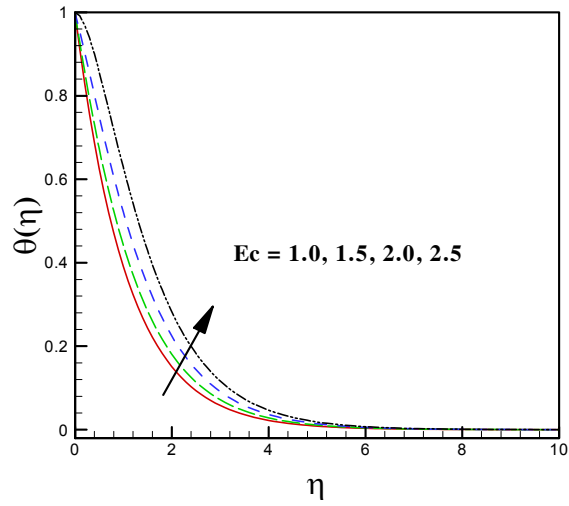
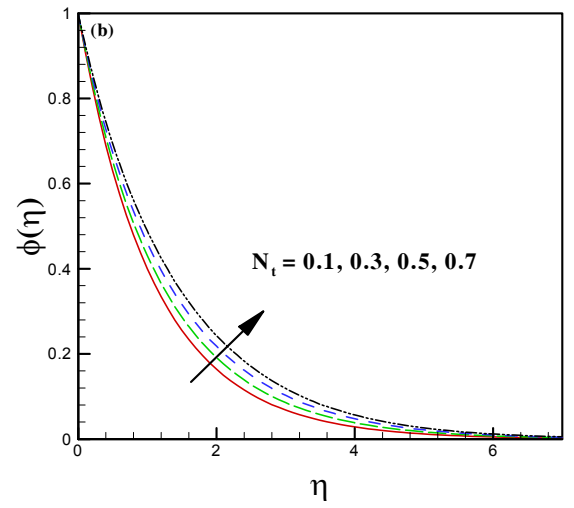
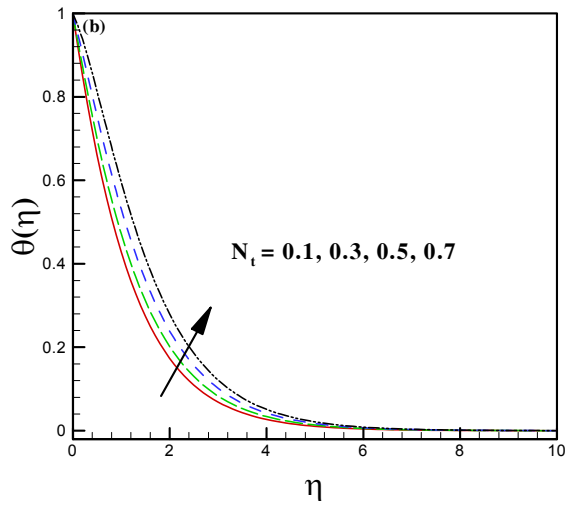
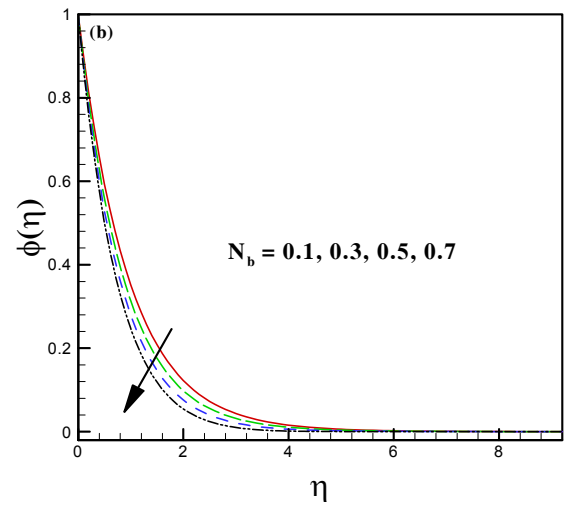
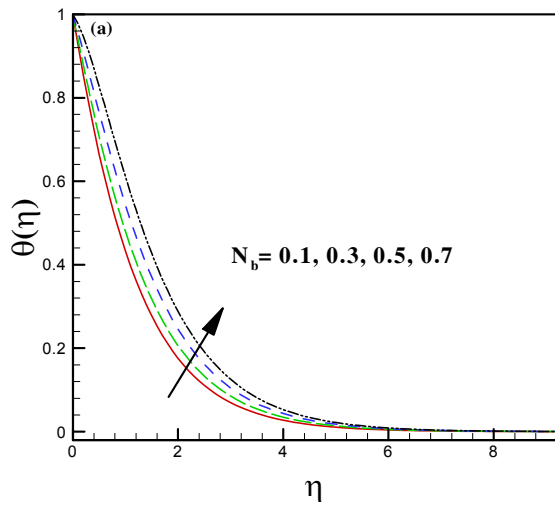


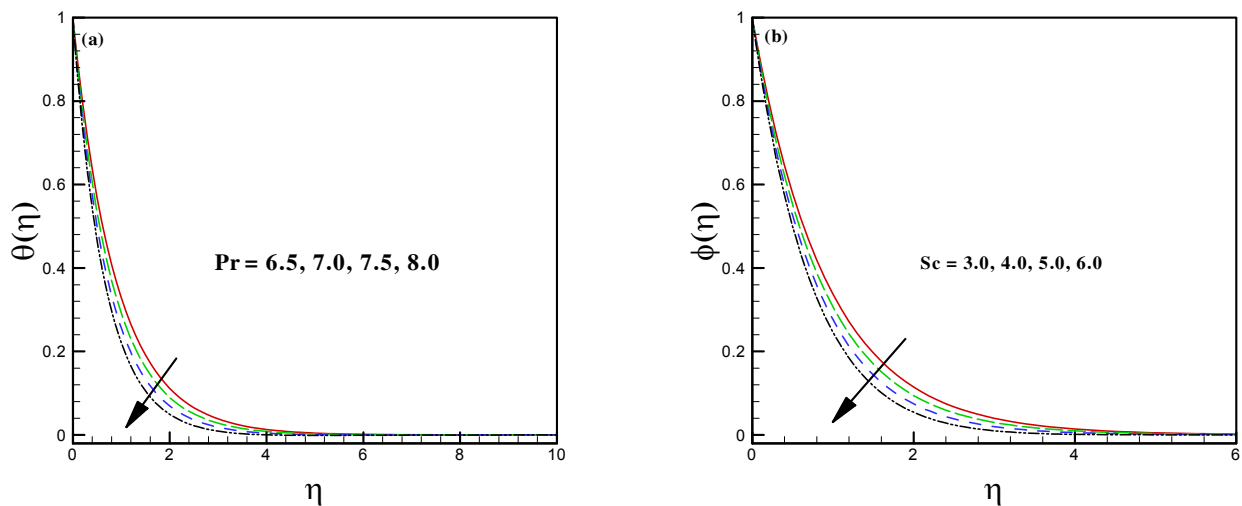
Fig. 6.5: Impact of Ec on temperature profile.



Figs. 6.6(a, b): Impact of N_t on thermal and solutal profiles.



Figs. 6.7(a, b): Impact of N_b on thermal and solutal profiles.



Figs. 6.8(a, b): Impact of Pr and Sc on thermal and solutal profiles.

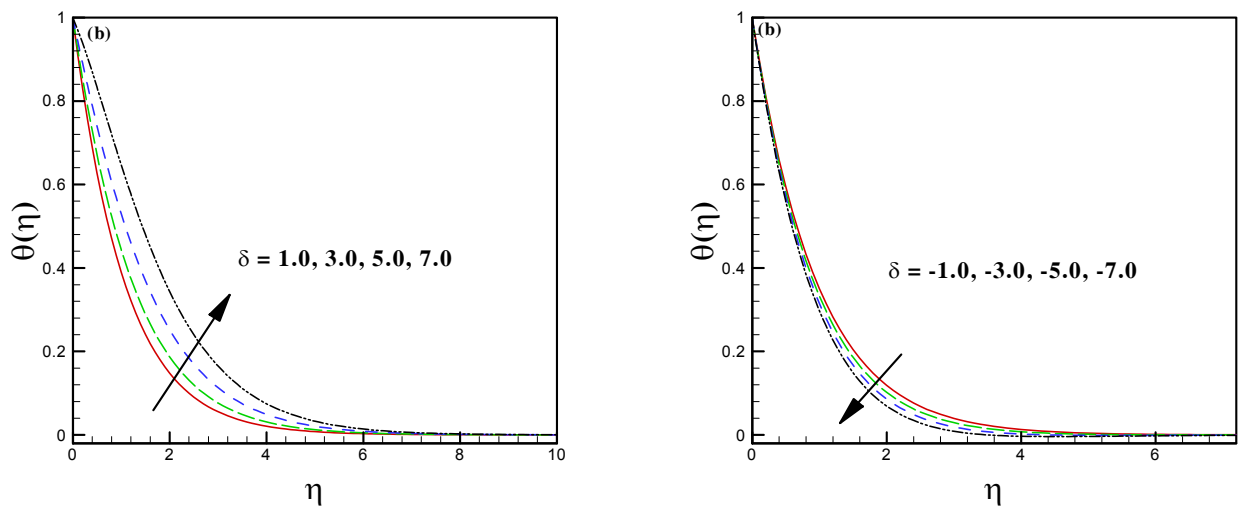


Fig. 6.9(a, b): Impact of δ on temperature profile.

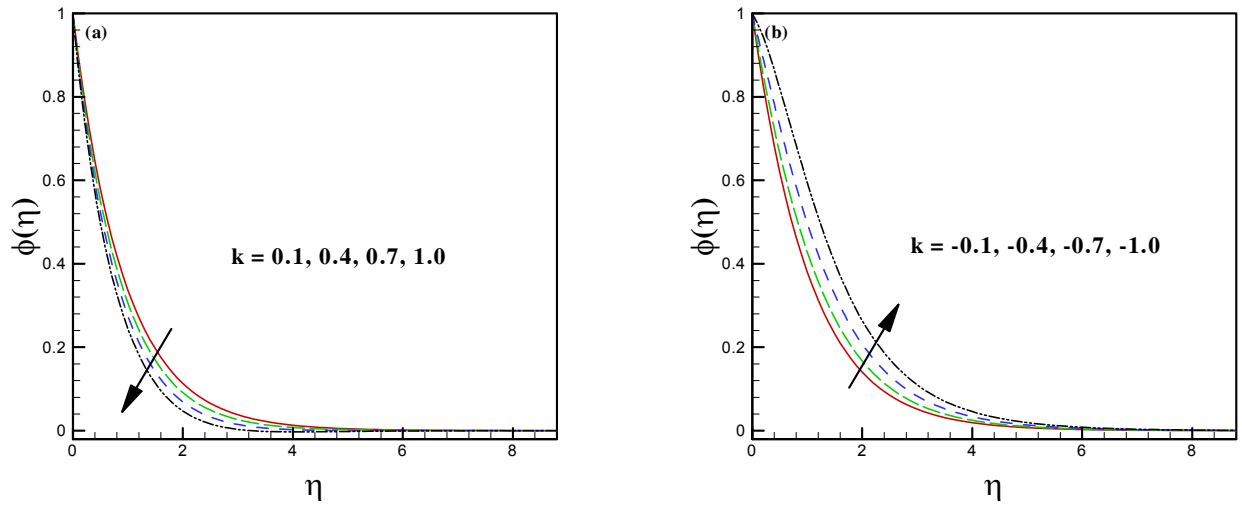


Fig. 6.10(a, b): Impact of k_1 on concentration profile.

Chapter 7

Features of thermophoretic and Brownian forces in Burgers fluid flow subject to Joule heating and convective conditions

Here we investigate the aspects of thermal and solutal energy transport in MHD flow of Burgers nanofluid caused by a unidirectional stretching cylinder. The well known Fourier's and Fick's laws are utilized to inspect the heat and mass transport phenomena. The convective energy transport at the surface of the cylinder is assumed and Fourier's law of thermal conduction is modelled in terms of non uniform heat source/sink and Joule heating. Additionally, the prescribed surface temperature (PST) with convective boundary conditions is considered here. Governing partial differential equations (PDEs) are transformed into ordinary differential equations (ODEs) by utilizing suitable similarity transformations. To deal with these ODEs, a numerical technique namely BVP midrich scheme in Maple is utilized. The behavior of different physical parameters is explored and depicted in form of graphs and discussed with reasonable arguments. Basic physical intimation of gained results is that the higher Eckert number intensifies the thermal profile of nanofluid. Moreover, the nano particles concentration profile builds up for higher

amount of thermophoretic force constraint. Solutal distribution of Burgers nanofluid depicts growing trend for larger solutal Biot number.

7.1 Mathematical Formulation

In this portion of study, a mathematical model to the flow of Burgers nanofluid due to a stretching cylinder is presented. The flow is caused by the stretching cylinder. Further it is assumed that the velocity field for $2D$ incompressible flow is $\mathbf{V} = [u, 0, w]$, where u and w are considered as the velocity components along r and z axes, respectively. Furthermore, a uniform magnetic field of strength $B = [B_0, 0, 0]$ is applied along normal to the flow direction. Cylindrical polar coordinates (r, θ, z) are considered to model the flow, energy and concentration equations. Fourier's law of heat conduction is modelled in terms of non uniform heat source/sink and Joule heating. Here the stretching velocity of the cylinder is taken as $w = \frac{U_0 z}{l}$ along z -direction, where U_0 is considered as the reference velocity and l the specific length. Moreover, it is assumed that the temperature and concentration at wall of the cylinder are (T_w, C_w) respectively. The geometry of the problem is depicted in Fig. 4.1 (cf. Chapter 4).

The governing PDEs for continuity equation, momentum equation, heat transport equation and the concentration equation (2.1 – 2.7) (cf. Chapter 2) under above assumptions are given below

$$\frac{\partial u}{\partial r} + \frac{u}{r} + \frac{\partial w}{\partial z} = 0, \quad (7.1)$$

$$\begin{aligned}
& u \frac{\partial w}{\partial r} + w \frac{\partial w}{\partial z} + \lambda_1 \left[u^2 \frac{\partial^2 w}{\partial r^2} + w^2 \frac{\partial^2 w}{\partial z^2} + 2uw \frac{\partial^2 w}{\partial z \partial r} \right] \\
& + \lambda_2 \left[\begin{aligned}
& u^3 \frac{\partial^3 w}{\partial r^3} + w^3 \frac{\partial^3 w}{\partial z^3} + 2u^2 \left(\frac{\partial u}{\partial r} \frac{\partial^2 w}{\partial r^2} + \frac{\partial w}{\partial r} \frac{\partial^2 w}{\partial r \partial z} \right) - u^2 \left(\frac{\partial w}{\partial r} \frac{\partial^2 u}{\partial r^2} + \frac{\partial w}{\partial z} \frac{\partial^2 w}{\partial r^2} \right) \\
& + 2w^2 \frac{\partial u}{\partial z} \frac{\partial^2 w}{\partial r \partial z} + w^2 \left(\frac{\partial w}{\partial z} \frac{\partial^2 w}{\partial z^2} - \frac{\partial w}{\partial r} \frac{\partial^2 u}{\partial z^2} \right) + 3uw \left(u \frac{\partial^3 w}{\partial r^2 \partial z} + w \frac{\partial^3 w}{\partial z^2 \partial r} \right) \\
& + 2uw \left(\frac{\partial u}{\partial r} \frac{\partial^2 w}{\partial z \partial r} + \frac{\partial u}{\partial z} \frac{\partial^2 w}{\partial r^2} + \frac{\partial w}{\partial r} \frac{\partial^2 w}{\partial z^2} - \frac{\partial w}{\partial r} \frac{\partial^2 u}{\partial r \partial z} \right)
\end{aligned} \right] \\
& = \nu \left[\frac{\partial^2 w}{\partial r^2} + \frac{1}{r} \frac{\partial w}{\partial r} \right] + \nu \lambda_3 \left[\begin{aligned}
& u \frac{\partial^3 w}{\partial r^3} + w \frac{\partial^3 w}{\partial r^2 \partial z} + \frac{u}{r} \frac{\partial^2 w}{\partial r^2} - \frac{\partial w}{\partial r} \frac{\partial^2 u}{\partial r^2} + \frac{w}{r} \frac{\partial^2 w}{\partial r \partial z} \\
& - \frac{1}{r} \frac{\partial u}{\partial r} \frac{\partial w}{\partial r} - \frac{1}{r} \frac{\partial w}{\partial r} \frac{\partial w}{\partial z} - \frac{\partial w}{\partial z} \frac{\partial^2 u}{\partial r^2}
\end{aligned} \right] \\
& - \frac{\sigma B_0^2}{\rho} \left[\begin{aligned}
& w + \lambda_1 u \frac{\partial w}{\partial r} + \\
& \lambda_2 \left(w \frac{\partial u}{\partial z} \frac{\partial w}{\partial r} - u \frac{\partial w}{\partial z} \frac{\partial w}{\partial r} + uw \frac{\partial^2 w}{\partial r \partial z} + w^2 \frac{\partial^2 w}{\partial r^2} \right)
\end{aligned} \right], \quad (7.2)
\end{aligned}$$

$$u \frac{\partial T}{\partial r} + w \frac{\partial T}{\partial z} = \alpha_1 \frac{1}{r} \left[\frac{\partial}{\partial r} \left(r \frac{\partial T}{\partial r} \right) \right] + \tau \left[D_b \frac{\partial C}{\partial r} \frac{\partial T}{\partial r} + \frac{D_T}{T_\infty} \left(\frac{\partial T}{\partial r} \right)^2 \right] + \frac{1}{(\rho c_p)} q''' + \frac{\sigma B_0^2}{\rho c_p} w^2, \quad (7.3)$$

$$u \frac{\partial C}{\partial r} + w \frac{\partial C}{\partial z} = \frac{D_B}{r} \frac{\partial}{\partial r} \left(r \frac{\partial C}{\partial r} \right) + \frac{D_T}{T_\infty} \frac{1}{r} \frac{\partial}{\partial r} \left(r \frac{\partial T}{\partial r} \right) - k_c (C - C_\infty), \quad (7.4)$$

with boundary conditions

$$w = w_s = \frac{U_0 z}{l}, \quad u = 0, \quad -k \frac{\partial T}{\partial r} = h_f [T_w - T], \quad -D_B \frac{\partial C}{\partial z} = h_m [C_w - C] \text{ at } r = R, \quad (7.5)$$

$$w \rightarrow 0, \quad \frac{\partial w}{\partial r} \rightarrow 0, \quad T \rightarrow T_\infty, \quad C \rightarrow C_\infty \text{ as } r \rightarrow \infty. \quad (7.6)$$

The non-uniform heat generation/absorption q''' is considered as

$$q''' = \frac{k w_s}{x \nu} [A_* (T_w - T_\infty) f'(\eta) + B_* (T - T_\infty)]. \quad (7.7)$$

In above equations, A_* and B_* represent the coefficients of space and temperature dependent heat source/sink, respectively. The case $A_* > 0$ and $B_* > 0$ demonstrates the internal heat

generation whereas, $A_* < 0$ and $B_* < 0$ signifies internal heat absorption.

By adopting the similarity transformations given in Eq. (4.7) (cf. Chapter 4), equation (7.1) satisfied explicitly and equations (7.2) – (7.4) take the form as

$$\begin{aligned}
& (1 + 2\alpha\eta)^2 \beta_1 \left[2ff'f'' - f^2f''' \right] - (1 + 2\alpha\eta) \alpha\beta_1 f^2 f'' - 4\alpha^2 \beta_2 f''' f'' + (1 + 2\alpha\eta)^3 f''' \\
& - (1 + 2\alpha\eta)^2 \beta_2 \left[3f^2(f'')^2 + 2f(f')^2 f'' - f^3 f^{iv} \right] - 4\alpha\beta_3 (1 + 2\alpha\eta)^2 f f''' \\
& + (1 + 2\alpha\eta) \alpha\beta_2 \left[3f^2 f' f'' + f^3 f''' \right] + (1 + 2\alpha\eta)^2 \left[2\alpha f'' + f f'' - (f')^2 \right] \\
& + (1 + 2\alpha\eta)^3 \beta_3 \left[(f'')^2 - f f^{iv} \right] - (1 + 2\alpha\eta)^2 M^2 \left[\beta_2 f f''' - \beta_1 f f'' + f' \right] = 0, \quad (7.8)
\end{aligned}$$

$$\begin{aligned}
& (1 + 2\alpha\eta) \theta'' + 2\alpha\theta' + \text{Pr}(\theta' f - \theta f') + \text{Pr}[\delta f' + \delta_1 \theta] + \text{Pr} M E c (f')^2 \\
& + \text{Pr} N_b \phi' \theta' (1 + 2\alpha\eta) + \text{Pr} N_t \theta'^2 (1 + 2\alpha\eta) = 0, \quad \text{(PST)} \quad (7.9)
\end{aligned}$$

$$(1 + 2\alpha\eta) \phi'' + 2\alpha\phi' + Le \text{Pr} f \phi' + (1 + 2\alpha\eta) \left(\frac{N_t}{N_b} \right) \theta'' + 2\alpha \left(\frac{N_t}{N_b} \right) \theta' - k_1 Le \text{Pr} \phi = 0, \quad (7.10)$$

and transformed boundary conditions from equations (7.5) and (7.6) are as follows

$$f = 0, \quad f' = 1, \quad \theta'(0) = -\gamma_1(1 - \theta(0)), \quad \phi'(0) = -\gamma_2(1 - \phi(0)) \quad \text{at } \eta = 0, \quad (7.11)$$

$$f' \rightarrow 0, \quad f'' \rightarrow 0, \quad \theta \rightarrow 0, \quad \phi \rightarrow 0 \quad \text{as } \eta \rightarrow \infty. \quad (7.12)$$

Here U_0 is the reference velocity. Moreover, the curvature parameter α , Deborah numbers β_1 and β_3 , Burgers fluid parameter β_2 , magnetic parameter M , Prandtl number Pr , Lewis number Le , thermophoresis parameter N_t and Brownian motion parameter N_b , Eckert number Ec ,

thermal Biot number γ_1 , solutal Biot number γ_2 , chemical reaction parameter k_1 , space and temperature dependent heat source/sink parameters δ, δ_1 , respectively, are defined as follows:

$$\begin{aligned} \alpha &= \frac{1}{R} \sqrt{\frac{\nu l}{U_0}}, \quad \beta_1 = \lambda_1 \frac{U_0}{l}, \quad \beta_2 = \lambda_2 \left(\frac{U_0}{l}\right)^2, \quad \beta_3 = \lambda_3 \frac{U_0}{l}, \quad M = \left(\frac{\sigma l B_0^2}{\rho U_0}\right)^{1/2}, \\ \delta_1 &= \frac{B_*}{\alpha \nu (\rho c_p)}, \quad \text{Pr} = \frac{\nu}{\alpha_1}, \quad N_t = \frac{\tau D_T (T_w - T_\infty)}{\nu T_\infty}, \quad N_b = \frac{\tau D_B (C_w - C_\infty)}{\nu}, \quad Ec = \frac{w_s^2}{c_p (T_w - T_\infty)}, \\ Le &= \frac{\alpha_1}{D_B}, \quad \delta = \frac{A_*}{\nu (\rho c_p)}, \quad \gamma_1 = \frac{h_f}{k} \sqrt{\frac{\nu l}{U_0}}, \quad \gamma_2 = \frac{h_m}{D_B} \sqrt{\frac{\nu l}{U_0}}, \quad k_1 = \frac{k_{cl}}{U_0}. \end{aligned} \quad (7.13)$$

7.2 Engineering Concerned Quantities

Relations for heat transfer (Nu_z) rate and mass transfer (Sh_z) rate are

$$Nu_z = \frac{z q_s}{k(T_w - T_\infty)}, \quad Sh_z = \frac{z j_s}{D_B(C_w - C_\infty)}, \quad (7.14)$$

where q_s and j_s are the heat and mass flux respectively

$$q_s = -k \left(\frac{\partial T}{\partial r} \right)_{r=R}, \quad j_s = -D_B \left(\frac{\partial C}{\partial r} \right)_{r=R}. \quad (7.15)$$

The dimensionless form of Eq. (7.14) is given by

$$Nu_z \text{Re}^{-\frac{1}{2}} = -\theta'(0), \quad Sh_z \text{Re}^{-\frac{1}{2}} = -\phi'(0). \quad (7.16)$$

where $\text{Re}_z = \frac{w_s z}{\nu}$ is the local Reynolds number.

7.3 Validation of Numerical Scheme

We employed BVP midrich numerical technique described in section (1.3.1) (cf. Chapter 1) to solve the established ordinary differential equations (7.8 – 7.10) with corresponding boundary conditions (7.11) and (7.12). Table (7.1) is an computation table for values of $-f''(0)$ for different values of M with comparison of some existing studies. As a consequence, from this table we are assured that the recent results are identical with the investigations made by Hayat *et al.* [142] and Shehzad *et al.* [143]. Hence, the numerical scheme which we have used namely BVP Midrich is a valid technique. This technique is based on modified Euler’s method (explicit midpoint method) which has absolute error convergence up to 1×10^{-6} .

Table 7.1: A comparison table for values of $-f''(0)$ for different values of M when $\alpha = \beta_1 = \beta_2 = \beta_3 = 0$

M	Shehzad <i>et al.</i> [142]	Hayat <i>et al.</i> [143]	Present study
0.0	1.00000	1.00000	1.000000
0.2	1.01980	1.01980	1.019803
0.5	1.11803	1.11803	1.118027
0.8	1.28063	1.28063	1.280635
1.0	1.41421	1.41421	1.414213
1.2	1.56205	1.56205	1.562063
1.5	1.80303	1.80303	1.803028

7.4 Discussion of Outcomes

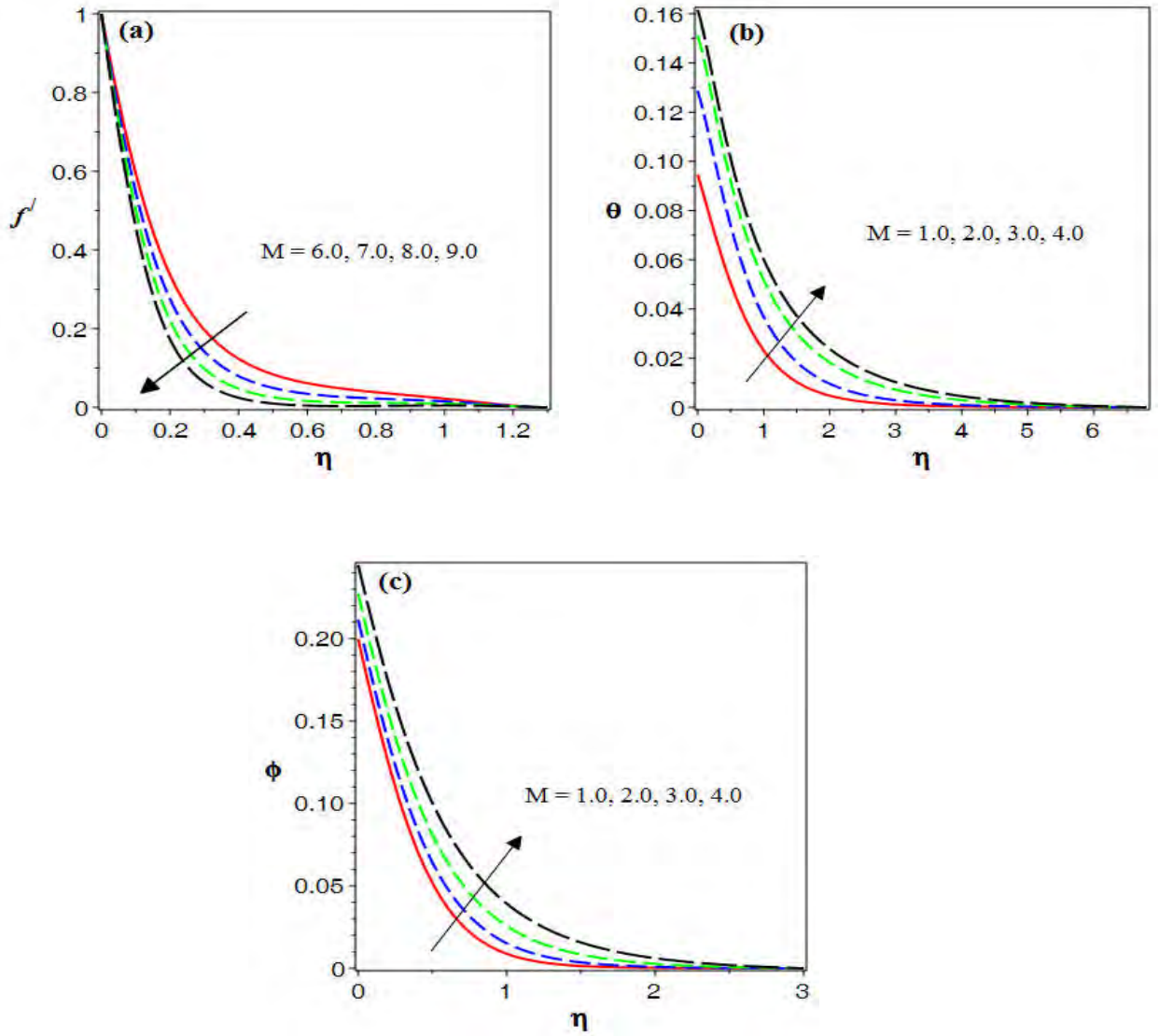
The numerical investigation of non linear coupled ordinary differential equations (7.8 – 7.10) in addition with convective boundary conditions written in Eqs. (7.11) and (7.12) is performed by employing BVP midrich scheme in Maple explained in section (1.3.1) (cf. Chapter 1). This section is designed to observe the influence of varying magnitudes of physical parameters on velocity $f'(\eta)$, thermal $\theta(\eta)$ and solutal $\phi(\eta)$ profiles of magnetized Burgers nanofluid. The physical behavior of several dimensionless parameters is examined, for instance, the impact of Burgers fluid parameter β_2 and magnetic parameter M on flow, thermal and concentration distributions. In similar pattern, the impact of Brownian motion parameter N_b , thermophoresis parameter N_t , Prandtl number Pr , space and temperature dependent heat source/sink parameters δ and δ_1 respectively, chemical reaction constraint k_1 , thermal Biot number γ_1 and Eckert number Ec on thermal distributions is explored. Moreover, the influence of Lewis number Le , Brownian motion constraint N_b , thermophoretic force parameter N_t , and solutal Biot number γ_2 on solutal profile is observed. The impacts of all these parameters are depicted through Figs. (7.1 – 7.9). We have assigned the following fixed values for main constraints such as $\alpha = 0.2$, $\beta_1 = 0.7$, $\beta_2 = 0.2$, $\beta_3 = 0.5$, $M = 0.5$, $N_t = 0.6$, $N_b = 0.4$, $\delta = 0.5$, $\delta_1 = 0.4$, $Ec = 0.9$, $Pr = 5.0$, $Le = 4.0$, $k_1 = 0.6$, $\gamma_1 = 0.2$, $\gamma_2 = 0.3$ during the whole computations.

We will discuss behavior of each parameter with complete physical judgment. Figs. 7.1(a–c) are displayed to enlighten the influence of magnetic parameter (M) on flow, thermal and solutal distributions of Burgers nanofluid. It is assessed that the flow profiles and momentum thickness to the boundary layer of Burgers nanofluid diminish for higher magnitude of magnetic parameter while, the thermal and solutal profiles depict converse trend to that of flow profile

for higher values of M . This situation arises because of the reason that when we intensify the magnitude of magnetic field then a resistive force called Lorentz force in the fluid flow become more stronger which oppose the flow phenomenon and therefore, the flow profile of the fluid deteriorates. Additionally, this intensified Lorentz force creates more interface between the fluid particles due to which friction increases among the fluid particles which results in the rise of the temperature and solutal distribution of the liquid. To visualize the influence of Burgers fluid parameter (β_2) on flow, thermal and solutal distributions of nanofluid Figs. 7.2(a – c) are depicted. From these Figs. diminution in flow profile of nano Burgers fluid is perceived with an escalation in the magnitude of β_2 . Also, it is seen that the temperature and solutal profiles of Burgers fluid show enhancing trend for higher values of β_2 . To envision the stimulus of thermophoretic force constraint (N_t) on thermal and concentration distributions of Burgers nanofluid Figs. 7.3(a, b) are portrayed. It is clear from these Figs. that both temperature distribution and nanoparticles volume fraction of Burgers nanofluid improve for escalating values of (N_t) and far field conditions at the boundary satisfy asymptotically throughout the solution region. These investigations are identical to the process of thermophoresis, i.e, molecules from warmer regions move towards cooler regions and therefore, collision between fluid particles enhances due to which thermal and concentration distributions of Burgers nanofluid boost. Figs. 7.4(a, b) are drawn to highlight the impact of Brownian motion constraint (N_b) on thermal and solutal profiles of Burgers nano fluid. It is clear from these Figs. that for larger values of N_b the temperature profile and thermal boundary layer thickness of nanofluid boost up while the nano particles volume fraction profile depicts opposite trend to that of thermal profile. The reason behind this is that the kinetic energy of the system enlarges with escalation in the magnitude of N_b and consequently, the heat transfer rate boosts up which lead to

enhance the temperature of the fluid. Furthermore, due to intensification in N_b the motion of the particles increases due to which viscosity of the fluid lowers down which leads to diminish the concentration profile of the nanofluid. To disclose the effect of Prandtl number (Pr) and Lewis number (Le) on thermal and nano particles volume fraction profiles, respectively, Figs. 7.5(a, b) are inserted. These Figs. disclose that both the thermal and solutal profiles and depict diminishing trend and associated boundary layer thicknesses become thinner for higher magnitude of Pr and Le respectively. Mathematically, as Prandtl number is inversely proportional to thermal diffusivity. Hence larger magnitude of Pr is responsible to lowers down the thermal diffusivity of the nanofluid and obviously diminution in thermal diffusivity corresponds to deteriorate the thermal profile of nanofluid. In addition, larger Lewis number results in reduction of mass diffusivity as it is inversely proportional to Lewis number. Hence, ultimately lower mass diffusivity is considered as responsible for diminution of nano particles volume fraction distribution. The effects of space and temperature dependent heat source parameters ($\delta, \delta_1 > 0$) are demonstrated in Figs. 7.6(a, b). Enhancing trend of temperature profiles is being perceived for increasing values of space and temperature dependent heat source parameters. Also, far field boundary conditions throughout the solution region are satisfied asymptotically. These outcomes are according to our expectations, as more amount of heat is provided to the system by increasing the magnitude of heat source parameters which finally results in enhancement of thermal distribution of the nanofluid. Impact of thermal and solutal Biot numbers (γ_1, γ_2) on thermal and solutal distributions are demonstrated in Figs. 7.7(a, b) respectively. It is detected that the thermal as well as solutal distributions of Burgers nanofluid boost up for growing magnitude of thermal and solutal Biot numbers. Actually, larger thermal Biot number promotes the surroundings convection which results in rise of temperature in nanofluid. Furthermore, Figs.

7.8(*a, b*) elucidate the influence of Eckert number (Ec) on thermal and solutal distributions of nanofluid. It is scrutinized that the thermal profiles of nanofluid build up for augmented values of Ec . Higher Eckert number is responsible for rise of kinetic energy of the flow which then results in growing of the temperature distribution of the fluid. Basically, larger Eckert number leads to convert the mechanical energy of the flow into thermal energy and consequently thermal distribution enhances. Figs. 7.9(*a, b*) elucidate the impact of constructive and destructive chemical reaction impact on the transport of solutal energy. It is realized that the growing range of constructive chemical reaction constraint demotivates the solutal transport in the flow whereas the destructive chemical reaction promotes the transport of solutal energy in the flow. Because, some amount of energy utilizes in the occurrence of chemical reaction due to which solutal curves deteriorate and when chemical reaction goes to be slow down then less amount of energy requires and ultimately solutal curves build up. Moreover, table 7.2 is depicted for numerical calculations to the rate of heat and mass transport coefficients at the boundary of the surface for pertinent values of M , β_2 , N_t , N_b , γ_1 and γ_2 by fixing all other parameters. From these results we observed that the thermal and solutal gradient enhance at the surface in case of higher thermophoretic and Brownian forces.



Figs. 7.1(a – c): Influence of M on velocity, thermal and concentration fields.

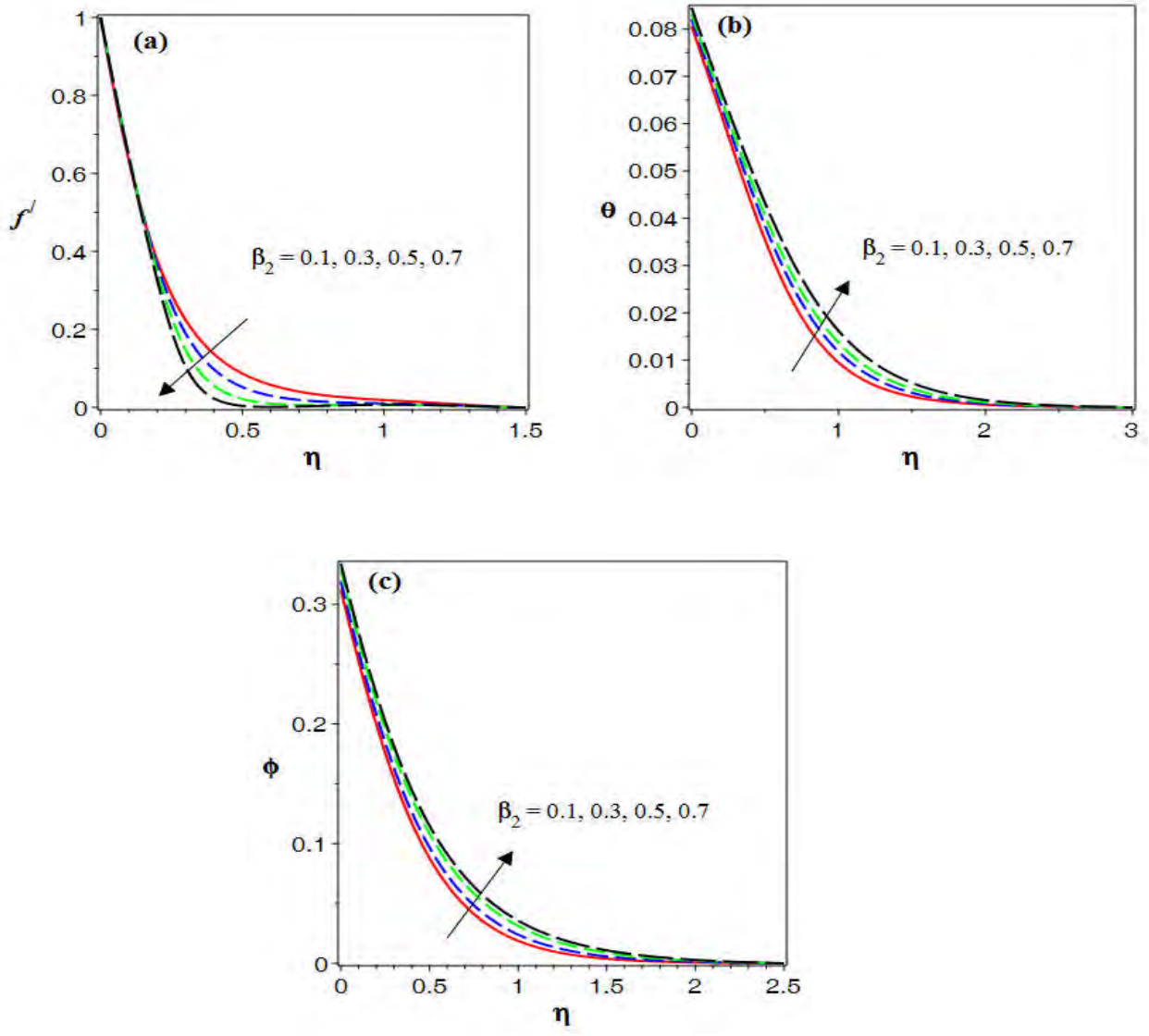
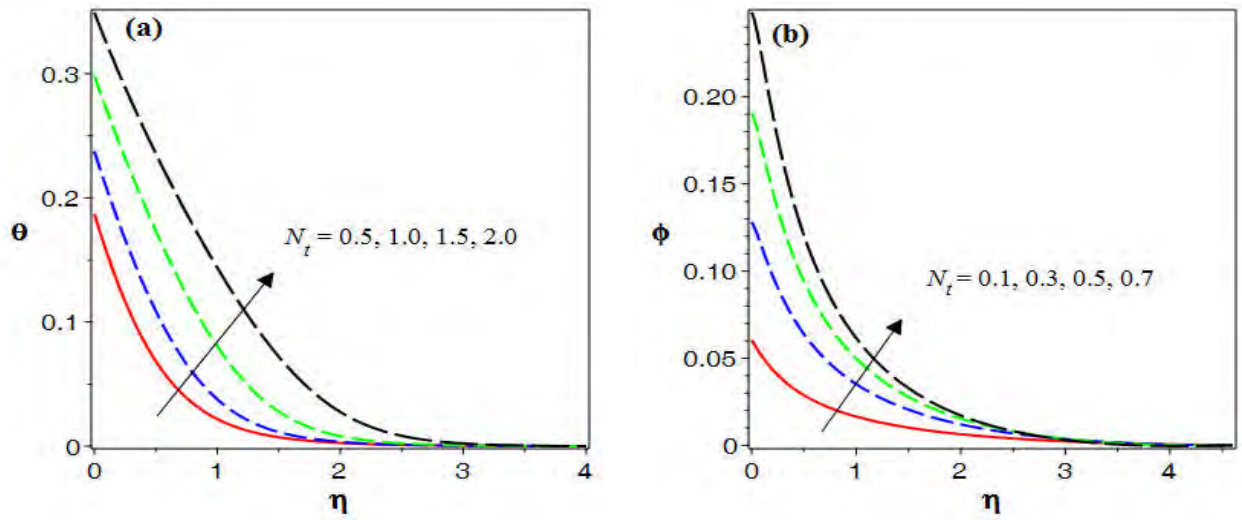
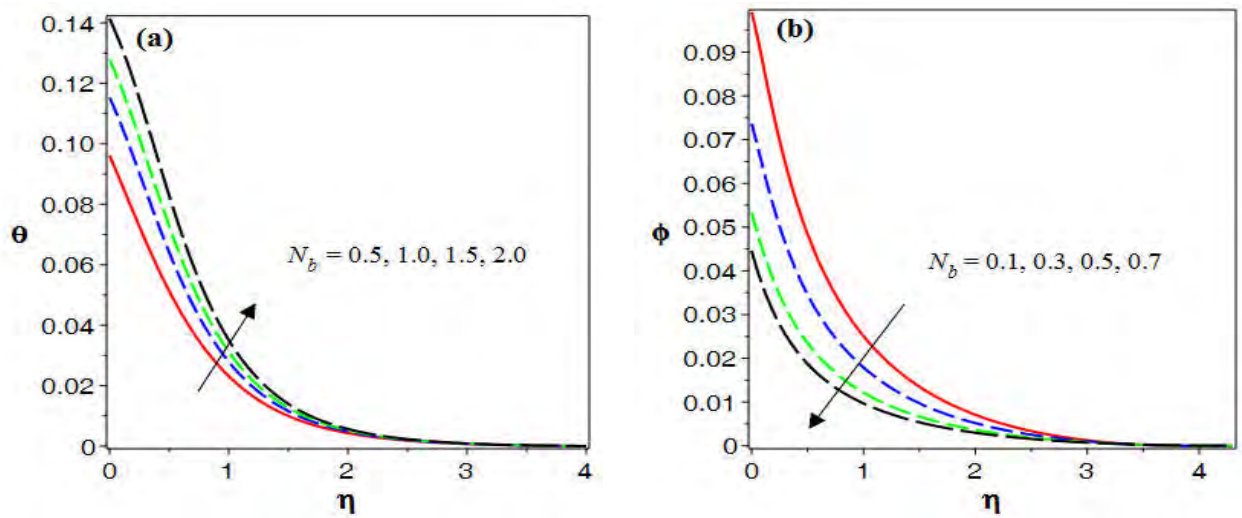


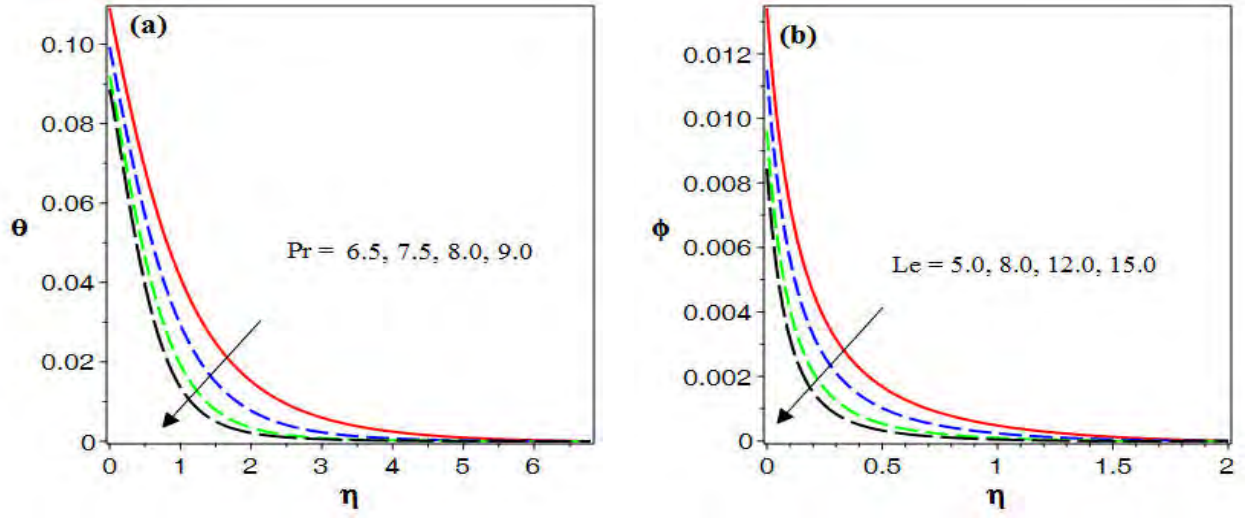
Fig. 7.2(a – c): Influence of β_2 on velocity, thermal and solutal fields.



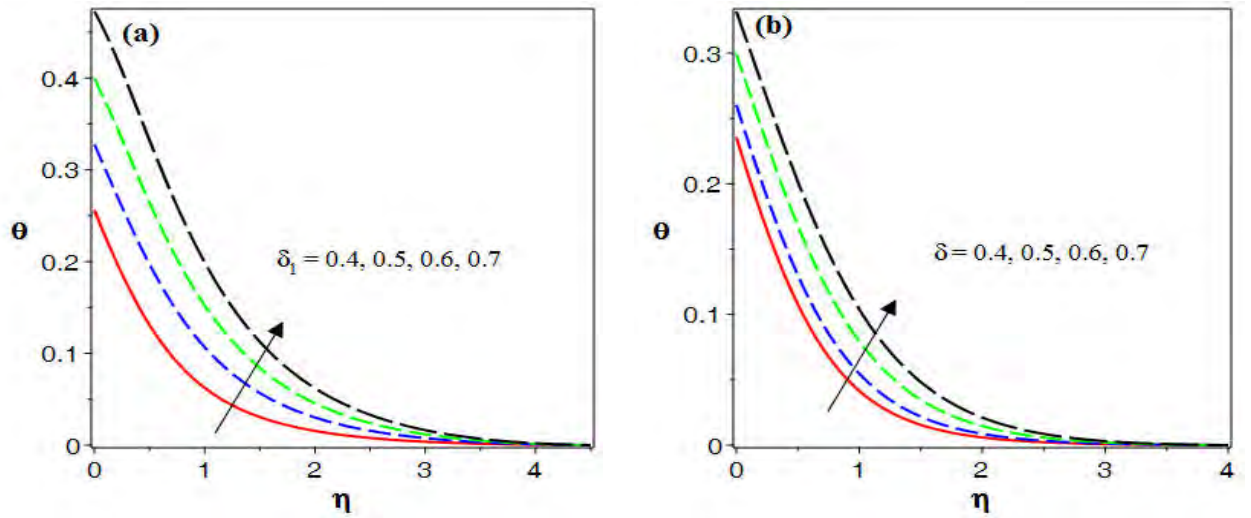
Figs. 7.3(a, b): Influence of N_t on thermal and concentration profiles.



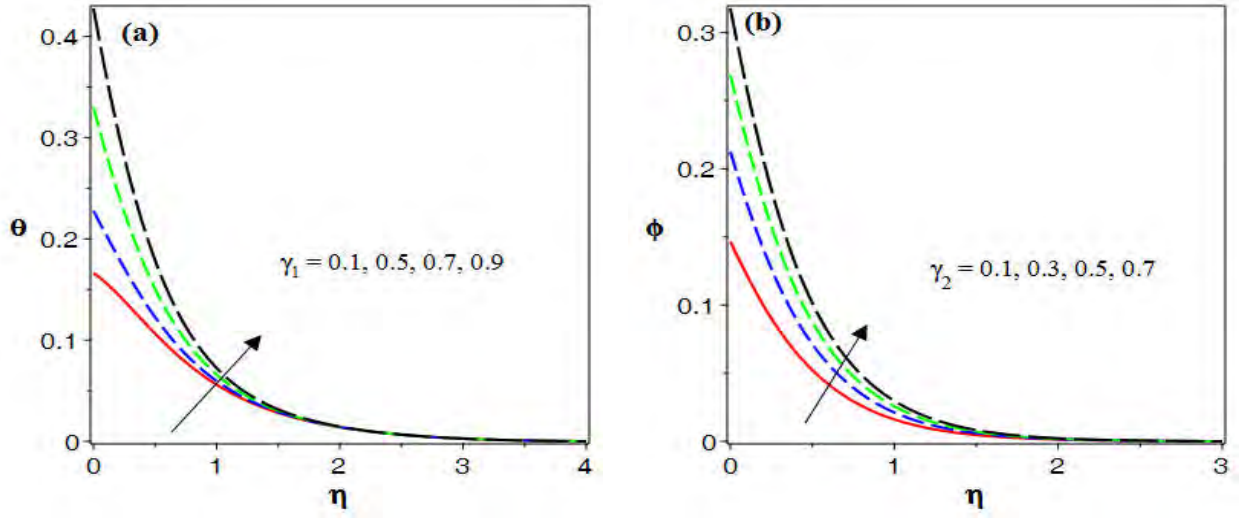
Figs. 7.4(a, b): Influence of N_b on thermal and concentration profiles.



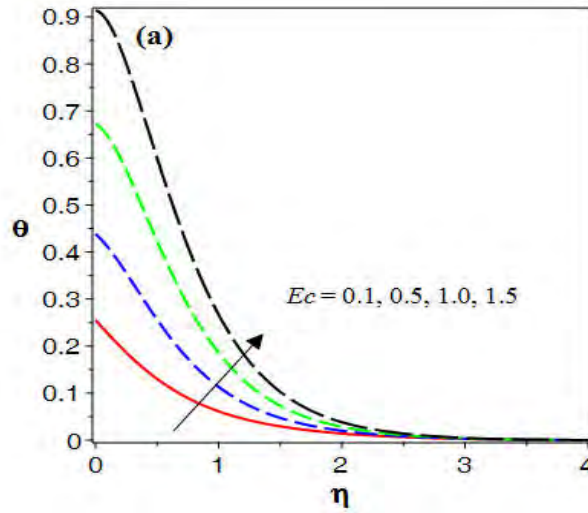
Figs. 7.5(a, b): Influence of Pr and Le on thermal and concentration profiles.



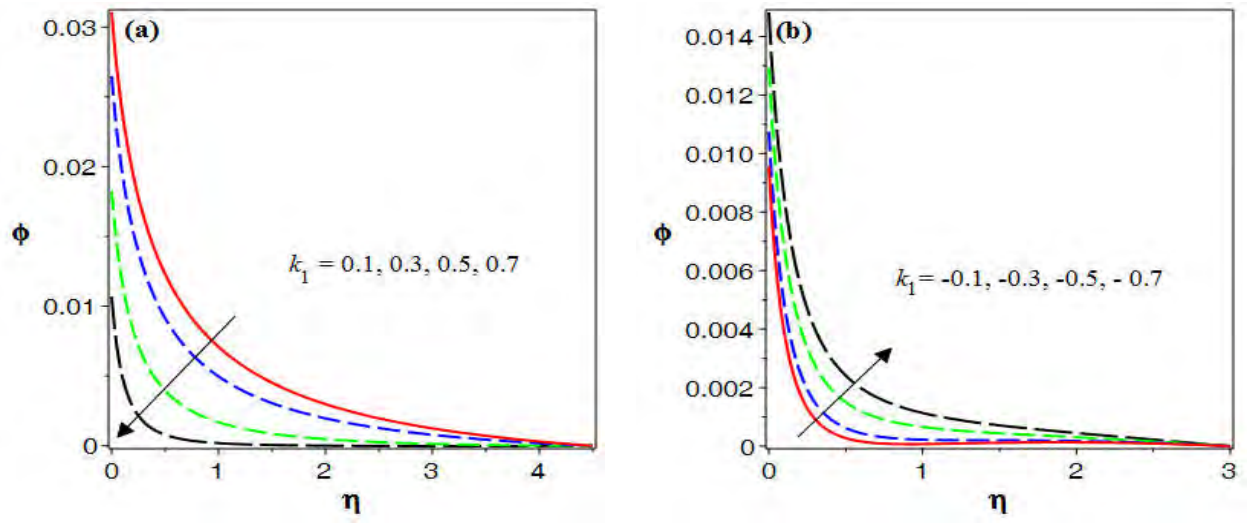
Figs. 7.6(a, b): Impact of δ and δ_1 on thermal profile.



Figs. 7.7(a, b): (a) Influence of γ_1 on thermal profile (b) Influence of γ_2 on solutal profile.



Figs. 7.8: Influence of Ec on thermal profile.



Figs. 7.9(a, b): Influence of k_1 on solutal profiles.

Table 7.2: The illustration of numerical computations of rate of heat transfer coefficient and Sherwood numbers for pertinent values of M , β_2 , N_t , N_b , γ_1 and γ_2 when $\alpha = 0.2$, $\beta_1 = 0.7$, $\beta_3 = 0.5$, $\delta = 0.5$, $\delta_1 = 0.4$, $Ec = 0.9$, $Pr = 5.0$, $Le = 4.0$, $k_1 = 0.3$.

M	β_2	N_t	N_b	$-\theta'(0)$	$-\phi'(0)$
1	0.3	0.1	0.5	0.06448	0.09381
2				0.06603	0.09389
3				0.07011	0.09401
3	0.1	0.1	0.5	0.04480	0.08010
	0.3			0.04911	0.08541
	0.5			0.05320	0.08992
3	0.3	0.1	0.5	0.06837	0.09396
		0.2		0.06969	0.08718
		0.3		0.07084	0.08094
3	0.3	0.1	0.1	0.02401	0.05081
			0.2	0.02015	0.04920
			0.3	0.01622	0.04801

Chapter 8

On modified Fourier heat flux in stagnation point flow of magnetized Burgers fluid subject to homogeneous-heterogeneous reactions

In the current chapter, an effort has been made to model the forced convection flow phenomenon of magnetized viscoelastic fluid near a stagnation point. Moreover, Cattaneo-Christov heat flux model and the impact of uniform heat rise/fall are employed to examine the aspects of thermal energy transport. Additionally, the scrutiny of the fluid concentration feature by utilizing homogeneous-heterogeneous reactions is also an important effort of the present investigation. Ordinary differential equations (ODE's) are achieved by adopting the method of similarity transformations. The characteristics of physical parameters are assessed by employing numerical technique BVP midrich scheme. Pertained outcomes are depicted in the form of graphs. The thermal distribution of Burgers fluid exhibits a diminishing trend for escalation in the extent of thermal relaxation heat flux parameter. Moreover, the concentration rate of the fluid deteriorates for higher strength of homogenous response whereas, it augments for greater magnitude of heterogenous response. The validation of the present investigation is ensured by comparing

with already published studies. The numerical values for the coefficient of heat transfer rate of Burgers fluid are also computed and depicted in graph.

8.1 Mathematical Formulations

The mathematical formulation of the present flow phenomenon is divided into following three sub sections.

8.1.1 Flow Profile

In this portion, mathematical modelling for the axisymmetric 2D flow of Burgers fluid is established. Moreover, it is assumed that the flow is incompressible and generated due to stretching the boundary of cylinder and having velocity and stress fields as $\mathbf{V} = [u, 0, w]$ and $\mathbf{S} = \mathbf{S}(r, z)$ respectively. Here, u is taken as the component of velocity along radial direction ($r - axis$) of the surface while, w is the component of the velocity profile along horizontal direction ($z - axis$). The boundary of the cylinder is stretched along $z - axis$ with velocity $w = \frac{U_0 z}{l}$, where, U_0 and l are specified as the reference velocity and the specific length respectively. Additionally, the flow is influenced by the uniform magnetic force of strength $B = [B_0, 0, 0]$ in the perpendicular direction of flow. We are utilizing cylindrical polar coordinates (r, θ, z) to model the flow phenomenon. The geometry of the problem is depicted in Fig. 4.1 (cf. Chapter 4).

The basic continuity and momentum equations (2.2) and (2.3) (cf. Chapter 2) under above assumptions given by

$$\frac{\partial u}{\partial r} + \frac{u}{r} + \frac{\partial w}{\partial z} = 0, \quad (8.1)$$

$$\begin{aligned}
& u \frac{\partial w}{\partial r} + w \frac{\partial w}{\partial z} + \lambda_1 \left[u^2 \frac{\partial^2 w}{\partial r^2} + w^2 \frac{\partial^2 w}{\partial z^2} + 2uw \frac{\partial^2 w}{\partial z \partial r} \right] \\
& + \lambda_2 \left[\begin{aligned}
& u^3 \frac{\partial^3 w}{\partial r^3} + w^3 \frac{\partial^3 w}{\partial z^3} + 2u^2 \left(\frac{\partial u}{\partial r} \frac{\partial^2 w}{\partial r^2} + \frac{\partial w}{\partial r} \frac{\partial^2 w}{\partial r \partial z} \right) - u^2 \left(\frac{\partial w}{\partial r} \frac{\partial^2 u}{\partial r^2} + \frac{\partial w}{\partial z} \frac{\partial^2 w}{\partial r^2} \right) \\
& + 2w^2 \frac{\partial u}{\partial z} \frac{\partial^2 w}{\partial r \partial z} + w^2 \left(\frac{\partial w}{\partial z} \frac{\partial^2 w}{\partial z^2} - \frac{\partial w}{\partial r} \frac{\partial^2 u}{\partial z^2} \right) + 3uw \left(u \frac{\partial^3 w}{\partial r^2 \partial z} + w \frac{\partial^3 w}{\partial z^2 \partial r} \right) \\
& + 2uw \left(\frac{\partial u}{\partial r} \frac{\partial^2 w}{\partial z \partial r} + \frac{\partial u}{\partial z} \frac{\partial^2 w}{\partial r^2} + \frac{\partial w}{\partial r} \frac{\partial^2 w}{\partial z^2} - \frac{\partial w}{\partial r} \frac{\partial^2 u}{\partial r \partial z} \right)
\end{aligned} \right] \\
& = \nu \lambda_3 \left[\begin{aligned}
& u \frac{\partial^3 w}{\partial r^3} + w \frac{\partial^3 w}{\partial r^2 \partial z} + \frac{u}{r} \frac{\partial^2 w}{\partial r^2} - \frac{\partial w}{\partial r} \frac{\partial^2 u}{\partial r^2} + \frac{w}{r} \frac{\partial^2 w}{\partial r \partial z} - \\
& \frac{1}{r} \frac{\partial u}{\partial r} \frac{\partial w}{\partial r} - \frac{1}{r} \frac{\partial w}{\partial r} \frac{\partial w}{\partial z} - \frac{\partial w}{\partial z} \frac{\partial^2 w}{\partial r^2}
\end{aligned} \right] + w_e \frac{\partial w_e}{\partial r} \\
& + \nu \left[\frac{\partial^2 w}{\partial r^2} + \frac{1}{r} \frac{\partial w}{\partial r} \right] - \frac{\sigma B_0^2}{\rho} \left[\begin{aligned}
& (w - w_e) + \lambda_1 u \frac{\partial w}{\partial r} + \\
& \lambda_2 \left(w \frac{\partial u}{\partial z} \frac{\partial w}{\partial r} - u \frac{\partial w}{\partial z} \frac{\partial w}{\partial r} + uw \frac{\partial^2 w}{\partial r \partial z} + w^2 \frac{\partial^2 w}{\partial r^2} \right)
\end{aligned} \right], \quad (8.2)
\end{aligned}$$

subject to the boundary conditions

$$w(r, z) = w_s = \frac{U_0 z}{l}, \quad u(r, z) = 0 \text{ at } r = R, \quad (8.3)$$

$$w(r, z) \rightarrow w_e = \frac{U_\infty z}{l}, \quad \frac{\partial w}{\partial r} \rightarrow 0 \text{ as } r \rightarrow \infty. \quad (8.4)$$

Here λ_1 is the fluid relaxation time, λ_2 the material parameter of Burgers fluid, λ_3 ($\leq \lambda_1$) the fluid retardation time and ν the kinematics viscosity of the fluid.

By utilizing equation (4.7) (cf. Chapter 4) into equations (8.1–8.4), equation (8.1) satisfied

automatically and equations (8.2 – 8.4) take the following form

$$\begin{aligned}
& (1 + 2\alpha\eta)^2 \beta_1 \left[2ff'f'' - f^2f''' \right] - (1 + 2\alpha\eta) \alpha\beta_1 f^2f'' + (1 + 2\alpha\eta)^3 f''' \\
& - (1 + 2\alpha\eta)^2 \beta_2 \left[3f^2(f'')^2 + 2f(f')^2f'' - f^3f^{iv} \right] - 4\alpha^2\beta_2 f'''f'' \\
& + (1 + 2\alpha\eta) \alpha\beta_2 \left[3f^2f'f'' + f^3f''' \right] + (1 + 2\alpha\eta)^2 \left[2\alpha f'' + ff'' - (f')^2 \right] \\
& + (1 + 2\alpha\eta)^3 \beta_3 \left[(f'')^2 - ff^{iv} \right] - 4\alpha\beta_3 (1 + 2\alpha\eta)^2 ff'' \\
& - (1 + 2\alpha\eta)^2 M^2 \left[\beta_2 ff''' - \beta_1 ff'' + f' - A \right] + (1 + 2\alpha\eta)^2 A^2 = 0, \tag{8.5}
\end{aligned}$$

$$f = 0, \quad f' = 1 \text{ at } \eta = 0, \text{ and } f' \rightarrow A, \quad f'' \rightarrow 0 \text{ as } \eta \rightarrow \infty. \tag{8.6}$$

Here $\alpha = \frac{1}{R} \sqrt{\frac{\nu l}{U_0}}$ is the curvature parameter, $\beta_1 = \lambda_1 \frac{U_0}{l}$ the relaxation time parameter, $\beta_2 = \lambda_2 \left(\frac{U_0}{l}\right)^2$ the Burgers fluid parameter, $\beta_3 = \lambda_3 \frac{U_0}{l}$ the fluid retardation time parameter, $M = \left(\frac{\sigma l B_0^2}{\rho_f U_0}\right)^{1/2}$ the magnetic force parameter and $A = \frac{w_e}{w_s}$ the velocity ratio parameter.

8.1.2 Thermal Features of Burgers Fluid

The heat equation (1.7) (cf. Chapter 1) in view of Cattaneo-Christov heat flux given in equation (2.5) (cf. Chapter 2) and non-uniform heat source/sink takes the following form

$$\begin{aligned}
& \left(u \frac{\partial T}{\partial r} + w \frac{\partial T}{\partial z} \right) = \alpha_1 \left(\frac{\partial^2 T}{\partial r^2} + \frac{1}{r} \frac{\partial T}{\partial r} \right) + \frac{Q_0}{\rho c_p} (T - T_\infty) + \lambda_t \frac{Q_0}{\rho c_p} \left(u \frac{\partial T}{\partial r} + w \frac{\partial T}{\partial z} \right) \\
& - \lambda_t \left[u^2 \frac{\partial^2 T}{\partial r^2} + w^2 \frac{\partial^2 T}{\partial z^2} + 2uw \frac{\partial^2 T}{\partial r \partial z} + \frac{\partial T}{\partial r} \left(u \frac{\partial u}{\partial r} + w \frac{\partial u}{\partial z} \right) + \frac{\partial T}{\partial z} \left(u \frac{\partial w}{\partial r} + w \frac{\partial w}{\partial z} \right) \right], \tag{8.7}
\end{aligned}$$

with the relative boundary conditions

$$T = T_w \text{ at } r = R \text{ and } T \rightarrow T_\infty \text{ as } r \rightarrow \infty. \tag{8.8}$$

By using the dimensionless temperature from equation (4.7) (cf. Chapter 4) into Eqs. (8.11, 8.12)

we get

$$(1 + 2\alpha\eta)\theta'' + 2\alpha\theta' + \text{Pr} f\theta' + \text{Pr}\beta_t[-ff'\theta' - f^2\theta''] + \delta\theta + \delta\beta_t f\theta' = 0, \quad (8.9)$$

$$\theta = 1 \text{ at } \eta = 0, \text{ and } \theta \rightarrow 0 \text{ as } \eta \rightarrow \infty. \quad (8.10)$$

Here $\left(\text{Pr} = \frac{\nu}{\alpha_1}\right)$ is the Prandtl number, $\beta_t (= \lambda_t \frac{U_0}{T})$ the thermal relaxation time constant and $\delta \left(= \frac{lQ_0}{U_0(\rho c)_f}\right)$ the heat rise/fall parameter.

8.1.3 Relation for Chemical Species

Here we are considering (G, H) as chemical reactants having (a, b) as concentrations with (k_c, k_s) as rate constants respectively. The homogeneous response for cubic autocatalysis is considered as below



whereas the isothermal response of first order at the surface of catalyst (heterogeneous) is presented as



Furthermore, it is supposed that the reactants are isothermal and are farther from the surface at the ambient liquid, a_0 is considered as the uniform concentration of reactant A while the autocatalyst doesn't exist. Such limitations lead to the following governing equations for species

$$u \frac{\partial a}{\partial r} + w \frac{\partial a}{\partial z} = D_G \left(\frac{1}{r} \frac{\partial a}{\partial r} + \frac{\partial^2 a}{\partial r^2} \right) - k_c ab^2, \quad (8.13)$$

$$u \frac{\partial b}{\partial r} + w \frac{\partial b}{\partial z} = D_H \left(\frac{1}{r} \frac{\partial b}{\partial r} + \frac{\partial^2 b}{\partial r^2} \right) + k_c a b^2, \quad (8.14)$$

with associated boundary conditions as

$$D_G \frac{1}{r} \frac{\partial a}{\partial r} = k_s a, \quad D_H \frac{1}{r} \frac{\partial b}{\partial r} = -k_s a \text{ at } r = R, \quad (8.15)$$

$$a \rightarrow a_0, \quad h \rightarrow 0 \text{ as } r \rightarrow \infty. \quad (8.16)$$

Here D_G is the coefficient of diffusion for the specie G whereas D_H is the diffusion coefficient for specie H .

Making use of following transformations

$$a = a_0 \Phi(\eta), \quad b = b_0 \Psi(\eta). \quad (8.17)$$

By utilizing above transformations in Eqs. (8.13 – 8.16) we get

$$\left((1 + 2\alpha\eta)\Phi'' + 2\alpha\Phi' \right) \frac{1}{Sc} + f\Phi' - k_1\Phi\Psi^2 = 0, \quad (8.18)$$

$$\left((1 + 2\alpha\eta)\Psi'' + 2\alpha\Psi' \right) \frac{\lambda^*}{Sc} + f\Psi' + k_1\Phi\Psi^2 = 0, \quad (8.19)$$

$$\Phi'(0) = k_2\Phi(0), \quad \lambda^*\Psi'(0) = -k_2\Phi(0), \quad (8.20)$$

$$\Phi \rightarrow 1, \quad \Psi \rightarrow 0 \text{ as } \eta \rightarrow \infty. \quad (8.21)$$

Here $\lambda^* = \frac{D_H}{D_G}$ is the diffusion coefficient, k_1 the homogeneous reaction constant, k_2 the heterogeneous reaction constant and $Sc = \frac{\nu}{D_a}$ the Schmidt number.

Now, by assuming the equality of the coefficients of diffusion i.e., $D_H = D_G$ implies that $\lambda^* = 1$. This implies that

$$\Phi(\eta) + \Psi(\eta) = 1. \quad (8.22)$$

Therefore, we finally arrived at the following

$$\left((1 + 2\alpha\eta)\Phi'' + 2\alpha\Phi' \right) \frac{1}{Sc} + f\Phi' - k_1(1 - \Phi)^2\Phi = 0, \quad (8.23)$$

$$\Phi'(0) = k_2\Phi(0) \text{ and } \Phi \rightarrow 1 \text{ as } \eta \rightarrow \infty. \quad (8.24)$$

8.2 Validation of Numerical Scheme

Tables 8.1 and 8.2 are evaluation tables of $-f''(0)$ for several values of β_1 and M , respectively with comparison of some already published articles. Finally, from these tables we are assured that the our recent investigations are authentic and the numerical scheme BVP Midrich written in section (1.3.1) (cf. Chapter 1) is a valid technique.

Table 8.1: A comparison table for $-f''(0)$ against different values of β_1 in limiting case when $\alpha = \beta_2 = \beta_3 = M = A = 0$.

β_1	Hayat <i>et al.</i> [135]	Khan <i>et al.</i> [12]	Present case
0.0	1.000000	1.0000000	1.00000000
0.2	1.051995	1.0519893	1.05198926
0.4	1.101930	1.1019281	1.10192772
0.6	1.150175	1.1501695	1.15016960
0.8	1.197689	1.1977124	1.19771371

Table 8.2: A comparison table for $-f''(0)$ against different values of M in limiting case when $\alpha = \beta_1 = \beta_2 = \beta_3 = A = 0$.

M	Fathizadeh <i>et al.</i> [144]	Ahmed <i>et al.</i> [145]	Present case
0.5		1.224745	1.2247447
1.0	1.41421	1.414213	1.4142134
1.5			1.5811367
2.0			1.7320451
5.0	2.44948	2.449474	204494738

8.3 Discussion of Results

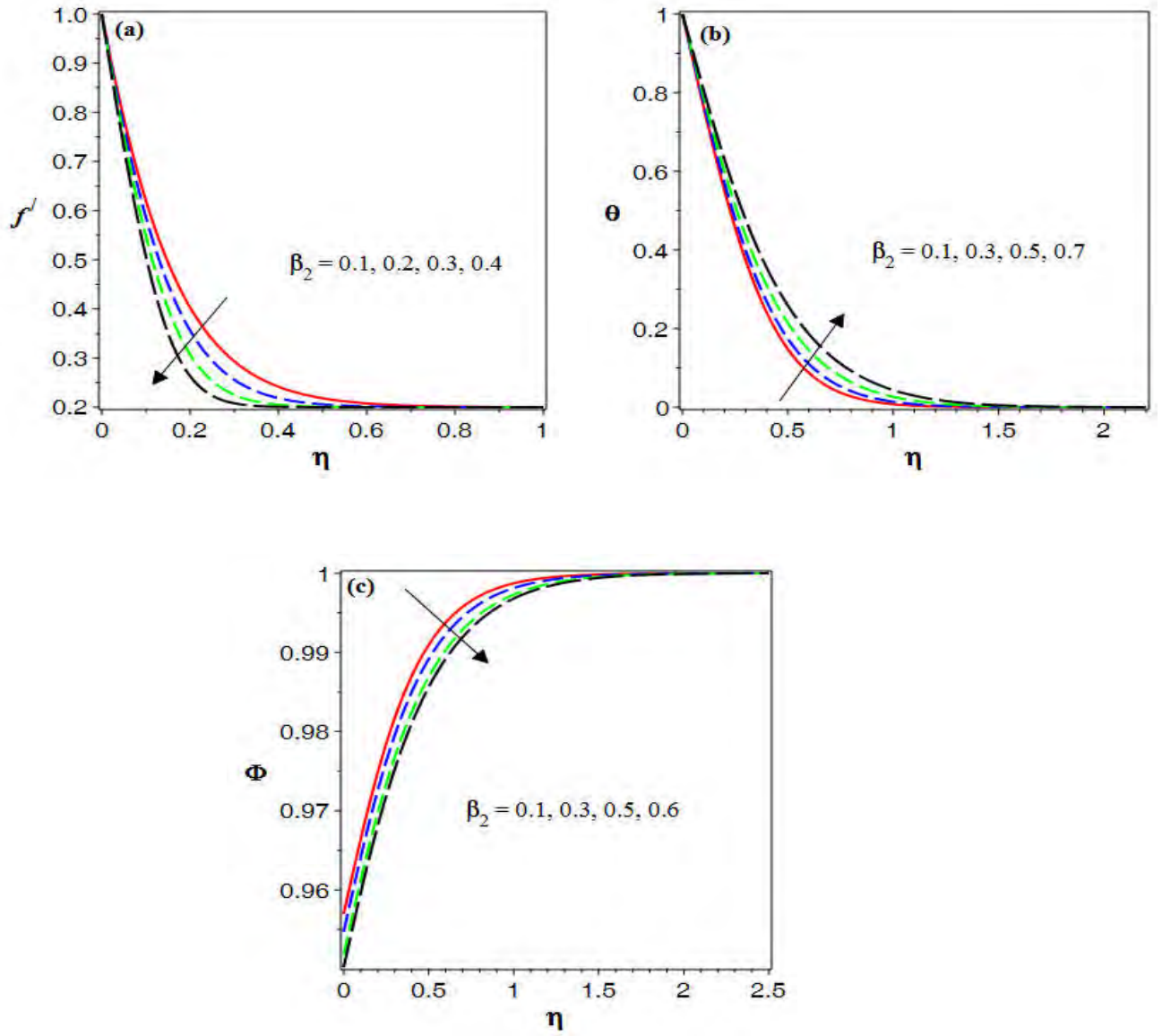
We have planned this part of the study to disclose the characteristics of all physical constraints involved in the ODE's of mathematical formulation section. We have utilized the BVP midrich numerical scheme of MAPLE explained in section (1.3.1) (cf. Chapter 1) to encounter the

investigation of physical behavior of numerous parameters. We have encountered the ODE's depicted in equations (8.5), (8.9) and (8.23) with associated boundary conditions mentioned in Eqs. (8.6), (8.10) and (8.24). The physical impacts of several parameters on flow, temperature and solutal distributions are explored and depicted through Figs. 8.1 – 8.9. Fixed values are allocated to all leading parameters during numerical simulations like, $\alpha = 0.1$, $\beta_1 = 0.7$, $\beta_2 = 0.25$, $\beta_3 = 0.5$, $M = 2.0$, $A = 0.2$, $Pr = 5.0$, $\beta_t = 0.4$, $k_1 = 0.4$, $k_2 = 0.5$, $Sc = 6.0$ and some are mentioned in graphs.

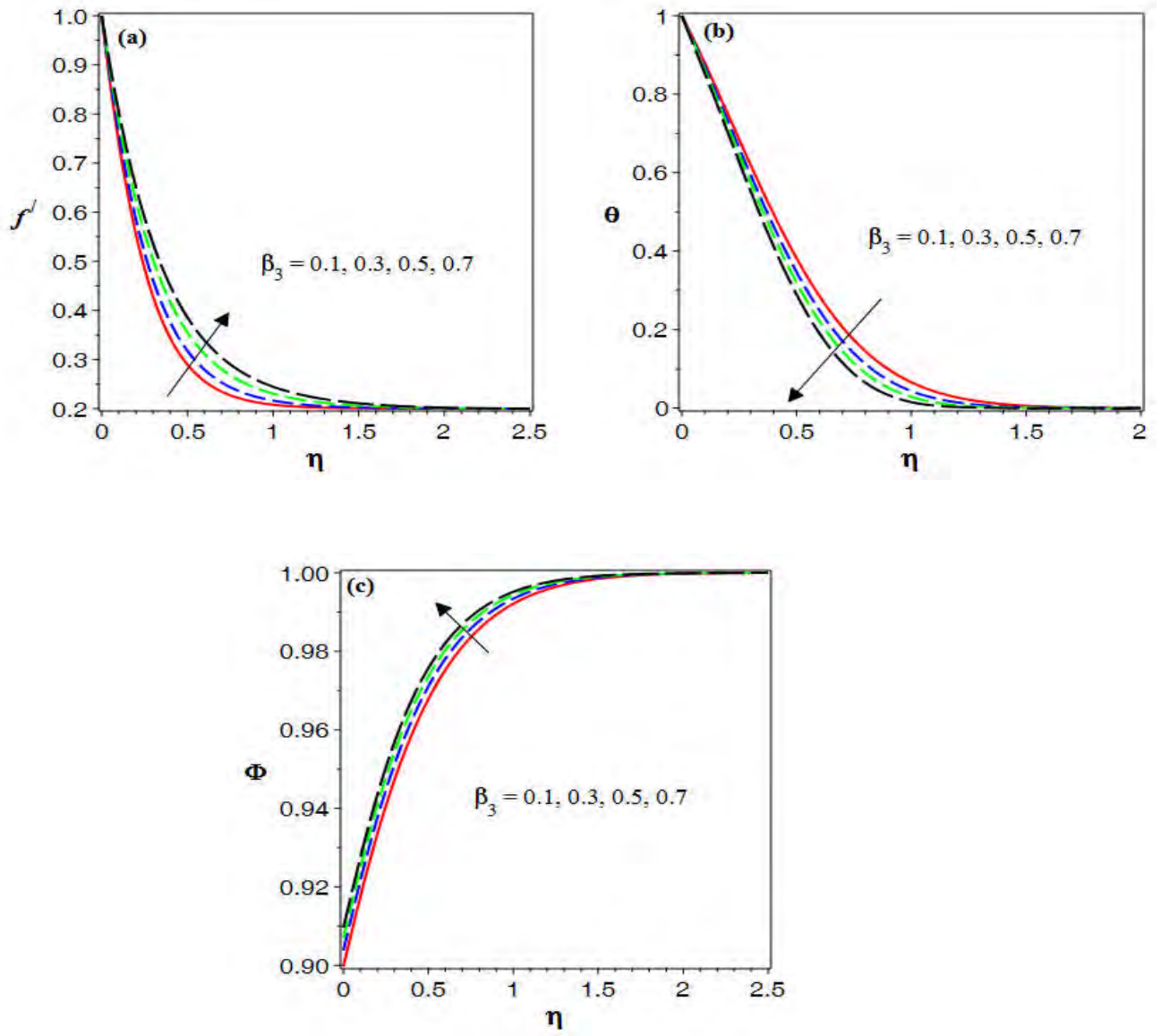
We are deliberating the physical intimation of all involved parameters with a reasonable justification. We have plotted Figs. 8.1(a – c) to ensure the physical interpretation of Burgers fluid parameter towards velocity, thermal and concentration profiles of Burgers fluid. It can be judged from these plots that the flow profile of Burgers fluid becomes more weaker as we intensify the magnitude of Burgers fluid parameter whereas, an upsurge is shown in temperature distribution for escalating values of Burgers fluid parameter. Actually, when we increase the Burgers fluid parameter then it means stress relaxation time (λ_2) enhances due to which fluid tends to behave like solid type and consequently the flow profile deteriorates, and thermal profile rises. Additionally, the concentration rate founds to be declined when we assign larger values to Burgers fluid parameter. The characteristics of retardation time parameter (β_3) against flow, temperature and solutal distributions are depicted in Figs. 8.2(a – c). The flow and concentration profiles of Burgers fluid rise while the thermal energy transport diminishes for escalating values of Deborah number β_3 . Physically, it happens because of enlargement in retardation time λ_3 . Moreover, the influence of magnetic force parameter (M) on velocity, thermal and solutal distributions of Burgers fluid can be seen in Figs. 8.3(a – c). It is found that the velocity of the fluid declines for intensifying effects of magnetic parameter whereas,

opposite trend is depicted for thermal and solutal distributions when compared to velocity profile of Burgers liquid. Lorentz force is responsible for this behavior. Resistance between fluid elements rises and consequently velocity reduces while, temperature profile and concentration rate of species boost up. To highlight the features of temperature distribution for Prandtl number and concentration rate for Schmidt number Figs. 8.4(*a, b*) are portrayed. From these plots, diminution in thermal distribution is assessed for higher amount of Prandtl number whereas, for larger Schmidt number concentration rate of chemical species shows an enhancing trend. Physically, Prandtl number has inverse relation with thermal diffusivity and obviously larger amount of Prandtl number results in lower thermal diffusivity which ultimately decreases the fluid temperature. Moreover, Schmidt number has an inverse relation with molecular diffusion rate and has a direct relation with momentum diffusion rate (viscosity). Hence by increasing Schmidt number the viscosity of the fluid increases which results in the augmentation of concentration rate. Fig. 8.5 elucidates the graphical illustration of velocity ratio parameter (*A*) for flow distribution of Burgers liquid. Form this plot it is detected that the flow phenomenon and the associated thickness of boundary layer of Burgers liquid increase with an escalation in the magnitude of velocity ratio constraint ($A < 1$). Basically, $A = \frac{w_e}{w_s}$ is the ratio of free stream velocity (w_e) to the stretching velocity of the cylinder (w_s). Here the condition ($A < 1$) corresponds to the situation that depicts that the velocity of the free stream is lesser as compared to the velocity of the stretching cylinder. Physically, it makes sense that when we intensify the magnitude of *A* then ultimately velocity of the free stream rises and therefore the fluid flows with more speed. Here it is important to mention that at $A = 1$ boundary layer will not be achieved it is due to the situation that the velocity of free stream equals to the velocity of the stretching cylinder which elaborates that the fluid motion and boundary

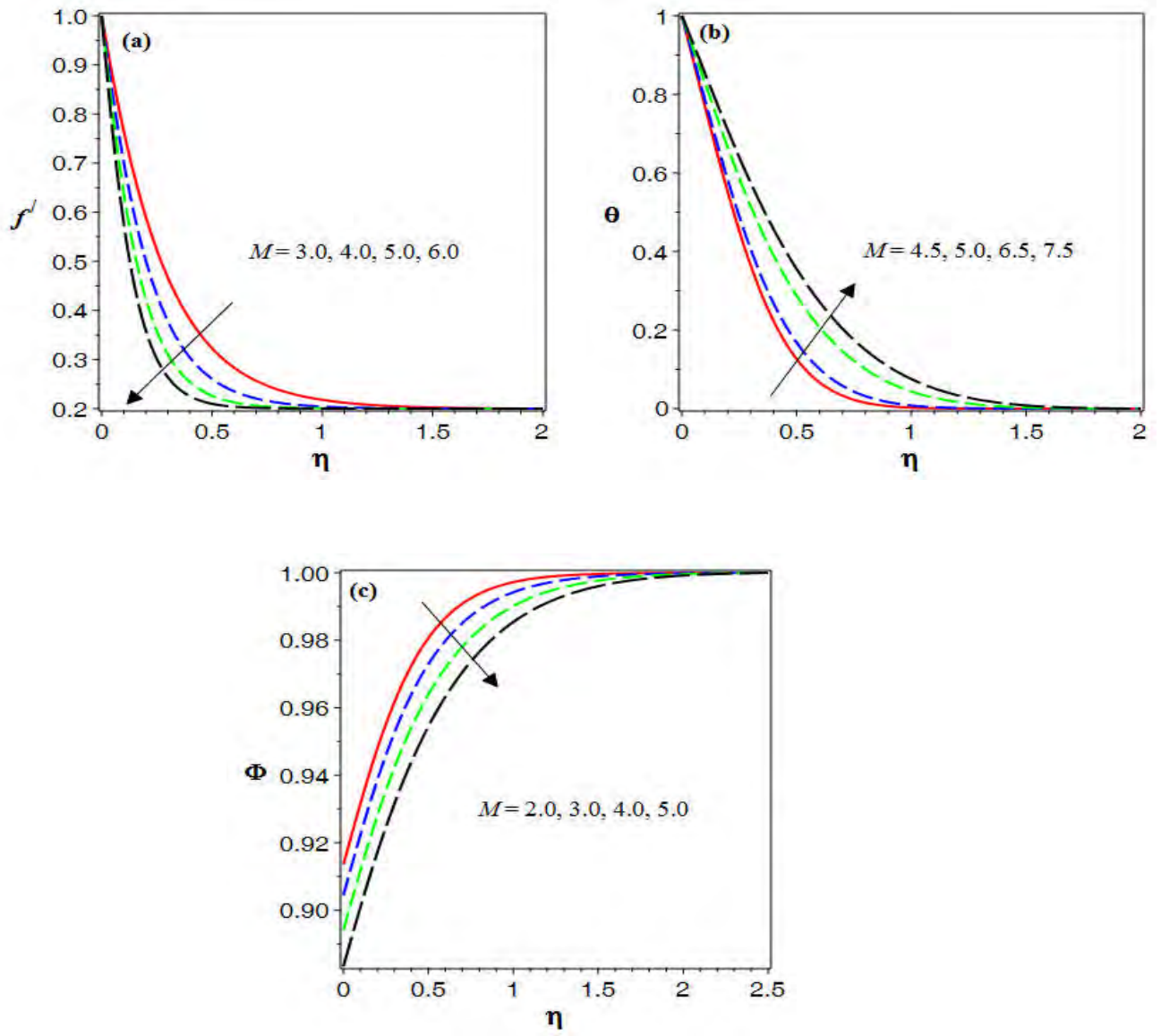
motion are at equal rates. Figs. 8.6(a, b) are depicted to highlight the physical influence of heat rise/fall parameter against thermal distribution of Burgers liquid. From these graphs, it is assessed that the thermal distribution of fluid significantly affected by the heat source/sink parameter. A clear upsurge is detected in temperature profile of Burgers fluid due to escalation in the extent of heat rise parameter ($\delta > 0$) whereas, it declines by increasing the scale of heat fall parameter ($\delta < 0$) as expected. These results were expected because escalation in the heat rise scale ultimately assures the addition of more heat in the system which results in upsurge of thermal state of the liquid. Moreover, increasing the scale of heat fall parameter means that extra amount of heat leaves the system which ultimately declines the thermal state of liquid. To ensure to physical behavior of thermal relaxation time parameter (β_t) on thermal state of liquid in the form of graphical representation we have designed Fig. 8.7. From this sketch, it can be verified that the thermal distribution of Burgers liquid depreciates with stronger impacts of β_t . Physically, the escalation in scale of β_t implies that the larger heat flux relaxation time and this means that more time is needed to the fluid elements to pass waves to their adjacent elements and consequently this phenomenon corresponds to decline the thermal state of the entire system. Moreover, it is observed that in case ($\lambda_t = 0$) this Cattaneo-Christov heat flux model converted into the classical Fourier's law of thermal conduction. To envision the homogeneous and heterogenous reaction parameters (k_1 and k_2) impacts on solutal distribution Figs. 8.8(a, b) are portrayed. We found that the solutal distribution of Burgers fluid become weaker for stronger strength of homogenous response (k_1) while it enlarges for higher strength of heterogenous reaction constraint (k_2). It is the fact that some of the reactants utilize during homogeneous process due to which viscosity of the concentration deteriorates and hence solutal profile declines for increasing the strength of homogeneous reactions.



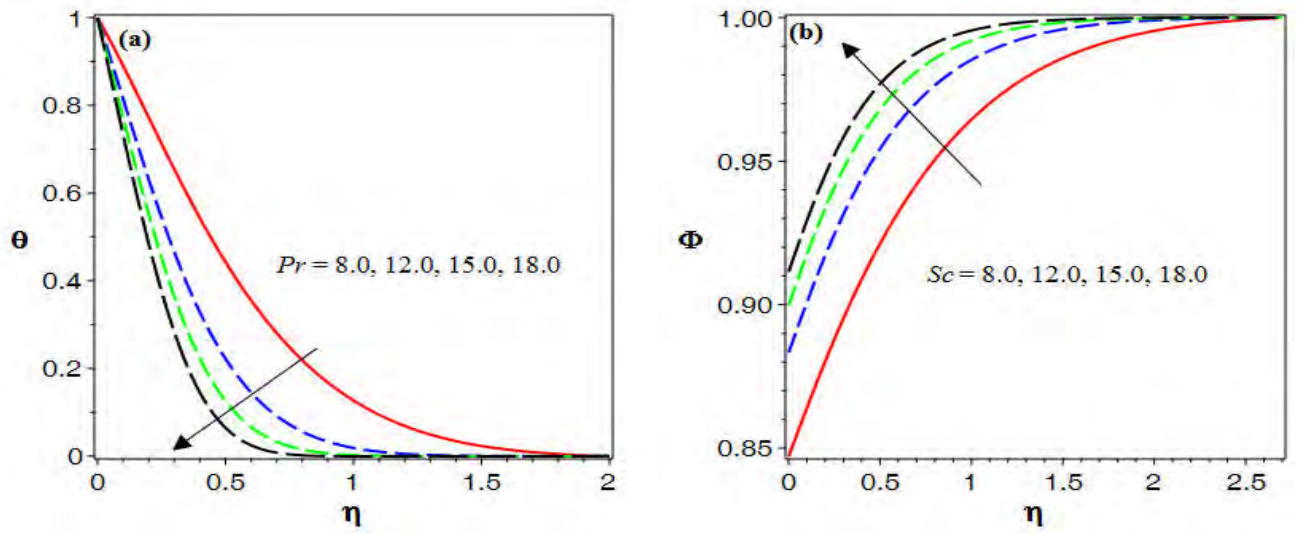
Figs. 8.1(a – c): Impact of β_2 on flow, thermal and concentration profiles.



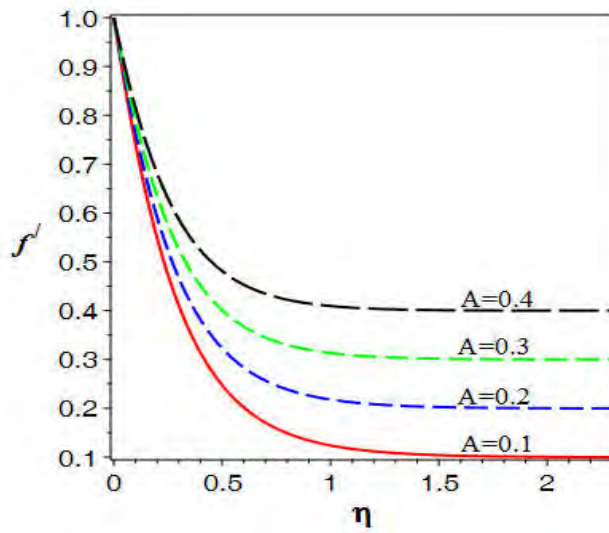
Figs. 8.2(a – c): Impact of β_3 on flow, thermal and concentration profiles.



Figs. 8.3(a – c): Effect of M on flow, thermal and concentration profile.



Figs. 8.4(a, b): Effect of Pr and Sc on θ and ϕ .



Figs. 8.5(a - c): Effect of A on flow profile.

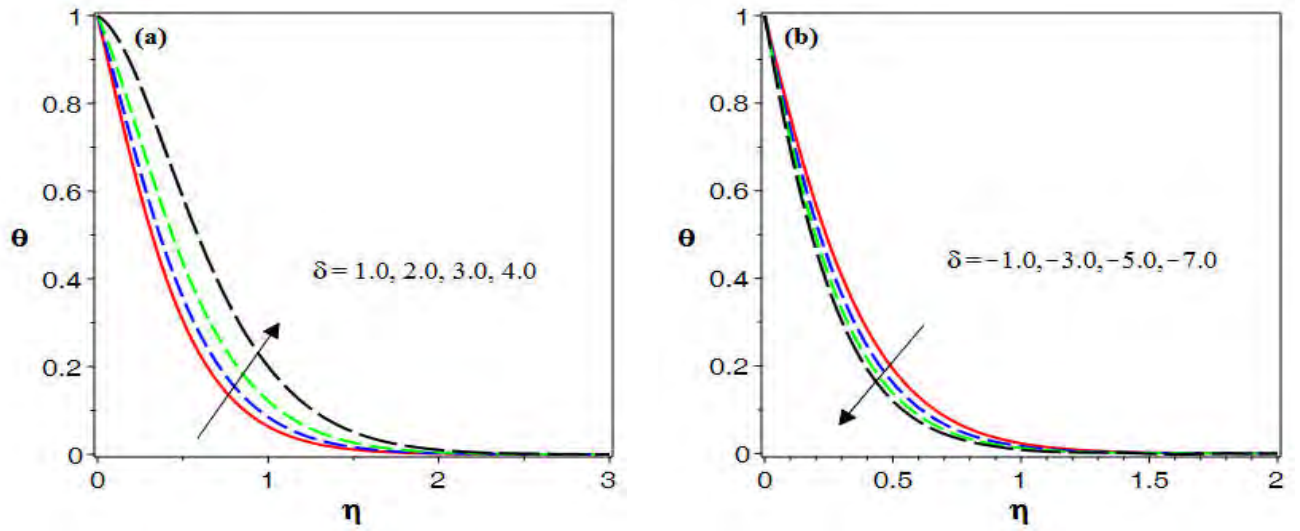


Fig. 8.6(a, b): (a) Impact of $\delta > 0$ on θ , (b) Impact of $\delta < 0$ on θ .

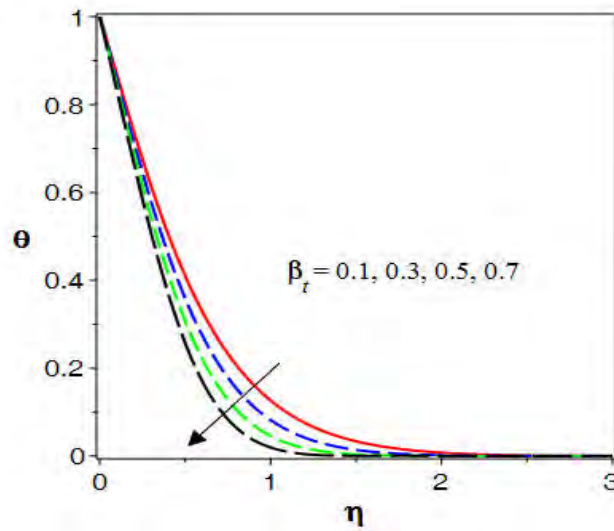


Fig. 8.7: Impact of β_t on θ .

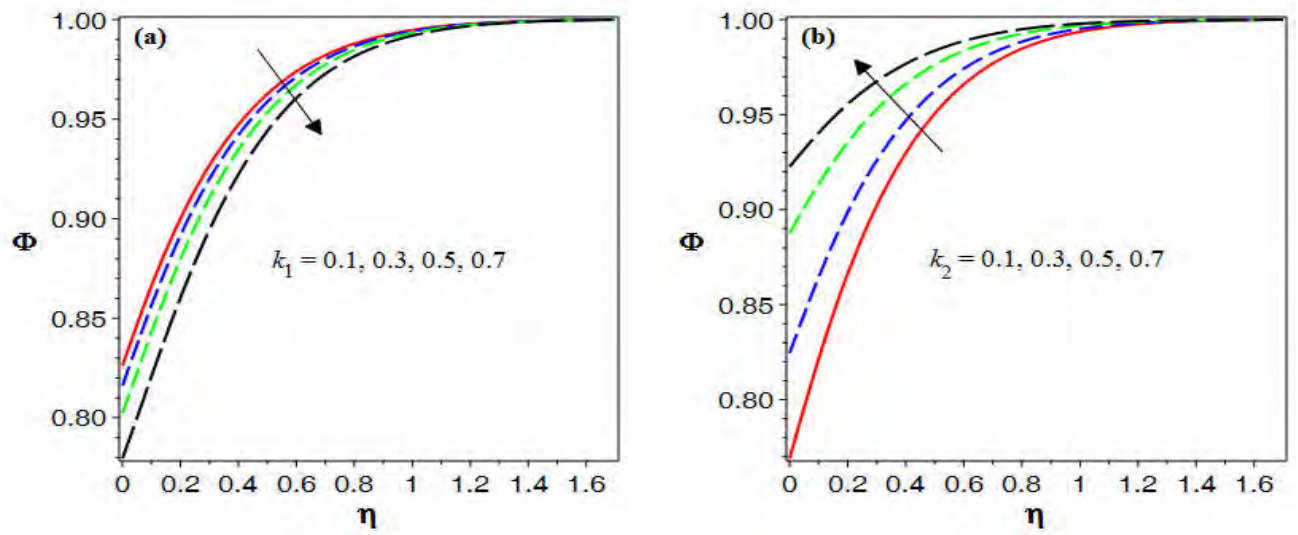


Fig. 8.8(a, b): Impact of k_1 and k_2 on concentration profile.

Chapter 9

Conclusions and Forthcoming Work

The main findings from the present research are given in Section **9.1** and some useful recommendations for forthcoming work are mentioned in Section **9.2**.

9.1 Conclusions

The aim of this thesis was to explore the thermal transport features in the steady flow of non-Newtonian viscoelastic Burgers fluid accelerated by stretching surfaces. Mathematical modelling has been carried out for the flow of Burgers fluid due to unidirectional stretching sheet, bidirectional stretching sheet and stretching cylinder. Different physical effects are considered to investigate their impacts on the fluid flow and heat transport. The analytic and numerical solutions of governed differential equations are developed by employing homotopy analysis method and BVP midrich numerical scheme. The main results of this work are summarized as below.

- The developing strength of fluid relaxation time parameter and material parameter of

Burgers fluid de-accelerated the momentum transport whereas, incrementing magnitude of fluid retardation time parameter accelerated the momentum transport in the flow.

- Diminution in flow velocity along x -direction of the flow was noted for developing magnitude of stretching strength parameter while along y -direction of the flow velocity profile showed opposite trend.
- The flow profile of Burgers nanofluid boosted up for augmenting values of velocity ratio parameter and declined for larger magnetic parameter.
- Thermal and solutal transport in the flow improved for augmenting values of fluid relaxation time parameter and material parameter of Burgers fluid.
- Reduction in thermal and solutal distributions of Burgers nanofluid was noted for escalating values of retardation time fluid parameter.
- It is observed that the rate of heat transfer in the flow was promoted due to escalating magnitude of Eckert number, heat rise parameter, thermophoretic force parameter and fluid relaxation time parameter.
- Thermal distribution of nanofluid showed enhancing trend for escalating magnitude of Brownian motion constraint whereas, converse trend was being noticed for solutal distribution.
- Thermal and concentration profiles of Burgers liquid declined for thermal relaxation time parameter and solutal relaxation time parameter respectively.
- Thermal and solutal distributions of nanofluid deteriorated for larger Prandtl and Lewis numbers, respectively.

- Enhancing trend of the temperature distribution of Burgers nano liquid was being noticed for improving values of radiation parameter and temperature ratio parameter.
- The thermal profiles of Burgers nanoliquid depicted significant variation and shows a rising trend for intensifying effects thermal Biot number as well as temperature and space dependent heat source parameters.
- The impacts of fluid relaxation time parameter and fluid retardation time parameter were quite opposite on momentum and energy transport profiles.

9.2 Forthcoming work

The foremost concern of this thesis is to develop the analytical and numerical solutions to the steady flow of Burgers fluid over stretching surfaces like, unidirectional and bidirectional stretching sheets as well as stretching cylinder. The results developed in this thesis give birth to a new area of research. Some of the suggestions for the forthcoming work are mentioned as below:

- The unsteady flow features of Burgers fluid accelerated by stretching geometries may be further study.
- It could be more interesting to explore the flow features of Burgers fluid over rotating as well as swirling geometries.
- To investigate the flow phenomenon and heat transfer in generalized Burgers fluid over stretching cylinder may of great importance.

- Burgers fluid flow can be investigated over complex surfaces like, flow in a nozzle, flow in a channel, flow in air ducts, flow in a cavity, flow generated over the curved surface, flow inside the annular pipe and flow caused by the bundles of circular surfaces.
- We are planning to explore the flow and thermal characteristics of Burgers fluid by adopting advanced numerical methods like, finite element method (FEM), finite difference method (FDM), finite volume method (FVM), and lattice Boltzmann method (LBM).

Bibliography

- [1] J.M. Burgers, Mechanical considerations-model systems-phenomenological theories of relaxation and of viscosity (1939).
- [2] J.C. Maxwell, On the dynamical theory of gases, *Philos. Trans. R. Soc. Lond.*, **157** (1866) 26–78.
- [3] J.G. Oldroyd, On the formulation of rheological equations of state, *Proc. R. Soc. Lond. Ser. A*, **200** (1950) 523–591.
- [4] P. Ravindran, J.M. Krishnan and K.R. Rajagopal, A note on the flow of a Burgers' fluid in an orthogonal rheometer, *Int. J. Eng. Sci.*, **42** (2004) 1973.
- [5] T. Hayat, C. Fetecau and S. Asghar, Some simple flows of a Burgers' fluid, *Int. J. Eng. Sci.*, **44** (2006) 1423.
- [6] T. Hayat, Exact solutions to rotating flows of a Burgers' fluid, *Comput. Math. Appl.*, **52** (2006) 1413.
- [7] M. Khan, S. Asghar and T. Hayat Hall effect on the pipe flow of a Burgers' fluid: An exact solution, *Nonlinear Anal. Real World Appl.*, **10** (2009) 974-979.

- [8] T. Hayat, S. Ali, M. Awais and S. Obaidat, Stagnation point flow of Burgers' fluid over a stretching surface, *Prog. Comp. Fluid Dyn.*, **13** (2012) 48-53.
- [9] T. Hayat, M. Waqas, M.I. Khan A. Alsaedi and S.A. Shehzad, Magnetohydrodynamic flow of burgers fluid with heat source and power law heat flux, *Chin. J. Phy.*, **55** (2017) 318-330.
- [10] M. Khan, M. Irfan and W.A. Khan, Impact of nonlinear thermal radiation and gyrotactic microorganisms on the Magneto-Burgers nanofluid, *Int. J. Mech. Sci.*, **130** (2017) 375-382.
- [11] M. Waqas, M.I. Khan, T. Hayat and A. Alsaedi, A generalized Fourier and Fick's perspective for stretching flow of burgers fluid with temperature-dependent thermal conductivity, *Therm. Sci.*, **23** (2019) 3425-3432.
- [12] M. Khan, Z. Iqbal and A. Ahmed, Stagnation point flow of magnetized Burgers' nanofluid subject to thermal radiation, *Appl. Nanosci.*, **10** (2020), 5233-5246.
- [13] Z. Iqbal, M. Khan, A. Ahmed, J. Ahmed and A. Hafeez, Thermal energy transport in Burgers nanofluid flow featuring the Cattaneo–Christov double diffusion theory, *Appl. Nanosci.*, **10** (2020) 5331–5342
- [14] C.Y. Wang, The three-dimensional flow due to a stretching surface, *Phys. Fluids*, **27** (1984) 1915-1917.
- [15] P.D. Ariel, Generalized three-dimensional flow due to a stretching sheet, *Z. Angew. Math. Mech.* **83** (2003) 844–852.

- [16] I.C. Liu and H.I. Andersson, Heat transfer over a bidirectional stretching sheet with variable thermal conditions, *Int. J. Heat Mass Transf.*, **51** (20018) 4018-4024.
- [17] T. Hayat, S.A. Shehzad and A. Alsaedi, Three-dimensional flow of Jeffrey fluid over a bidirectional stretching surface with heat source/sink, *J. Aerosp. Eng.*, **27** (2014) 04014007.
- [18] B. Mahanthesh, B.J. Gireesha, R.S.R. Gorla, F.M. Abbasi and S.A. Shehzad, Numerical solutions for magnetohydrodynamic flow of nanofluid over a bidirectional non-linear stretching surface with prescribed surface heat flux boundary, *J. Magnet. Mag. Mater.*, **417** (2016) 189-196.
- [19] M. Khan and W.A. Khan, Three-dimensional flow and heat transfer to Burgers fluid using Cattaneo-Christov heat flux model, *J. Mol. Liq.*, **221** (2016) 651-657.
- [20] W.A. Khan, M. Khan and A.S. Alshomrani, Impact of chemical processes on 3D Burgers fluid utilizing Cattaneo-Christov double-diffusion: Applications of non-Fourier's heat and non-Fick's mass flux models, *J. Mol. Liq.*, **223** (2016) 1039-1047.
- [21] W.A. Khan, A.S. Alshomrani and M. Khan, Assessment on characteristics of heterogeneous-homogenous processes in three-dimensional flow of Burgers fluid, *Res. Phy.*, **6** (2016) 772-779.
- [22] S. Hina, M. Munir and M. Mustafa, A non-Fourier heat flux approach to model MHD Oldroyd-B fluid flow due to bidirectional stretching surface, *Int. J. Mech. Sci.*, **131** (2017) 146-154.

- [23] M. Khan, L. Ahmad, W.A. Khan, A.S. Alshomrani, A.K. Alzahrani and M.S. Alghamdi, A 3D Sisko fluid flow with Cattaneo-Christov heat flux model and heterogeneous-homogeneous reactions: A numerical study, *J. Mol. Liq.*, **238** (2017) 19-26.
- [24] S. Gupta and S. Gupta, MHD three dimensional flow of Oldroyd-B nanofluid over a bidirectional stretching sheet: DTM-Padé Solution, *Nonlin. Eng.*, **8** (2019) 744-754.
- [25] D. Lu, M. Mohammad, M. Ramzan, M. Bilal, F. Howari and M. Suleman, MHD boundary layer flow of Carreau fluid over a convectively heated bidirectional sheet with non-Fourier heat flux and variable thermal conductivity, *Symmetry*, **11** (2019) 668.
- [26] A.I. Alsabery, F. Selimefendigil, I. Hashim, A.J. Chamkha and M. Ghalambaz, Fluid-structure interaction analysis of entropy generation and mixed convection inside a cavity with flexible right wall and heated rotating cylinder, *Int. J. Heat Mass Transf.*, **140** (2019) 331-345.
- [27] Z. Iqbal, M. Khan and A. Ahmed, On modified Fourier heat flux in stagnation point flow of magnetized Burgers' fluid subject to homogeneous-heterogeneous reactions, *J. Therm. Anal. Calorim.*, 2020; <https://doi.org/10.1007/s10973-020-10308>.
- [28] M. Khan, Z. Iqbal and A. Ahmed, A mathematical model to examine the heat transport features in Burgers fluid flow due to stretching cylinder, *J. Therm. Anal. Calorim.*, 2020; <https://doi.org/10.1007/s10973-020-10224>.
- [29] H. Upreti, A.K. Pandey, M. Kumar and O.D. Makinde, Ohmic heating and non-uniform heat source/sink roles on 3D darcy–Forchheimer flow of CNTs nanofluids over a stretching surface, *Arab. J. Sci. Eng.*, **45** (2020) 7705-7717.

- [30] Z. Iqbal, M. Khan A. Ahmed and S. Nadeem, Features of thermophoretic and Brownian forces in Burgers fluid flow subject to Joule heating and convective conditions, *Phy. Scr.*, **96** (2020) 015211.
- [31] T. Javed, M. Faisal and I. Ahmad, Dynamisms of solar radiation and prescribed heat sources on bidirectional flow of magnetized Eyring-Powell nanofluid, *Case Stud. Therm. Eng.*, **21** (2020) 100689.
- [32] L.J. Crane, Boundary layer flow due to a stretching cylinder, *Z. Angew. Math. Phys.*, **26** (1975) 619–622.
- [33] C.Y. Wang, Fluid flow due to a stretching cylinder, *Phys. Fluids*, **31** (1988) 466–468.
- [34] C.Y. Wang, and C.O. Ng, Slip flow due to a stretching cylinder, *Int. J. Non-Linear Mech.*, **46** (2011) 1191–1194.
- [35] H.R. Ashorynejad, M. Sheikholeslami, I. Pop and D.D. Ganji, Nanofluid flow and heat transfer due to a stretching cylinder in the presence of magnetic field, *Heat Mass Transf.*, **49** (2013) 427–436.
- [36] M. Sheikholeslami, M.T. Mustafa and D.D. Ganji, Nanofluid flow and heat transfer over a stretching porous cylinder considering thermal radiation, *Iran. J. Sci. Technol.*, **39** (2015) 433–440.
- [37] M. Tamoor, M. Waqas, M.I. Khan, A. Alsaedi and T. Hayat, Magnetohydrodynamic flow of Casson fluid over a stretching cylinder, *Res. Phys.*, **7** (2017) 498–502.

- [38] Hashim, A. Hamid and M. Khan, Transient flow and heat transfer mechanism for Williamson-nanomaterials caused by a stretching cylinder with variable thermal conductivity, *Microsys. Tech.*, **25** (2019) 3287–3297.
- [39] Z. Iqbal, M. Khan, A. Ahmed, J. Ahmed and A. Hafeez. Thermal energy transport in Burgers nanofluid flow featuring the Cattaneo–Christov double diffusion theory, *Appl. Nanosci*, **10** (2020) 5331–5342
- [40] M. Khan, A. Ahmed, M. Irfan and J. Ahmed, Analysis of Cattaneo–Christov theory for unsteady flow of Maxwell fluid over stretching cylinder, *J. Therm. Anal. Calorim.*, **144** (2021) 145–154
- [41] D. Pal and H. Mondal, Hydromagnetic convective diffusion of species in Darcy–Forchheimer porous medium with non-uniform heat source/sink and variable viscosity, *Int. Commun. Heat Mass Transf.*, **39** (2012) 913-917.
- [42] R. Sivaraj and B.R. Kumar, Viscoelastic fluid flow over a moving vertical cone and flat plate with variable electric conductivity, *Int. J. Heat Mass Transf.*, **61** (2013) 119-128.
- [43] D. Mythili and R. Sivaraj, Influence of higher order chemical reaction and non-uniform heat source/sink on Casson fluid flow over a vertical cone and flat plate, *J. Mol. Liq.*, **216** (2016) 466-475.
- [44] M. Durairaj, S. Ramachandran and R.M. Mehdi, Heat generating/absorbing and chemically reacting Casson fluid flow over a vertical cone and flat plate saturated with non-Darcy porous medium, *Int. J. Num. Meth. Heat Fluid Flow*, **27** (2017) 156-173.

- [45] T. Hayat, S. Qayyum, A. Alsaedi and S. Asghar, Radiation effects on the mixed convection flow induced by an inclined stretching cylinder with non-uniform heat source/sink, *PLOS ONE*, **12** (4), e0175584.
- [46] T. Hayat, I. Ullah, M. Waqas and A. Alsaedi, MHD stratified nanofluid flow by slandering surface, *Phys. Scr.*, **93** (2018) 115701.
- [47] M. Irfan, M. Khan and W.A. Khan, Impact of non-uniform heat sink/source and convective condition in radiative heat transfer to Oldroyd-B nanofluid: A revised proposed relation, *Phy. Lett. A*, **383** (2019) 376-382.
- [48] M. Ijaz, M.S. Alqarni, F. Salah and M.Y. Malik, Numerical simulation of Joule heating and Arrhenius activation energy for nonlinear radiative flow of Casson nanofluid with Cattaneo–Christov heat flux model, *Phys. Scr.*, **95** (2019) 025401.
- [49] S.S. Ghadikolaei, K. Hosseinzadeh and D.D. Ganji, Investigation on magneto Eyring-Powell nanofluid flow over inclined stretching cylinder with nonlinear thermal radiation and Joule heating effect, *World J. Eng.*, **16** (2019) 51-63.
- [50] N.S. Khashi'ie, N.M. Arifin, I. Pop and N.S Wahid, Flow and heat transfer of hybrid nanofluid over a permeable shrinking cylinder with Joule heating: A comparative analysis, *Alex. Eng. J.*, **59** (2020) 1787-1798.
- [51] J.B.J. Fourier, *Théorie Analytique De La Chaleur*, Paris, 1822.
- [52] C. Cattaneo, Sulla conduzione del calore, *Atti Semin. Mat. Fis, Univ. Modena Reggio Emilia*, **3** (1948) 83–101.

- [53] C.I. Christov, On frame indifferent formulation of the Maxwell–Cattaneo model of finite-speed heat conduction, *Mech. Res. Commun.*, **36** (2009) 481–486
- [54] B. Straughan, Thermal convection with the Cattaneo–Christov model, *Int. J. Heat Mass Transf.*, **53** (2010) 95–98.
- [55] M. Ciarletta and B. Straughan, Uniqueness and structural stability for the Cattaneo–Christov equations, *Mech. Res. Commun.*, **37** (2010) 445–447.
- [56] S.A.M. Haddad, Thermal instability in Brinkman porous media with Cattaneo-Christov heat flux, *Int. J. Heat Mass Transf.*, **68** (2014) 659–668.
- [57] V. Tibullo and V. Zampoli, A uniqueness result for the Cattaneo-Christov heat conduction model applied to incompressible fluids, *Mech. Res. Commun.*, **38** (2011) 77-79.
- [58] S. Han, L. Zheng, C. Li and X. Zhang, Coupled flow and heat transfer in viscoelastic fluid with Cattaneo-Christov heat flux model, *Appl. Math. Lett.*, **38** (2014) 87-93.
- [59] T. Hayat, M.I. Khan, M. Farooq, A. Alsaedi, M. Waqas and T. Yasmeen, Impact of Cattaneo–Christov heat flux model in flow of variable thermal conductivity fluid over a variable thicked surface, *Int. J. Heat Mass Transf.*, **99** (2016) 702-710.
- [60] M. Waqas, T. Hayat, M. Farooq, S.A. Shehzad and A. Alsaedi, Cattaneo-Christov heat flux model for flow of variable thermal conductivity generalized Burgers fluid, *J. Mol. Liq.*, **220** (2016) 642-648.
- [61] R. Malik, M. Khan and M. Mushtaq, Cattaneo-Christov heat flux model for Sisko fluid flow past a permeable non-linearly stretching cylinder, *J. Mol. Liq.*, **222** (2016) 430-434.

- [62] M. Khan, L. Ahmad, W.A. Khan, A.S. Alshomrani, A.K. Alzahrani, and M.S. Alghamdi, A 3D Sisko fluid flow with Cattaneo-Christov heat flux model and heterogeneous-homogeneous reactions: A numerical study, *J. Mol. Liq.*, **238** (2017) 19-26.
- [63] M. Irfan, M. Khan and W.A. Khan, On model for three-dimensional Carreau fluid flow with Cattaneo-Christov double diffusion and variable conductivity: a numerical approach, *J. Braz. Soc. Mech. Sci. Eng.*, **40** (2018) 577.
- [64] S.Z. Alamri, A.A. Khan, M. Azeez and R. Ellahi, Effects of mass transfer on MHD second grade fluid towards stretching cylinder: A novel perspective of Cattaneo-Christov heat flux model, *Phy. Lett. A*, **383** (2019) 276-281.
- [65] Z. Iqbal, M. Khan, A. Ahmed, J. Ahmed and A. Hafeez, Thermal energy transport in Burgers nanofluid flow featuring the Cattaneo-Christov double diffusion theory, *Appl. Nanosci.*, **10** (2020) 5331-5342.
- [66] S. Ahmed, S. Nadeem, N. Muhammad and M.N. Khan, Cattaneo-Christov heat flux model for stagnation point flow of micropolar nanofluid toward a nonlinear stretching surface with slip effects, *J. Therm. Anal. Calorim.*, **143** (2021) 1187-1199.
- [67] V.J. Rossow, On flow of electrically conducting fluids over a flat plate in the presence of a transverse magnetic field, *NACA TN*, (1957) 3971.
- [68] H. I. Andersson, MHD flow of a viscoelastic fluid past a stretching surface, *Acta Mech.*, **95** (1992) 227-230.

- [69] R. Bhargava, L. Kumar and H.S. Takhar, Numerical solution of free convection MHD micropolar fluid flow between two parallel porous vertical plates, *Int. J. Eng. Sci.*, **41** (2003) 123-136.
- [70] P.S. Datti, K.V. Prasad, M.S. Abel and A. Joshi, MHD visco-elastic fluid flow over a non-isothermal stretching sheet, *Int. J. Eng. Sci.*, **42** (2004) 935-946.
- [71] T. Hayat, M. Khan and S. Asghar, On the MHD flow of fractional generalized Burgers' fluid with modified Darcy's law, *Acta Mech. Sin.*, *23* (2007) 257-261.
- [72] M. Sajid and T. Hayat, The application of homotopy analysis method for MHD viscous flow due to a shrinking sheet, *Chaos, Sol. Frac.*, **39** (2009) 1317-1323.
- [73] S. Nadeem and S. Akram, Magnetohydrodynamic peristaltic flow of a hyperbolic tangent fluid in a vertical asymmetric channel with heat transfer, *Acta Mech. Sin.*, **27** (2011) 37-250.
- [74] S. Munawar, A. Ali and A. Mehmood, Thermal analysis of the flow over an oscillatory stretching cylinder, *Phy. Scr.*, **86** (2012) 065401.
- [75] S. Mukhopadhyay, MHD boundary layer slip flow along a stretching cylinder, *Ain Sham. Eng. J.*, **4** (2013) 317-324.
- [76] V. Rajesh, M.P. Mallesh and O.A. Bég, Transient MHD free convection flow and heat transfer of nanofluid past an impulsively started vertical porous plate in the presence of viscous dissipation, *Proc. Mater. Sci.*, **10** (2015) 80-89.

- [77] N.S. Akbar, D. Tripathi and O.A. Bég, MHD convective heat transfer of nanofluids through a flexible tube with buoyancy: A study of nano-particle shape effects, *Adv. Pow. Tech.*, **28** (2017) 453-462.
- [78] N. Shukla, P. Rana, O.A. Bég, B. Singh and A. Kadir, Homotopy study of magnetohydrodynamic mixed convection nanofluid multiple slip flow and heat transfer from a vertical cylinder with entropygeneration, *Prop. Pow. Res.*, **8** (2019) 147-162.
- [79] M. Suleman, M. Ramzan, S. Ahmad and D. Lu, Numerical simulation for homogeneous–heterogeneous reactions and Newtonian heating in the silver-water nanofluid flow past a nonlinear stretched cylinder, *Phys. Scr.*, **94** (2019) 085702.
- [80] S.A. Khan, M.I. Khan, T. Hayat and A. Alsaedi, Physical aspects of entropy optimization in mixed convective MHD flow of carbon nanotubes (CNTs) in a rotating frame, *Phys. Scr.*, **94** (2019) 125009.
- [81] D.D. Vo, Z. Shah, M. Sheikholeslami, A. Shafee and T.K. Nguyen, Numerical investigation of MHD nanomaterial convective migration and heat transfer within a sinusoidal porous cavity, *Phys. Scr.*, **94** (2019) 115225.
- [82] T.K. Nguyen, M. Sheikholeslami, S.A. Shehzad, A. Shafee and M. Alghamdi, Solidification entropy generation via FEM through a porous storage unit with applying a magnetic field, *Phys. Scr.*, **94** (2019) 095207.
- [83] S. Nadeem, M.R. Khan and A.U. Khan, MHD oblique stagnation point flow of nanofluid over an oscillatory stretching/shrinking sheet: existence of dual solutions, *Phys. Scr.*, **94** (2019) 075204.

- [84] M. Khan, Z. Iqbal and A. Ahmed, Stagnation point flow of magnetized Burgers' nanofluid subject to thermal radiation, *Appl. Nanosci.*, (2020), doi.org/10.1007/s13204-020-01360-8.
- [85] A. Ahmed, M. Khan, J. Ahmed, A. Hafeez and Z. Iqbal, Unsteady stagnation point flow of Maxwell nanofluid over a stretching disk with joule heating, *Arabian J. Sci. Eng.*, (2020), doi.org/10.1007/s13369-020-04468-9.
- [86] S.U.S. Choi, Enhancing thermal conductivity of fluids with nanoparticles, The proceedings of the 1995. In: ASME international mechanical engineering congress and exposition. *San Francisco, USA: ASME*, (1995) 99–105.
- [87] S.U.S. Choi, Z.G. Zhang, W. Yu, F.E. Lockwood and E.A. Grulke, Anomalously thermal conductivity enhancement in nanotube suspensions, *Appl. Phys. Lett.*, **4** (2001) 2252-79
- [88] H.U. Kang, S.H. Kim and J.M. Oh, Estimation of thermal conductivity of nanofluids for the application of heat transfer fluids, *Exp. Heat Transf.*, **19** (2006) 181–91.
- [89] D.H. Yoo, K.S. Hong and H.S. Yang, Study of thermal conductivity of nanofluids for the applications of heat transfer fluid, *Thermochim. Acta*, **9** (2006) 455-66
- [90] D.D. Ganji and M. Hatami, Squeezing Cu–water nanofluid flow analysis between parallel plates by DTM-Padé Method, *J. Mol. Liq.*, **193** (2014) 37–44.
- [91] M. Hatami and D.D. Ganji, Natural convection of sodium alginate (SA) non-Newtonian nanofluid flow between two vertical flat plates by analytical and numerical methods, *Case Stud. Therm. Eng.*, **2** (2014) 14–22.

- [92] M.Y. Malik, I. Khan, A. Hussain and T. Salahuddin, Mixed convection flow of MHD Eyring-Powell nanofluid over a stretching sheet: a numerical study, *AIP Adv.*, **5** (2015) 117–118.
- [93] E. Seiyed, Ghasemi, M. Vatani, M. Hatami and D.D. Ganji, Analytical and numerical investigation of nanoparticle effect on peristaltic fluid flow in drug delivery systems, *J. Mol. Liq.*, **215** (2016) 88–97.
- [94] R. Ellahi, M. Hassan, A. Zeeshan & A.A. Khan, The shape effects of nanoparticles suspended in HFE-7100 over wedge with entropy generation and mixed convection, *Appl. Nanosci.*, **6** (2016) 641–651.
- [95] N.S. Akbar, M. Raza and R. Ellahi, Impulsion of induced magnetic field for Brownian motion of nanoparticles in peristalsis, *Appl. Nanosci.*, **6** (2016) 359–370.
- [96] M. Irfan, M. Khan and W.A. Khan, Numerical analysis of unsteady 3D flow of Carreau nanofluid with variable thermal conductivity and heat source/sink, *Res. Phys.*, **7** (2017) 3315–3324.
- [97] K. Hosseinzadeh, A.J. Amiri, S.S. Ardahaie and D.D. Ganji, Effect of variable lorentz forces on nanofluid flow in movable parallel plates utilizing analytical method, *Case Stud. Therm. Eng.*, **10** (2017) 595–610.
- [98] S.S. Nourazar, M. Hatami, D.D. Ganji and M. Khazayinejad, Thermal-flow boundary layer analysis of nanofluid over a porous stretching cylinder under the magnetic field effect, *Pow. Technol.*, **317** (2017) 310–319.

- [99] K.L. Hsiao, Micropolar nanofluid flow with MHD and viscous dissipation effects towards a stretching sheet with multimedia feature, *Int. J. Heat Mass Transf.*, **112** (2017) 983-990.
- [100] K.L. Hsiao, To promote radiation electrical MHD activation energy thermal extrusion manufacturing system efficiency by using Carreau-Nanofluid with parameters control method, *Energy*, **130** (2017) 486-499.
- [101] M. Hatami, J. Zhou, J. Geng and D. Jing, Variable magnetic field (VMF) effect on the heat transfer of a half-annulus cavity filled by Fe_3O_4 -water nanofluid under constant heat flux, *J. Magn. Magn. Mater.*, **451** (2018) 173-182.
- [102] Hashim, M. Khan and A. Hamid, Numerical investigation on time-dependent flow of Williamson nanofluid along with heat and mass transfer characteristics past a wedge geometry, *Int. J. Heat Mass Transf.*, **118** (2018) 480-491.
- [103] S. Nasir, S. Islam, T. Gul, Z. Shah, M.A. Khan, W. Khan, A.Z. Khan and S. Khan, Three-dimensional rotating flow of MHD single wall carbon nanotubes over a stretching sheet in presence of thermal radiation, *Appl. Nanosci.*, **8** (2018) 1361-1378.
- [104] A. Hamid, M. Khan and A.S. Alshomrani, Non-linear radiation and chemical reaction effects on slip flow of Williamson nanofluid due to a static/moving wedge: a revised model, *Appl. Nanosci.*, **10** (2019) 3171-3181.
- [105] I. Ahmad, M. Faisal and T. Javed, Bi-directional stretched nanofluid flow with Cattaneo-Christov double diffusion, *Res. Phys.*, **15** (2019) 102581.

- [106] Z. Ahmed, S. Nadeem, S. Saleem, R. Ellahi, CNT-based MHD nanofluid with variable viscosity over a permeable shrinking surface, *Int. J. Num. Meth. Heat Fluid Flow*, **29** (2019) 4607-4623.
- [107] R. Ellahi, F. Hussain, S.A. Abbas, M.M. Sarafraz, M. Goodarzi and M.S. Shadloo, Study of two-phase Newtonian nanofluid flow hybrid with hafnium particles under the effects of slip, *Invention*, **5** (2020) 6.
- [108] M.M. Sarafraz, O. Pourmehran, B. Yang, M. Arjomandi and R. Ellahi, Pool boiling heat transfer characteristics of iron oxide nano-suspension under constant magnetic field, *Int. J. Therm. Sci.*, **147** (2020) 106131.
- [109] R. Ellahi, S.M. Sait, N. Shehzad and Z. Ayaz, A hybrid investigation on numerical and analytical solutions of electro-magnetohydrodynamics flow of nanofluid through porous media with entropy generation, *Int. J. Num. Meth. Heat Fluid Flow*, **30** (2020) 834-854.
- [110] K. Hiemenz, Die Grenzschicht an einem in den gleichförmigen Flüssigkeitsstrom eingetauchten geraden Kreiszylinder, *Dinglers Polytech. J.*, **4** (1911) 326-321.
- [111] F. Homann, Der Einfluss grosser Zähigkeit bei Strömung um Zylinder, *Z. Angew. Math. Mech.*, **16** (1936) 153-164.
- [112] L. Howarth, The boundary layer in three dimensionless flow-Part II, The flow near a stagnation point, *Philos. Mag.*, **42** (1951) 1433-40.
- [113] T.C. Chiam. Stagnation-point flow towards a stretching plate, *J. Phys. Soc. Japan*, **63** (1994) 2443-44.

- [114] T.R. Mahapatra and A.S. Gupta, Magneto hydrodynamic stagnation point flow towards a stretching sheet, *Acta Mech.*, **6** (2001) 152-191.
- [115] T.R. Mahapatra and A.S. Gupta. Heat transfer in stagnation point flow towards a stretching sheet, *Heat Mass Transf.*, **38** (2002) 517-521.
- [116] R. Nazar, N. Amin, D. Filip and I. Pop. Stagnation-point flow of a micropolar fluid towards a stretching sheet, *Int. J. Non-linear Mech.*, **39** (2004) 1227–1235.
- [117] M. Reza and A.S. Gupta. Steady two-dimensional oblique stagnation point flow towards a stretching surface, *Fluid Dyn. Res.*, **37** (2005) 334–340.
- [118] Y.Y. Lok, N. Amin and I. Pop, Non-orthogonal stagnation point flow towards a stretching sheet, *Int. J. Non-linear Mech.*, **41** (2006) 622–627.
- [119] Y.Y. Lok, I. Pop, D.B. Ingham and N. Amin. Mixed convection flow of a micropolar fluid near a non-orthogonal stagnation point on a stretching vertical sheet, *Int. J. Num. Meth. Heat Fluid Flow*, **19** (2009) 459–83.
- [120] M. Farooq, M. I. Khan, M. Waqas, T. Hayat, A. Alsaedi and M. I. Khan, MHD stagnation point flow of viscoelastic nanofluid with non-linear radiation effects, *J. Mol. Liq.*, **221** (2016) 1097-1103.
- [121] K.L. Hsiao, Stagnation electrical MHD nanofluid mixed convection with slip boundary on a stretching sheet, *Appl. Therm. Eng.*, **98** (2016) 850-861.
- [122] S. S. Ghadikolaei, M. Yassari, H. Sadeghi, K. Hosseinzadeh and D. D. Ganji, Investigation on thermophysical properties of $\text{TiO}_2\text{-Cu}/\text{H}_2\text{O}$ hybrid nanofluid transport dependent on shape factor in MHD stagnation point flow, *Pow. Tech.*, **322** (2017) 428-438.

- [123] K.L. Hsiao, Combined electrical MHD heat transfer thermal extrusion system using Maxwell fluid with radiative and viscous dissipation effects, *Appl. Therm. Eng.*, **112** (2017) 1281-1288.
- [124] N. Abbas, S. Saleem, S. Nadeem, A. A. Alderremy and A.U. Khan, On stagnation point flow of a micro polar nanofluid past a circular cylinder with velocity and thermal slip, *Res. Phys.*, **9** (2018) 1224-1232.
- [125] M. I. Khan, T. Hayat, F. Shah, M. Rahman and F. Haq, Physical aspects of CNTs and induced magnetic flux in stagnation point flow with quartic chemical reaction, *Int. J. Heat Mass Transf.*, **135** (2019) 561-568.
- [126] M.A. Chaudhary, J.H. Merkin, A simple isothermal model for homogeneous–heterogeneous reactions in boundary-layer flow. I equal diffusivities, *Fluid Dyn. Res.*, **16** (1995) 311-333.
- [127] J.H. Merkin, A model for isothermal homogeneous–heterogeneous reactions in boundary layer flow. *Math. Comput. Model.*, **24** (1996) 125-136.
- [128] T. Hayat, M.I. Khan, M. Farooq, T. Yasmeen, A. Alsaedi, Stagnation point flow with Cattaneo-Christov heat flux and homogeneous-heterogeneous reactions, *J. Mol. Liq.* **220** (2016) 9-55.
- [129] H. Xu, A homogeneous–heterogeneous reaction model for heat fluid flow in the stagnation region of a plane surface, *Int. Commun. Heat Mass Transf.*, **87** (2017) 112–117.

- [130] T. Hayat, F. Haider, T. Muhammad, B. Ahmad, Darcy–Forchheimer flow of carbon nanotubes due to a convectively heated rotating disk with homogeneous-heterogeneous reactions, *J. Therm. Anal. Calorim.*, **137** (2019) 1939-1949.
- [131] T. Hayat, A. Aziz, T. Muhammad and A. Alsaedi, Significance of homogeneous–heterogeneous reactions in Darcy-Forchheimer three-dimensional rotating flow of carbon nanotubes, *J. Therm. Anal. Calorim.*, **139** (2020) 183-195.
- [132] J. Ahmed, M. Khan and L. Ahmed, Effectiveness of homogeneous-heterogeneous reactions in Maxwell fluid flow between two spiraling disks with improved heat conduction features, *J. Therm. Anal. Calorim.*, **139** (2020) 3185-3195.
- [133] M. Khan, J. Ahmed, W. Ali, An improved heat conduction analysis in swirling viscoelastic fluid with homogeneous-heterogeneous reactions, *J. Therm. Anal. Calorim.*, **143** (2021) 4095–4106.
- [134] S. Mukhopadhyay, Heat Transfer Analysis of the Unsteady Flow of a Maxwell Fluid over a Stretching Surface in the Presence of a Heat Source/Sink, *Chin. Phys. Lett.*, **29** (2012) 054703.
- [135] T. Hayat, S.A. Khan, M.I. Khan, S. Momani and A. Alsaedi, Cattaneo-Christov (CC) heat flux model for nanomaterial stagnation point flow of Oldroyd-B fluid, *Comp. Meth. Prog. Bio.*, **187** (2020) 105247.
- [136] C.Y. Wang, Free convection on a vertical stretching surface, *J. Appl. Math. Mech. (ZAMM)*, **69** (1989) 418-420.

- [137] R.S.R. Gorla and I. Sidawi, Free convection on a vertical stretching surface with suction and blowing, *Appl. Sci. Res.*, **52** (1994) 247-257.
- [138] T. Hayat, S.A. Shehzad and A. Alsaedi, Three-dimensional flow of an Oldroyd-B fluid over a bidirectional stretching surface with prescribed surface temperature and prescribed surface heat flux, *J. Hydro. Hydromech.*, **62** (2014) 117-125.
- [139] M.S. Abel, J.V. Tawade and M.M. Nandeppanavar, MHD flow and heat transfer for the upper-convected Maxwell fluid over a stretching sheet. *Meccanica*, **47** (2012) 385–393.
- [140] M. Waqas, M.I. Khan, T. Hayat and A. Alsaedi, Stratified flow of an Oldroyd-B nanoliquid with heat generation. *Res. Phys.*, **7** (2017) 2489–2496.
- [141] M. Irfan, M. Khan and W. A. Khan, Impact of homogeneous–heterogeneous reactions and non-Fourier heat flux theory in Oldroyd-B fluid with variable conductivity, *J. Braz. Soc. Mech. Sci. Eng.*, **41** (2019) 41-135.
- [142] S.A. Shehzad, T. Hayat and A. Alsaedi, Influence of convective heat and mass conditions in MHD flow of nanofluid, *Bull. Pol. Ac. Sci. Tech. Sci.*, **63** (2015), 10.1515/bpasts-2015-0053.
- [143] T. Hayat, M. Waqas, S.A. Shehzad and A. Alsaedi, On model of Burgers fluid subject to magneto nanoparticles and convective conditions, *J. Mol. Liq.*, **222** (2016) 181-187.
- [144] M. Fathizadeh, M. Madani, Y. Khan, N. Faraz, A. Yildirim and S. Tutkun, An effective modification of the homotopy perturbation method for MHD viscous flow over a stretching sheet, *J. King. Saud. Univ. Sci.*, **25** (2013) 107-113.

- [145] A. Ahmed, M. Khan, M. Irfan and J. Ahmed, Transient MHD flow of Maxwell nanofluid subject to non linear thermal radiation and convective heat transport, *Appl. Nanosci.*, **10** (2020) 5361–5373.

From DRSM (DRSM L)

- Processed on 11-Oct-2021 10:06 PKT
- ID: 1670789826
- Word Count: 34533

Similarity Index

14%

Similarity by Source

Internet Sources:

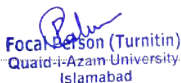
9%

Publications:

9%

Student Papers:

2%



Focal Person (Turnitin)
Quaid-i-Azam University
Islamabad

sources:

- 1 1% match (Internet from 23-Aug-2021)
<https://www.sciencegate.app/keyword/72757>
- 2 1% match (Internet from 23-Aug-2021)
<https://www.sciencegate.app/keyword/8545>
- 3 1% match (publications)
[Masood Khan, Zahoor Iqbal, Awais Ahmed. "Energy transport analysis in the flow of Burgers nanofluid inspired by variable thermal conductivity", Pramana, 2021](#)
- 4 1% match (publications)
[Zahoor Iqbal, Masood Khan, Aamir Hamid, Awais Ahmed. "Energy transport analysis in flow of Carreau nanofluid inspired by variable thermal conductivity and zero mass flux conditions", Advances in Mechanical Engineering, 2021](#)
- 5 < 1% match (student papers from 21-Jun-2014)
[Submitted to Higher Education Commission Pakistan on 2014-06-21](#)
- 6 < 1% match (student papers from 11-May-2012)
[Submitted to Higher Education Commission Pakistan on 2012-05-11](#)
- 7 < 1% match (student papers from 07-Nov-2017)
[Submitted to Higher Education Commission Pakistan on 2017-11-07](#)
- 8 < 1% match (student papers from 25-Apr-2017)
[Submitted to Higher Education Commission Pakistan on 2017-04-25](#)
- 9 < 1% match (student papers from 06-Jun-2018)
[Submitted to Higher Education Commission Pakistan on 2018-06-06](#)